Year : 2014

ASIC1a oligomerization Structure-function of its extracellular vestibule and Functional characterization of αS243Pßγ ENaC

Huser Delphine

UNIL | Université de Lausanne
Faculté de biologie et de médecine

Département de Pharmacologie et Toxicologie

ASIC1a oligomerization
Structure-function of its extracellular vestibule

and

Functional characterization of αS243Pβγ ENaC

Thèse de doctorat ès Sciences de la vie (PhD)

Présentée à la Faculté de biologie et de médecine de l'Université de Lausanne par

Delphine Huser

Master ès Sciences en biologie médicale

Université de Lausanne

Jury

Prof. Lee-Ann Laurent-Applegate, Présidente

Prof. Laurent Schild, Directeur de thèse

Prof. Raimund Dutzler, Expert

PD Dr. Ian Cameron Forster, Expert

Lausanne 2014

Imprimatur

Vu le rapport présenté par le jury d'examen, composé de

Président	Madame	Prof. Lee Ann	**Laurent-Applegate**
Directeur de thèse	Monsieur	Prof. Laurent	**Schild**
Experts	Monsieur	Prof. Raimund	**Dutzler**
	Monsieur	Prof. Ian	**Forster**

le Conseil de Faculté autorise l'impression de la thèse de

Madame Delphine Huser

Master en biologie médicale de l'Université de Lausanne

intitulée

Structure

ASIC1a oligomerization
Stucture-function of its extracellular vestibule and
functional characterization of ~~d'~~αS243Oβγ ENaC

αS243 Pβγ

Lausanne, le 14 février 2014

pour Le Doyen
de la Faculté de Biologie et de Médecine

Prof. Lee Ann Laurent-Applegate

Acknowledgments

Résumé

Oligomérisation d'ASIC1a et structure-fonction de son vestibule extracellulaire
Caractérisation fonctionnelle d'αS243Pβγ ENaC

Delphine Huser, Département de Pharmacologie et Toxicologie

Quatre cristaux du canal ASIC1a ont été publiés et soutiennent une stœchiométrie trimérique. Cependant, ces données contredisant de précédentes analyses fonctionnelles effectuées sur des canaux de la même famille, notre intérêt fut porté sur l'oligomérisation d'ASIC1a. Dans ce sens, un nouvel essai couplant la méthode d'analyse par substitution de cystéines (SCAM) avec l'utilisation de réactifs sulfhydryls bifonctionnels (crosslinkers) a été mis en place. Le but étant de stabiliser, puis sélectionner les canaux fonctionnels, pour ensuite les séparer selon leur taille par SDS-PAGE. Grâce à cette technique, nous avons démontré que le complexe stabilisé a une taille coïncidant avec une organisation tétramérique.

En plus de son oligomérisation, le chemin emprunté par les ions pour traverser le canal n'est pas clairement défini dans ces structures. De ce fait, utilisant une approche électrophysiologique, nous avons étudié le lien entre la structure et la fonction du vestibule extracellulaire d'ASIC1a. Dans ce but, nous nous sommes intéressés l'accessibilité de cystéines spécifiques localisées dans ce vestibule pour des réactifs méthanethiosulfonates (MTS). Ainsi, nous avons pu corréler les cinétiques de modification de ces cystéines par les MTS avec les effets sur le courant sodique, et donc avoir des informations supplémentaires sur la voie empruntée par les ions. De plus, la simulation informatique de liaison de ces réactifs illustre le remplissage total de ce vestibule. Fonctionnellement, cette interaction ne perturbe pas le passage de ions, c'est pourquoi il nous apparaît probable que le vestibule présente une taille plus large que celle illustrée par les cristaux.

Dans un deuxième temps, notre intérêt fut porté sur ENaC. Ce canal est composé des trois sous-unités (α, β et γ) et est exprimé dans divers épithéliums, dont les tubules des reins. Il participe à l'homéostasie sodique et est essentiellement régulé par voie hormonale *via* l'aldostérone et la vasopressine, mais également par des sérines protéases ou le Na^+. Nous avons étudié la répercussion fonctionnelle de la mutation αS243P, découverte chez un nouveau-né prématuré atteint de pseudohypoaldostéronisme de type 1. Cette maladie autosomale récessive se caractérise, généralement, par une hyponatrémie liée à d'importantes pertes de sel dans les urines, une hyperkaliémie, ainsi qu'un niveau élevé d'aldostérone.

Tout d'abord aucune des expériences biochimiques et électrophysiologiques n'a pu démontrer un défaut d'expression ou une forte diminution de l'activité soutenant les données cliniques. Cependant, en challengeant αS243PβγENaC avec une forte concentration de Na^+ externe, une hypersensibilité de canal fut observée. En effet, ni les phénomènes régulateurs de « feedback inhibition » ou de « Na^+ self-inhibition » n'étaient semblables au canal sauvage. De ce fait, ils apparaissaient exacerbés en présence de la mutation, amenant ainsi à une diminution de la réabsorption de Na^+. Ceci corrobore entièrement l'hyponatrémie diagnostiquée. Le rein d'un prématuré étant immature, la quantité de Na^+ atteignant la partie distale du néphron est plus élevée, du fait que les autres mécanismes de réabsorption en amont ne sont probablement pas encore en place. Cette hypothèse est renforcée par l'existence d'un frère présentant la même mutation, mais qui, né à terme, ne présentait aucun signe d'hyponatrémie.

Summary

ASIC1a oligomerization and structure-function of its extracellular vestibule
Functional characterization of αS243Pβγ ENaC

Delphine Huser, Department of Pharmacology and Toxicology

The main topic of my thesis is the structure-function relationship of the ENaC/Deg family of ion channels, namely the Acid-Sensing Ion Channel ASIC1a and the Epithelial Na Channel ENaC.

The primary part of this research is dedicated to the structure of ASIC1a. Four channel crystals have been published, which support a trimeric stoichiometry, although these data contradict previous functional experiments on other ENaC/Deg members. We are therefore interested in ASIC1a oligomerization and have set up a new assay combining the Substituted-Cysteine Accessibility Method (SCAM) with bifunctional sulfhydryl reagents (crosslinkers) allowing its study. The aim was to first stabilize the channels, then select those that are functional and then resolve them according to their size on SDS-PAGE. We demonstrated that the stabilized complex has a molecular weight corresponding to a tetrameric stoichiometry.
In addition to our interest in the oligomerization of the ENaC/Deg family of ion channels, we also wanted to investigate the thus far undefined way of permeation for these channels. Therefore, taking the advantage of a more electrophysiological approach, we studied the accessibility of specific cysteines for methanethiosulfonate reagents (MTS) and were able to correlate the MTS association kinetics on cysteine residues with Na^+ currents. These results have given us an insight into ion permeation and our functional evidence indicates that the extracellular is larger than that depicted by the crystal structures.

As a side project, we focused on ENaC, which is made up of three subunits (α, β and γ) and is expressed in various epithelia, especially in the distal nephron of the kidneys. It plays a role in Na^+ homeostasis and is essentially regulated by hormones *via* aldosterone and vasopressin, but also by serine proteases or Na^+. We have studied the functional impact of the αS243P mutation, discovered in a premature baby suffering from pseudohypoaldosteronism of type 1. This autosomal recessive disease is characterized by hyponatremia, hyperkalemia and high aldosterone levels. Firstly, neither biochemical nor electrophysiological experiments indicated an expression defect or a strong decrease in activity. However, challenging αS243PβγENaC with increased external Na^+ concentration showed channel hypersensitivity. Indeed, both the "feedback inhibition" and the "Na^+ self-inhibition" regulatory mechanisms are impaired, leading to a decrease in Na^+ reabsorption, entirely supports the diagnosis. The kidneys in preterm infants are immature and Na^+ levels reaching the distal nephron are higher than normally observed. We hypothesize that the upstream reabsorption machinery is unlikely to be sufficiently matured and this assumption is supported by an asymptomatic sibling carrying the same mutation, but born at term.

Résumé destiné à un large public

Oligomérisation d'ASIC1a et structure-fonction de son vestibule extracellulaire
Caractérisation fonctionnelle d'αS243Pβγ ENaC

Delphine Huser, Département de Pharmacologie et Toxicologie

La cellule, unité fonctionnelle du corps humain, est délimitée par une membrane plasmique servant de barrière biologique entre les milieux intra et extracellulaires. Une communication entre cellules est indispensable pour un fonctionnement adéquat. Sa survie dépend, entre autres, du maintien de la teneur en ions dans chacun des milieux qui doivent pouvoir être réabsorbés, ou sécrétés, selon les besoins. Les protéines insérées dans la membrane forment un canal et sont un moyen de communication permettant spécifiquement à des ions tel que le sodium (Na^+) de traverser. Le Na^+ se trouve dans la plupart des aliments et le sel, et est spécifiquement réabsorbé au niveau des reins grâce au canal sodique épithélial ENaC. Cette réabsorption se fait de l'urine primaire vers l'intérieur de la cellule, puis est transporté vers le sang. Pour maintenir un équilibre, une régulation de ce canal est nécessaire. En effet, des dysfonctionnements impliquant la régulation ou l'activité d'ENaC lui-même sont à l'origine de maladies telles que la mucoviscidose, l'hypertension ou encore, le pseudohypoaldostéronisme (PHA). Cette maladie est caractérisée, notamment, par d'importantes pertes de sel dans les urines. Des pédiatres ont diagnostiqué un PHA chez un nouveau-né, ce dernier présentant une modification du canal ENaC, nous avons recréé cette protéine afin d'étudier l'impact de ce changement sur son activité. Nous avons démontré que la régulation d'ENaC était effectivement perturbée, conduisant ainsi à une forte réduction de la réabsorption sodique.

Afin de développer des molécules capables de moduler l'activité de protéines. Il est nécessaire d'en connaître la structure. Celle du canal sodique sensible à l'acidification ASIC1, un canal cousin d'ENaC, est connue. Ces données structurales contredisant cependant les analyses fonctionnelles, nous nous sommes penchés une nouvelle fois sur ASIC1. Une protéine est une macromolécule biologique composée d'une chaîne d'acides aminés (aa). De l'enchaînement d'aa à la protéine fonctionnelle, quatre niveaux de structuration existent. Chaque aa donne une indication quant au repliement et plus particulièrement la cystéine. Arborant un groupe sulfhydryle (SH) capable de former une liaison spécifique et stable avec un autre SH, celle-ci est souvent impliquée dans la structure tridimensionnelle de la protéine. Ce type de liaison intervient également dans la stabilisation de la structure quaternaire, qui est l'association de plusieurs protéines identiques (homomère), ou pas (hétéromère).
Dans cette partie, nous avons remplacé des aa par des cystéines à des endroits spécifiques. Le but était de stabiliser plusieurs homomères d'ASIC1 ensemble avec des réactifs créant des ponts entre deux SH. Ainsi, nous avons pu déterminer le nombre de protéines ASIC1 participant à la formation d'un canal fonctionnel. Nos résultats corroborent les données fonctionnelles soutenant un canal tétramérique. Nous avons également étudié l'accessibilité de ces nouvelles cystéines afin d'obtenir des informations supplémentaires sur la structure du chemin emprunté par le Na^+ à travers ASIC1 et plus particulièrement du vestibule extracellulaire.

Abbreviations

Å	Angstrom
aa	amino acid
AD	Autosomal Dominant
ADN	Acid desoxyribonucleic
ANG	Angiotensin
APETx2	*Anthopleura elegantissima* Toxin-2
AR	Autosomal Recessive
ASDN	Aldosterone Sensitive Distal Nephron
ASIC	Acid-sensing Ion Channel
ASL	Airway Surface Liquid
ATP	Adenosine TriPhosphate
AVP	Vasopressin
BLINaC	Brain-Liver Na Channel
BMOE	Bismaleimidoethane
BN-PAGE	Blue-Native-PAGE
CaCC	Ca-activated Cl Channel
cAMP	cyclic Adenosine MonoPhosphate
CAP	Channel Activating Protease
CCD	Cortical Collecting Duct
C_{Ct}	C-ter Cysteine mutated Channel
CD	Collecting Duct
CF	Cystic Fibrosis
CFTR	Cystic Fibrosis Transmembrane Regulator channel
CHO	Chinese Hamster Ovary
CNS	Central Nervous System
CNT	Connected Tubule
CRD	Cysteine-Rich Domain
DCT	Distal Convoluted Tubule
Deg	Degenerin
DRASIC	Dorsal Root ASIC
DRG	Dorsal Root Ganglia
DTT	Dithiothreitiol
ECL	Extracellular Looop
ENaC	Epithelial Na Channel
FaNaC	FMRFamide Na Channel
GluR	Glutamate receptor
GMQ	Guanidine-4-MethylQuinazoline
GR	Glucocorticoid Receptor
hINaC	human Intestine Na Channel
HT	Hypertension
HyNaC	Hydra Na Channel
IC_{50}	Inhibitory Concentration for half of the maximum

	effect
Imax	maximum current
I_{Na+}	Na^+ current
I_{peak}	Peak current
$I_{sustained}$	Sustained current
k_2	Association rate constant
KcsA	*Streptomyces lividans* K Channel
Kir	K inward rectifier
LTP	Long Term Potentiation
MDCK	Madin-Darby canine kidney
MDEG	Mammaliam Deg
MEC	Mechanosensitive Channel
MitTx	*Micrurus tenertener* Toxin
MR	Mineralocorticoid Receptor
MTS	Methanethiosulfonate
N	number
NaTT	Sodium Tetrathionate
NCC	Na Cl Channel
n_H	Hill coefficient
NKCC2	Na, K, 2Cl Cotransporter
NM	Nafamostat mesilate
NMDA	N-methyl-D-aspartic
NMDG	N-methyl-D-glucosamine
NPFF	Neuropeptide FF
NPSF	Neuropeptide SF
ns	non significant
NSAID	Nonsteroid Anti-inflammatory Drug
OCAM	Oligomer Characterization by Addition of Mass
PCT	Poximal Tubule
PcTx1	Psalmotoxin
pH	potential Hydrogen
$pH_{0.5}$	pH of half activation
$pH_{0.5in}$	pH of half inactivation
PHA1	Pseudohypoaldosteronism type 1
PNS	Peripheral Nervous System
P_o	Open Probability
PPK	Pickpocket
pS	pico Siemens
PST	Proximal Straight Tubule
PY	PxxYxx
R	Receptor
RAAS	Renin-Angiotensin-Aldosterone System

ROMK	Renal Outer Medullary K Channel
RPK	Ripped Pocket
SCAM	Substituted-Cysteine Accessibility Method
SDS	Sodium Dodecyl Sulfate
SDS-PAGE	SDS-Polyacrylamide Gel Electrophoresis
SEC	Size Exclusion Chromatography
Sf9	Spodoptera frugiperda cell
Sgk1	Serum-glucocorticoid kinase
SP	Serine protease
SPASIC	Spinal cord ASIC
τ	Tao
TAL	Thick Ascending Limb
τ_D	Tao of desensitization
TEVC	Two-Electrodes Voltage Clamp
TL	Thin descending Limb
TM	Transmembrane
τ_{rec}	Tao of recovery
ub	Ubiquitin
UNC	Uncoordination Channel
wt	wild-type

List of amino acids

Ala	**A**	Alanine
Arg	**R**	Arginine
Asn	**N**	Asparagine
Asp	**D**	Aspartate
Cys	**C**	Cysteine
Gln	**Q**	Glutamine
Glu	**E**	Glutamate
Gly	**G**	Glycine
His	**H**	Histidine
Ile	**I**	Isoleucine
Leu	**L**	Leucine
Lys	**K**	Lysine
Met	**M**	Methionine
Phe	**F**	Phenylalanine
Pro	**P**	Proline
Ser	**S**	Serine
Thr	**T**	Threonine
Trp	**W**	Tryptophan
Tyr	**Y**	Tyrosine
Val	**V**	Valine

Table of contents

Introduction

Ion channels, as well as aquaporins or the porins, are macromolecular pores inserted in the cell membrane. They appeared more than 3 billion years ago with primitive replicating forms surrounded by the first lipid envelope (1). While protecting cell from the loss of vital components, the envelope also prevents the access of ionized necessary substrates and the loss of ionized waste products. Thus, transport mechanisms (membrane proteins) have evolved in parallel, each of them with specific transport devices and physiological functions. Their roles are to regulate the distribution of ions and water in the intracellular and extracellular compartments. The transport can be either passive or active, depending whether molecules cross the membrane passively or actively through membrane proteins. In the passive or facilitated transport, molecules (such as ions or glucose) cross the transmembrane proteins following their electrochemical gradients. Both intra- and extracellular milieus have a heterogenic ionic composition influenced by the selective permeability of the membrane for ions. This characteristic renders the membrane electrically polarized. The pores (i.e. aquaporins), the carriers (i.e. glucose transporters GLUT), as well as the ionic channels, belong to the facilitated pathway. Ion channels present diversity and are classified into gene families and subfamilies; among them are the voltage-gated, the ligand-gated, the transient-receptor potential TRP or the ENaC/Degenerin family of ion channels.

ENaC/Degenerin family

The epithelial sodium channel (ENaC)/degenerin (Deg) gene family have been discovered lately at the beginning of the 1990s. All members form Na^+-selective channels sharing a common subunit organization characterized by two hydrophobic transmembrane (TM) domains, short N- and C- termini, and a large extracellular loop (ECL) containing two to three cysteine-rich domains.

The Figure 1 depicts the phylogenetic relationship of the ENaC/Deg family members classified into taxa. Until recently ENaC/Deg channels were found only in Metazoa. Formerly restricted to the Bilateria, the identification of new members isolated from the Cnidaria *Hydra magnipapillata* (namely HyNaC1 to 4) moved backwards the first appearance of the ENaC/Deg family prior to the Radiata-Bilateria dichotomy. The fact that HyNaC channels are gated by the Hydra Arg-Phe-NH$_2$ (RFamide) peptides supports the theory that the peptide-gated ion channels

1

have evolved in organisms bearing a primitive nervous system where transmission occurred extensively *via* neuropeptides (2). Bilateria have another peptide-gated channel subfamily, i.e. the FaNaC. Belonging of Protostomia to the subdivision Lophotrochozoa, FaNaC channels have been identified from the snail *Helix aspersa* (Molluska) and are directly gated by the peptide Phe-Met-Arg-Phe-NH_2 (FMRFamide) (3). In the same branch the Ecdysozoa contains the two largest subfamilies of ENaC/Deg channels; the Nematoda and the Insecta. The Degenerins of the worm *Caenorhabditis elegans* are composed of 30 members, with DEG-1 and MEC-4 as the first discovered *via* a screening of mutations that caused neurodegeneration (4,5). Expressed in mechanoreceptor neurones (MEC, DEG) and muscles (UNC), they are activated by mechanical stimuli such as stretch (6). Additionally, *C. elegans* has distinct members of the degenerins, namely FLR, which were isolated through fluoride ion resistant mutants (7). Beside Nematoda, Insecta with the *Drosophila melanogaster* contain no less than 31 related-genes, namely ripped pocket (RPK) and pickpocket (PPK) (8). Cell functions and patterns of expression are as various as the number of genes, going from a role in mechanosensation to a chemosensory function in male courtship behaviors, an implication in salt taste, tracheal liquid clearance or synaptic plasticity (9-16). To date, a lot remains to be investigated in order to understand the physiological functions of most pickpocket proteins. The final branch of the Metazoa displaying ENaC/Deg genes encompasses the vertebrates. We can distinguish two subfamilies; the H^+-activated ASIC and the constitutively open ENaC. Vertebrates also have the brain-liver-intestine Na^+ channel (BLINaC), isolated from the rat brain and the human intestine sodium channel (hINaC). A recent study, searching for ENaC/Deg homologs from unicellular eukaryotes to multicellular Metazoans, pointed out the existence of homologs in the *Naegleria gruberi* genome, a eukaryotic microbe from the Excavata. Authors raised the question of the ENaC/Deg family presence in the *N. gruberi* and confronted two hypotheses, one supporting a common ancestor and the consequent vertical inheritance of the gene family and the other inclining for a lateral gene transfer (17).

Despite a well-conserved topology of the subunits between the ENaC/Deg family members, the homology between the subfamilies is quite low, whereas it increases within subfamilies. Indeed, within ENaC and Deg subfamilies, the average homology between amino acids (aa) sequences reaches 33 and 35 %, respectively, while it attains 38, 43 and 68 % in

HyNaC, ASIC and FaNaC, respectively. Regarding PPK members, the sequence homology falls to 20 % (see Percent Identity Matrix (Clustal Omega) for detailed values).

Between subfamilies, conserved motifs exist. The ECL is rich in cysteines and contains seven disulfide bridges widely conserved among homologs; the cysteine-rich domains "CRD". The N-terminal region contains two residues (His-Gly) highly conserved, this is the "HG motif". The conservation of HG is complete within the ASIC, ENaC, HyNaC, FaNaC and Deg proteins. However, it is not within the PPK family. Indeed, 58 % arbor HG, 22 % have a half-conserved motif (HN, SG, NG or AG), and 20 % display no conservation or deletion of HG. Then, the FPxxTxC sequence following M1 (post-M1, yellow) displays the same kind of conservation than HG; F, P, T and C residues display a conservation of 90, 97, 61 and 97 % within the PPK members, respectively. The TM domains are a feature fully-conserved throughout the ENaC/Deg family. Analyzing the aa identity of the TM1 (respectively TM2) within subfamilies demonstrates that the conservation is pretty much higher for the TM2 than the TM1. Indeed, the average values are 37 and 71 % for ASIC TM1 versus TM2, 31 and 46 % for ENaC, 28 and 56 % concerning HyNaC, as well as 24 and 51 % for Deg proteins.
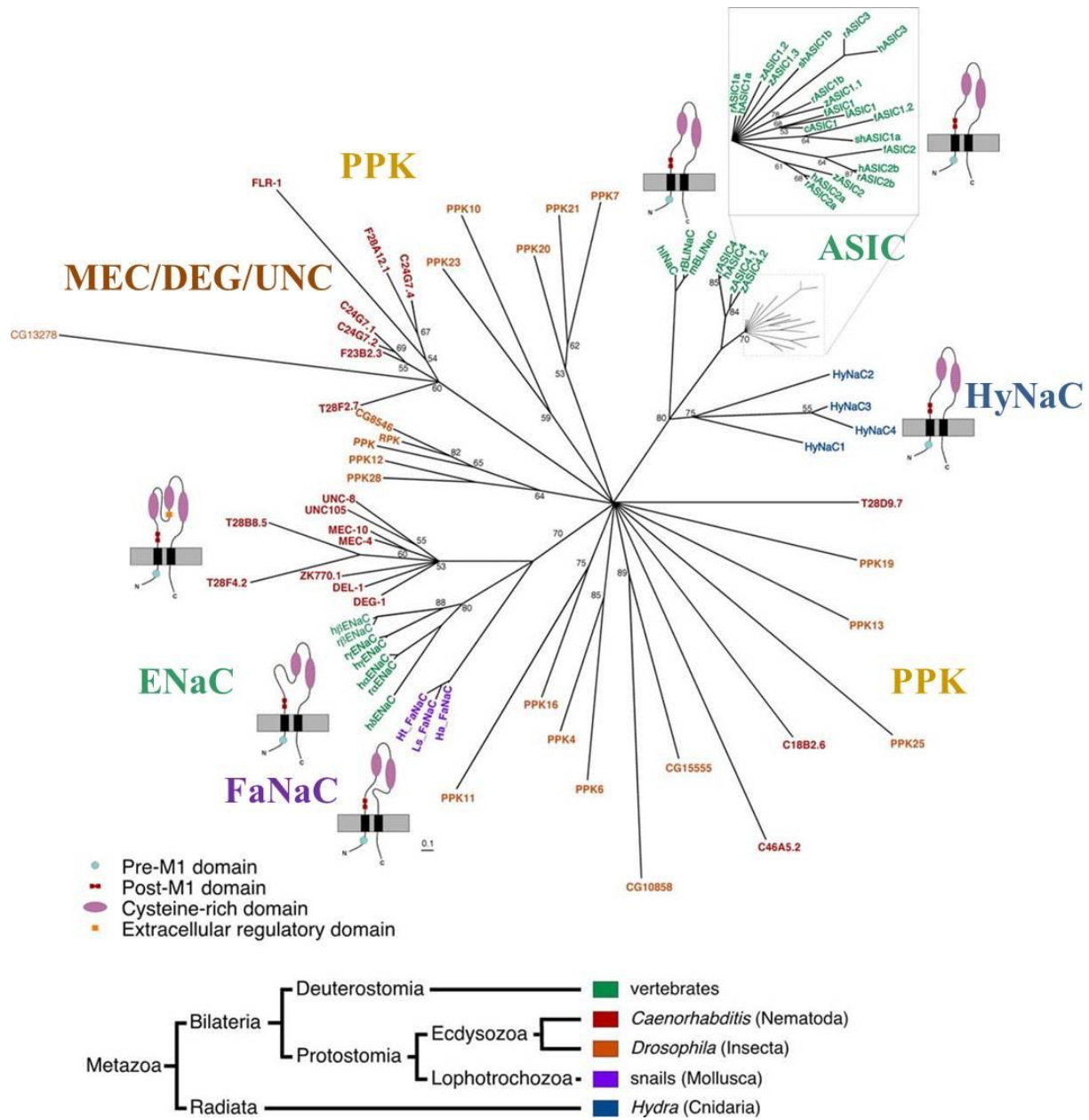
Figure 1 Quartet-puzzling consensus tree for the DEG/ENaC family members. The tree has been constructed from molecular sequence data by maximum likelihood, with the program TREE-PUZZLE; branch lengths represent the evolutionary distance. Support values below 90% are indicated. The ASIC branch is shown also at higher magnification. Figure modified from Golubovic *et al.* 2007 (2).

ENaC

The existence of an epithelial Na^+ channel was known prior the cloning thanks to experiments of Ussing on frog skin (18). Single-channels recordings on rat kidney performed by Palmer and Frindt also confirmed the presence of an epithelial Na^+ channel (19). ENaC is a heteromultimeric membrane protein. To date, four subunits of ENaC have been cloned; α, β, γ (20-22) and δ1/2 (23,24). They have been the first members of the ENaC/Deg family expressed in a heterologous system. Analyzing the percent of aa sequence homology between them indicates an average of 33 %. The highest similarities have been found between α and δ (39 %), as well as between γ and β (36 %) (Figure 2).

	SCNN1A	SCNN1B	SCNN1G	SCNN1D
SCNN1A	100.00			
SCNN1B	31.41	100.00		
SCNN1G	33.17	35.79	100.00	
SCNN1D	39.12	29.20	29.97	100.00

Figure 2 Amino acids sequence identity matrix of ASIC channels obtained from basic local alignment of amino acid sequences using Clustal Omega (http://www.ebi.ac.uk/Tools/msa/clustalo/).

To be functional, channels must be composed at least of an α or α-like subunit (δ). However, when expressed individually, β or γ does not induce an amiloride-sensitive current. When co-expressed with α subunit, β and γ demonstrate a 3- to 5- fold potentiation of the currents. Finally, co-expression of αβγ is required to have a maximal channel activity. This maximal current is 25 to 50-fold higher than αβ or αγ currents (25). Co-expression of δ2βγ in *Xenopus laevis* oocytes leads to smaller currents than channels made of αβγ subunits. Due to a decreased level of expression at the cell surface, it might result from a lower efficiency of assembly and/or a trafficking defect (26).

αβγENaC is a constitutively open channel characterized by high selectivity for small cations such as Li^{2+} and Na^+ and non-selectivity for larger cations (K^+ or NH_4^+). Permeability (P) is higher for Li^{2+} than Na^+ which in turn is 20-fold bigger than P_K ($P_{Li} > P_{Na} \gg P_K$). Patch-clamp analyses on rat collecting tubules have demonstrated that the ENaC unitary conductance reaches 4-5 pS for the Na^+ and 8 pS for the Li^{2+}. Moreover, the Michaelis constant (K_m), that is the concentration required for half-maximal conductance, indicates that Na^+ has an apparent binding

affinity higher than Li^{2+} with K_m of 20-50 mM and 90 mM, respectively. Regarding the gating, ENaC is characterized by long spontaneous and closed times (0.5-5 sec at room temperature). The duration is shortened to hundreds of millisecond in rat cortical collecting duct (CCD) at 37°C (27). Channels made of two subunits ($\alpha\beta$ or $\alpha\gamma$) have functional characteristics slightly different. For instance, the magnitude of amiloride-sensitive current has a similar profile between $\alpha\beta\gamma$ and $\alpha\gamma$ channels ($Li^+ > Na^+ >> K^+$), whereas $\alpha\beta$ has larger Na^+ current than Li^+. Moreover, single channel conductances of $\alpha\beta$ channels (5.1 pS and 4.2 pS for Na^+ and Li^+, respectively) are smaller than for $\alpha\gamma$ (6.5 and 10.8 pS for Na^+ and Li^+, respectively) (28).

1.   ENaC physiology

$\alpha\beta\gamma$ENaC is expressed at the apical side of polarized epithelial cells. ENaC has been detected in the kidney and the lung (for details, see next section), as well as in salivary glands (29) and taste buds (30,31). Colonic epithelial cells also express ENaC and play a role in Na^+ homeostasis (32). In the epidermis, ENaC has also been detected in human primary keratinocytes and murine epithelium (33,34). ENaC is the rate-limiting step for Na^+ transport. The model of the Figure 3 illustrates the movement of Na^+ ions; according to their electrochemical gradient, Na^+ ions enter the cell and are then actively extruded through the Na, K-ATPase. This polarized cell model is the base of the Na^+ transport and is found in various epithelia. In the lung ENaC is co-expressed with the Cl^- channel CFTR responsible of the Cl^- secretion, whereas in the kidney it is with the K^+ channel ROMK secreting K^+.
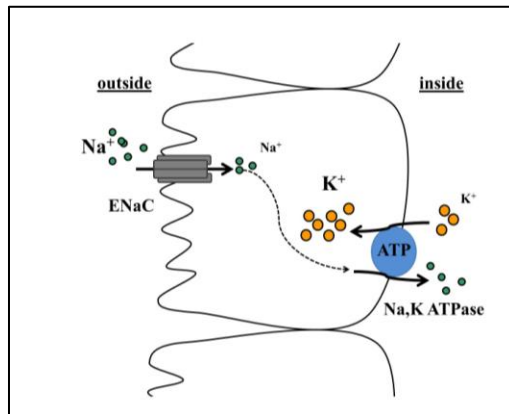
Figure 3 Scheme of the transcellular Na^+ transport in a polarized epithelial cell. At the apical membrane, ENaC (in gray) transports Na^+. Basolaterally, the Na, K-ATPase (in blue) extrudes it from the cell and reabsorbs K^+.

The δ1 and 2 subunits expression is, however, not restrained to epithelia. Indeed, these proteins

have been detected in non-epithelial tissues as in the CNS (telencephalon) or spermatogenic cells (35,36). Surprisingly, neither β nor γ ENaC appeared to be co-expressed with δ. Few works have highlighted the presence of δ transcripts in epithelia, as for instance in lung tissue (37). However, the expression profile of δ proteins still remains unknown.

Several domains have been shown to be important for ENaC structure and function. Some of them have been cited before *via* their conservation throughout the ENaC/Deg family, other not. Extracellular cysteines of the "CRD" are involved in disulfide bonds, except the C275. These bridges likely play a role in the proper protein folding (38,39). The "HG motif" in the N-terminus has been discovered *via* a human mutation where a serine replaced a glycine in βENaC (βG37S). This mutation led to an ENaC loss of function due to an opening probability decrease and, consequently, to an excessive Na^+ loss in the urine. (40).

ENaC channels share common features with ASIC; the degenerin and the amiloride binding sites, as well as the selectivity filter. The Deg site has been identified thanks to the mutation of a conserved alanine in the pre-M2 region of MEC-4 that led to neuronal cell swelling and degeneration in *C. Elegans* degenerins (5). This mutation leads to the destabilization of the closed state that becomes shorter (41). The replacement of the corresponding alanine, serine or glycine into ASIC, ENaC, RPK, BLINaC and hINaC by bulkier residues (valine, phenylalanine, threonine or lysine) promotes the activation of channel (9,42-45). ENaC and ASIC are inhibited by the potassium-sparing diuretic amiloride. The binding site is located in the middle of the TM2. ENaC is blocked by nanomolar concentrations, whereas the affinity is 100-fold lower for ASIC. Residues involved in the binding have been identified using site-directed mutagenesis; αS583, βG525 and γG537 in the rat ENaC (46), G437 in the human ASIC2 (47), and G440 in the human ASIC1a (Amiloride dose-response curves Figure 49) (48). Given that these residues are located in the conducting pore, more precisely in the middle of the TM2, the amiloride behaves as a plug preventing ion permeation (49). This block can be modulated by different factors such as the extracellular pH since the amiloride blocks the channel in its positively charged form (50). Thus, the more the pH increases the less the amiloride will be protonated. The extracellular Na^+ concentration also modifies the block by increasing the association rate constant. This underlines a competition between permeating ions and amiloride (51). The amiloride-channel interaction depends on the transmembrane voltage too (52). The stretch of residues responsible for the

permeability of ENaC/ASIC channels for small cations is called the selectivity filter. This preference for small ions shows that the filter constitutes the narrowest part of the pore. It is composed of a three amino acid sequence G/SxS, (αG587-9 in rat ENaC). Mutation of αS589 allows the passage of larger ions such as K^+. Bulkier is the mutant residue, the higher will be the permeability to large ions. This suggests an enlargement of the permeation pathway and a side chain pointing away from the pore (53-56). ENaC subfamily contains the conserved "PY motif" (PPPxYxxL) in the C-terminus, which is involved in the regulation of the channel's cell surface expression by the ubiquitin system (ENaC Regulation) (57).

1.1. ENaC in the lung

The airway surface liquid (ASL) is composed of the periciliary layer and the mucus. To keep the ASL well-hydrated, the water flow varies according to the osmotic gradients and depends on the activity of membrane proteins expressed at the air-liquid interface, which are ENaC, the Ca^{2+}-activated Cl^- channel CaCC and CFTR. Through these proteins, the cells secrete Cl^- (CFTR, CaCC) and absorb Na^+ (ENaC) to maintain an appropriate volume. In cystic fibrosis, the ASL is dehydrated. That reflects an imbalance between the absorption of and secretion of salt. Actually, it is not well known which of the CFTR or the $[Cl^-]_i$ regulates ENaC (Figure 4) (58,59).
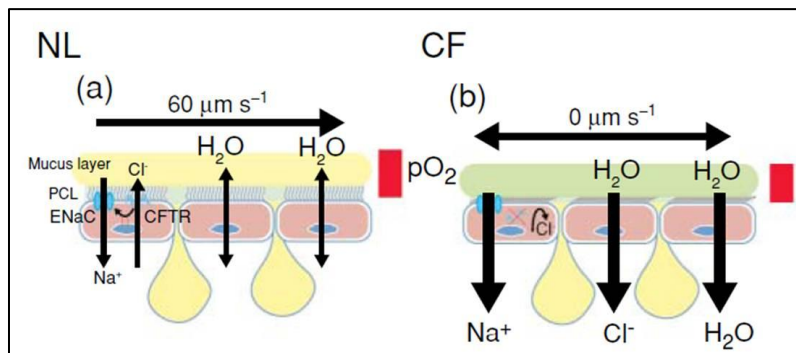
Figure 4 Mechanisms of mucus clearance, normal (NL) versus cystic fibrosis (CF) airway surfaces. *A,* In NL airways, ENaC absorbs Na^+ and cystic fibrosis transmembrane regulator CFTR secretes Cl^- and regulate ENaC. *B,* In CF, the absence of CFTR protein/function leads to unregulated Na^+ and water absorption. Bars depict O_2 tension in ASL (red and blue for oxygenated and hypoxic, respectively). Figure modified from Boucher *et al.*, 2007 (60).

In the distal lung airway, ENaC is expressed at the air-liquid interface. Loss-of-function mutations of ENaC in the salt-losing syndrome named pseudohypoaldosteronism type 1 are often associated with neonatal respiratory distress syndrome (see ENaC and pathologies) (61,62). Moreover, transgenic mice overexpressing βENaC in the airway epithelia exhibit depleted ASL hydration, slowed mucus clearance, mucus adhesion and death prior to weaning, a phenotype

similar to cystic fibrosis disease (63). Altogether, these findings suggest a role of ENaC in the airways.

1.2. ENaC in the kidney

In the kidney, ENaC is expressed in the aldosterone-sensitive distal nephron (ASDN) in which it is the rate-limiting step for the Na^+ uptake allowing the Na^+ flux out of the primary urine. As shown on Figure 5, the Na, K-ATPase, expressed basolaterally, creates the electrochemical gradient that is the driving force behind Na^+ reabsorption through ENaC (64). The transepithelial movement of Na^+ creates osmotic forces that drive the transepithelial absorption of water. The K^+ channel ROMK is responsible of extruding K^+ out of the cell.
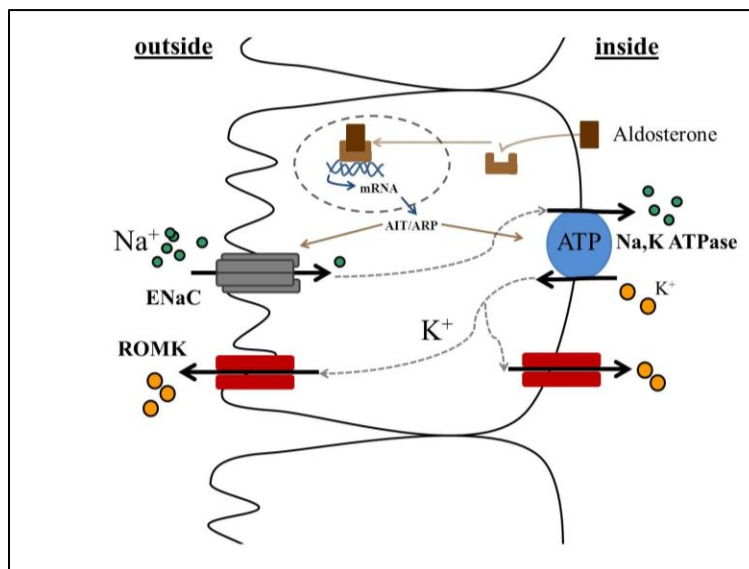
Figure 5 Transepithelial transport in the principal cells of the cortical collecting duct (CCD). The aldosterone binds to its receptor (MR), then the complex translocates into the nucleus where it induces/represses transcription of targeted genes (AIT/ARP). ENaC expression, and thus Na^+ transport, is increased.

The mineralocorticoid hormone aldosterone plays a critical role by controlling the Na^+ reabsorption and the K^+ secretion. There are two corticoid receptors (R) in the nephron; the glucocorticoid and the mineralocorticoid R (GR and MR). To insure the specificity of mineralocorticoids the enzyme 11β-hydroxysteroid dehydrogenase type 2 (11β-HSD2) converts cortisol or corticosterone into an inactive metabolite that prevents the binding of MR by glucocorticoids (65,66). The three key players in the fine tuning of Na^+ reabsorption, that are; ENaC, MR and 11β-HSD2, are expressed in the ASDN (67).

2. ENaC Regulation

Na^+ intake varies during the day, thus its reabsorption *via* ENaC needs constant adjustment. Many steps control ENaC expression at the apical membrane of epithelial cells. Transcription of α, β and γ subunits are under the control of aldosterone. Translation and post-translational modifications occur through phosphorylation, proteolytic cleavage, ubiquitylation and deubiquitylation. This leads to a fast overall turnover of 45 to 60 minutes for each subunit. Circadian rhythms also influence the sodium transport independently of blood pressure, body water or salt intake (68-70).

In response to a decrease of the extracellular volume or blood pressure or hyponatremia, an increase in plasmatic K^+ and angiotensin (ANG) II is observed. Both of them induce the production of aldosterone and thus an increase in the Na^+ reabsorption. The renin-angiotensin-aldosterone cascade (RAAS) is initiated by the angiotensinogen synthesis in the liver. The renin, synthetized by granular cells of the juxtaglomerular apparatus in the kidney, then cleaves angiotensinogen to ANG I. In a final step, ANG I is cleaved by the angiotensin converting enzyme to ANG II. The binding of ANG II on its receptor stimulates the phospholipase C, leading to the formation of diacyglycerol and inositol 1,4,5-triphosphate. Subsequent increase in $[Ca]_i$ depolarizes the plasma membrane of glomerulosa cells and thus induces the production of aldosterone (71).

In vivo, injection of aldosterone in adrenalectomized rats induces an increased αENaC expression in the ASDN (β and γ levels unchanged) and a redistribution of ENaC to the apical membrane within two hours (72). These results support previous experiments performed on either NaCl-restricted or aldosterone-perfused rats. Subsequently, the γENaC cleavage is clearly linked to an increase in ENaC-mediated I_{Na+} (73). ENaC current measurements from cortical collecting tubule cells of mice expressing β-truncated subunit demonstrate that the mineralocorticoid regulation of ENaC is still maintained and does not imply the PY motif and hence NEDD4-2 dependent down regulation (74). *In vitro* experiments on ENaC endogenously expressed in a cell line derived from *Xenopus laevis* kidney have highlighted the impact of aldosterone on ENaC. The hormone enhances both the transcription and translation of α, β and γ subunits by a two- and four-fold increase respectively. Consistently, a similar enlargement of the amiloride-sensitive currents is observed and unlinked with any change in the P_o, the kinetics of single channels or in the rate of

degradation of ENaC subunits (75). *In vivo* and *in vitro* studies diverge; the former shows an overexpression of αENaC only, whereas the latter demonstrates a transcriptional increase of α, β and γENaC together.

In the distal nephron, the binding of the antidiuretic hormone arginine vasopressin to its basolateral V2-receptor increases the expression of type 2 aquaporins at the apical membrane. This leads to an enhancement of water reabsorption. The PKA/cAMP signaling pathway is stimulated, inducing the activation of Na^+ transport *via* ENaC, and Na, K-ATPase. cAMP increases the quantity of ENaC and the Na, K-ATPase at the cell membrane, while PKA activates the serum-glucocorticoid kinase (Sgk1), an inhibitor of the ubiquitine-ligase NEDD4-2 (76,77).

Focusing now on the translational and post-translational modifications, proteolytic cleavage and ubiquitylation are known to regulate the Na^+ transport *via* ENaC. To date, it has been demonstrated that the proteolysis of ENaC is associated with a channel activity increase (78-82). Serine proteases (SP) can be classified according to sequence and structure similarities. ENaC-activating SPs belong to two subfamilies. The first subfamily contains proteases with His-Asp-Ser (HDS) as catalytic residues and a primary specificity for Ala, Glu, Phe, Gly, Lys, Gln, Arg, Trp and Tyr. A representative member is trypsin. The second subfamily has a catalytic domain made of DHS and is specific for Phe, Trp and Tyr residues. TMPRSS (CAP2), elastase, prostasine (CAP1) or matriptase, and Furin-like protein convertases are known to activate ENaC by four- to seven-fold depending on experimental conditions through an increase in P_o and without any change in the number (N) of cell surface expressed channels (81). αβγENaC co-expression is required for the cleavage and thus the full activation of the channel. Indeed, subunits expressed alone in CHO or MDCK epithelial are not cleaved (83). Western blot analysis demonstrated that α and γ subunits are cleaved, whereas β is not. The absence of β cleavage is due to a lack of cleavage site (Figure 6).
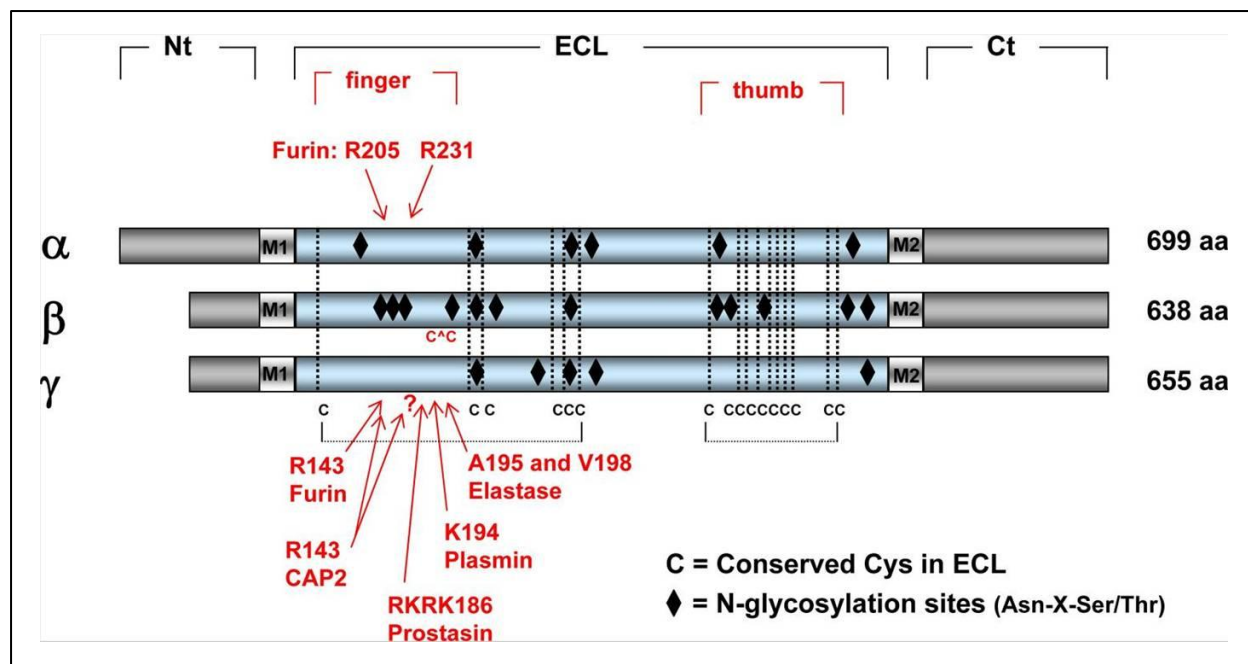
Figure 6 Linear models of the ENaC subunits. The finger domain contains the cleavage sites by furin for α subunit and by furin, prostasin (CAP1), CAP2, elastase, and plasmin for the γ subunit. This alignment also shows that the β subunit lacks the consensus motifs for protease recognition but has supplementary sites for glycosylation, as well as an additional Cys pair. Figure from Kleyman *et al.*, 2009 (84).

To exert their function, SPs have to be activated. This activation is tightly controlled, and occurs through transcriptional/translational regulation, protease activation and degradation (85), or *via* protease inhibitors (SPIs), such as the protease nexin-1 (86).

ENaC arbors a motif for degradation called the "PY motif". It has been shown that the PY motifs of β and γ subunits are involved and lead to a reduction of ENaC density at the apical cell membrane *via* ubiquitylation (87,88). The ubiquitin (ub) is a polypeptide made of 76 amino acids. Through an isopeptide bond, ub is conjugated to the lysine (ε amino group). Three kinds of proteins are involved in the ubiquitylation cascade: The ub-activating enzyme (E1), the ub-conjugating enzyme (E2), and the ub-protein ligase (E3). This process is reversible thanks to the deubiquitylating enzymes DUBs. It has been described that the E3 Nedd4.2 specifically binds to the PY domains of β and γ ENaC, thus leading to the ubiquitylation and finally to the endocytosis of ENaC (89). Several years later, the DUB USP-45 was shown to be upregulated by aldosterone, thus increasing the ENaC content at the apical membrane (90).

Ions are also involved in the regulation of ENaC. The Na^+ is a modulator of channel activity by two distinct phenomena. The increase intracellular Na^+ content slowly inhibits ENaC currents with a time constant of 10 to 20 min (91); the so-called "feedback inhibition". The rapid

increase of external Na^+ concentration (0 to 100 mM) induces the fast relaxation of the large I_{Na} peak to a lower steady-state value (92-94). This mechanism is the "self-inhibition" and, unlike the "feedback inhibition", has a rapid time constant of ~3 seconds and is temperature-dependent (95). Self-inhibition is also observed upon fast amiloride removal.

3.   ENaC and pathologies

ENaC mutations have been found in patients suffering of salt-dependent symptoms, such as impaired blood pressure, excessive salt-loss, or pulmonary emphysema. Single point mutations are helpful in the understanding of protein function. Mutagenesis studies *in vitro* have brought important progresses in the understanding of protein structure-function relationship.

Several evidence support the fact that the precise salt handling by the kidneys is very important for blood pressure (96). Genetically, animal models, as well as mutations in 18 human genes have been associated either with a salt loss (hypotensive) phenotype or a salt retaining (hypertensive) phenotype. The major key players that determine blood pressure are Na^+ and K^+ transporters in the kidney; NKCC2, NCC, ENaC and ROMK. Actually, they are the targets of the clinically useful diuretics (67). To date, the hypertension (HT) is the most common disease with over 1 billion affected individuals worldwide. It is also a risk factor in cardiovascular diseases including stroke, myocardial infarction, and heart and kidney failure. It has been shown that ENaC gain of function mutations lead to HT, as well as mutations in components of the ENaC regulating pathways, for example in the MR or the 11β-HSD2 (67). Besides human genetics, experiments using rodents have also demonstrated the link between HT and the kidney. For example, a report has shown that transplantation of a HT kidney into a normotensive animal leads to HT, indicating that something in the kidney is responsible for the high blood pressure (97). Moreover, in the early 60's, the introduction of the diuretic thiazide, a blocker of NCC, has been the first effective treatment of HT and is still used (98).

Furthermore, several transgenic mouse models have been developed to study the roles of ENaC *in vivo*. The phenotypes of these mice demonstrate the importance of each α, β, or γ subunit for survival and regulation of Na^+ transport (99). Indeed, the three models of ENaC subunit-deficient mice die within two days after birth; αENaC$^{-/-}$ of pulmonary edema (100), whereas β and γENaC$^{-/-}$ of hyperkalemia (101,102).

The phenotype of β and γENaC$^{-/-}$ mice is similar to that of humans suffering of pseudohypoaldosteronism type 1 (PHA1). This is a monogenic disorder of mineralocorticoid resistance characterized, in the first week of life, by severe dehydration, urine salt-wasting, hyperkalemia, high aldosterone levels, and failure to thrive (103). An autosomal recessive form (AR-PHA1) is caused by loss-of-function mutations in ENaC usually with severe and persisting multiorgan symptoms (104), whereas the autosomal dominant form of PHA1 (AD-PHA1) is due to mutations in the mineralocorticoid receptor causing milder and transient symptoms restricted to the kidney (105).

Another disease is linked to ENaC mutations, but rather than reducing the Na$^+$ reabsorption, it increases it. This is the Liddle's syndrome, an autosomal dominant form of salt-sensitive hypertension with early onset of elevated blood pressure during adolescence. This hypertension is associated with hypokalemia, metabolic alkalosis, low plasma aldosterone and suppressed plasma renin activity (106). Mutations in the PY motif of β and γ subunits have been shown to prevent the interaction of NEDD4-2, the subsequent ubiquitylation and endocytosis of the channels. Consequently, instead of being decreased, the Na$^+$ absorption is maintained (57,107).

4.   Pharmacology

Amiloride, as well as another inhibitor named triamterene, are used as diuretics to treat arterial hypertension, whereas benzamil is reserved for laboratory purposes.
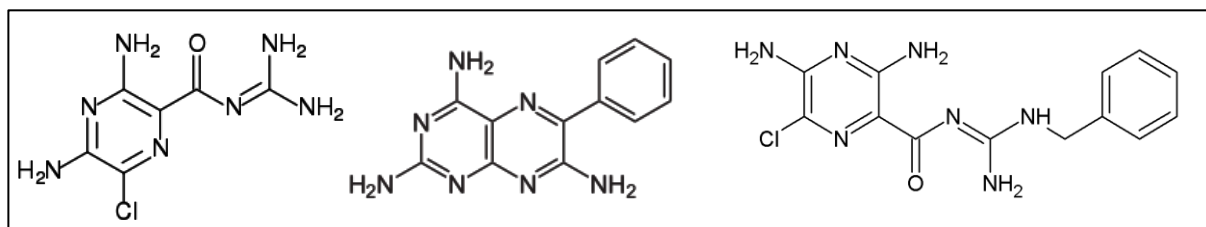
Figure 7 Inhibitors of ENaC. From left to right: the amiloride, the triamterene and the benzamil.

The amiloride has been discovered in the 1960s as a potassium-sparing diuretic able to inhibit the transepithelial Na$^+$ absorption through the frog skin and the toad blatter (108-111). The cloning of ENaC then allowed the target of this compound to be discovered, as well as residues implicated in the block (for details, ENaC physiology).

Actually, it would be interesting to focus on the ENaC-dependent pulmonary edema. Indeed, some PHA1 patients display an excess of airway liquid (112,113). The role of ENaC in the transition from liquid-filled to air-filled lung has been supported by ENaC-deficient mice (100,114). To get round of this ENaC loss-of function, one possibility is to target the deg site which mutation led to an increase open probability or to develop SP-like molecule that would increase the activity of the channel. An activator of ENaC has been identified. This molecule increases the open probability via an interaction with the ECL of β subunit and can reverse the loss-of-function phenotype observed in a PHA1 case (αβG37Sγ) (115). Thus, the activation of ENaC function in PHA1 patients could correct dehydration and salt-wasting, or promote lung function in neonatal respiratory distress syndrome and pulmonary edema by increasing both the Na^+ and lung fluid ENaC-dependent reabsorption (116).

ASIC

As opposed to the epithelial sodium transport mediated by ENaC, the existence of acid-sensing ion channel was unknown until the cloning of the ASIC genes. Based on its sequence homology with DEG and ENaC, ASIC2 (previously known as MDEG for mammalian DEG or BNC1 for Brain Na^+ channel) has been the first ASIC identified from the human brain. It has been initially called Brain Na^+ channel, and then ASIC after the finding that acidification activates it (117,118). Furthermore, ASIC1, ASIC3 (formerly DRASIC), and finally ASIC4 (initially SPASIC for spinal cord) have been cloned (119-121). Finally, the screening of a human genomic library with BLINaC as probe leads to the identification of the human intestine Na^+ channel hINaC, initially called ASIC5 (43). Actually, both hINaC and BLINaC have been classified in another subgroup within the ENaC/Deg family; the BASIC, for bile-acid sensitive channels. Regarding the sequence homology, BASIC are closer to ASIC than ENaC. Whereas they are not sensitive to protons, the bile is able to activate them in *Xenopus laevis* oocytes (122). Later, new members of ASIC subfamily have been identified from the lamprey, the shark, the toadfish and the chicken. It appears that the ASIC from lamprey and shark were insensitive to protons implying that different agonists activate ASIC1 in lower vertebrates (123). In mammals, seven proteins have been identified; ASIC1a, ASIC1b, ASIC2a, ASIC2b, ASIC3, ASIC4 and ASIC5, with 1b and 2b the splicing variants of ASIC1a and 2a.

The size of ASIC proteins ranges from 512 to 563 aa. Between human ASIC channels, the sequence homology varies, the average being 43 %, as depicted on the Table 1 below. The highest homology is found between ASIC1, ASIC2 and ASIC3, whereas ASIC4 and ASIC5 are a little bit less conserved; this might explain their insensitivity to protons differentiating them from the formers.

	ASIC1	ASIC2	ASIC3	ASIC4	ASIC5
ASIC1	100.00				
ASIC2	67.38	100.00			
ASIC3	50.70	51.45	100.00		
ASIC4	49.69	46.38	47.35	100.00	
ASIC5	28.85	30.11	30.41	26.71	100.00

Table 1 Amino acids sequence identity matrix of ASIC channels obtained from basic local alignment of amino acid sequences using Clustal Omega (http://www.ebi.ac.uk/Tools/msa/clustalo/).

The left part of the Figure 8 shows typical traces for ASIC channels; a transient peak current is induced by a switch from pH 7.4 to pH 6.0, and the channel directly desensitizes. The shape of the peak (the time necessary to go from one state to another or the kinetics of activation and inactivation) can vary. Different time constants characterize the kinetics; τ is the time required for the channel to open and τ_D the time necessary for desensitization. Another parameter is τ_{rec} which is the time required between two pH drops to recover the same current amplitude. The activity of ASIC channels can be described as being the transition between three states; (1) the closed (resting) state at alkaline physiological pH (about 7.4), (2) the transient and open conducting state after a fast extracellular pH drop, and (3) the inactivated/desensitized state following an extent acidification of the milieu (Figure 8).
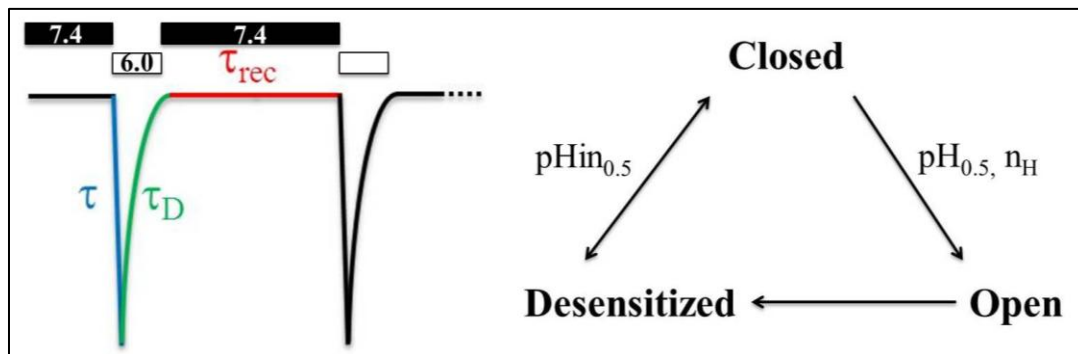
Figure 8 *Left,* scheme of typical ASIC recordings; at pH 7.4 the channel is close, then it opens transiently thanks to a drop of the pH (6.0), and desensitized rapidly. τ represents the time required for activation (blue), τ_D the time necessary for the channel to desensitize (green) and τ_{rec} the time required between two pH drops to recover the same current amplitude (red). *Right,* The three states of ASIC: closed, open and desensitized. The transition between each state is pH dependent. The pH50 determines the pH dependency of the activation whereas the pHin50 the pH dependency of the inactivation (transition from closed to desensitized).

The pH dependences of activation and inactivation also varies between ASIC channels. The $pH_{0.5}$ of activation is the pH that induces half of the maximum current (I_{max}). ASIC1a opens upon a fast extracellular pH decrease from pH 7.4 to below 6.9. The current increases until pH 6.0 and then saturates. The dose-response curve is defined by the Hill equation. The pH dependency of half maximal inactivation is described by the $pH_{in0.5}$, being the pH where one half of the channels are closed (and still able to open) and the others are inactivated/desensitized. It is obtained by switching from variable conditioning pH solutions slightly acidic to pH 4.0. The Hill coefficient (n_H) represents the cooperativity of the ligand binding to its receptor.

ASIC subunits can assemble to form homo- or heteromultimeric channels (124). The biophysical properties of ASIC homomers are in the Table 2. ASIC are permeable to monovalent ions with a P_{Na+}/P_{K+} ratio smaller than the Na^+ permeability of ENaC channels (125). Permeabilities and conductances of ASIC channels are summarized in the Table 2. Its permeability, even low, for Ca^{2+} and H^+ distinguishes ASIC1a from the other ASIC. Physiologically, this entry of Ca^{2+} being small it should not increase a lot the intracellular Ca^{2+} concentration. However, it could induce the calcium release of intracellular Ca^{2+} stores (126). The P_{H+} might acidify locally the intracellular milieu and regulate some channels (118,126). Structurally, the selectivity filter (GAS motif 444-446 in human ASIC1a) is responsible for this ionic specificity (see introduction for details). Strikingly, despite the total conservation of this aa stretch, permeability characteristics can change between ASIC channels. This feature is linked to the N-terminal part of ASIC. Indeed, mutagenesis studies have shown that residues A22, I33 and F34 of ASIC1a (127); I19, F20 and T25 of ASIC2 (128); and T26 of ASIC3 (128), are important for selectivity.

	ASIC1a	ASIC1b	ASIC2a	ASIC3
Selectivity	P_{Na}/P_K 5.5-13	P_{Na}/P_K 14	P_{Na}/P_K 10	P_{Na}/P_K $I_{peak} >= 10$ $I_{sustained}$ 1.62
	P_{Na}/P_{Ca} 5.5-18.5			
	P_{Na}/P_H <0.3-0.8	$P_{Na}>>P_{Ca}$		P_{Na}/P_{Ca} >100
Conductance (gNa)	14.3 pS	ND	10.4-13.4 pS	12.6-15 pS
τ (ms)	5.8-13.7	9.9	ND	<5
$τ_D$ (s)	0.64 ± 0.09	0.89 ± 0.11	1.4 ± 0.2	0.29 ± 0.02
$τ_{rec}$ (s)	5.3-13	4.4-7-7	0.6	0.4-0.6
$pH_{0.5}$	5.8-6.8	6.1-6.2	4.5-4.9	I_{peak} 6.4-6.6 $I_{sustained}$ 3.5
$pH_{0.5in}$	7.2-7.4	7.0	6.0	7-7.1
nH	0.75-4.5	4.8	2.2	1.6

Table 2 Biophysical properties of ASIC channels. The selectivity of ASIC subtypes is indicated by the ratios of P_{Na} over P_K, P_{Ca} or P_H. Conductance of ASIC channels are represented in pS. This table also contains representative range of time constant of activation (τ), inactivation ($τ_D$) and recovery ($τ_{rec}$), and pH_{50}, pH_{in50} and nH values. ND=not determined (129) (130) (131) (118) (132) (133) (126) (134) (135) (124,136-139) (140).

1. ASIC physiology

In the central nervous system, ASIC1a and 2a are widely expressed in brain areas such as the hippocampus, cingulate cortex, striatum, amygdala, cerebellar cortex and olfactory bulb. ASIC2a is found predominantly in dendrites, dendritic spines and synaptosomes (141,142). The synaptic vesicles being acidic, the release of neurotransmitters into the synaptic cleft goes along with an acidification that could potentially activate acid-sensing ion channels expressed in the postsynaptic buttons (143,144).

Studies on ASIC1a$^{-/-}$ mice have demonstrated that ASIC1a was required for long-term potentiation and acid-induced inward currents, associated with learning and memory related phenotypes or with pain transmission and processing phenotypes. Both of these features were decreased in the ASIC1a knockout model, as well as the acid-evoked Ca^{2+} entry at dendritic spines and the dendritic spines number in hippocampal slices (145,146). However, another recent report suggests that ASIC1a was not necessary for normal long term potentiation and spatial memory (147). ASIC1a$^{-/-}$ mice also present a fear conditioning deficit as supported by a slower freezing response to fear conditioning stimuli (142).

The reduction of blood flow that accompanies ischemia provokes hypoxia. This deprivation of oxygen increases anaerobic metabolism leading to the accumulation of lactic acid. Both the ATP

hydrolysis and the increase amount of lactate induce a strong pH decrease to 6.0 (148-150). It is known that the tissue acidosis resulting from ischemic stroke induces neuronal injury in the brain. The precise mechanism is unclear, but several possibilities exist; the Ca^{2+} toxicity being essential for ischemic neuronal injury, an overload induced by GluR was an explanation (151,152). However, GluR antagonists having failed to protect the brain, this hypothesis has been ruled out (153). The second theory is based on the H^+-induced Ca^{2+} release induced by ASIC1a. This increase of intracellular Ca^{2+} would also provoke neuronal injury (152,154,155). The pharmacological block of ASIC1a with psalmotoxin, as well as the ASIC1$^{-/-}$ mouse model, supports the fact that ASIC1a is a neuroprotective therapeutic target for brain ischemia (126,152,156).

A decrease in the pH also occurs during seizure, intensive neuronal excitation and at the end of an epileptic activity (157-159). Thus, the role of ASIC1a has been investigated during these events. It results that knockout mouse model have a more pronounced seizure, whereas the ASIC1a overexpression decreases it. Moreover, the activation of ASIC1a in inhibitory interneurons eases the epileptic activity (160). In these situations, ASIC1a agonists would be used to improve seizure.

The ASIC1a contribution to axonal degeneration in multiple sclerosis is also known. In this autoimmune inflammatory disease lesions are accompanied by tissue acidosis. Again, the increase Ca^{2+} is the responsible and leads to axonal degeneration. The use of the non-specific blocker amiloride gave promising neuroprotective results (161).

At sensory neuron terminals, H^+ and other chemicals are thought to activate ASIC channels. Two studies on ASIC2$^{-/-}$ mouse model support the role of ASIC2 in mechanosensation. Firstly, the expression of ASIC2 has been shown adjacently to the hair follicule. While the hair movements excite mechanoreceptors in rodent skin, they tested the response of ASIC2$^{-/-}$ mice to mechanical touch stimuli. They observed a decrease in their sensitivity suggesting a role in mechanosensation (162). Another study has figured out that ASIC2 was an important determinant of the arterial baroreceptor reflex. Usually, baroreceptor reflex causes a decrease in heart rate when there is an increase in blood pressure, and *vice versa*. Lu *et al*. first localized ASIC2 in aortic baroreceptor neurons in the nodose ganglia, and then demonstrated that ASIC2$^{-/-}$ mice suffered of hypertension and an impaired baroreceptor reflex (163).

Studies on ASIC3 have shown its expression in sensory neurons, in particular in nerve endings where mechanical stimuli are converted into electrical signals (121,164). Moreover, ASIC3 is co-expressed with the calcitonin gene related peptide, an important vasodilator peptide involved in pressure-induced vasodilatation (PIV). Thus, Fromy *et al.* decided to investigate the role of ASIC3 in PIV. Using ASIC3$^{-/-}$ mouse model and pharmacological block of ASIC3 (APETx2, see ASIC pharmacology) they have demonstrated that the deletion of ASIC3 leads to an absence of PIV directly linked to a failure of pressure detection. Then, they have carried on experiments with stronger and longer pressure. This led to ischemia associated with H$^+$ and lactate production that can activate ASIC3 and is necessary for reactive hyperemia after compression. They concluded that ASIC3 was benefic for the microcirculation and protects against pressure ulcers (165). Taken together, these results demonstrate a role of ASIC2 and 3 in mechanosensation. However, unlike pH, mechanical stimulation has not been shown to directly gate ASIC, as it does for mechanosensitive channels (166), thus there are still debates on the role of ASIC in mechanosensation.

During inflammation, ischemic stroke, infections and cancer, there is a tissue acidosis. In such conditions, pH levels can drop near 6 or even lower (167,168). When a tissue is injured, it releases mediators of inflammation; substance P, bradykinin, histamin, serotonin, glutamate, ATP, interleukin-1, nerve growth factor and H$^+$ (169).

To assess the roles of ASIC in pain, several pharmacological studies have been performed. Use of peripheral injections of APETx2 revealed the involvement of ASIC3 in the maintenance of primary hyperalgesia (170). Moreover, the role of ASIC1b-containing channels has been demonstrated by injection of mambalgins, which induces analgesic effects on acute heat pain and inflammatory heat hyperalgesia (171). Recently, Bohlen et al. highlighted the involvement of ASIC1 in pain using MiTx injection (172). Moreover, PcTx1 injections (intrathecal and intracerebro-ventricular) have demonstrated the role of ASIC1a in the pain pathway. Indeed, PcTx1 led to a potent analgesic effect in several models of acute and chronic pain (173,174). Knockout mice models additionally delivered new insights into the role of ASIC1a in brain function. Formerly, those animals presented an impaired hippocampal long-term potentiation and defects in spatial learning and memory (145). Actually, however, those data are no longer supported (147) except for the role of ASIC1a in hippocampus through the detection of ASIC1a and 2a hippocampal neurons and postsynaptic membranes of the dendritic tree and

spines (145,146,175-178). Finally, the use of ASIC1a blockers has also demonstrated the implication of ASIC1a in Huntington's and Parkinson's diseases (179,180).

Taken together, these studies show the importance of developing highly specific and potent blockers against ASIC1a. Several modulators of ASIC are known and would be described in the next chapter.

2. ASIC pharmacology

Several endogenous factors are known to modulate ASIC channels. In the class of neuropeptides, dynorphins, opioid peptides involved in analgesia, have been shown to limit the steady-state desensitization of ASIC1a (133). Normally, steady-state desensitization occurs when incremental pH reductions are applied, the channel then desensitizes and activation is prevented (181). In a dose-dependent manner, dynorphin A and big dynorphin (EC$_{50}$ of 32.8±11.5 μM and 26.4±14.8 nM, respectively) inhibit the ASIC1a steady-state desensitization. Indeed, without dynorphin, a conditioning pH7.0-solution leads to the desensitization of the channel, which is represented by the absence of a pH5.0-induced current. This process is prevented by dynorphins [140]. The steady-state desensitization of ASIC2-containing heteromeric channels is influenced by big dynorphin in a similar manner. Indeed, conditioning pH of 7.1 and 6.8, usually prevent the opening of ASIC1a/2b and 1a/2a at pH 4.5. However, this is disrupted in presence of big dynorphin with EC$_{50}$ of 3.5±1.6 nM and 256.5±76.2 nM, respectively (182). Such slight pH decrease occurs during pathophysiological conditions within the acidosis extends over several minutes, i.e. ischemia. Dynorphin level being increased under pathological conditions (183), it is possible that it enhances neuronal damage following ischemia by preventing the steady-state desensitization of ASIC channels.

FMRFamide is a peptide found in invertebrate nervous system and is able to gate FaNaC channels at mM concentrations (3). This tetrapeptide also acts on ASIC channels by potentiating H^{+}-evoked currents and altering inactivation, thus leading to a sustained current in most cases. However, the FMRFamide has not been isolated from mammals. Endogenous mammalian RFamide peptides, such as the neuropeptide FF "NPFF", exist and modulate ASIC but are not as potent. Indeed, whereas 50 μM FMRFamide induces a sustained current in ASIC1a, 50 μM NPFF only slightly delays its inactivation (129). Regarding ASIC3, both neuropeptide create a

sustained current and postpone the inactivation. However, the kinetics of the peak current are different with a τ_D shortened in presence of NPFF and extended with FMRFamide (129,184). Belonging to the polyamines, the arginine metabolite agmatine, as well as its analog arcaine, has been demonstrated to activate ASIC3 and ASIC3/1b channel, *via* an extracellular non-proton ligand-sensing domain (185). In addition, spermine (0.25 mM) has been shown to induce a two-fold increase ASIC1a and ASIC1b mediated currents through a 0.2 pH units shift of their steady-state inactivation curves towards more acidic values (186). Furthermore, various cations can inhibit ASIC channels, among them, the Cd^{2+}. A 1 mM of Cd^{2+} decreases roughly half of the current or rASIC2a and rASIC3, but has no effect on rASIC1a activity (187). The hASIC1a is inhibited by Cd^{2+} with an IC_{50} of 0.37 ± 0.01 mM (127). Another divalent, the Ca^{2+}, is known to modify the affinity for H^+; a high Ca^{2+} concentration is reducing the affinity and *vice versa* (181). Extracellular Ca^{2+} has a dual action on ASIC1a; Currents are very small in presence of low $[Ca^{2+}]_o$, then they increase with augmented $[Ca^{2+}]_o$, and finally are reduced with higher $[Ca^{2+}]_o$. Moreover, depletion of Ca^{2+} leads to an absence of ASIC1a current. Concerning ASIC2a, we observe an opposite relation; the currents being decreased with increasing $[Ca^{2+}]_o$ (138). A study on ASIC3 argues that H^+ and Ca^{2+} compete at a binding site with H^+ catalyzing the release of Ca^{2+} from that site (188). However, disruption of two Ca^{2+} (and H^+) binding sites on ASIC1a by mutation of the negatively charged aa Glu425 and Asp432 relieves the Ca^{2+} block, without constitutively opening the channel suggesting the existence of another Ca^{2+}/H^+ binding site (189).

Inflammatory mediators also modulate the activity of ASIC. The arachidonic acid (ASIC1a and ASIC3), the lactate (ASIC1a and ASIC3), the nitric oxide (ASIC1-3), the ATP (ASIC3) or the serotonin (ASIC3), are able to increase pH-induced currents (150,190-193). As for synthetic molecules, the inhibitory activity of Nonsteroid Anti-Inflammatory Drugs (NSAID), such as ibuprofen, aspirin or salicylic acid, influences ASIC. Indeed, the application of NSAID prevents the increase mRNA content of ASIC-expressed sensory neurons. Moreover, they directly inhibit ASIC currents (194). The diuretic amiloride and its derivatives are also known to reduce the currents in ASIC subtypes, whereas ASIC1a is inhibited with an IC_{50} of 14.6 µM, ASIC2a is almost insensitive (IC_{50} 72.5 µM), ASIC1a/2a represents an intermediate with 36.2 µM reducing half of the maximal current (138). On ASIC3, the sustained current is unaffected whereas the peak current is inhibited with an IC_{50} of 36.9 µM (195). The blocker behaves as a plug binding

the middle of the TM2. Residues involved in the block are the G440 in the human ASIC1a (Appendix 5, Figure 49 and (48)) and the G437 in the human ASIC2 (47).

The first ASIC blocker being more potent and specific than amiloride is the compound A-317567. ASIC currents are inhibited with IC_{50} of 2.0, 29.1 and 9.5 µM in ASIC1- ASIC2- and ASIC3-like neurons from adult rat DRG (196). The synthetic compound 2-guanidine-4-methylquinazoline (GMQ) shifts pH activation of ASIC3 towards alkaline values. This leads to the opening of the channel independently of H^+ at pH 7.4 (197). Diverse effects were observed for ASIC1a and 1b with an opposite shift of the pH activation curves towards more acidic pH (48). In both cases, however, the steady state inactivation is shifted towards acidic values, meaning that the channel inactivation becomes less favorable in term of energy and that the recovery is easier. Nafamostat mesilate (NM) has also been tested on ASIC channels thanks to its side effect (inhibition of ENaC) in the treatment of pancreatitis (198). For ASIC1a and 3, this amidine-guanidine compound seems more potent than amiloride, whereas for ASIC2a it appears to be less potent; IC_{50} are 13.5, 70.6 and 2.5 µM for ASIC1a, ASIC2a and ASIC3 (195).

There are presently no pharmacological blockers for ASIC channels displaying high potency, but natural molecules extracted from venoms specifically modulate ASIC channels. The peptide Psalmotoxin 1 (PcTx1) in the venom of tarantula *(Psalmopoeus cambridgei)* selectively inhibits the human ASIC1a channels with an IC_{50} of 13 nM, whereas a higher concentration potentiates it (EC_{50} 60 nM) (199,200). Human ASIC1b and chicken ASIC1 currents are enhanced by the toxin (EC_{50} of 100 and 189 nM, respectively) (201,202). This toxin acts by a binding to the extracellular loop at the Cysteine-Rich Domains I/II (201,203). This inhibition is Ca^{2+}-dependent, meaning that an increase of Ca^{2+} leads to a decrease of the PcTX1 inhibition (186). Three other toxins extracted from black mamba venom, mambalgins (1 to 3), inhibit currents mediated by hASIC1a (IC_{50} 127 nM), rASIC1a (IC_{50} 11-55 nM) and rASIC1b homomers (IC_{50} 44-192 nM), hASIC1a/2a (IC_{50} 220 nM), rASIC1a/2a (IC_{50} 25-252 nM), rASIC1a/2b (IC_{50} 61 nM) and rASIC1a/1b (IC_{50} 72 nM) heteromers (171). Mambalgins inhibit all the ASIC-channels combinations in the CNS, compared to PcTx1 that inhibits 30 % of these currents. Moreover, they inhibit 60 % of ASIC currents in sensory neurons, while PcTx1 about 40 % (171). Only ASIC3 and ASIC3-containing channels are not targeted by mambalgins. However, the peptide APETx2, isolated from sea anemone *Anthopleura elegantissima,* inhibits them (IC_{50} 37-63 nM for ASIC3, and 2 µM, 900 nM and 117 nM for ASIC1a/3, 1b/3 and 2b/3, respectively) (204-206).

23

Studies have also shown the inhibitory activity of APETx2 on $Nav_{1.2}$, and $Nav_{1.8}$ channels (IC_{50} 114 nM and 55 nM to 19 µM), and to $Nav_{1.6}$ (1 µM, 17 % inhibition) (207,208). Extracted from the venom of Texas coral snake *Micrurus tenertener*, MitTx is a heteromeric complex functioning as a potent, persistent and selective agonist of ASIC, in particular rat ASIC1a and ASIC1b (EC_{50} 9 and 23 nM, respectively) channels, and more slightly on rat ASIC3 (EC_{50} of 830 nM). Moreover, MitTx does not activate ASIC2a, but strongly potentiates the currents, *in vitro,* by shifting the activation curve towards less acidic pH (172).

These toxins are a precious tool in the investigations of physiological and pathophysiological ASIC roles *in vivo* especially in pain. Indeed, CNS injections (intrathecal and intracerebroventricular) of both PcTx1 and mambalgins in mice induce an analgesic effect in acute and inflammatory pain. Furthermore, PcTx1 effects are sensitive to naloxone, whereas mambalgins are not. This suggests that ASIC are involved in two different pathways linked to pain transmission and/or modulation (171,173,209). Peripheral injections of APETx2, MitTx and mambalgins also highlight the role of ASIC in pain and sensory perception. It has been shown that the application of APETx2 reduces the mechanical hypersensitivity in a mouse model of joint inflammation, as well as in a rat model of cutaneous inflammatory pain (210,211). Then, continuous intra-articular APETx2 injection has demonstrated a reduction in pain-related behavior and secondary mechanical hyperalgesia in a rat model of ostheoarthritis (212). Subcutaneous injections of mambalgins in the mice hindpaw also provide pain relief, as demonstrated by the resulting analgesic effect on acute heat pain and inflammatory heat hyperalgesia (171). Moreover, peripheral injection of MitTx elicits pain behavior through ASIC1. Indeed, ASIC1$^{-/-}$ mice spent less time to lick compared to the wt after toxin administration (172).

Beside their roles in pain, neuroprotective effects of PcTx1 have been shown in various studies, to mention but a few; in ischemia, using mouse cultured hippocampal neurons deprivated in oxygen and glucose, as well as in extracellular acidosis, using spinal motoneurones (154,213). Furthermore, central injection of PcTx1 (or venom) demonstrates a reduction of fear, as well as antidepressant and anxiolytic-like effects. Both fear and depression have been linked to ASIC1a channels (in ASIC1a$^{-/-}$ animal studies), thus their inhibitions are directly responsible of the improvement (142,145,214,215). Anxiolytic-like effects have also been observed after PcTx1 venom injection, however the mechanism is still unknown (216).

3.   Structure and function relationship

ENaC

The membrane topology of ENaC has been determined by investigating the glycosylation of putative glycosylation sites on ENaC. Site-directed mutagenesis has shown that the putative residues at both N- and C-termini were not glycosylated. This supports the fact that both N- and C-termini are located intracellularly, whereas the large domain between the termini is extracellular. Moreover, the use of the truncated αENaC fused with the Na^+-K^+-ATPase β-subunit (known to be glycosylated) has demonstrated that both transmembrane domains were signals for start- and stop-transfer, respectively (217,218).

Regarding the ENaC stoichiometry, Snyder and colleagues have assessed it taking the advantage of α, β and γ subunits containing mutations that alter channel inhibition by methanethiosulfonate reagents. The use of different ratios of γwt versus γG536C (γ*) mutant which are, respectively, insensitive and sensitive to MTSET, has permitted to conclude that there should be three γ subunits. As a second independent test, the MTSEA has been used. MTSEA inhibited αβγENaC, and the mutation of the deg site into cysteine disrupted the inhibitory effect (αS549C, βS520C and γS529C). The comparison of channel properties of wt and ratios of single mutant, allows concluding, as for the experiments with MTSET that ENaC is made of three γ subunits, as well as three α and three β, leading to a nine-subunits stoichiometry. To further investigate this arrangement, a sucrose gradient analysis has been used. It confirmed their previous results (219). The sucrose gradient sediment technique has also been chosen by Cheng and Dijkink, as well as Coscoy to assess ENaC and FaNaC stoichiometries. The former study confirmed the nine-subunits oligomerization of Snyder *et al.*, whereas the latter report did not. Indeed, the report of Dijkink and colleagues has demonstrated the tetrameric arrangement of ENaC (220). Similarly, the study of Coscoy and collaborators has concluded that FaNaC molecular weight corresponds to a tetramer and confirmed it with SDS-PAGE analyzing of crosslinked channels. For that purpose, the bifunctional crosslinkers NHS-ASA (5.7 Å) and SADP (13.9 Å) harboring a photo- and a primary amino-reactive group, or the DSS (11.4 Å) interacting with two amine groups have been used (221). A study taking advantage of a quantitative analysis of cell surface expressed ENaC has investigated the channel oligomerization. The authors have worked with Flag-tagged subunits (F) recognized by an

iodinated monoclonal antibody. The binding signal has then been correlated with the measured amiloride-sensitive current. The comparison of each tagged subunit co-expressed with increasing concentrations of the untagged subunits ($\alpha^F\beta\gamma$, $\alpha\beta^F\gamma$, $\alpha\beta\gamma^F$) led to the observation that the relative abundance of ENaC subunits followed the order $\alpha > \beta > \gamma$ suggesting that the channel is made of more than three subunits, α being the most abundant. Moreover, looking at concatemers of mutants altering the sensitivity to Zn^{2+} (αS583C) or amiloride (αS583C, βG525C and γG537C) supported a tetramer with an $\alpha\beta\alpha\gamma$ organization (222). Another report on the same ENaC mutants has assessed the composition of the channel by testing its sensitivity to either MTSEA or amiloride. Kosari *et al.* have concluded that ENaC was made of four subunits, consistent with the results of Firsov *et al.* (223). Another study has investigated the composition of ENaC channel with the freeze-fracture electron microscopy. This technique examines cross-sectional area of ENaC in the plasma membrane and permits to estimate the number of transmembrane α-helices. This has suggested the presence of an integral membrane protein complex made of eight or nine subunits (224). Given that the stoichiometry remained uncertain with electrophysiology and biochemical experiments, Staruschenko and colleagues have taken the advantage of an independent biophysical approach; the fluorescence resonance energy transfer FRET. This mechanism describes the energy transfer between two chromophores. A donor initially in its electronic excited state (cyan fluorescent protein CFP), may transfer energy to an acceptor (YFP), if they are close enough (50 % efficiency with a distance of 35 Å (225)). In three independent experiments (eCFP_αeYFP-$\alpha\beta\gamma$) or (αeCFP_βeYFP_$\beta\gamma$) or ($\alpha\beta$eCFP_γeYFP_γ) have been expressed. These experiments supported that ENaC was a nonamer made of $\alpha_3\beta_3\gamma_3$ (226). Anantharam and Palmer have looked at individual mutations lining the pore and altering the single-channel conductance of ENaC. Wt subunits have been co-expressed with equimolar amount of either a αS589D (or αS592T), βG529A, or γG534E mutant and the channels conductance has been measured. $\alpha\alpha$S592D$\beta\gamma$ channels (0.5:0.5;1;1) presented an additional intermediate conductance different from the small wt and the large mutant conductances (4.2±0.2 and 7.2±0.2, respectively). This suggested that a channel made of $\alpha\alpha$S592D$\beta\gamma$ exist. Neither $\alpha\beta\beta$G529Aγ, nor $\alpha\beta\gamma\gamma$G534E displayed this supplementary conductance. Thus, this report arrived to the conclusion that ENaC is made of $\alpha_2\beta\gamma$ (227). Later, two studies have investigated again the structure of ENaC. As Cl$^-$ ions of unknown function are present on the ASIC crystal

26

structure (coordination via Arg310, Glu314 and Lys212 (228)), Collier *et al.* have decided to work on the equivalent Cl$^-$ binding sites on ENaC. Based on their sequence, homologous residues have been identified; αMet321, βAsn288 and γMet299. Whereas β and γ mutants decreased the inhibitory effect of Cl$^-$, α did not lead to any significant difference compared to the wt. Cl$^-$ being coordinated by more than one residue, the pairing of palm and thumb domains according to either an αβγ or an αγβ orientation has been examined. βAsn288 paired with αHis418 on a αγβ model, whereas it paired with γHis396 on αβγ. Given that only βAsn288-αHis418 had an effect on Cl$^-$ inhibition, the αγβ model is supported. Reduction of the Cl$^-$ inhibitory effect of γMet299-βArg388 further confirmed this model (229). Stewart *et al.* have then developed a method based on AFM imaging in order to determine the stoichiometry and arrangement of ENaC. To start, each subunit has been tagged; αV5 or FLAG, βV5 or His$_6$ and γV5. Then, αFLAGβHis$_6$γV5 has been purified *via* the FLAG tag and used for AFM. The use of anti-His$_6$ antibodies and anti-V5 Fab fragments has allowed the subunit differentiation and the calculation of angles. Altogether, these results supported a trimeric organization (230).

These studies have been made on ENaC, mainly because this channel is made of three distinct subunits. Indeed α, β and γ can be distinguished from the others through individual mutations. These mutations modify the channel affinity for inhibitors (amiloride, Cd^{2+}) or MTS reagents. Experiments that correlate the channel function to the structure are more relevant. Indeed, if we focus only on a structural analysis of the channel subunit composition, how to be sure that our results are relevant for the functional channel. From my point of view, electrophysiological experiments analyzing the effect of α, β or γ mutations on the single channel conductance and on their affinity for ligands are of primary interest (219,222,223,227). However, these reports do not support the same ENaC stoichiometry and lead the question about the number of subunits that compose ENaC/Deg channels still open.

ASIC

Gao *et al.*, working with heteromers made of ASIC1a and ASIC2b, took advantage of the inability of ASIC2b to form homomeric channels. Similarly to Staruschenko *et al.*, they have created distinct constructs and co-expressed them. Each condition led to a positive FRET signal, in details; (2a+1a_CFP+1a_YFP) and (1a+2a_CFP+2a_YFP) have a FRET efficiency of 34 and 22 %, indicating that channels are made of at least two ASIC1a and two ASIC2a. Furthermore,

(1a_CFP+1a_YFP+2b) 44 %, (1a+2b_CFP+2b_YFP) 39 %, (2a_CFP+2a_YFP+2b) 21 % and (2a+2b_CFP+2b_YFP) 31% mean that in heteromeric channels, there are at least two copies of the different subunit types, thus at least four subunits form an ASIC channel (231). Subsequent studies addressing ASIC oligomerization have concluded to a trimeric organization, in agreement with the crystal structure. Carnally and colleagues have developed a method based on atomic force microscopy (AFM) imaging, in order to directly determine the arrangement of subunits. The distribution of measured molecular volumes has allowed them to find ASIC1a stoichiometry (232). A crosslinking approach has highlighted the importance of the four C-terminal cysteines (C464, C469, C495 and C526) of mASIC1a. Using H_2O_2 as oxidizing agent, they have pointed out that these four cysteines were involved in the stabilization of high molecular weight complexes *via* intersubunit disulfide bonds on SDS-PAGE and western blots. The presence of high molecular weight complexes has been confirmed by crosslinking experiments with sulfo-EGS and sulfo-DSP, two amino-reactive crosslinkers of 12 Å. Authors have observed four bands on their blots referring to them as ASIC1 monomer, two disulfide-linked ASIC1a subunits, trimer and higher ASIC1a disulfide-linked subunits. They concluded that ASIC1a was present under a trimeric organization, arguing that higher complexes were either, an inter-trimer complex or, ASIC1a crosslinked with another protein (233).

Crystal structures

To date, four X-ray crystal structures of ASIC have been published. The first one has been obtained from the chicken ASIC1 overexpressed in Sf9 cells with deletion in the N- and C-termini (26 to 463 amino acids instead of 527) (228). This led to a non-functional channel. Biochemical experiments combining glutaraldehyde crosslinking with SDS-PAGE gel and Light Scattering analyses revealed a channel molecular weight of 165 kDa, consistent with a trimeric stoichiometry. Looking into details, this 1.9 Å resolution structure gave a nice depiction of the ECL. The figure 9 shows the ECL domains rearrangement that resembles an upright forearm and clenched hand. Within the hand, the main piece is the palm made of seven-strand sheet that connect directly the extracellular part to both transmembrane domains. Above the palm stands the knuckle domain and close-by the finger. The tip of the finger is in contact with the thumb domain rich in disulfide-bonds. The palm, the finger and the thumb encircle the 5-strand-β-ball domain. This hand is rich in conserved cysteines involved in disulfide bridges ("CRD" discussed in the chapter about the ENaC/Degenerin family). Likely, the integrity provided by these bonds

28

facilitates the transmission of conformational changes to the transmembrane domains leading to the pore opening. In the extracellular region resides the putative H^+ binding site, which is not clearly established yet. The Cl^- also has a binding site there; however its physiological relevance remains unknown.
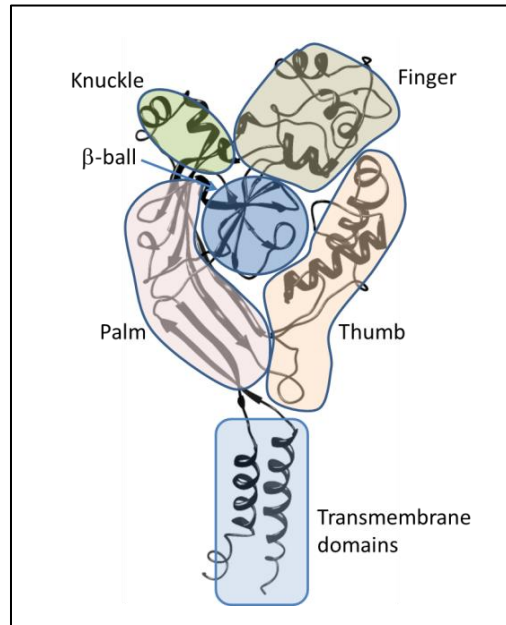
Figure 9 Overview of a cASIC1 subunit. It looks like a hand holding a ball (β-ball domain) with the palm, the knuckle, the finger and the thumb highlighted in light pink, green, orange and brown, respectively.

Another crystal structure has been obtained by overexpressing a C-terminus truncated cASIC1 into Sf9 cells. Actually, this protein is longer (N terminus included and C terminus stopped at residue 466) and led to a functional channel in CHO cells while the function has not been assessed in Sf9 cells (234). This crystallization provides a clear picture of the role of the TM2 as a pore lining structure. The orientation of the TM2 with respect to the ion permeation pathway is consistent with previous functional studies. For instance, both the degenerin (G432 and αS576) and the amiloride (G439 and αS583) binding sites have been described as being accessible for MTS reagents, Zn^{2+}, and the pore blocker amiloride (41,222,223,235,236), whereas the residue αS589 of the ion selectivity filter is not accessible for MTSEA (Figure 10) (53,54). In addition, the side chain of αS589 has been proposed to point towards the subunit-subunit interface (237). These accessibility studies have been made using the substituted-cysteine accessibility method (SCAM). Residues are first mutated into cysteine and their accessibility then tested using thiol reactive reagents such as the Cd^{2+} or methanethiosulfonate reagents (MTSEA or MTSET).
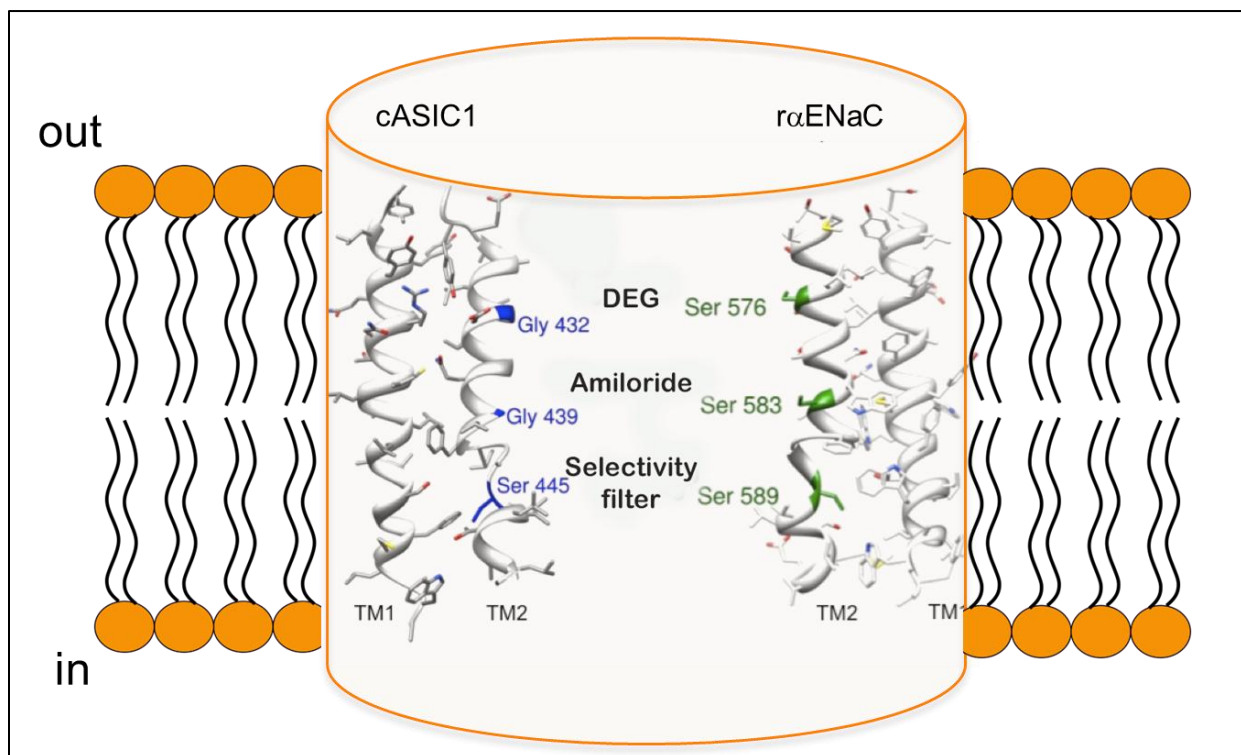
Figure 10 Comparison of the cASIC1 (pdb 3HGC) and the αENaC TM2. The cylinder depicts the TM domains of a channel with the pore in its middle surrounded by TM segments of the cASIC1 on the left (blue residues) and of the rαENaC on the right (green residues). The side chains of the degenerin site (DEG, cGly432 and αSer 576), the amiloride binding site (cGly439, αSer583) and the selectivity filter (cSer445, αSer589).

Despite the good correlation between the TM domains of this second crystal structure and the functional studies, there is still a problem. Indeed, due to a crossing of the TM2, this structure does not allow the flow of Na^+ ions through the pore, nor the binding of the amiloride. More generally, the available ASIC crystal structures do not identify a clear ion permeation pathway for permeant cations.

The surface of the ASIC1 structure based on the electrostatic potential (Figure 11) shows that the only access to the pore is across the lateral fenestrations, and no continuous pathway is possible through the extracellular loop.
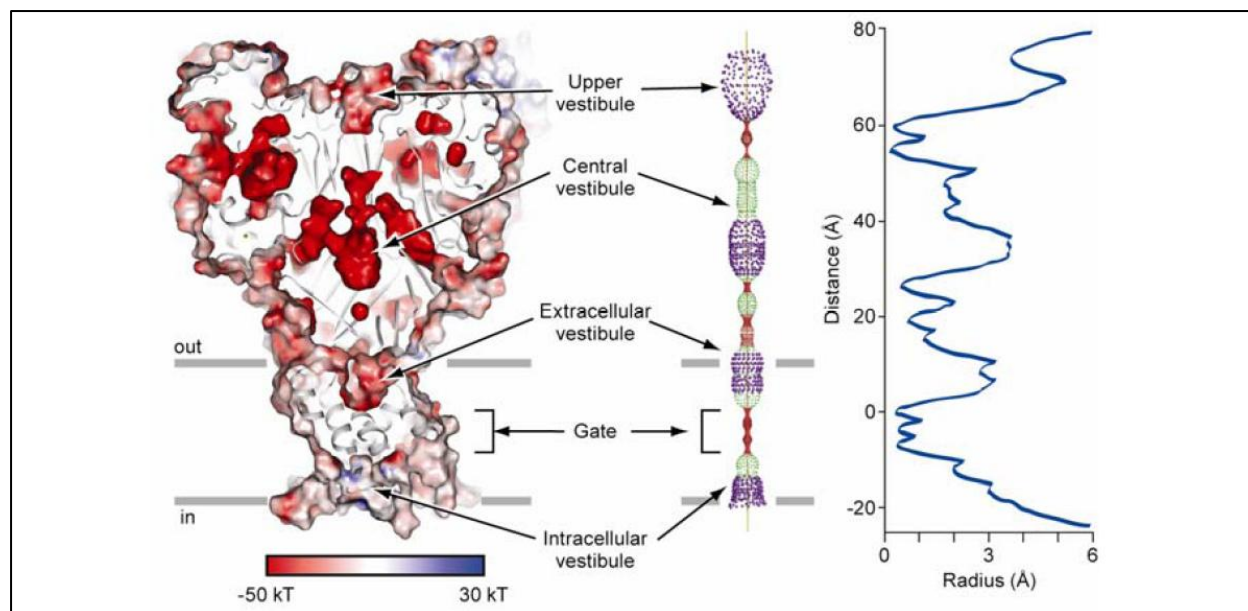
Figure 11 *Left,* Vestibules and possible ion permeation pathways. An electrostatic potential surface and cartoon representation of the mfc cASIC1 cutted along the 3-fold axis of symmetry. Colors from red to blue depict the electrostatic potential from −50 kT to +30 kT. White is 0 kT. *Right,* Radius of the putative permeation pathways along the 3-fold axis. This was generated with HOLE, a program allowing the analysis and the visualization of the pore dimensions (red < 1.4 Å < green < 2.3 Å < purple). Figure taken from Gonzales *et al.*, 2009 (234).

These two structures of ASIC1 show an ion channel non-conducting for permeant ions (228,234). Two interpretations can be formulated; the first proposed by the authors is that the crystal has been made at an acidic pH of 6.5 and represents a desensitized channel. According to them, ions might reach the extracellular vestibule through lateral fenestrations. The second proposed that since the protein was crystallized from Sf9 cells in which the function was not assessed, it is possible that this structure does not correspond to the functional channel. The lipid composition of insect cells is different from mammalian cell lines (lower cholesterol to phospholipid ratio) and can account for a less active or even an inactive membrane protein (238,239).

More recently the complex made of psalmotoxin and cASIC1 has been crystallized (201,203). The idea behind the use of PcTx1 was to stabilize the open state of the channel. Indeed, contrary to human or rat ASIC1a, cASIC1 is activated by PcTx1 (240). The toxin potentiates the cASIC1 (EC_{50} 189 nM) (202) and leads to the partial desensitization of the channel (201). Both articles confirm a previous functional study highlighting the binding of the toxin to the acidic pocket of ASIC1. As shown on the schematic view below, PcTx1 binds the interface between two subunits, namely the H^+-sensitive pocket (241).

31
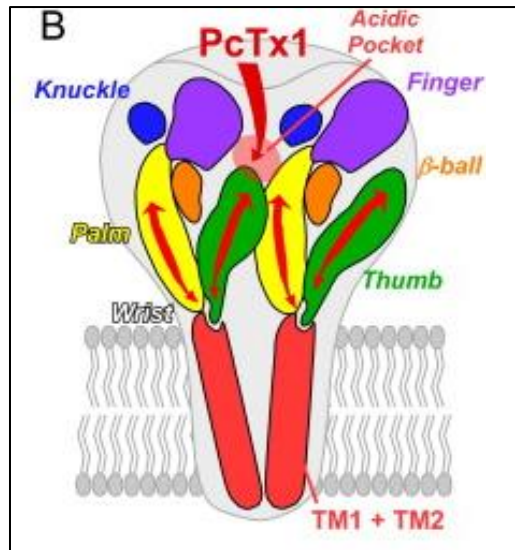
Figure 12 Schematic representations of two ASIC subunits. Red arrows indicate the domains proposed to be involved in channel gating by coupling the extracellular domain with the TM1 and TM2, the acidic pocket is depicted with the red circle, palm in yellow and thumb in green. Figure from Baron *et al.*, 2013 (242).

In the first paper published by Dawson *et al.*, a 3.0 Å resolution crystal structure at pH 5.5 has been obtained. Given that the study is based on the truncated construct (26-463) used in 2007 for the first crystallization, this led to disturbed transmembrane domains making difficult the decision of whatever the pore in an open or closed conformation was. However, this study allowed the characterization of the PcTx1-binding site and its molecular interaction with the channel. Three PcTx1 molecules were bound per trimeric channel in the H^+-sensitive pocket. This pocket is between the thumb and the palm domains of the adjacent subunit (Figure 12).

In the second report, Baconguis and Gouaux have used a longer and functional construct (14-463). Crystals of the PcTx1-cASIC1 complex have been obtained at two different pH. At pH 7.25 with a 3.3 Å resolution, the channel presents a large pore (10 Å) lined by TM2 and TM1 residues and not selective for Na^+. At pH 5.5, the structure (2.8 Å) displayed a 3.2 to 5.2 Å pore, large enough to selectively accommodate a hydrated Na^+ ion. The toxin binding site is identical in the two studies with a few discrepancies concerning the molecular interactions.

To date, none of the crystals displays trapped Na^+ ions in the putative permeation pathway neither in the desensitized, closed nor open conformation. This would be the evidence of an open and conducting channel state. Nevertheless, Baconguis and Gouaux found that the toxin prevented the complete desensitization of the channel leading to a small steady-state current at both pH 5.5 and 7.25 with some channels being open, while other are closed. In the present study,

both crystals are in an open conformation, pH 7.25 being unselective, whereas pH 5.5 specifically conducts Na^+ with a P_{Na+}/P_{K+} of ~10. Strikingly, this Na^+ selective pore is asymmetric and exposes one of its TM1 to the lumen as depicted on the mapping of the solvent accessible pathway of figure 13.
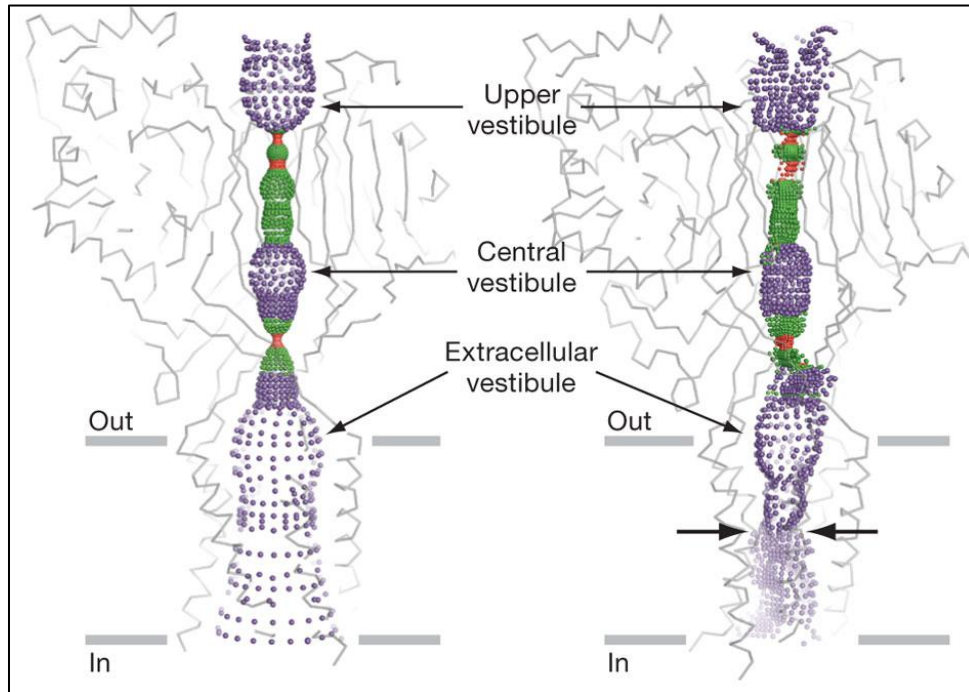
Figure 13 Mapping of solvent-accessible pathway along the three-fold axis. *Left,* High-pH structure (7.25) with a large pore. *Right,* Low-pH structure (5.5) with the opposite arrows depicting the constriction. Maps were generated using the HOLE software (243) (red < 1.4 Å < green < 2.3 Å < purple) Figure from Baconguis *et al.*, 2012 (201).

Regarding the ECL, movements are the same between the desensitized structure and both pH 7.25 and 5.5 crystals. There is an enlargement of the ECV with Val75 going from 7 Å to 11 and 12 Å in the selective and unselective states. The distance between Asn357 (thumb) and Arg85 (palm) also increases from 8 to 11 Å, as well as the peptide bond separating Thr84 and Arg85 flips by ~180°. Motions have also been observed in the β11-12 linker near to β1-2, confirming the crucial role of these linkers for desensitization (244,245).

In conclusion, stoichiometric studies (crosslinking, AFM and FRET) support a channel made of three or four subunits and all of the four crystal structures highlight a trimeric organization of ASIC1. However there are still open questions regarding these structures: what is the access pathway taken by the ion to cross the ASIC1 channel (central axis or lateral

fenestrations)? Why are they no permeant ion trapped in the open pore? Do these structures reflect the functional ASIC1 channel?

To answer these questions, it would be necessary to combine functional and structural investigations. Thus, we have decided to study the structure-function relationship of ASIC1a channels. Two parts compose this project: the stoichiometric analysis of the functional pool of ASIC1a channels expressed at the cell surface, and the functional study of the extracellular vestibule structure.

Material and Methods

1. *Xenopus laevis* oocytes

The biological expression model used in this work is the *Xenopus laevis* oocyte. By surgery, we remove stage V to VI oocytes from the ovarian tissues of animals anesthetized by immersion in MS-222 (2 g/l; Sandoz, Basel, Switzerland). Oocytes are then defolliculated and used for experiments. Oocytes are kept in an incubator at 19°C in a solution containing in mM: 10 NaCl, 2 KCl, 0.82 $MgSO_4$, 0.41 $CaCl_2$, 0.33 $Ca(NO_3)_2$, 80 NMDG and 5 HEPES.

2. Site-directed mutagenesis

We clone the coding sequence of hASIC1a in pSDEasy vector and introduce an octahistidine coding sequence (H8) into the multiple cloning site using XhoI and SalI restriction sites. H8-hASIC1a-C466A-C471A-C497A-C528Stop (ΔC_{Ct}) is used as template for mutagenesis. C49A, C59V, C61S, C59V-C61S, V74C, Y426C, G430C, G433C, N368A, N395A, and N368A-N395A point mutations are introduced in H8_hASIC1a and ΔC_{Ct} cDNA by Site-Directed Mutagenesis (Stratagene's QuickChange). Mutations have been verified by sequencing (Synergene Biotech, Zurich, Switzerland). Primers list is in the appendix (Primer sequences).

For experiments on human ENaC, the template for mutagenesis is pbluescript(+)-hENaCα.

3. *In vitro* transcription

The linearized and purified cDNA is transcript *in vitro* using the SP6 RNA polymerase (Promega, Dübendorf, Switzerland). After digestion of the template with an RNAse-free DNAse, RNA is purified with the Nucleospin RNA clean-up kit from MACHEREY-NAGEL.10 ng of RNA are pressure-injected per oocyte.

4. ASIC and ENaC expression in oocytes

ASIC-injected oocytes are kept in a Medium Barth Saline solution (MBS) containing in mM: 85 NaCl, 1 KCl, 2.4 $NaHCO_3$, 0.82 $MgSO_4$, 0.41 $CaCl_2$, 0.33 $Ca(NO_3)_2$, 10 HEPES and 4.08 NaOH at pH 7.2.Whereas ENaC-injected oocytes are maintained in a solution with low Na^+, in mM: 10 NaCl, 2 KCl, 0.82 $MgSO_4$, 0.41 $CaCl_2$, 0.33 $Ca(NO_3)_2$, 80 NMDG, 5 HEPES.

5.   Electrophysiological measurements

5.1.   Labeling with MTS reagents
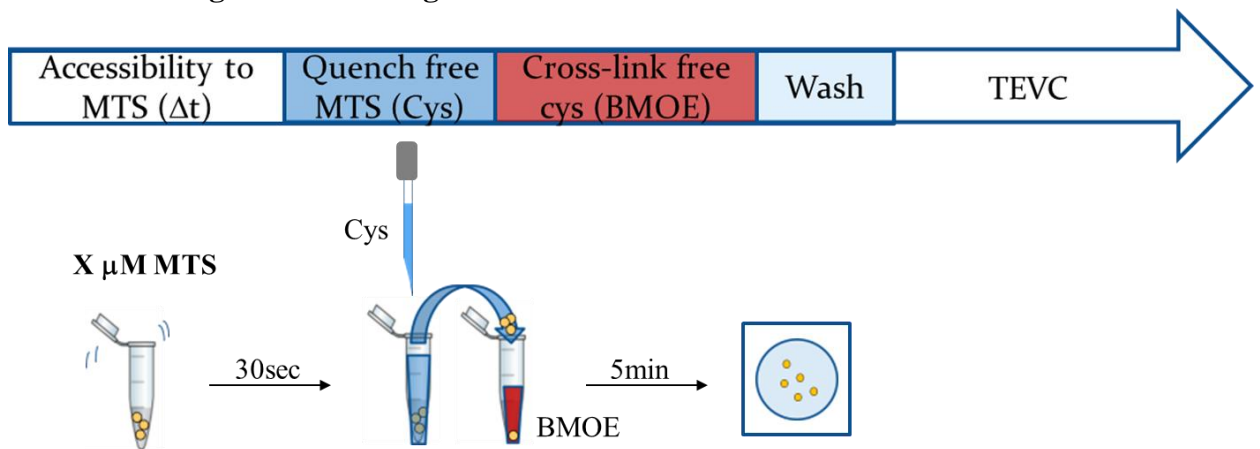
To assess the kinetics of MTS accessibility, we incubate oocytes in the control solution (pH 7.8) supplemented with x µM MTS. After varying time, we quench the MTS with 100 µM cysteine and directly crosslink the unoccupied cysteines of the protein with 2 mM BMOE. After three washing steps, we measure the currents using the Two-Electrodes Voltage Clamp (TEVC).

Then, currents are normalized over the maximum current (I_{Na+}/I_{Na+} max) and plotted in function of time. We apply the following equation for one phase association;

$$Y = Y_0 + (\text{Plateau} - Y_0)*(1 - e^{(-k*X)}),$$

with X the time and k the rate constant. The association constant k_2 is determined by dividing k by the concentration of MTS, and its unit is $M^{-1} * s^{-1}$. k_2 constants are calculated for each oocyte. Oocytes with aberrant or undefined k_2 are excluded from the analysis.

5.2.   Crosslinking in situ

To crosslink proteins *in situ*, we incubate intact oocytes in the incubation solution supplemented with 2 mM of BMOE (or 10 mM NaTT) at 19°C. After varying time (5 or 120 min), we wash the cells three times and proceed with the electrophysiological measurements and/or the biochemistry.

5.3. Two-electrodes voltage Clamp (TEVC)
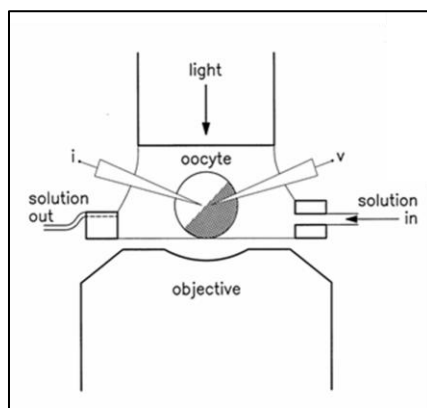
Figure 14 Setup of TEVC. The oocyte is impaled with two electrodes; one measuring the current (i) and the other the voltage (v). Figure from http://www.ionchannel.ku.dk/research/electrophysiology/

Electrophysiological measurements are made 24-48 hours after injection. Sodium currents are recorded using the TEVC technique (model TEV-200; Dagan Corp.). Measurements are carried out by placing the oocyte in a bath, perfused with different solutions, and impaled with two electrodes. One electrode measures the membrane potential (Vm) and the second one injects the current necessary to maintain the desired potential that would otherwise be modified by the channel activity. The two electrodes are realized using micropipettes containing a 1 M KCl solution. All electrophysiological experiments were performed at room temperature (22-25 °C). For hASIC1a sodium currents, we used an holding potential at -80 mV. The control solution at physiological pH contains in mM: 120 NaCl, 2 MgCl2, 10 HEPES°H$^+$, adjusted at pH 7.4 or 7.8 with N-Methyl-D-Glucosamine (NMDG). The acidic solution for the activation of hA1a contains in mM: 120 NaCl, 2 MgCl2, 10 MES and pH 6.0 is adjusted with NMDG. For each oocyte, three to four activations are performed at 40 seconds intervals. For ENaC recordings, the composition of the perfusion solution is in mM: 120 NaCl, 2.5 KCl, 1.8 CaCl$_2$-2H$_2$O, and 10 HEPES-H$^+$ for the Na$^+$ solution; NaCl is replaced by 120 mM NMDG-HEPES or KCl for the perfusion solutions devoid of Na$^+$. To determine amiloride-sensitive currents, we add amiloride (Sigma, 10 μM) in a separated fraction of each test solution. Inward Na$^+$ current is generated by switching from a solution without Na$^+$ (NMDG or KCl) to a perfusion solution containing 120 mM of Na$^+$. In the experiment with proteases, the oocytes are exposed to 5 μg/ml trypsin (Sigma-Aldrich Chemie) in the 120 mM NaCl-perfusion solution.

5.3.1. pH activation curves

Measurements are made by switching solutions from pH 7.8 to pH 7.4, 7.2, 7.0, 6.8, 6.5, 6.0, 5.5 and 5. Oocytes are stimulated twice at each pH solution. Currents are then normalized regarding the maximum I_{Na} that is pH 5.0. Points are then fitted with the equation:

$$Y=1/(1+(10^{\wedge}-pH/10^{\wedge}-x)^{\wedge}n) \;;$$

With, pH = pH of half activation and n = Hill coefficient

5.3.2. pH inactivation curves

Measurements are made by switching solutions from pH 7.8, 7.4, 7.2, 7.0, 6.8 to pH 5.0. Oocytes are stimulated twice at each pH solution. Currents are then normalized regarding the maximum I_{Na} that is after incubation at pH 7.8. Points are then fitted with the equation:

$$Y=z+((1-z)/(1+(10^{\wedge}-x/10^{\wedge}-pH)^{\wedge}n)) \;;$$

With pH = half max pH for inactivation, n = Hill coefficient and z = baseline

5.4. Cut-open technique
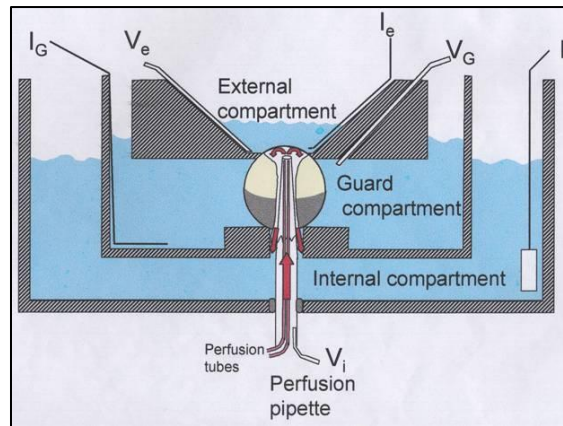
Figure 15 Setup of Cut-open

The cut-open technique allows the recording of macroscopic currents while both the inside and the outside of the oocyte are continuously perfused. *Xenopus laevis* oocytes are placed in an experimental holder divided in three chambers. The superior pole of the oocyte is in contact with the upper chamber and perfused with the extracellular solution. The lower pole is impaled by a microperfusion pipette used as well as microelectrode. The guard compartment isolates electrically the external (upper) and the internal (lower) compartments. The voltage clamp is performed using a Dagan cut-open oocyte voltage clamp apparatus (Dagan Corporation,

Minneapolis, MN; model CA-1 high performance oocyte clamp). 24-48 hours after RNA injection, oocytes are perfused intracellularly with either a control, 1 mM MTS or an acidic solution, and the sodium current is measured. In crosslinking experiments, oocytes are perfused either with BMOE or NaTT. To test if the MTSEA-biotin-mediated biotinylation specifically involved cysteines modification, some experiments are performed with oocytes perfused with a solution containing 1 mM MTSEA-biotin with or without 5 mM free cysteines (L-Cysteine*HCl, pH 7.35 with NMDG, Fluka).

6.   Biochemistry

6.1.   Pull-down on nickel-NTA-agarose beads

Oocytes are lysed with a lysis buffer (LB) containing 1% (v/v) Triton and, in mM: 100 NaCl, 20 Tris-HCl at pH 7.5, 10 N-Ethylmaleimide (NEM), 1 PMSF and 10 µg/ml each of Leupeptin, Pepstatin and Aprotinin (20 µl LB/oocyte). After 10 min centrifugation at ~15,000g (4°C), the intermediate phase comprising the solubilized protein fraction is recovered and subjected to batch affinity chromatography on nickel-NTA-Agarose beads (Qiagen, Hombrechtikon, Switzerland), incubating 2 h at 4°C in the presence of 20 mM imidazole to reduce non-specific binding.

After 2 min centrifugation at 2,000 rpm, the beads are washed 3 times with LB. 40 µl of sample buffer (25 mM DTT, final concentration) are added to the pellet containing the drained beads and heated at 95°C for 5 min. Bound proteins are then recovered by centrifuging through Evergreen mini-filters (EVE-208).

6.2.   Biotinylation of the cell-surface expressed ASIC

48h hours after cRNA injection, 30 oocytes/condition are labeled by 15 min incubation on ice in 1 ml of biotinylation buffer (in mM: 10 Triethanolamine, 150 NaCl and 2 $CaCl_2$) supplemented with 1 mg/ml of EZ-link sulfo-NHS-SS-biotin (Pierce, #21331). After aspiration of the bathing solution, oocytes are incubated for 5 min in 1 ml of quenching buffer (in mM: 192 Glycine, 25 Tris-HCl at pH 7.5, in MBS solution) and subsequently washed 3 times with MBS solution. Oocytes are finally lysed with a Streptavidin binding buffer (SBB, 20 µl LB/oocyte) containing 1% (v/v) Triton and, in mM: 5 EDTA, 100 NaCl, 40 Tris-HCl (pH 7.5), 1 PMSF and 10 µg/ml of each Pepstatin, Aprotinin and Leupeptin. After 10 min centrifugation at ~15,000g,

biotinylated proteins are isolated from the intermediate phase by a pull down assay. After incubation with 50μl of streptavidin-agarose (1h at RT, Immunopure immobilized streptavidin gel from Pierce #20349), beads are washed three times in SBB and bound proteins are then eluted as described above. Pilot studies using lysates from non-biotinylated oocytes are carried out to assess the absence of non-specific binding of His-tagged hASIC1a to streptavidin (not shown).

For *in situ* crosslinking studies, we supplement the SBB with 10 mM NEM to avoid crosslinking of free cysteines.

6.3. Blue native technique and Oligomer Characterization by Addition of Mass

CHO cells stably transfected with the $His_8\_sGFP\_TCS\_hASIC1a$ or $His_8\_sGFP\_TCS\_cASIC1\Delta$ are used and treated as described in the paper of Gandhi, Walton and Rees (246). Proteins are then resolved on a blue native polyacrylamide gel electrophoresis (BN-PAGE) according to the modified protocol of H. Schägger used by Swamy *et al.* (247).

Results

This section will be separated in two parts. The main part deals with the structure-function of ASIC: oligomerization and functional investigation of the apparent size of the extracellular vestibule. The other part is a side project on ENaC. It is the functional characterization of an ENaC mutation (αS243P$\beta\gamma$) found in a patient diagnosed with a PHA1.

ASIC

1.   Oligomerization of ASIC

Previous experiments on the stoichiometry of ENaC/Deg channels remain controversial. Moreover, the oligomerization of the functional ASIC channels *in situ* has never been addressed so far. Thus, we have investigated the subunit composition of the functional human ASIC1a channel using a crosslinking approach.

1.1.   Preliminary crosslinking experiments with sodium tetrathionate

When Jasti *et al*. published the crystal structure, we were already working on the crosslinking of human ASIC1a (hASIC1a). We assessed the effect of the oxidizing agent sodium tetrathionate (NaTT) on His_8_hASIC1a, either after the incubation of total lysates with the reagent, or after the NaTT injection into *Xenopus laevis* oocytes. SDS-PAGE and western blot analyses of crosslinked hASIC1a purified on nickel-beads led to the detection of three bands at 66±4, 147±13 and 304±33 kDa (mean±SD, n=4) (Figure 16). The distribution of these molecular weights follows a linear regression with a slope of 79.2±0.4 (R^2=1). Using a construct lacking the four cysteines of the C-terminus, we have noticed a disappearance of the highest band (304 kDa), a decrease of the intermediate (147 kDa) and an increase of the band at 66 kDa. Looking at the control condition without NaTT does not allow us to conclude that the NaTT crosslinking works. Indeed, the NaTT is an oxidizing agent that induces the disulfide bond formation. In order to see the effect of NaTT, we have to avoid the use of reducing agents (DTT) in the SDS-PAGE gels. Thus, it is impossible to distinguish disulfide bonds induced by NaTT from disulfide bridges already formed before the crosslinking treatment. However, this experiment shows the role of the C-terminal cysteines in the stabilization of high molecular weight complexes.
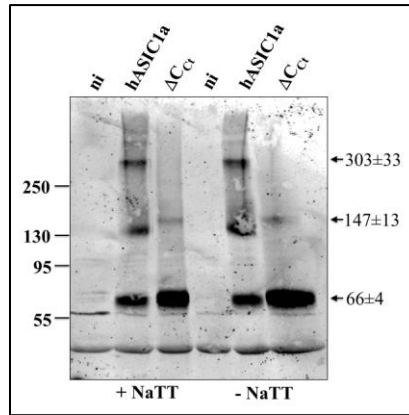
Figure 16 Analysis of the NaTT-crosslinked H$_8$hASIC1a. Stabilized ASIC1a wt is compared with ΔC$_{Ct}$ (construct lacking the four cysteines in the C-terminus). On a 5-15 % SDS-PAGE gel (non-reducing conditions (–DTT)), three bands are detected with the anti-His antibody (1/1000) at 66±4, 147±13 and 304±33 kDa (n=4). ni=non-injected oocytes.

Experiments performed by Jasti and colleagues on cΔASIC1 showed that glutaraldehyde stabilized a trimeric complex of ~165 kDa (monomer ~50 kDa) (228), whereas under our conditions, the NaTT stabilized a complex of 303±33 kDa closer to a tetramer (monomer 66±4 kDa). However, these experiments have been performed on total lysates and thus, do not make the distinction between functional cell surface expressed channels and cytosolic proteins. Moreover, the impact of the crosslinking on the channel activity was unknown. Thus we decided to assess the NaTT effect on channel function using the cut-open technique. As depicted on Figure 17, the crosslinker did not affect the hASIC1a activity of neither the wt nor the ΔC$_{Ct}$ (black circle and green squares, respectively, n=12 per condition). Then, proteins from the perfused oocytes have been separated on a non-reducing SDS-PAGE gel. This led to a migration pattern similar than for NaTT-injected oocytes (n=1, data not shown).
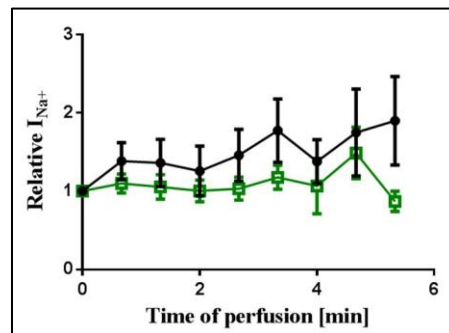
Figure 17 Analysis of the activity of hASIC1a perfused with 20 mM NaTT using the cut-open technique. hASIC1a wt is represented by the black circles and hASIC1a without the four cysteines of the C-terminus (ΔC$_{Ct}$) by the green squares (n=12/condition).

42

To summarize, on non-reducing SDS-PAGE gels, hASIC1a migrate under three molecular weight forms; 66±4, 147±13 and 303±33 kDa. The presence of the high molecular weight band is dependent of the C-terminal cysteines stabilizing high molecular weight complexes through intersubunit disulfide bonds formation.

1.2. Crosslinking experiments with bismaleimidoethane

The bismaleimidoethane (BMOE) is an 8 Å crosslinker for covalent and irreversible conjugation between thiol groups. Results are explained in the article "A crosslinking study of the human ASIC1a: evidence of 4 distinct oligomeric states at the cell surface" (Appendix).

In this article, we have developed a crosslinking approach to stabilize ASIC1a directly at the cell surface of *Xenopus laevis* oocytes. Similarly to NaTT, we have analyzed the effect of BMOE on the function of ASIC1a (wt and ΔC_{Ct}) using the cut-open technique (Figure 18 A). The BMOE does not change the ASIC1a activity. Moreover, SDS-PAGE gels (reducing condition) and western blot analyses of perfused oocytes confirm the BMOE-dependent crosslinking with three bands migrating at 72±2, 156±7 and 329±19 kDa (mean±SD, n=7) and their absence without BMOE treatment, as well as without the four cysteines in the C-terminus (Figure 18 B).
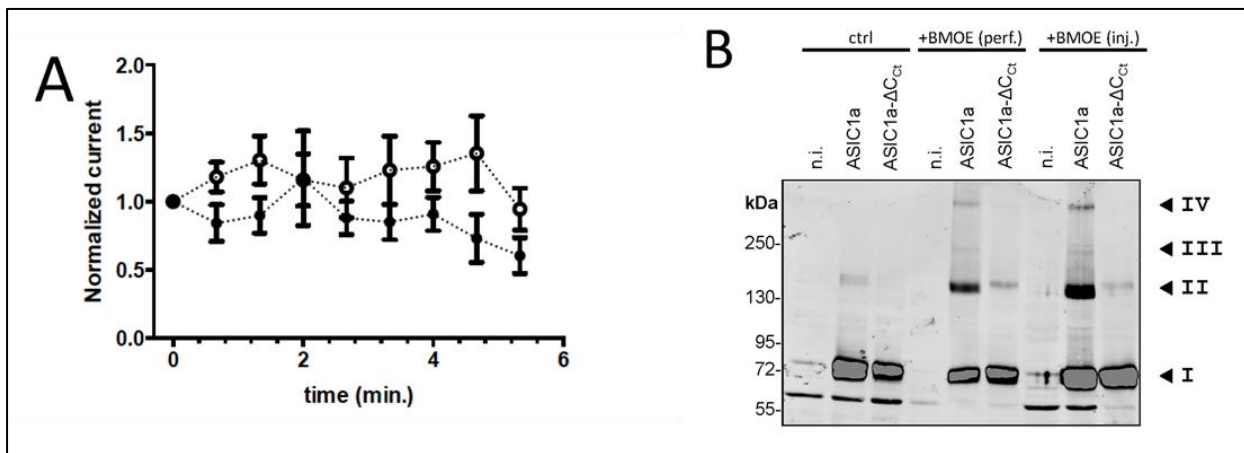
Figure 18 Effects of intracellularly applied BMOE on hASIC1a activity and oligomerization. *A,* Cut-open oocytes expressing either ASIC1a wild type (solid circles, n=18) or ASIC1a-ΔC_{Ct} (open circles, n=17) were intracellularly perfused with 2 mM BMOE; time 0 corresponds to the onset of perfusion with BMOE; currents (m±SD), elicited at pH 6.0 were normalized to the peak current at time zero in the absence of BMOE. *B,* Oligomerization of ASIC1a identified by an anti-ASIC1 western blot from oocytes, not injected (n.i.), or expressing ASIC1a or ASIC1a-ΔC_{Ct} lacking cysteines in the C-terminus, that were either untreated (ctrl), internally perfused (perf.), or intracellularly injected (inj.) with 2 mM BMOE. Numbers I to IV identify bands that are specific for ASIC1a and represent by Mw multiples of band I.

Given that C-terminal cysteines are able to form disulfide bridges between subunits (233), we cannot rule out that the 329 kDa-band is the result of the interaction of ASIC with an adjacent protein. Thus, we have engineered new cysteine mutants in a background where the four

cysteines of the C-terminus have been mutated (ΔC_{Ct} background). We have chosen these residues based on two criteria; their accessibility for MTS-reagents and the orientation of their side chains towards the pore lumen. These mutants are V74C and Y426C in the ECV (upper and bottom parts, respectively), as well as G430C and G433C in the TM2. They are functional and display an increased sensitivity for Cd^{2+}. Furthermore, BMOE treatment leads to a current inhibition for Y426C and G430C. Both results indicate that the residues are on the permeation way.

SDS-PAGE and western blot analyses of *in situ* crosslinked and cell surface purified channels allow the detection of four distinct bands. The distribution of their molecular weights follows a linear regression with a slope of 72±4 kDa consistent with a subunit mass (Figure 19).
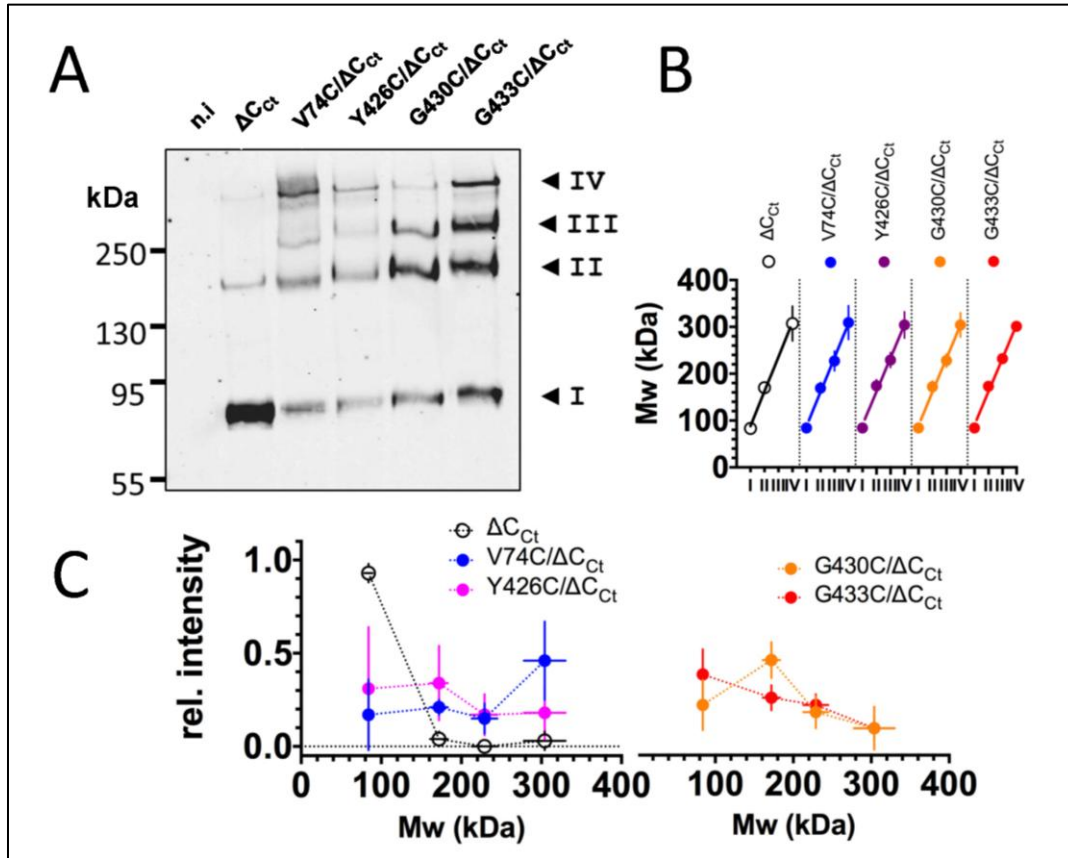
Figure 19 ASIC1 oligomeric states revealed by SDS-PAGE separation after crosslinking of cysteines in the ECV. *A,* Anti-His-tag western blot of the biotinylated fractions of surface proteins from non-injected oocytes (n.i.), from oocytes expressing either the His_8-tagged forms ASIC1a/ΔC_{Ct} (ΔC_{Ct}) lacking cysteines in the C-terminus, or the substitution mutants V74C/ΔC_{Ct}, Y426C/ΔC_{Ct}, G430C/ΔC_{Ct}, and G433C/ΔC_{Ct}. The crosslinking with 2 mM BMOE was performed at the cell surface; the biotinylated surface proteins were affinity-purified on streptavidin beads. Numbers I to IV, as in figure 18. *B,* Apparent Mw values of the ASIC1 oligomers (kDa, mean ±SD) estimated for each of the four main bands (I to IV) resolved by SDS-PAGE (see Methods) for the different constructs, as in A. *C,* Relative intensities (mean, vertical bars ±SD) of the four distinct bands I-IV identified in A: horizontal bars represent SD for the apparent Mw value for each band.

The engineered cysteine accounts only for two bands, while the others involve native cysteines of the TM1, in particular C59 and C61, as depicted on the Figure 20.
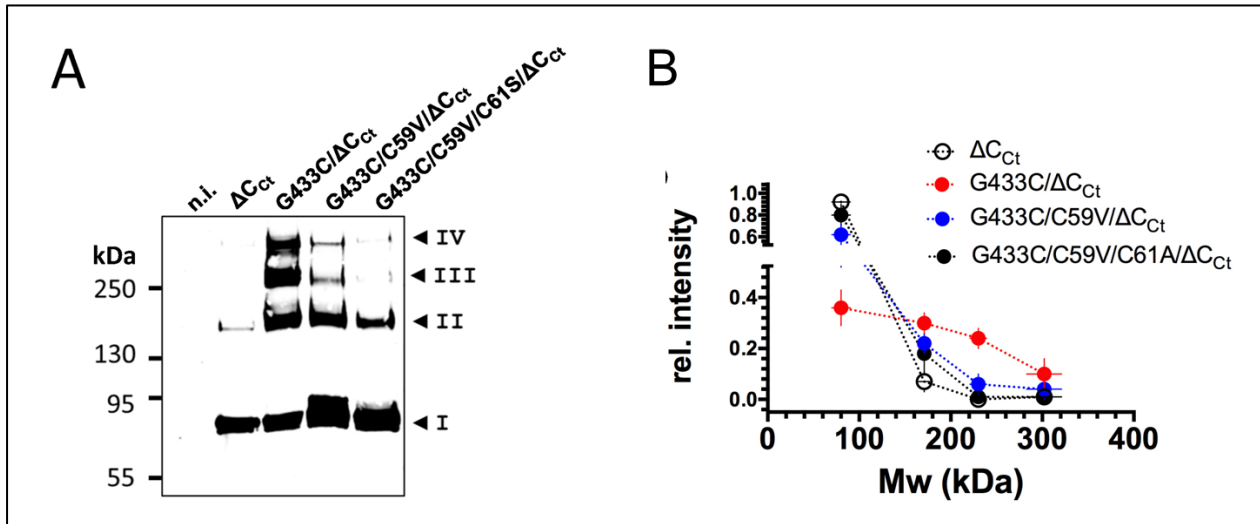
Figure 20 Contribution of the cysteines in the first transmembrane helix (TM1) to the subunit crosslinking by BMOE. *A*, ASIC1a oligomeric states identified by anti-His-tag western blot (using the same experimental procedure as in figure 3A) of the His$_8$-tagged forms of ASIC1a-ΔC_{Ct} (ΔC_{Ct}), and the cysteine substitution mutant G433C-ΔC_{Ct} associated or not with the C59V or C59V/C61S substitutions (G433C/C59V/ΔC_{Ct} or G433C/C59V/C61S/ΔC_{Ct}). Numbers I to IV have the same meaning as in figure 1. *B,* Relative intensities (arbitrary units, mean ±SD, n=4) of the bands identified on SDS-PAGE estimated for ASIC1a-$\Delta C_{Ct,}$ G433C/ΔC_{Ct}, G433C/C59V/ΔC_{Ct}, and G433C/C59V/C61S/ΔC_{Ct}. Horizontal bars represent ±SD of apparent molecular weight sizes.

Do these four bands reflect a diversity of ASIC1a oligomers at the cell surface or are they dissociated subunits coming from one unique oligomer? A way to discriminate between them is to optimize our crosslinking protocol (time, concentration, available cysteines). We have chosen to focus on the G433C mutant, mainly because it is not inhibited by BMOE, meaning that even after its stabilization we are still working on a functional channel. While the optimized conditions do not lead up to an enhancement of the crosslinking into *Xenopus* oocytes, they do in CHO cells. Indeed, as shown on Figure 21, the crosslinked ASIC1a wt is translated into four bands of 75±2, 160±13, 224±20 and 304±22 kDa (mean±SD, n=9). The engineered G433C increases the amount of high molecular weight complexes (224 and 304 kDa, 26 and 59 % of the total pool, respectively), whereas the 75 and 160 kDa bands have disappeared.

On the Figure 21, a doublet is present for the highest molecular weight complex. We hypothesize that the two bands represent two complexes made of four subunits that have been stabilized in two distinct conformations, i.e. a closed ring *versus* a linear configuration (248).

45
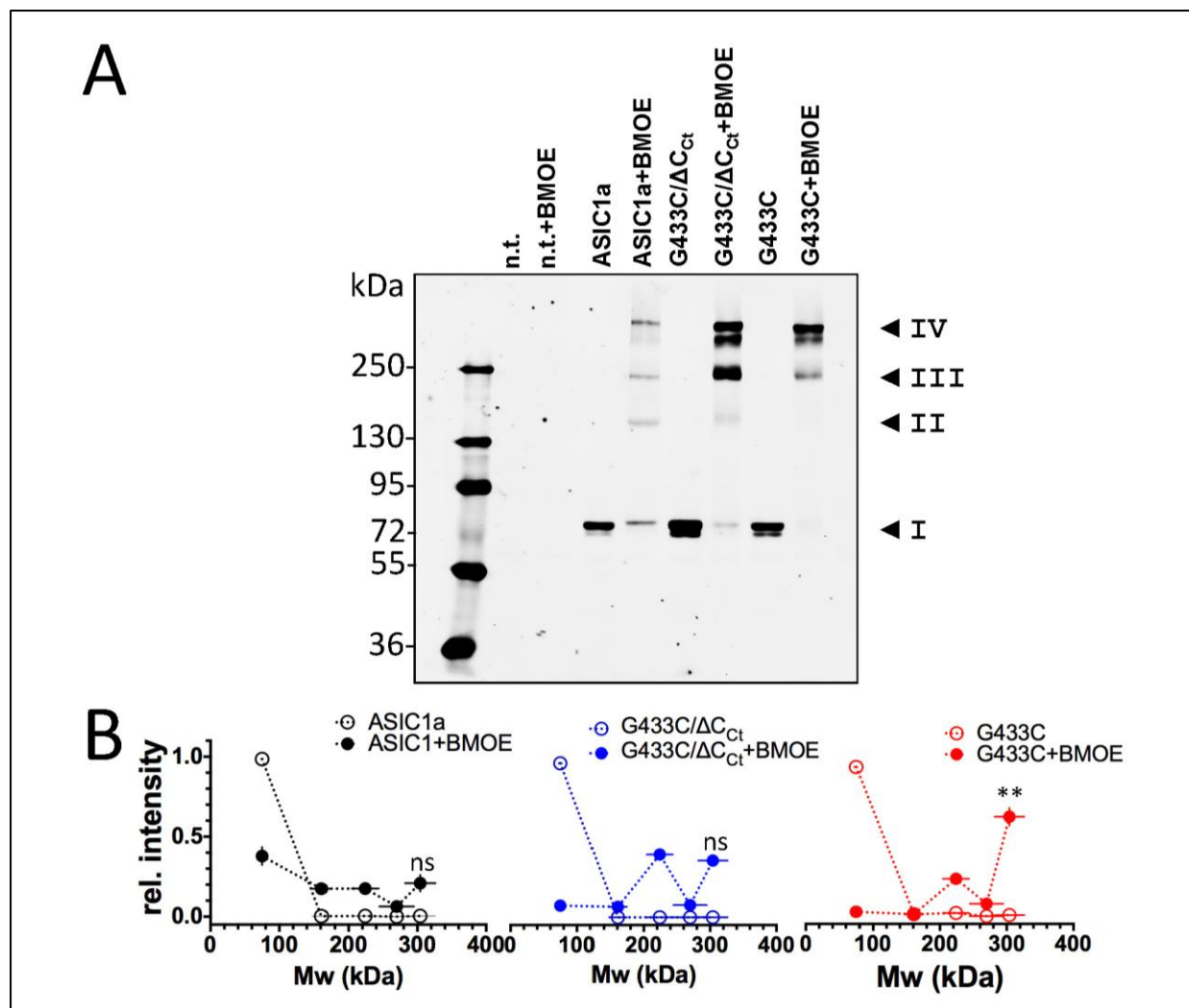
Figure 21 Stabilization of the ASIC1a channel complex at the cell surface of transfected CHO cells. *A,* Anti-His-tag western blot showing ASIC1a oligomeric states obtained from cell surface fractions of proteins expressed by CHO cells and transiently transfected with an empty vector (n.t.), or His$_8$-tagged forms of ASIC1a wt, ASIC1a-G433C/ΔC_{Ct}, or ASIC1a-G433C mutants, and treated with 2 mM BMOE or vehicle. Surface proteins were biotinylated, purified on streptavidin beads and analyzed by western blot.. Numbers I to IV have the same meaning as in figure 19. *B,* Relative intensities (mean ±SEM) measured of the different bands detected for the different constructs without (open circles) or with 2mM BMOE (filled circles). Horizontal bars represent apparent Mw values (±SEM) estimated for each band. Significant (** = p<0.01) difference in intensity between bands III and IV for each protein was determined by a paired, two-tailed *t*-test.

An increased number of cysteines available for crosslinking does not lead to an unique oligomer. We hypothesize that this could be a limitation of the BMOE itself. Indeed the number of free accessible and well-distanced cysteines might be too low. Thus we switch to the formaldehyde, a 2-3 Å amino crosslinker. The reaction of the formaldehyde with proteins is composed of three steps. Frist, a methylol adduct on amino groups is formed. This adduct is then partially dehydrated. This yields a labile Schiff-base that can crosslink with several aa residues. Arginine and tyrosine are the main residues, but asparagine, glutamine, histidine and tryptophan can also

be crosslinked (249). Consequently, no more difference is observed between ASIC1a wt and G433C mutant, because the number of formaldehyde-reactive residues is the same between both wt and cysteine mutant constructs. Furthermore, formaldehyde crosslinking is dose-dependent and leads finally to the stabilization of the 313±22 kDa oligomer representing between 70 and 80 % of all oligomeric states (Figure 22).
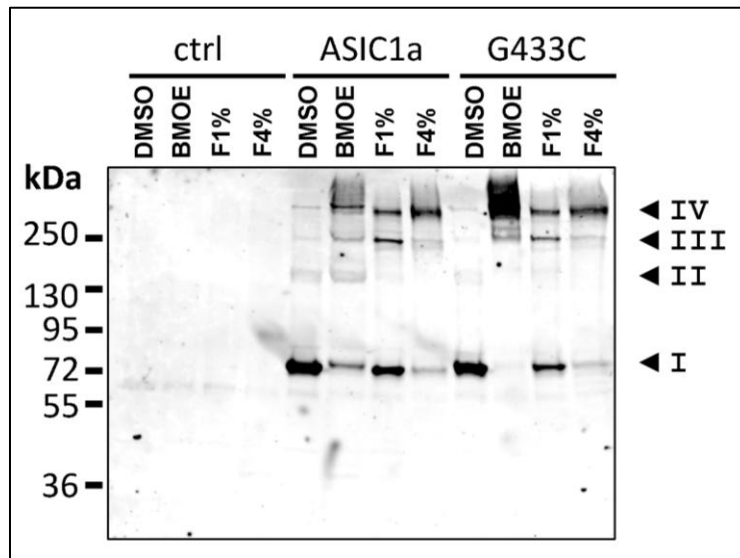
Figure 22 ASIC1a channel complex at the cell surface of CHO cells after crosslinking with formaldehyde. *A,* Anti-His-tag western blot of the biotinylated fractions of surface proteins in CHO cells transiently transfected either with empty vector (ctrl), or with His$_8$-tagged ASIC1a, or ASIC1a-G433C mutant (G433C). Cells were treated either with vehicle (DMSO), or BMOE (2 mM), or with 1 or 4% formaldehyde (1F, 4F, respectively). Surface proteins were biotinylated, purified on streptavidin beads before western blot analysis. Numbers I to IV have the same meaning as in figure 18.

In conclusion, stabilization of the functional hASIC1a expressed at the cell surface adds supplementary evidence in favor of a tetrameric ASIC1a channel, independently of the crosslinker, the expression system and the cysteine mutant.

2. Functional characterization of the extracellular vestibule size

In this part, we combine molecular, functional and biochemical approaches with bioinformatics to gain information on structural aspects of the extracellular vestibule (ECV). The aim was to evaluate functionally the size of the ECV. This has been done by testing the accessibility of specific residues, mutated in cysteines, for ligands of different molecular weight and shape. This technique is called SCAM for Substituted-Cysteine Accessibility Method.

Based on the crystal, we have identified pore-lining residues in the ECV. They are the E63, Y68, H73, V74, K423, A425, Y426, and G430 (Figure 23).

47
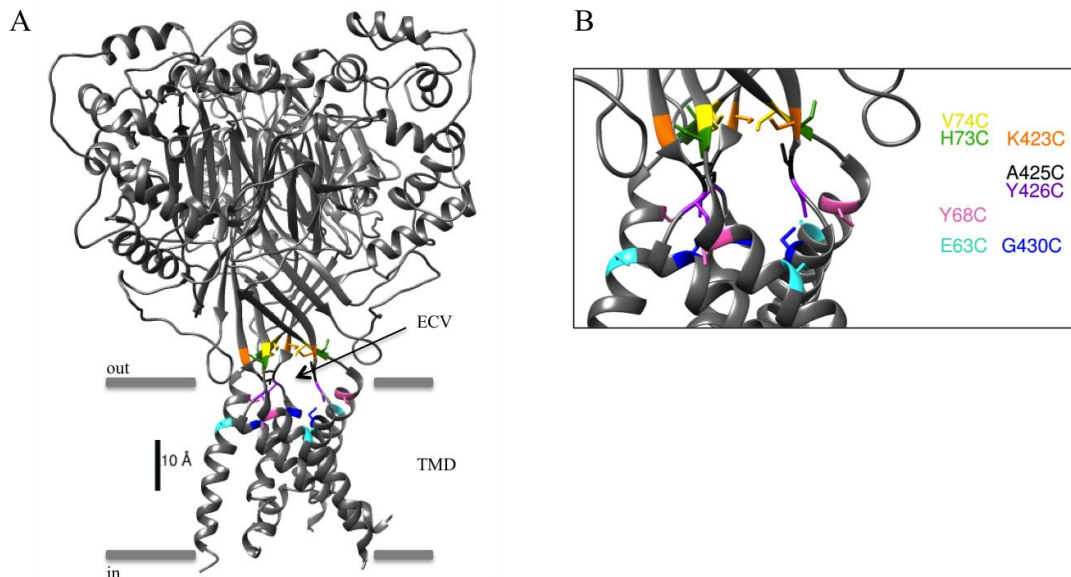
Figure 23 *A,* View of cASIC1 crystal with cysteines mutated residues in the extracellular vestibule (ECV). *B,* Inlet shows an enlarged representation of the ECV. Lining residues are H63, Y68, H73, V74, K423, A425, Y426, and G430, labeled in cyan, pink, green, yellow, orange, black, purple and blue.

2.1. Functional characteristics of the extracellular vestibule mutants

We have investigated by functional electrophysiological techniques the accessibility of E63C, Y68C, H73C, V74C, K423C, A425C, Y426C, and G430C ASIC mutants in the background of C-terminal deleted cysteines. Y68C, V74C and A425C show a lack or a strong reduction of current. V74C recovers its full activity after a reducing treatment (10 mM DTT), suggesting that disulfide bonds might be responsible of the loss of function (**Table 3**). No current was recovered after DTT treatment of Y68C and A425C. Thus, we further investigate the functional cysteine substitutions of E63, H73, V74, K423, Y426, and G430.

2.2. Electrophysiological analyses of the accessibility

2.2.1. Effect of Cd^{2+} on Na^+ currents

In order to assess the accessibility of these engineered cysteines, we use the Cd^{2+}. Having approximately the same size than the Na^+ ion, it is an indicator that a cysteine is along the permeation pathway. While the Cd^{2+} inhibits ASIC1a wt with an IC_{50} of 1.2 ± 0.1 mM, V74C is irreversibly blocked, and Y426C as well as G430C display an increased affinity (IC_{50} 0.032 ± 0.002 and 0.010 ± 0.001 mM, respectively), other mutants (E63C, H73C and K423C) do not present any change. This absence of modification in Cd^{2+} affinity suggests that these cysteines are not accessible. Thus we do not continue our investigations on them.

This first screen shows the accessibility of V74C, Y426C, and G430C for a small ligand like Cd^{2+}, and their subsequent inhibition (**Table 3**). This inhibition can result either from a pore occlusion or from the channel inability to open due to a crosslinking being two cysteines.

2.2.2. Effect of NaTT on Na⁺ currents

NaTT is an oxidizing agent that induces the formation of disulfide bonds between two cysteines that are close, in the range of a S-S, about 2 Å. We wonder if this treatment would lead to an inhibition, as observed for the Cd^{2+}. Neither the wt, the V74C, the Y426C nor the G430C displays a current significantly different after 10 min of incubation with 10 mM NaTT. This may indicate that two cysteines are not sufficiently close to form disulfide bridges, or that the S-S bond does not inhibit the current. As SDS-PAGE gel analysis has not been performed on these oocytes we are not able to distinguish between these two possibilities.

2.2.3. Effect of BMOE on Na⁺ currents

To further investigate the accessibility of these residues, we tested the effect of the homobifunctional disulfide crosslinker BMOE. Oocytes were incubated in 2 mM BMOE and then the currents recorded with TEVC. The BMOE drastically inhibits Y426C and G430C mutants compared to the ΔC_{Ct} wt channel, whereas V74C is not blocked (**Table 3**), the residual currents are 6.4±02, 9.5±0.2 and 115±24 %, respectively. The V74C inhibition is likely prevented by disulfide bridges as demonstrated by the absence of I_{Na+} of this mutant recovered after a reducing treatment with DTT. On SDS-PAGE analysis, the BMOE is able to crosslink V74C, Y426C and G430C resulting in the appearance of high molecular weight complexes (see the aforementioned article "*A crosslinking study of the human ASIC1a: evidence of 4 distinct oligomeric states at the cell surface*").

Thus, Y426C and G430C are accessible to Cd^{2+} and BMOE. The inhibition seems to be related with the crosslinking activity of BMOE as shown by the stabilization of dimers on SDS-Page (for details, see chapter: Crosslinking experiments with bismaleimidoethane, Figure 19).

hASIC1a	I_{Na} peak	+ BMOE Relative I_{Na} (% of control)	Cd^{2+} (IC_{50} mM)	I_{Na} peak + DTT
ΔC_{Ct}	45.06 ± 20.6	90.2 ± 10.0	1.16 ± 0.095	38.04 ± 15.24
V74C- ΔC_{Ct}	$2.9 \pm 2.4^{**}$	115.7 ± 24	Irreversible block	$25.84 \pm 15.72^{**}$
Y426C- ΔC_{Ct}	22.65 ± 14.22	$6.4 \pm 0.18^{**}$	$0.032 \pm 0.0016^{*}$	29.92 ± 16.8
G430C- ΔC_{Ct}	22.75 ± 14.73	$9.5 \pm 0.17^{**}$	$0.010 \pm 0.0008^{*}$	26.29 ± 19.37

Table 3 ASIC1a currents (µA) were elicited at pH 6.0 for the cysteine mutants in the C-terminal deleted cysteines background (ΔC_{Ct}). Effects of extracellular BMOE (2 mM), Cd^{2+} and DTT (10 mM). Data are means ± SD. ** denotes $p<0.01$ and * $p<0.05$ (Student T-test).

We do not know whether the current inhibition is due to the upholding of the channel in a closed conformation or to a steric hindrance that prevents the Na^+ flux. To gain information about the process of inhibition, we turn on ligand with one reactive group; the methanethiosulfonate reagents (MTS).

2.2.4. Effect of methanethiosulfonate reagents on Na^+ currents

In a search for evidence that MTS-reagents can access the ECV and cysteines in the ion permeation pathway, we have first tested the effects of MTSET, MTS-PTrEA, MTS-TBAE or MTSEA coupled to biotin or fluorescein (MTSEA-biotin, MTSEA-fluorescein) on ASIC currents. MTS-reagents only have one reactive group, thus, they should occlude the vestibule without freezing it in an inactive conformation. The structure of the MTS, as well as the scheme of the reaction is depicted in the appendix 3. MTSET, MTS-PTrEA and -TBAE are positively charged MTS. MSTET with its 5.8 Å head group is the smallest, whereas -PTrEA and -TBAE are bulkier analogues. The neutral MTSEA-biotin has a head group of 12 Å. Its longer analogue is the -biotinCap with an extent linker separating the reactive from the head group. MTSEA-fluorescein is the biggest MTS we have used.

We have incubated the oocytes with MTS and then measured the ASIC activity. Due to disulfide bridges between V74C residues, the accessibility of this cysteine to MTS-reagents cannot be tested directly. A pre-treatment with DTT is necessary for V74C to become free. The accessibility of V74C for MTS-reagents still has to be performed. Both Y426C and G430C have increased peak currents after incubation in MTS (details in the next chapter). Moreover,

incubation of Y426C and G430C with MTSEA-biotin induces a partial desensitization of the channel leading to a sustained current (Figure 24).
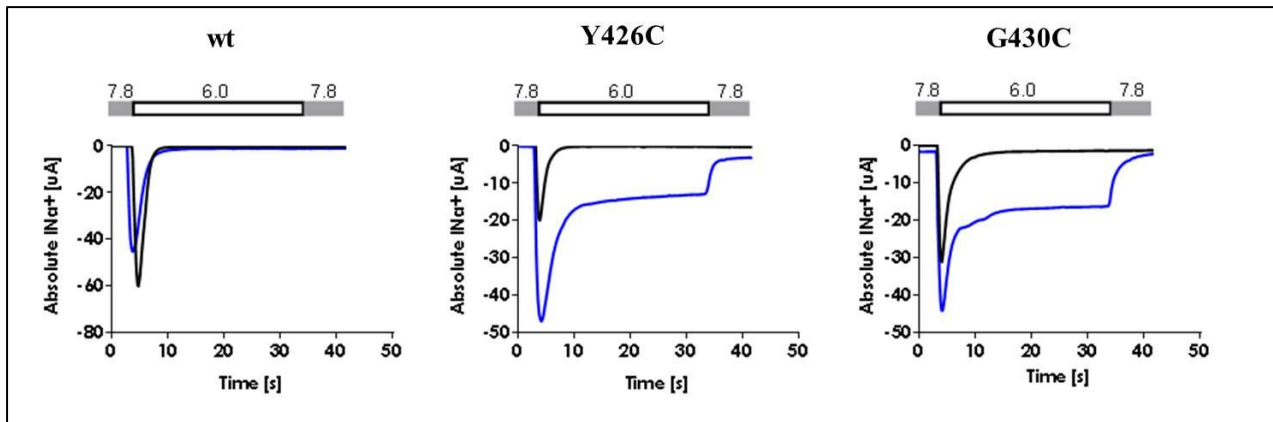
Figure 24 Representative traces of hASIC1a wt, Y426C and G430C with or without MTSEA-biotin (in blue and black, respectively). Currents are obtained by switching from a solution at pH 7.8 to pH 6.0.

2.2.4.1.   The peak current

The Figure 25 summarizes the peak current in the presence of MTS-reagents. It shows that the peak current (I_{peak}) of G430C (25.33±4.40 µA) is significantly increased after incubation in MTSEA-biotin (58.95±28.73 µA) and MTS-TBAE (46.17±7.64 µA), whereas both MTSET (25.85±4.05 µA) and MTS-PTrEA (27.49±7.88 µA) did not affect it. The I_{peak} of Y426C (19.81±3.21 µA) is significantly increased after incubation in MTSEA-biotin (36.38±5.12 µA), whereas MTS-PTrEA, MTSET and MTS-TBAE (27.39±6.93, 22.64±4.07 and 9.48±1.5 µA, respectively) did not affect it. The incubation in MTS-TBAE has been made another day. The corresponding control (unmodified Y426C) had less current (8.03±1.45 µA, n=27). Thus, the difference in current between Y426C treated or not with MTS-TBAE is non-significant.

51
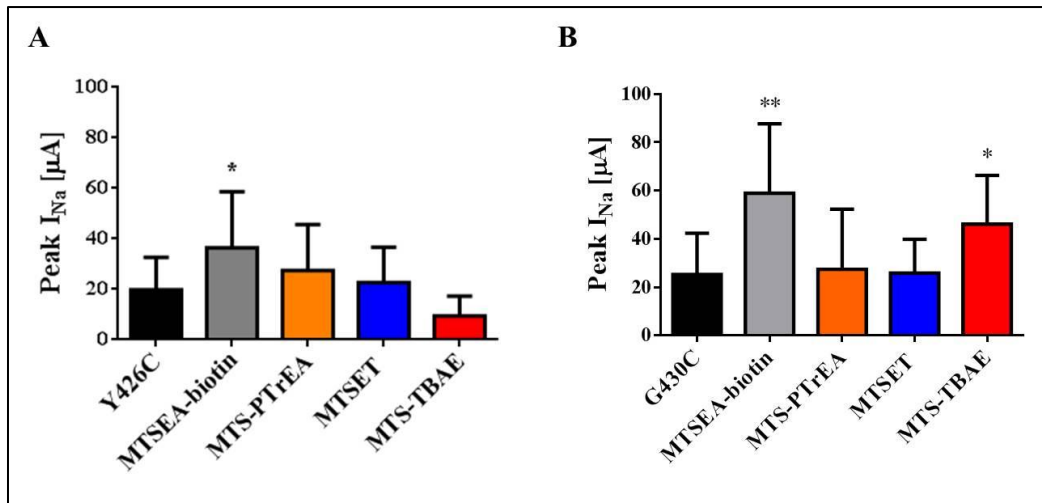
Figure 25 Effect of MTS on the peak currents. *A,* Y426C without MTS (black, n=16). Y426C modified with MTSEA-biotin (1 mM, gray, n=19), MTS-PTrEA (1 mM, orange, n=7), MTSET (1 mM, blue, n=12) and MTS-TBAE (1 mM, red, n=29). *B,* G430C without MTS pre-treatment (black, n=15) and G430C modified with MTSEA-biotin (1 mM, gray, n=11), MTS-PTrEA (1 mM, orange, n=10), MTSET (1 mM, blue, n=12) or MTS-TBAE (1 mM, red, n=7). MTS incubations last 10 min. Unpaired Student T-test: * and ** stand for *P* values smaller than 0.05 and 0.001, respectively. Errors are SD.

Then, we wonder if the pH dependence of activation was changed for the MTS-modified channels. Starting at pH 7.8, each oocyte is stimulated with different pH-solutions (pH 7.4, 7.2, 7.0, 6.8, 6.5, 6.0, 5.5 and 5.0). Currents are then normalized regarding the maximum peak current.

First, we look at the effect of the cysteine mutation on the $pH_{0.5}$ values. The V74C mutation shifts the $pH_{0.5}$ towards more alkaline values compared to the wt, (6.34±0.02, n=31 for the wt and 6.52±0.02, n=35, for V74C, $pH_{0.5}$±SE, *P*<0.0001). Y426C behaves similarly with a $pH_{0.5}$ of 6.50±0.02 (n=10, *P*=0.001). G430C has a pH of half activation unchanged compared to the wt (6.37±0.02, n=4). The effect of MTS-incubations on the $pH_{0.5}$ values is shown on the Figure 26; MTSEA-biotin, MTSET, MTS-TBAE and -PTrEA shift pH activation curve of Y426C ($pH_{0.5}$±SE is 6.50±0.02) towards more alkaline values (6.90±0.01, 7.08±0.02, 6.58±0.01, and 7.18±0.03, respectively). MTSEA-fluorescein, however, does not modify the affinity for H^+ (6.40±0.03). This is similar for G430C channels with $pH_{0.5}$ (±SE) without MTS or with MTSEA-biotin, -TBAE, -fluorescein and MTS-PTrEA of 6.37±0.02, 6.84±0.04, 6.60±0.02, 6.32±0.03, and 7.03±0.02, respectively. The amplitude of the shift is not dependent of the MTS size. Indeed, the shift induces by the MTS-PTrEA is larger than with MTSET, which in turn is larger than in presence of MTSEA-biotin.

The pH dependence of inactivation is unchanged for V74C compared to the wt (7.21±0.03, n=10 and 7.15±0.02, n=10, respectively ($pH_{0.5in}$±SE)), as well as for G430C (7.05±0.05, n=4). Y426C

as a pH inactivation curve shifted towards more alkaline values compared to the wt (7.11±0.01, n=11, and 7.02±0.01, n=5, *P*=0.0001).The binding of MTSEA-biotin slightly modifies the pH dependency of inactivation for the Y426C (7.16±0.02, n=11, *P*=0.03). The $pH_{0.5in}$ of G430C is shifted towards more alkaline values in presence of MTSEA-biotin (7.23±0.01, n=10, *P*=0.015) (Figure 27).
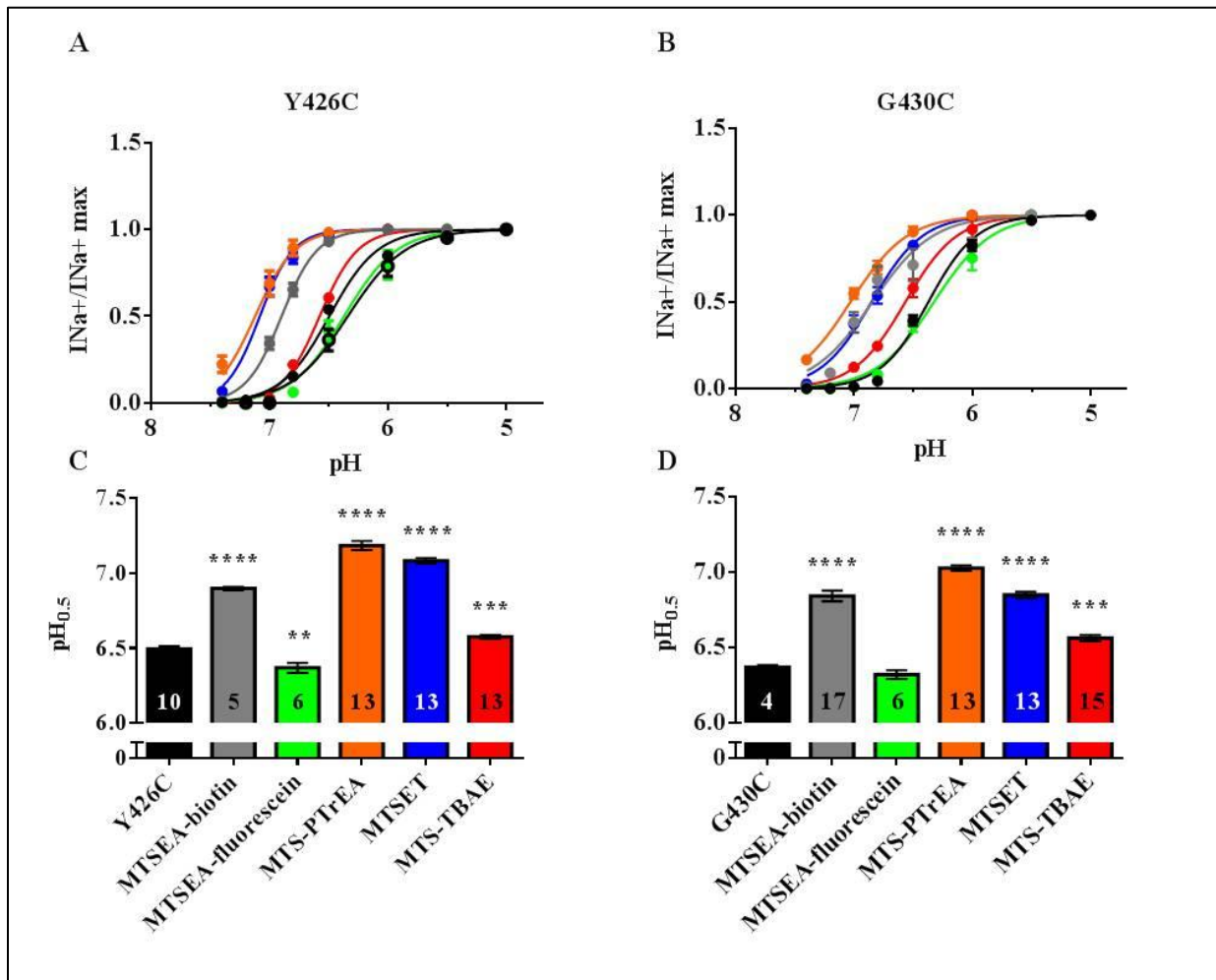
Figure 26 pH dependence of activation of Y426C and G430C. *A,* Y426C without MTS pre-treatment (black circle, n=10). Y426C modified with MTSEA-biotin (1 mM, gray, n=5), MTS-PTrEA (1 mM, orange, n=13), MTSEA-fluorescein (0.1 mM, green, n=6), MTSET (1 mM, blue, n=13) or MTS-TBAE (1 mM, red, n=13). *B,* G430C without MTS pre-treatment (black circle, n=4) and G430C modified with MTSEA-biotin (0.1 mM, gray, n=17), MTS-PTrEA (1 mM, orange, n=13), MTSEA-fluorescein (0.1 mM, green, n=6), MTSET (1 mM, blue, n=13) or MTS-TBAE (1 mM, red, n=15). MTS incubation last 10 min, except for MTSEA-fluorescein that lasts 15 min. *C-D,* $pH_{0.5}$ of activation values, colors are described in *A* and *B*. Unpaired Student T-test: **, *** and **** stand for *P* values smaller than 0.01, 0.001 and 0.0001, respectively.
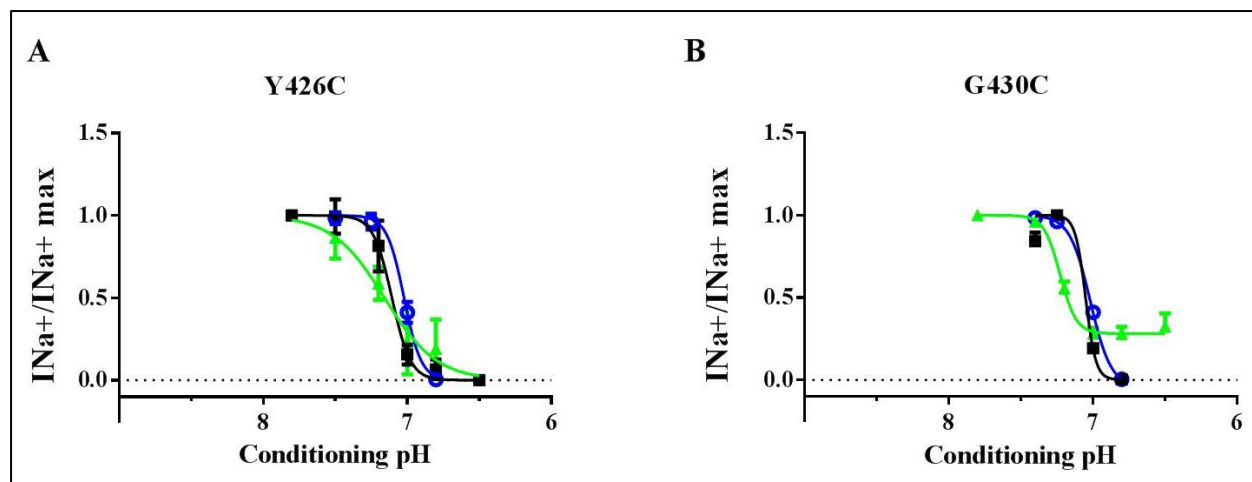
Figure 27 pH dependence of inactivation of Y426C and G430C. *A,* Y426C without MTS pre-treatment (black, n=11). Y426C modified with MTSEA-biotin (green, n=11). ASIC wt (blue, n=5) without MTS pre-treatment. *B,* G430C without MTS pre-treatment (black, n=4) and G430C modified with MTSEA-biotin (green, n=10). ASIC wt (blue, n=5) without MTS pre-treatment.

To summarize, the MTS-reagents (except MTSEA-fluorescein) shift the pH activation of Y426C and G430C mutants. Indeed, a pH-drop to 6.0 would open almost all the MTS-labeled channels (100% of them, except Y426C labeled with MTS-TBAE (97 %)), whereas 92 and 86 % of the unlabeled-Y426C and G430C channels. The amplitude of the shift explains partially the amount of increased I_{peak}. Indeed, the shift is not correlated with the amount of I_{peak}; whereas the MTS-PTrEA leads to the largest $pH_{0.5}$ shift for both Y426C and G430C mutants, it only increases by two-fold the I_{peak} of Y426C and does not change the I_{peak} of G430C. MTSEA-biotin induces the largest I_{peak} increases for both Y426C (4.7-fold) and G430C (2.3-fold).

2.2.4.2.   The sustained current

Beside the increased peak current, the binding of MTS also leads to a change in the kinetic of the current with a partial desensitization leading to a sustained component as previously shown on Figure 24. For G430C, this current represents 28.6±3.3 % of the I_{peak} with MTSEA-biotin, 25.0±5.0 % with MTSET, 37.9±3.2% with MTS-PTrEA, and 8.9±1.2 % with MTS-TBAE (mean±SD). For Y426C, this current represents 14.1±3.2 % of the I_{peak} with MTSEA-biotin, 23.7±12.3 % with MTSET, and 2.9±0.4% with MTS-PTrEA. MTS-TBAE does not induce a sustained Y426C current. Results are depicted on the Figure 28.
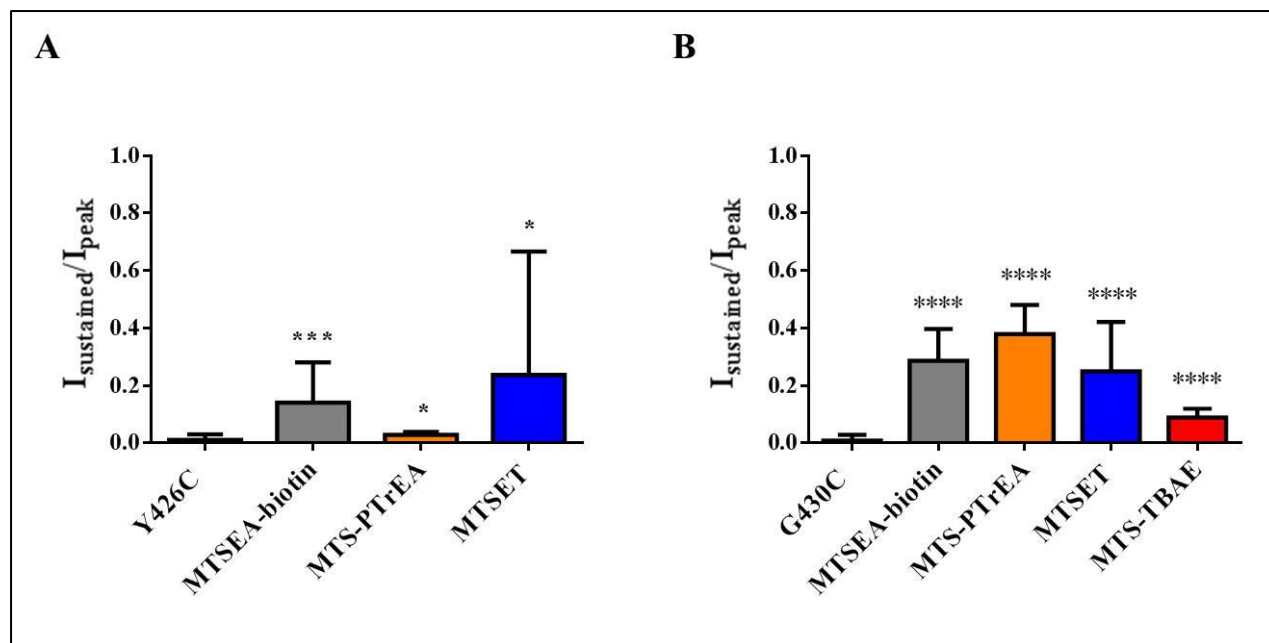
Figure 28 MTS-induced sustained currents. *A,* Y426C without MTS (black, n=16). Y426C modified with MTSEA-biotin (1 mM, gray, n=19), MTS-PTrEA (1 mM, orange, n=7), and MTSET (1 mM, blue, n=12). *B,* G430C without MTS pre-treatment (black, n=15) and G430C modified with MTSEA-biotin (1 mM, gray, n=11), MTS-PTrEA (1 mM, orange, n=10), MTSET (1 mM, blue, n=12) or MTS-TBAE (1 mM, red, n=7). MTS incubations last 10 min. Unpaired Student T-test: *, *** and **** stand for *P* values smaller than 0.05, 0.001 and 0.0001, respectively. Errors are SD.

2.2.5. Competitive interaction between MTS and Cd^{2+} for cysteines in the vestibule

To confirm that the effect of MTS-binding occurs via the same residue that coordinates Cd^{2+}, we have set up a competitive interaction for cysteine mutants between Cd^{2+} and MTS. Given that both Y426C and G430C are more sensitive to Cd^{2+}, we hypothesize that this enhanced affinity for Cd^{2+} should be reversed by a pre-incubation in MTS. Cd^{2+} dose-response curves of both Y426C and G430C mutants are shifted towards the left, as consequence of a higher sensitivity (Figure 29, red curves). This shift occurs independently of the incubation solution pH (either at pH 7.5 or 6.5), whenever the channel in a closed or desensitized state is. Concerning Y426C, MTEST and MTSEA-biotin are able to reverse this effect. On the other hand, MTSEA-biotin or –biotinCap totally reverses this phenomenon for G430C (blue and purple curves), whereas the MTSET does not (orange). This suggests that Cd^{2+} and MTS compete for the same binding site. MTSET does not shift the Cd^{2+} dose-response curve of G430C. This could be due to the non-binding of MTSET to G430C.
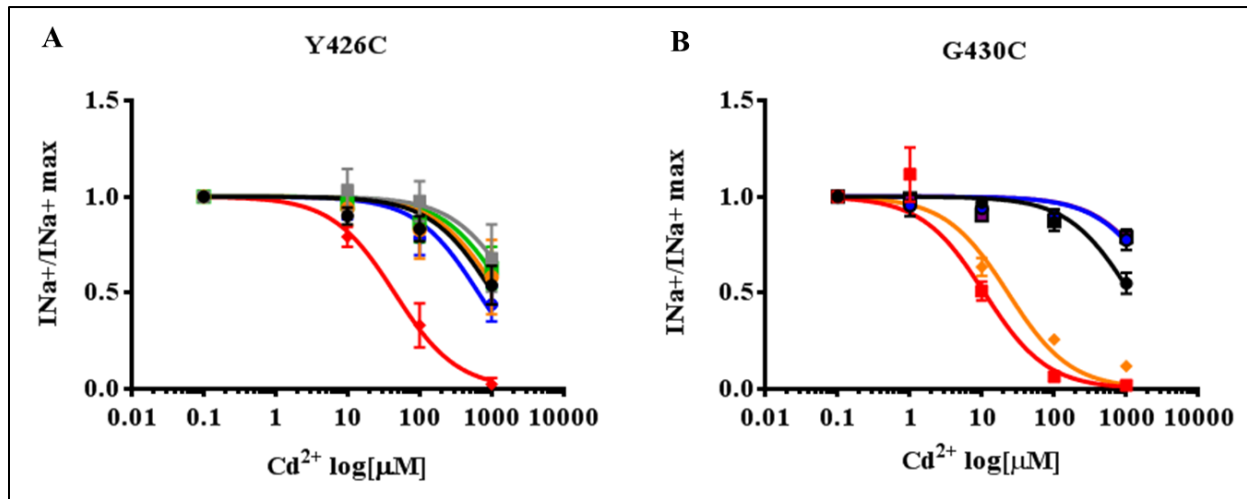
Figure 29 Cd^{2+} dose-response curves. *A,* hASIC1a wt is depicted in black and Y426C mutant in red (n=12 for each condition). Cd^{2+} dose-response curves of wt and Y426C mutant incubated either in MTSET or MTSEA-biotin are represented in grey and green and, orange and blue respectively (n=14, 17, 16 and 10). *B,* hASIC1a wt is depicted in black and G430C mutant in red (n=9 and 11). Cd^{2+} dose-response curves of G430C mutant incubated either in MTSET, MTSEA-biotin or –biotinCap are represented in orange, blue and purple respectively (n=4, 10 and 6).

2.2.6. Competitive interaction for G430C between MTSET and BMOE

To confirm the MTSET absence of binding to G430C, we have made another competitive interaction for this cysteine between the MTSET and BMOE. Previously, we have shown that BMOE inhibited G430C mutant channels. Thus, we have pre-incubated oocytes into MTS and, again challenge the channels for BMOE block. On the Figure 30, we have compared the ability of MTSET to prevent the BMOE block for the wt (in gray) and the G430C (in blue). Although there is an important variability for the relative currents of oocytes incubated with MTSET and BMOE, results suggest that the BMOE block (0.20±0.04 µA, n=5, mean±SD) is prevented by the pre-incubation of G430C in MTSET (2.21±0.45, n=5).
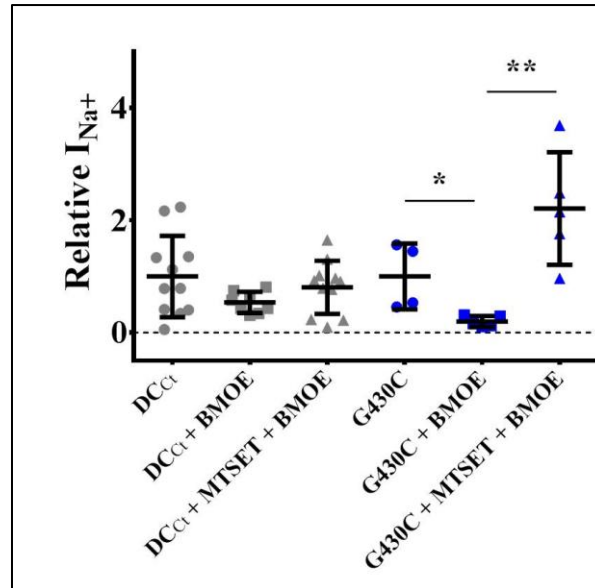
Figure 30 Competitive interaction for G430C between MTSET and BMOE. ΔC_{Ct} and G430C are depicted in grey and blue, respectively. We compare I_{Na+} from MTSET- and BMOE-untreated (circle), BMOE-treated (square) and MTSET- and BMOE-treated oocytes (triangle). n=4-11 oocytes/condition, 2 batches. Student T-test: * and ** for *P* values smaller than 0.5 and 0.01, respectively. Results are mean±SD.

Under this condition, the MTSET is able to prevent the BMOE block of G430C mutants, demonstrating a competition for the same residue. These experiments confirm the effective binding of MTSET to G430C.

2.2.7. Kinetics of accessibility of the MTS

Our data show that the MTS-reagents bind Y426C and G430C residues. We would like to investigate the kinetics of the binding reaction of the MTS-reagents to the cysteines. This would give you an indication of how easy/difficult it would be for a MTS to reach its binding site. We have set up an assay in which oocytes are incubated in a control solution at pH 7.8 supplemented with a constant concentration of MTS. The reaction is quenched with free cysteines at different time points. Then, oocytes are incubated in BMOE and ASIC activity recorded. With this protocol we measure the current recovery of the MTS-modified channels.
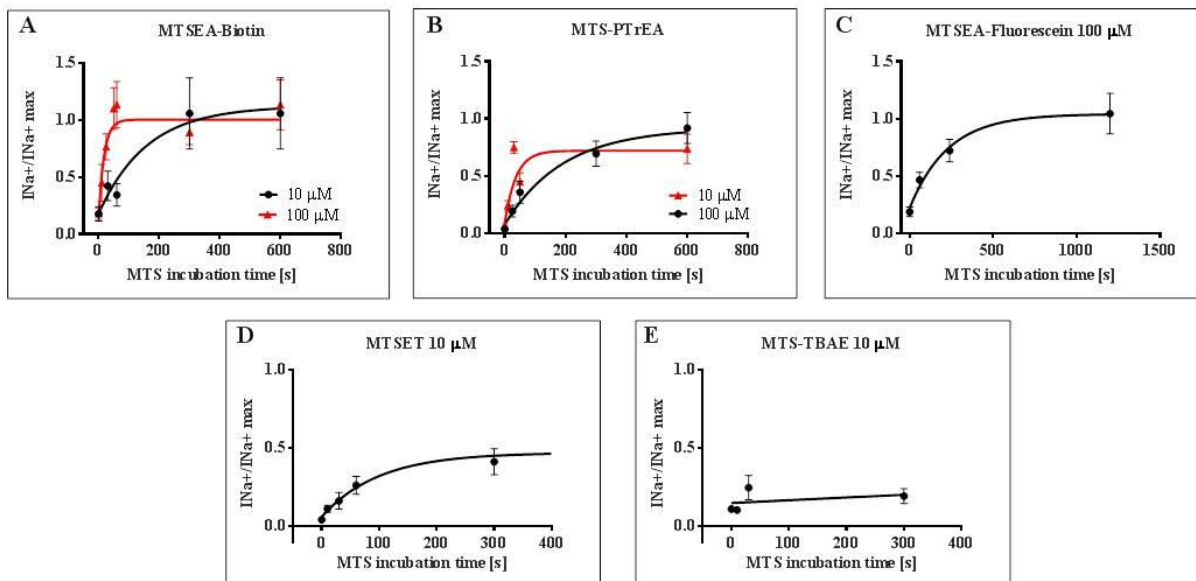
Figure 31 Kinetics of accessibility of MTS to C426. *A,* MTSEA-biotin at 10 and 100 μM, in black (n=7) and red (n=7), respectively. *B,* MTS-PTrEA at 10 and 100 μM, in red (n=8) and black (n=8), respectively. *C,* MTSEA-fluorescein at 100 μM (n=6). *D,* MTSET at 10 μM (n=6). *D,* MTS-TBAE at 10 μM (n=5). I_{Na+} are normalized on the maximum I_{Na+} that is the condition without MTS and without BMOE. Symbols are mean ± SEM.

The graphs on the Figure 31 represent the current recovery from the BMOE block of Y426C ($I_{Na+}/I_{Na+\ max}$) in function of the MTS incubation time. Looking at the condition with 10 μM MTSEA-biotin (panel A, black curve): At time zero, BMOE inhibits Y426C currents. After 30 s of incubation in MTSEA-biotin, 45 % of the current is recovered. This indicates that BMOE is still able to block 55 % of the current, whereas the MTS-binding prevents the block of the remaining 45 %. After 300 and 600 s of MTS-incubation the curve saturates. The current recovery reaches is maximum ($I_{Na+}/I_{Na+\ max}$ equal to 1.0) with the absence of BMOE block, meaning no more cysteine available for crosslinking. With 100 μM of MTSEA-biotin, the current recovery is faster, with a saturation reached after 60 s of MTS-incubation. The current recovery in presence of MTS-PTrEA (panel B) is similar than MTSEA-biotin. However, the MTS-PTrEA does not lead to a complete current recovery. Indeed, 20 % of the current remains sensitive to BMOE. This suggests that MTS-PTrEA does not occupy all the available Y426C that are still crosslinked by BMOE. MTSEA-fluorescein also leads to the complete current recovery (panel C). The difference with the MTSEA-biotin is that the saturation is reached after a longer time (800 s). Increasing MTSET incubation time leads to the recovery of 50 % of the current (panel D). The small size of this MTS might explain its difficulty to find and interact with a residue that is located in a large vestibule. The MTS-TBAE is not able to prevent the BMOE block as shown

58

by the straight line connecting the points (panel E). It indicates that there is no current recovery after MTS-TBAE suggesting an absence of binding to Y426C.
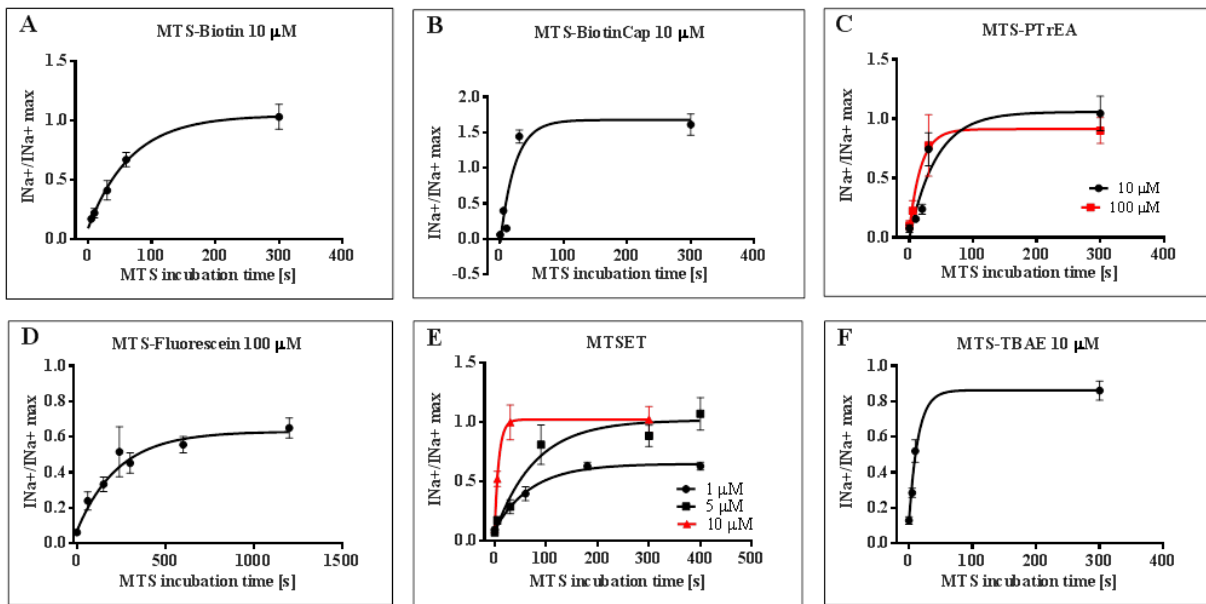
Figure 32 Kinetics of accessibility of MTS to G430C. *A,* MTSEA-biotin at 10 µM (n=10). *B,* MTSEA-biotinCAP at 10 µM (n=9). *C,* MTS-PTrEA at 10 µM (n= 9) and 100 µM (n=4), in black and red, respectively. *D,* MTSEA-fluorescein at 100 µM (n=17). *E,* MTSET at 1, 5 and 10 µM, black circle (n=3), black square (n=11), and red (n=4), respectively. *F,* MTS-TBAE at 10 µM (n=10). I_{Na+} are normalized on the maximum I_{Na+} that is the condition without MTS and without BMOE. Symbols are mean ± SEM.

The panels of Figure 32 represent the current recovery from the BMOE block of G430C after increasing MTS incubation times. In presence of MTSEA-biotin, MTSEA-biotinCap, as well as MTS-PTrEA, the current recovery is complete after 300 s (panels A to C). Incubation into MTSEA-fluorescein allows the recovery of 60 % of the current. 40% of the channels are still available for a block by BMOE after 1200 s. (panel D). 5 and 10 µM of MTSET lead to the complete current recovery after 300 s, whereas 1 µM recovers 50 % of the current from the BMOE block (panel E). MTS-TBAE leaves 20 % of current unrecovered (panel F).

Second order constants are then calculated (for details, refer at the section: Labeling with MTS reagents). k_2 values are similar for Y426C and G430C mutants ranging from ~1000 to ~7300 [$M^{-1}*s^{-1}$] and thus supporting a free access to both residues. The k_2 of MTSEA-fluorescein is smaller ~60 [$M^{-1}*s^{-1}$], indicating that the largest MTS has more difficulties to reach C426 and C430. However, looking more into details the Figure 31 and Figure 32 shows that neither MTSET nor MTS-TBAE is able to completely recover the current from the BMOE block of C426. Indeed, MTSET leads to a 50 % current recovery and MTS-TBAE 25 %.
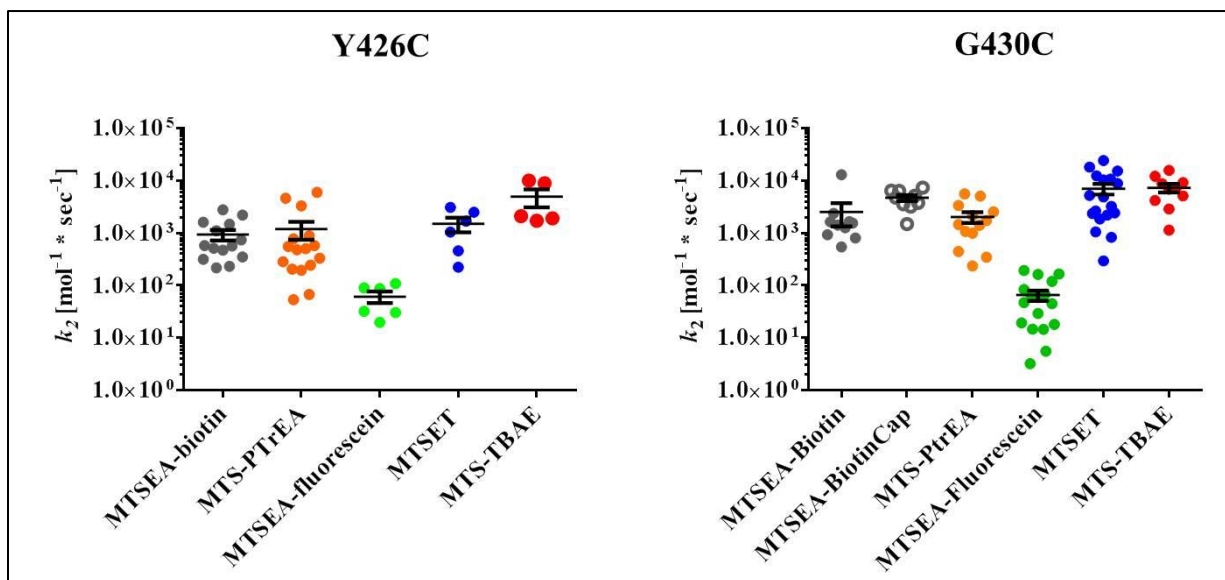
Figure 33 Association rate constants (k_2) of MTS for Y426C and G430C. *A,* Mean values for MTSEA-biotin, -PTrEA, -fluorescein, MTSET and MTS-TBAE are 938 ± 212 (n=14), 1193 ± 463 (n=16), 61 ± 16 (n=6), 1497 ± 463 (n=6) and 4937 ± 1864 (n=5) [$M^{-1}*s^{-1}$], respectively. *B,* Mean values for MTSEA-biotin, -biotinCap, -PTrEA, -fluorescein, MTSET and MTS-TBAE are 2516 ± 1174 (n=10), 4694 ± 625 (n=9), 2033 ± 475 (n=13), 66 ± 15 (n=17), 7066 ± 1617 (n=18) and 7344 ± 1387 (n=10) [$M^{-1}*s^{-1}$], respectively. Results are mean $\pm$ SE.

These competitive experiments for the binding of MTS to Y426C and G430C indicate that the extracellular vestibule can accommodate MTS-reagents as bulky as the MTSEA-fluorescein. This binding prevents the BMOE current block without interfering with the Na$^+$ flux. The association rate constants of the MTS to Y426C and G430C are equivalent and do not support a correlation between the MTS-shape and the localization of the residue. In most cases, this binding modifies the pH dependency of the activation leading to a channel that opens at less acidic pH. The pH dependency of the inactivation is also changed but in a less extent.

2.3.   Biochemical evidence of methanethiosulfonate reagents binding

These observations support that large ligands are able to coordinate C426 or C430 residues into the vestibule. This is further supported by biochemical experiments using a pull-down assay of MTSEA-biotin-modified ASIC on streptavidin beads.
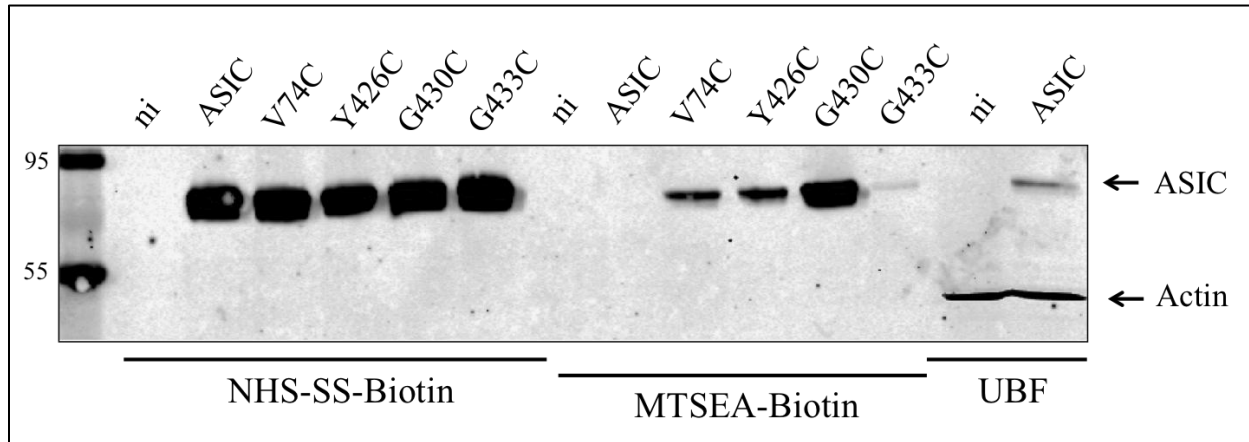
Figure 34 SDS-PAGE and western blot analysis of the streptavidin-bound fractions from NHS-SS-biotin or MTSEA-biotin labeled hASIC1a wt and mutants oocytes. n=40 oocytes/condition (2 batches), ni = non-injected oocytes. n=5 independent experiments. Anti-His and anti-actin antibodies are diluted 1/1000 before use.
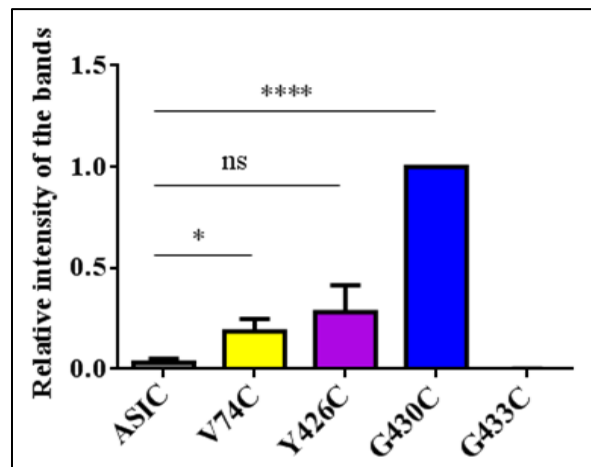
Figure 35 Quantification of the pull-down with MTSEA-biotin. The MTSEA-biotin labeled proteins are expressed in function of the surface expressed channels (MTSEA-biotin/NHS-SS-biotin). Then, to compare binding efficacy between mutants, we normalize regarding to G430C binding signal plotted as equal to 1. n=5 (n=2 for G433C). Unpaired Student T-test: * stands for $P = 0.456$, ns for $P = 0.1026$ and **** for $P = 0.0001$. Results are mean ± SD.

We compare the binding of MTSEA-biotin on residue V74C, Y426C, G430C or G433C to the wt. MTSEA-biotin binds most efficiently to G430C, with almost the same signal for cell surface expressed channels and MTSEA-biotin labeled channels. Therefore, we use it for normalization.

Next, we catch significantly more V74C (20%) than the wt. Regarding Y426C, there is only a tendency but the absence of significance is likely due to the high variability between experiments. Functionally, MTSEA-biotin is able to recover 100% of the Y426C BMOE block (Figure 31). However, the pull-down assay shows that only ~30% of Y426C channels expressed at the cell surface are caught by the streptavidin beads. There are two possibilities to explain this value; first, not all the channels are modified. And second, the streptavidin is less efficient to interact with MTSEA-biotin-modified Y426C than with MTSEA-biotin-modified G430C. Given that the MTSEA-biotin recovers 100% of the Y426C BMOE inhibition, I would support the second hypothesis.

2.4. Amiloride block of MTSEA-biotin-modified channels

Because MTS-reagents bind in the ECV without blocking the Na^+ flux, we wonder if the pore blocker amiloride would still reach its binding site in the middle of the TM2 (αS583, βG537 and γG525 on ENaC). In our laboratory, we have observed that mutation of the corresponding glycine into alanine on hASIC1a (G440A) completely disrupts the inhibition (see Appendix, Amiloride dose-response curves). To assess whether the MTS impaired the access to G440, we have performed dose-response analyses of G430C mutant channels, pre-treated either with, MTSEA-biotin, MTS-TBAE, or MTSEA-fluorescein (Figure 36).
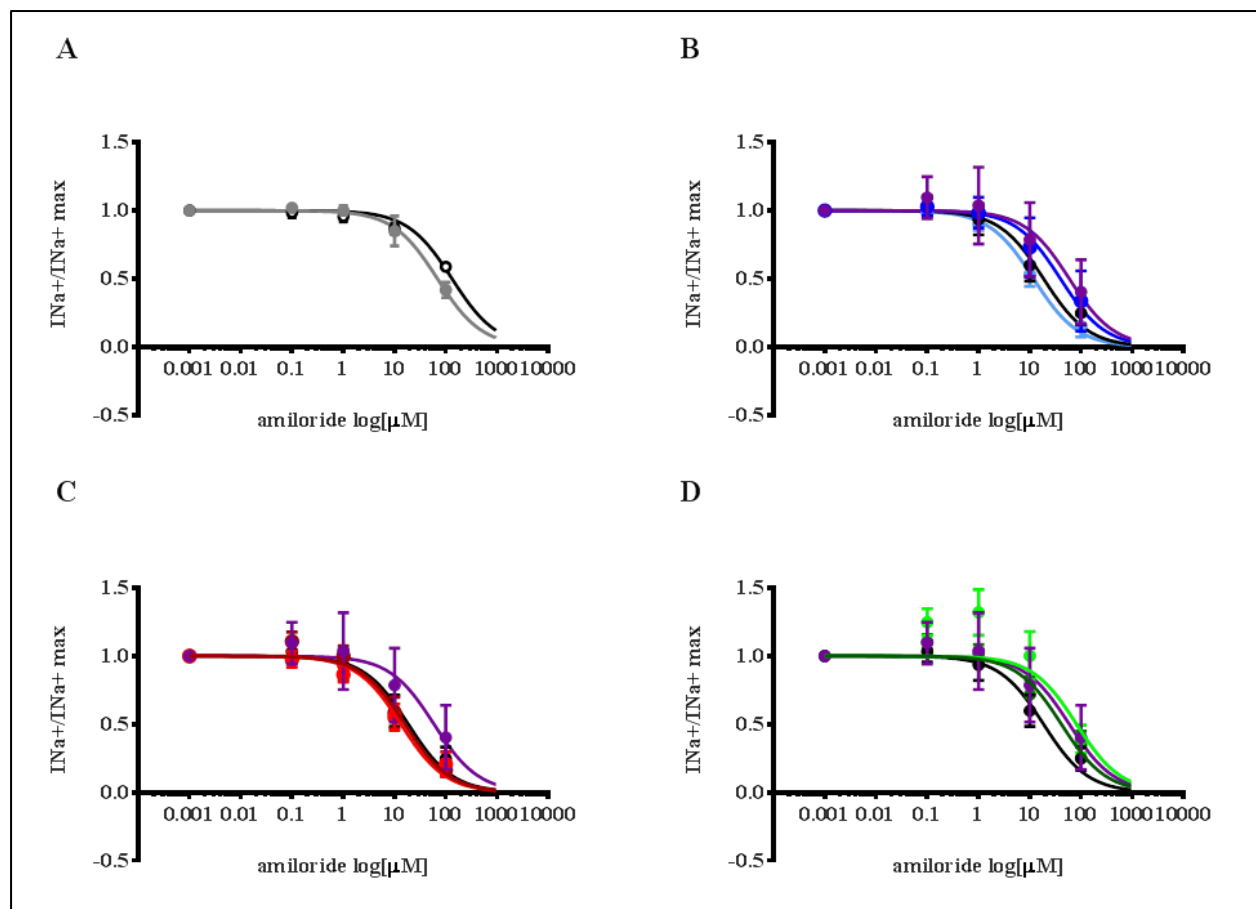
Figure 36 Amiloride dose-response curves. *A,* hASIC1a with or without MTSEA-biotin (1 mM, 5 min) in grey (n=4) and black (n=4), respectively. *B,* G430C treated with MTSEA-biotin (1 mM, 5 min) or MTSEA-biotin + BMOE are in dark (n=23) and light blue (n=6), respectively. *C,* G430C treated with MTS-TBAE (1 mM, 10 min) or MTS-TBAE + BMOE are in red (n=6) and brick (n=5), respectively. *D,* G430C treated with MTSEA-fluorescein (10 mM, 5 min) or MTSEA-fluorescein + BMOE are in light (n=6) and dark green (n=6), respectively. *B-D,* BMOE-treated oocytes are represented in black (2 mM, 5 min, n=12). Non-treated G430C expressing oocytes are depicted in purple (n=20).

The presence of MTS does not impair the amiloride block. Indeed, the blocker is still able to reach its binding site in the transmembrane domain. Statistical analysis shows a significant difference between the amiloride affinity of the G430C mutant and the wt (IC$_{50}$ of 59.07±10.99 and 132.40±11.84 µM, respectively, *P*<0.0001). These values support that the engineered cysteine 430 increases the affinity of the amiloride for ASIC. To assess the impact of MTS binding on the block efficacy, we compare untreated to MTS- and BMOE-treated oocytes. While unmodified channels are blocked, we only take notice of the MTS-modified channels being still functional. In this way, we point out that neither MTSEA-biotin (11.90±1.05 µM), MTS-TBAE (15.97±2.36 µM) nor MTSEA-fluorescein (41.45±6.69 µM) decrease the amiloride affinity for G430C mutant channels. The sensitivity of G430C is even increased after modification with

MTSEA-biotin, MTS-TBAE and MTSEA-fluorescein ($P=0.0011$, $P<0.0001$ and $P=0.0011$, respectively).

In conclusion, these experiments indicate that thiol modifying reagents of different shape and size are able to modify cysteines introduces at positions Y426 and G430. The increased affinity of Y426C and G430C for Cd^{2+} indicates that these residues are accessible for a cation of similar size than Na^+. This observation supports that both of these cysteines line the ion permeation pathway. The current block by BMOE shows that Y426C and G430C are accessible to a bifunctional crosslinker of 8 Å-length. The binding of BMOE induces an inhibition of the current, suggesting that the modified channel is blocked in a closed conformation. Accessibility experiments with MTS-reagents of different shape show the MTS-binding into the ECV. These bindings prevent neither the Na^+ nor the amiloride to flow through the pore. The interaction of most tested-MTS with Y426C and G430C even increases the I_{peak} and shifts the pH dependences of activation and inactivation towards more alkaline pH, and leads to a partial desensitization. Furthermore, MTS-reagents increase the affinity of G430C channels for the pore blocker amiloride.

3.   Contributions

I have generated the ASIC constructs, as well as I have transcript and expressed them into *Xenopus laevis* oocytes. I have done the whole biochemistry experiments and the electrophysiological analyses with the help of Ivan Gautschi. I have made the size exclusion chromatography and the blue native gels. Miguel van Bemmelen has done the experiments with CHO cells. Concerning the bioinformatics section, Dr. Simon Bernèche and Dr. Justyna Iwaszkiewicz (Molecular Modeling Group, Swiss Institute of Bioinformatics, Lausanne) have provided us with the trimeric structure of cASIC1 and done the MTS docking.

ENaC

The side project focuses on the description of a novel Ser243Pro mutation in the αENaC subunit associated with a transient AR-PHA1.

At birth, a premature boy (32 weeks of gestation) was hypotonic and had feeding problems. 16 days after birth, he suffered from severe hyponatremia, hyperkalemia as well as mild metabolic acidosis, and both his plasma renin activity and his aldosterone level were high. Moreover, his urinary ratio Na^+/K^+ was four-fold too high. The boy did not present any respiratory distress nor any excess of Cl- in the sweat. Thanks to NaCl supplementation and cation-exchange resins, the patient improved (normal levels of Na^+ in the serum and normal Na^+ excretion) and the treatment stopped at 6 months of age. Altogether these symptoms supported a severe salt-losing syndrome and suggested a pseudohypoaldosteronism of type 1 (PHA1). The symptoms being restricted to the kidneys, clinicians opted for an AD-PHA1 and sequenced the mineralocorticoid receptor (MR) gene. The absence of mutation made them investigate the trail of ENaC genes and the AR-PHA1 even if the symptoms were not multi-systemics. Thus they discovered a missense mutation in the in the αENaC subunit leading to the replacement of the Serine 243 by a Proline.

We have performed the characterization of αSer243Proβγ channel function, *in vitro*, by expressing it in *Xenopus laevis* oocytes, the results are reported in the paper named: "A homozigous missense mutation in SCNN1A is responsible for a transient neonatal form of pseudohypoaldosteronism type 1" (Appendix, A homozygous missense mutations in SCNN1A is responsible for a transient neonatal form of pseudohypoaldosteronism type 1).

Traces of ENaC-mediated Na^+ current (I_{Na+}) are obtained by rapidly changing the perfusion solution from a Na^+-depleted to a 120 mM Na^+ containing solution. This leads to a I_{Na+} characterized by a large peak (I_{peak}) followed by a relaxation and then a steady state current (I_{ss}). The relaxation is a physiological inhibitory response of the channel to extracellular Na^+ ions, known as self-inhibition (for details, see ENaC Regulation). Qualitatively, both wt and mutant channel display similar I_{Na+}. However the quantity is different; currents are decreased in the αS243Pβγ ENaC by 30 % compared to wt channels (Figure 37, A and B) and an impaired cell surface expression does not account for this lower activity (Figure 38).
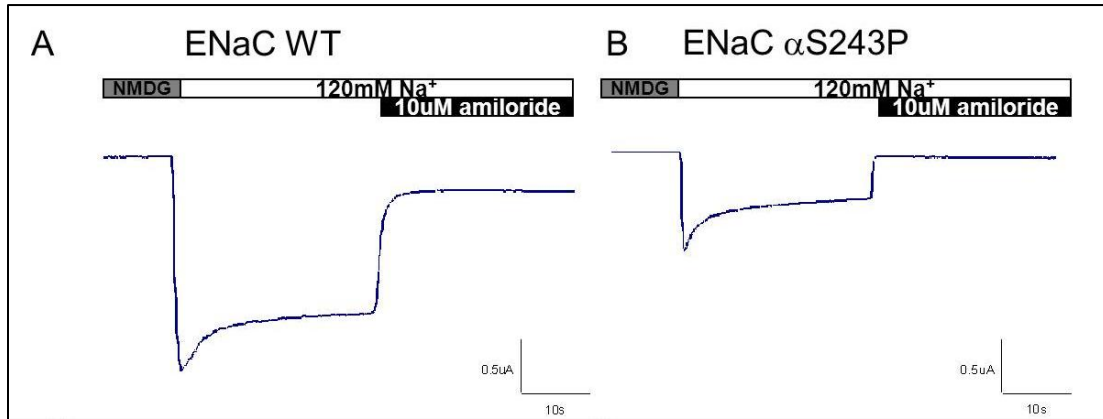
Figure 37 ENaC mediated Na$^+$ currents in oocytes expressing ENaC wild type (WT) and ENaC αS243P mutant. A and B. Representative recordings of amiloride-sensitive Na$^+$ current in oocytes expressing ENaC wild type (WT αβγ) and ENaC αS243Pβγ mutant.
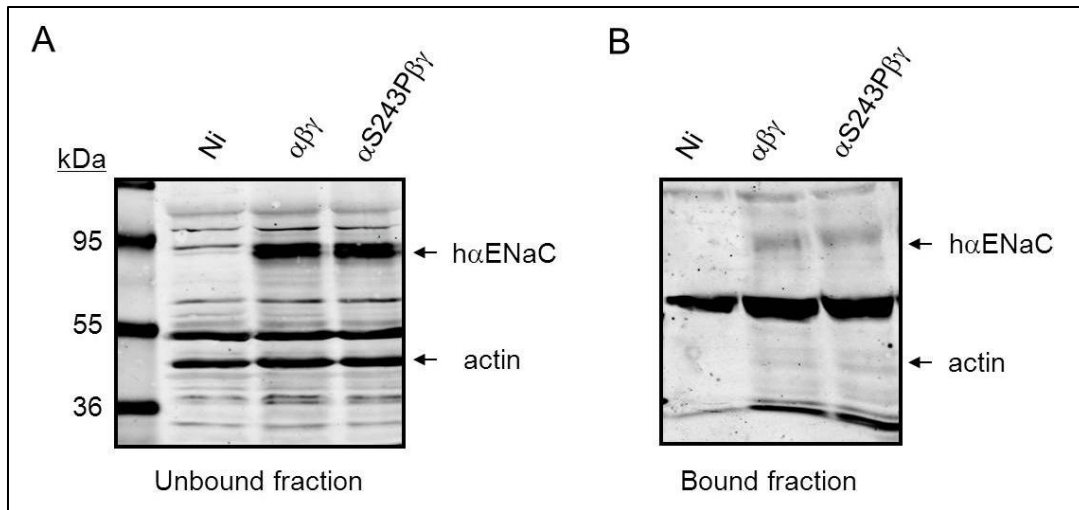
Figure 38 Surface expression of ENaC wild type (WT) and αS243P mutant. A. Western blot using anti-α ENaC and anti-actin antibodies of the unbound fraction to streptavidin beads (non biotinylated fraction) of total proteins from oocytes expressing ENaC wild type or the αS243P mutant. B. Similar Western blot of the biotinylated fraction of total proteins bound to streptavidin beads representing the surface expression of αENaC wild type and mutant.

In the introduction, I mentioned that the Na$^+$ ion regulated ENaC function. Thus, we challenged the channel with different concentration of extracellular Na$^+$. We compare currents of oocytes incubated either in a low (10 mM) or in a high Na$^+$ medium (85 mM). ENaC being constitutively open, both extracellular and intracellular contents of Na$^+$ will be the same. In response to an increase in intracellular Na$^+$ load, I$_{Na+}$ decreases in order to prevent an excessive accumulation of Na$^+$ that would be toxic for the cell. It appears that the response of αS243Pβγ is exacerbated compared to the wt channels with an 80 % stronger diminution of the I$_{ss}$ (Figure 39, C and D). This supports an impaired "feedback inhibition".
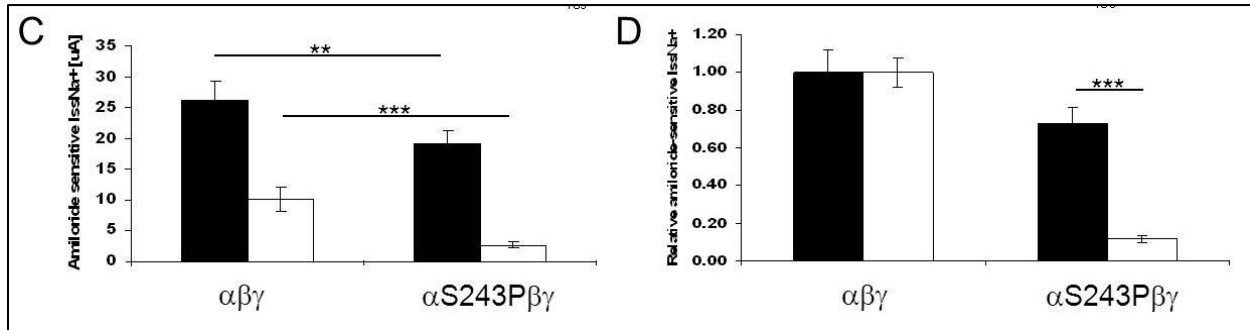
Figure 39 ENaC mediated Na$^+$ currents in oocytes expressing ENaC wild type (WT) and ENaC αS243P mutant. C. Absolute amiloride-sensitive steady state Na$^+$ currents measured in oocytes incubated for 24 hours (see methods section of the article in the Appendix) in a low Na$^+$ containing solution (filled bars, n=12 experiments) and in a high Na$^+$ solution (open bars, n=8 experiments). Oocytes expressed either αβγ wild type or αS243Pβγ mutant. ** denotes $P<0.01$, *** denotes $P<0.001$. D. Relative changes in the ENaC mediated amiloride-sensitive current in oocytes expressing the αS243Pβγ mutant relative those expressing ENaC αβγ WT, after incubation in a low Na$^+$ containing solution (filled bars) and in a high Na$^+$ solution (open bars). *** denotes $P<0.001$.

A second mechanism involving the Na$^+$ and known to modify ENaC activity is the "self-inhibition". To measure it, we calculate the ratios I$_{ss}$/I$_{peak}$ of wt and mutant channels. We observe that it is apparently slightly stronger for the αS243Pβγ (Figure 40).
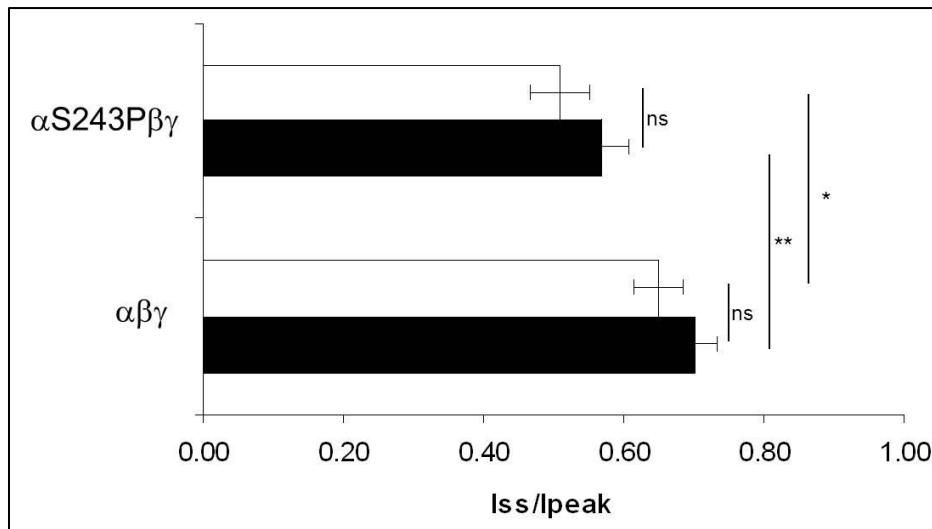
Figure 40 ENaC self-inhibition of the wild type (WT) channel and the αS243P mutant. Channel self-inhibition was defined as the ratio of the steady-state current (Iss) measured after 20 seconds over the peak current (Ipeak) (see Fig. 2A and 2B). Filled and open bars denote respectively low and high Na$^+$ incubation conditions. Iss/Ipeak ratio was for the αS243Pβγ and the WT 0.57 ± 0.04 and 0.70 ± 0.03 respectively ($P<0.05$, Student's T-test, n=12), and 0.51 ± 0.04 versus 0.65 ± 0.04 ($P<0.01$, Student's T-test, n=8).

The parents being heterozygotes, we compared the I$_{Na+}$ of αβγ, with ααS243Pβγ (0.5:0.5:1:1) and αS243Pβγ channels. We observed that the magnitude of the ααS243Pβγ current was intermediate (40 % decrease) to that of the wt and the mutant channels. The parents being

heterozygotes and asymptomatic, this suggests that a reduction of 40 % is tolerated and without any consequence for the maintenance of Na^+ homeostasis.

Finally, we wondered if the decreased I_{Na+} could be due to an impaired regulation by serine proteases. To assess it, we applied trypsin externally and measured the change in I_{Na+}. For both wt and mutant channels, independently of the low or high Na^+ load, the trypsin increased by two-fold the currents, indicating that this mechanism of regulation was retained.

To summarize our results, the mechanisms of regulation implying Na^+ are impaired in this premature boy; namely, the "feedback inhibition" and the "Na^+ self-inhibition", leading to decreased ENaC activity and thus a severe salt-losing syndrome. Neither the expression of the channel nor its regulation by serine proteases is affected. Interestingly his brother, born at term and carrying the same mutation did not lose salt. This could be explained thanks to studies on newborn rabbits. Indeed, rabbits being born with immature kidneys they are representative for human kidneys of preterm babies. The immature kidneys do not have any significant Na^+ transport and no conducting ENaC channels (250,251). It is known that not only ENaC reabsorbs Na^+, but also other transporters located upstream; the Na^+,K^+,Cl^- co-transporter (NKCC2) and the thiazide-sensitive NaCl transporter (NCC). Salt-losing diseases distinct from PHA1 involve these transporters, namely the Barter and the Gitelman syndromes, respectively (67). We can hypothesize that NCC and/or NKCC2 are immature in the preterm kidney, leading to a too elevated Na^+ concentration in the distal part of the nephron where ENaC is expressed.

1.   Contributions

For this project, I have created the αS243P ENaC mutant using site-directed mutagenesis. I have done the *in vitro* transcription of α, β and γ ENaC cDNA, injected them into *Xenopus laevis* oocytes and performed all the electrophysiological, as well as the biochemical analyses.

Discussion/Conclusion

ASIC

1. Stoichiometry

We have demonstrated that the crosslinking of cysteines located in the C-terminal domain, the first transmembrane domain, and the extracellular vestibule of ASIC1a allows the covalent stabilization of ASIC1a subunit interactions and the subsequent identification of four distinct ASIC1a oligomeric states. These complexes weigh ~75, ~160, ~224 and ~304 kDa as determined by SDS-PAGE under reducing conditions and correspond to multiples of one ASIC1a oligomer (~75 kDa).

Independent from the ASIC1a construct used (native or engineered cysteines), the expression cell system (*Xenopus laevis* oocytes or CHO cells) and the crosslinker (NaTT, BMOE or formaldehyde), the estimated molecular weight of these complexes was highly reproducible. Moreover, optimizing the experimental conditions using an increased number of accessible cysteines or the amino-reactive crosslinker formaldehyde, led to the identification of the predominant ASIC1a oligomer expressed at the cell surface, which weighed ~310 kDa and corresponded to the expected mass of a homotetrameric ASIC1a channel. In the sections below, I present evidence that supports our theory that ASIC1a has indeed a tetrameric assembly and that the tetrameric structure we identify is not just a result of the crosslinking to a neighboring protein.

1.1. Crosslinked oligomers are homomultimers of ASIC1a subunits

Several observations from this research indicate that crosslinking leads to the stabilization of homomultimers of ASIC1a subunits rather than between two ASIC1a channels.

- The differences in mass between the four identified stabilized complexes correspond to the size of one subunit.
- The stabilization of the high molecular weight complexes depends upon the interaction of G433C with native cysteines of the TM1 (C59 and C61).
- The length of the BMOE ranges from 6 to 11 Å and given that G430C and G433C residues are located in the TM2, it is very unlikely that they form inter-channel crosslinking.

69

- The calculated masses of the four stabilized complexes were comparable from both solubilized and membrane bound ASIC1a, with clusters of channels unlikely to form from the solubilized form.

Thus, under our experimental conditions, we conclude that crosslinking only occurs between cysteines within the same homomultimeric channel complex expressed at the cell surface.

1.2. Stabilization of a predominant ASIC1a complex at the cell surface

We have shown that cysteines in the TM1, as well as in the C-terminal, are important for the stabilization of high molecular weight complexes. Using an ASIC1a channel with its native TM1 and C-terminal cysteines along with an engineered cysteine, increases the possibility of BMOE to stabilize a high molecular weight complex, allowing the stabilization of the predominantly homotetrameric complex observed for ASIC1a. The stabilization of the homotetrameric ASIC1a is further confirmed by the use of the formaldehyde. With both crosslinkers, the amount of tetrameric complexes identified by SDS-PAGE, increases while the quantity of smaller molecular weight complexes decreases, i.e. monomers, dimers and trimers.

1.3. The homotetramer and the literature

1.3.1. Crosslinking studies

Our results, which show the stabilization of a predominantly homotetrameric ASIC1a complex are in accordance with two previously published crosslinking studies. Zha *et al*., showed that the formation of a disulfide-bond with the oxidizing agent H_2O_2 and the crosslinking with sulfo-EGS allowed the stabilization of ASIC1a complexes expressed at the cell surface. By SDS-PAGE, they observed a migration pattern composed of monomers, dimers, trimers and higher-order ASIC1a oligomers that they interpreted as inter-channel complexes (233). Their identified oligomers migrated at sizes equivalent to ours, yet we have excluded the hypothesis of inter-channel crosslinking. Supporting the possibility of a four-subunit stoichiometry for ASIC1a, Coscoy *et al*., identified a tetrameric stoichiometry for another member of the ENaC/Deg family; the FMRFamide Na$^+$ channel (FaNaCh). Using photo-inducible and amino-reactive crosslinkers they obtained a similar pattern of migration on SDS-PAGE gels with four distinct oligomeric states corresponding to monomeric (74-82 kDa), dimeric (151-164 kDa), trimeric (205-230 kDa) and tetrameric forms (305-327 kDa) (221).

An additional study into ASIC1, based on the use of double cysteine mutants, demonstrated the presence of a disulfide bond between Y426C and G430C residues of adjacent subunits (252). On non-reducing SDS-PAGE, these disulfide bonds led to the stabilization of one single high-order molecular weight band of 190 kDa, which was reported as being a homotrimer based on the monomer size of ~60 kDa (252). This is different from the other crosslinking studies presented above, which revealed the presence of distinct oligomers, i.e. four different complexes (221) (233), In our experimental conditions, using single cysteine mutants and thiol reactive crosslinkers, we were unable to stabilize one single oligomer. This incomplete crosslinking could be perceived as a limitation of the technique, but on the other hand, it did enable us to count the number of subunits and estimate the molecular weight separating each complex.

1.3.2. Other biochemical and functional studies

In addition to the above described crosslinking studies, other methods have been employed to elucidate the stoichiometry of other members of the ENaC/Deg ion channels family. For ENaC, for example, methods have included the use of concatemers, the channels affinity for pore blockers, mutant constructs or biochemistry and most of these studies have supported the tetrameric oligomerization of ENaC made of 2α, 1β and 1γ subunits (220,222,223,227).

1.3.3. Crystal structures

The crystal structures of the C-terminal truncated chicken ASIC1 (cASIC1) revealed a trimeric organization of the channel (201,203,228,234). These structures challenge previous studies, as well as our own, which support a tetrameric stoichiometry of ENaC/Deg members.

These discrepancies could be due to a number of structural aspects of these crystal structures. First of all, the construct used for crystallization was C-terminal truncated. As demonstrated in our study, as well as in the report by Zha *et al.* (233), cysteines found in this C-terminal region are crucial for subunit-subunit interactions and aid to prevent the dissociation of high molecular weight oligomers. Moreover, there is no distinction between cytosolic and cell surface expressed proteins with the crystallized cASIC1. Therefore, it would have been difficult to separate the functional from non-functional channels, the latter of which might have been incompletely assembled. For this reason, we stabilized and purified exclusively the cell surface functional full-length ASIC1a channels.

1.3.4. Alternative approaches

We have used alternative approaches to investigate the molecular weight of non-denatured hASIC1a complexes. Such an example is size exclusion chromatography, which estimates the size of a native complex, by measuring the time required for a protein to go through a column filled of porous polymer beads. Smaller proteins will have a longer path length and a subsequent longer retention time. This technique is generally used for the purification of a high volume of protein such as those required for structural studies; for instance, the purification of the beta-adrenergic receptor prior to its crystallization (253). The molecular weight of the beta-adrenergic receptor obtained by size exclusion chromatography was 120 kDa, whereas its theoretical predicted size was 46 kDa (253). The difference is attributed to the detergent, which can have a variable impact on molecular weight determination depending both upon the type of detergent used and the membrane protein. Thus, it is difficult to differentiate between complexes made of three or four subunits using this technique.

Another additional approach is the use of blue native gels, which allows the separation of native proteins with blue native polyacrylamide gel electrophoresis. Coomassie blue is a negatively charged dye that binds to protein, and therefore, the proteins electrophoretic mobility is determined both by the interaction with the dye and by the size and the shape of the protein (254). We have used this technique to investigate the oligomerization of the chicken ASIC1 channel construct used for the second cASIC1 crystal structure (234). For our research, the minimal functional construct (mfc) was kindly provided by Eric Gouaux (Vollum Institute, Oregon Health and Science University), which is a truncated chicken ASIC1 (cASIC1Δmfc) fused to a His_8_sGFP with a Thrombin cleavage site present in the sequence of the linker. We have used this blue native technique for two main reasons. Firstly, the channel stays under its native state. Secondly, proteins are detected because of the Coomassie blue, overcoming the unavailability of a chicken ASIC1 antibody. However, as this technique requires a higher amount of protein than SDS-PAGE, we decided to switch from *Xenopus laevis* oocytes to CHO cells, where we could obtain these higher volumes. Expressed in CHO cells, $H_8\_GFP\_cASIC1\Delta mfc$ produces functional ASIC1 channels. After purification on Ni^{2+}-beads the ASIC1 complex was treated with or without thrombin and run on a blue native gel. The cleaved cASIC1Δmfc complex migrated at a molecular weight higher than 240 kDa (n=1), but it was difficult to distinguish a trimer from a tetramer, with insufficient resolution between bands corresponding to 242 and 480

kDa. Thus, we turned to another protocol, the Oligomerization Characterization by Addition of Mass (OCAM). The principle of this is to expose the native H_8_GFP_TCS_cASIC1Δmfc complex to thrombin, and depending of the time of exposure, different cASIC1 complexes would be observed on the gel, i.e. those having none, one, two, three or more added His_8_sGFP.
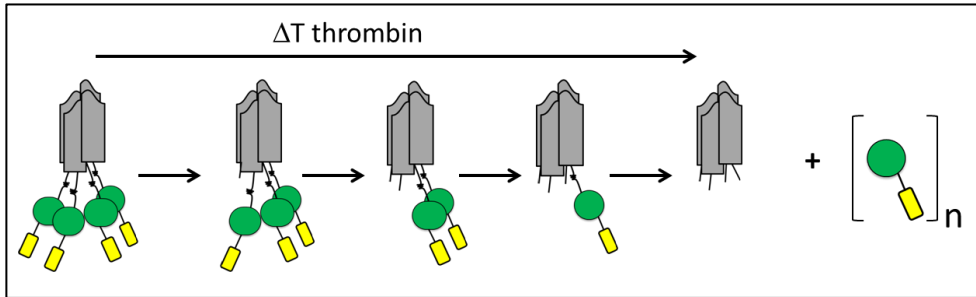
Figure 41 Scheme of the OCAM.

As cleaved His_8_sGFP has a fixed mass of 27 kDa, the cleaved complexes would have, depending on digestion time, different weights, which should easily be separable on a gel. In theory, the number of subunits constituting the channel would be deducible and thus the number of homologous subunits that constitutes the ASIC1 channel complex could be directly determined. In practice, however, we could not obtain the required resolution to distinguish between cleaved complexes. This could be due to the degradation of the protein leading to smeary bands, or to the insufficient quality of our home made gradient gels. Either way, we stopped our OCAM investigations to pursue more reliable techniques.

2.   Functional characterization of the extracellular vestibule size

To functionally evaluate the size of the ECV, we tested the accessibility to specific residues mutated in cysteines (V74C, Y426C and G430C) for ligands of different shapes and sizes. The binding of a bulky ligand to one of these cysteines would suggest a large extracellular vestibule, whereas an absence of binding would indicate that there is not enough space to accommodate such a reagent. Starting with Cd^{2+} and BMOE, we then investigated the binding of methanethiosulfonate reagents into the vestibule. Both Cd^{2+} and BMOE have an inhibitory effect on ASIC1a mutants, whereas MTS activates them. Detailed results regarding these aformentioned ligands are discussed below.

73

2.1. Accessibility for Cd^{2+}

The small ligand Cd^{2+} has a similar radius to the permeate Na^+ ion, and is therefore a useful indicator to study ASIC1a permeation. Cd^{2+} can be coordinated by sulfhydryl groups, as well as negative residues, such as glutamate or aspartate. V74C channels are irreversibly blocked by the Cd^{2+}, whereas Y426C and G430C channels show an increased sensitivity to Cd^{2+}. In the three cases, our results support that the Cd^{2+} is able to access and modify the cysteine residues.

Baconguis *et al*., have shown that V74C residues move between two conformational states, from 7 Å at an acidic pH, to 12 Å at pH 7.25 (201). In our experiments, we have shown that a disulfide bond between two V74C residues makes the V74C mutant channel non-functional. This loss of function supports the requirement of an increased distance between two V74C residues for opening. Indeed, the full activity of V74C channel is restored upon extracellular reducing treatment with DTT. Therefore, a dynamic constraint on V74C channels (either with the coordination of Cd^{2+} or with a disulfide bond) might interfere with the activity of the channel and thus maintain it in a closed conformation.

In collaboration with the Swiss Institute of Bioinformatics (SIB, Lausanne), we have simulated the docking of Cd^{2+} in the extracellular vestibule of the V74C channel. As depicted in Figure 42, distances from the thiol group to Cd^{2+} are about 3.5 Å. The analysis of high-resolution PDB files with Cd^{2+} coordination has shown that distances range from 2 to 2.6 Å between the sulfhydryl atom and the Cd^{2+}. Taking into account that the resolution of the crystal structure is about 3 Å, the coordinated distances are plausible.
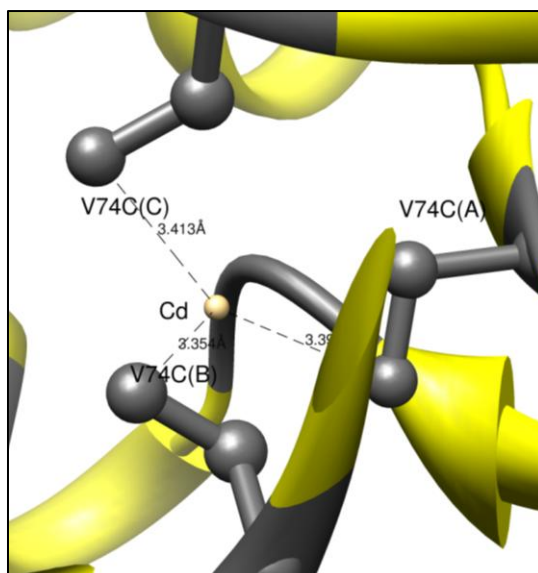
Figure 42 Cd^{2+} docking on V74C. Side chains of the V74C residues are depicted with the sticks and balls, ribbons are in yellow.

We can rule out that the increased Cd^{2+} affinity to Y426C and G430C is due to coordination by two Y426C or two G430C as pairing residues 10 and 15 Å apart with Cd^{2+} is impossible. Thus, the observed increased affinity could be attributed to coordination between the engineered cysteine and a nearby negative residue. D434 and E427 being at 6 and 4.7 Å from G430C, respectively, are the closest putative candidates. It is difficult to explain the Cd^{2+} coordination on the desensitized crystal structure. Indeed, Y426 and G430 are too far apart and the distance does not decrease in the open state. Indeed, the two open state crystal structures of PcTx1-cASIC1 (Baconguis (pH5.5) and Dawson) pointed out that the distance between the side chains of V74 (V75 in the cASIC1) increases from 7 to ~11 Å, as well as the increase in distances observed between Y426C or G430C residues (201,203).

In conclusion, Cd^{2+} coordination requires a channel where candidate residues of distinct subunits (Y426C, E427, G430C and D434) become closer to each other. This might be possible by adding a fourth subunit.

2.2. Accessibility for BMOE

As previously shown (Crosslinking experiments with bismaleimidoethane), BMOE irreversibly decreases the activity of both the Y426C and G430C mutants but not of the V74C mutant. According to the distributor, BMOE has an 8 Å spacer length (Thermo scientific #22323). However, this can vary substantially, as has been demonstrated by a method based on

stochastic dynamic simulations, which gives new quantitative data on widely used crosslinkers. Briefly, this technique simulates the effect of a solvent on the conformation of molecules, and indicates that BMOE is able to crosslink residues separated by 6.3 to 10.5 Å (255). Desensitized structure analysis shows that there are 15 and 10 Å between two C426 and two C430 residues, respectively. As the resolution of this crystal is about 3 Å, a BMOE crosslinking between C426 (or C430) residues is conceivable. In the open-state structure of Baconguis, the measured distances between two Y426C or two G430C increases to ~18 and 12-15 Å. Thus, it is possible that BMOE prevents the enlargement of the extracellular vestibule. The lack of effect that BMOE has on V74C could be explained by the pre-existing disulfide bond.

2.3. Mechanism of block by crosslinking reagents

Together with the biochemical analysis (SDS-PAGE analysis of the crosslinked complexes), these functional (electrophysiological) experiments indicate that V74C, Y426C and G430C residues are accessible to an extracellularly-applied thiol ligand or reagent and that V74C forms spontaneous disulfide bonds in the extracellular vestibule of the functional channel. Cd^{2+} reacts with a cysteine and a negative amino acid, while BMOE reacts with two cysteines, both of which maintains the connected residues in a constrained distance impairing either the opening of the channel or the flux of ions.

2.4. Accessibility for methanethiosulfonate reagents

We do not know if BMOE blocks the ASIC1 channel by maintaining it in an inactive conformation or if because the size of the reagent physically prevents ions from passing. To test the possibility that ligand binding at Y426C and G430C inhibits ASIC1a by interfering with the flux, we used methanethiosulfonate reagents (MTS) such as MTSET, MTS-PTrEA, MTS-TBAE or MTSEA coupled to biotin or fluorescein. Given that MTS reagents have one reactive group, they will not constrain the channel in a non-conducting conformation. However, due to their size and shape, the reagents would still prevent ions to go through the channel.

We did not observed any block in the activity of the cysteine mutant channels, but there were several indications that MTS does bind the ECV:

- An increase in the peak currents was observed after incubation with MTS-reagents.
- There was a shift in the pH activation curves towards more alkaline values.
- MTS was responsible for the partial desensitization of Y426C and G430C.

- The observed competitive interaction of MTS with Cd^{2+} (and BMOE) for Y426C and G430C supports the specificity of the MTS-binding.
- Using a pull-down assay with streptavidin beads, we isolated MTSEA-biotin-labeled Y426C and G430C channels.

Because the ion flux is not decreased or inhibited by MTS, it indicates that Cd^{2+} and BMOE interfere with the conformational rearrangement occurring at channel opening as opposed to interference of the ion flux.

2.4.1. Shift in the $pH_{0.5}$ of activation

Upon MTS binding we observed a shift in the pH activation curve leading to a channel that opens at more alkaline value. Each of the above mentioned MTS have different characteristics, such as size and shape. The extent of the shift in the pH activation curves varies according to the reagent. The size order of the reagents is as follows: MTSEA-fluorescein < MTS-TBAE < MTSEA-biotin < MTSET < MTS-PTrEA, but there was no correlation between the size and the shift for either of the mutants.

A study investigating pore opening mechanisms on Y426C and G430C residues of mouse ASIC1 (252) also demonstrated that G430C was accessible to a positively charged MTS, such as MTSET, and that its binding induced a shift in the pH of activation curve, which is in line with our work. Moreover in this study carried out by Tolino *et al.*, MTSET promoted the sustained opening of the channel when perfused at pH 7.0. They also showed the induction of MTSET-dependent sustained currents for Y426C mutant channels, but we were never able to observe this in our study. We did observe a sustained current following the I_{peak} when we opened the channel by switching from pH 7.8 to 5.5, but, not with pH 7.0 solution supplemented with MTSET as they did. Tolino *et al.* argue that the opening of the modified channel occurs *via* a steric repulsion between the G430C-MTS and the side chain of Y426 initiating thus a conformational rearrangement of the TM2 and pore gating (252).

Another report by Li *et al.* described the accessibility of TM2 residues in the lamprey ASIC1 (256). MTSEA was perfused either from the extracellular or the intracellular side, in both the open and the closed conformations. Accessibility of residues varies according to the state and the perfusion site enables them to show the movement of the TM2 from an open to a closed state. They demonstrated that in both conformations there was a narrowing of the pore. In the open

conformation, the narrowing is located midway of the TM2, whereas in the closed state it is at the external end of the pore. In accordance with our results, the G430C residue was accessible independently of the channel state (256).

In addition, the accessibility of Y426C for MTSET under both closed and desensitized states has also been confirmed (257). Similarly, we have shown a shift in the pH activation curve of Y426C in presence of MTSET supporting its binding.

Finally, investigations into the degenerin site of ASIC2 (G430 corresponding to G433 in the hASIC1a) have highlighted the accessibility of this residue for MTS reagents in the open state and its subsequent non-inactivating current. MTSET, as well as the bulky MTS-4-fluorescein reaches the middle of the TM2. These authors suggest that the modified residue would sterically hinder the rotation of the TM required to close the channel (258). We have tried, unsuccessfully, to modify hASIC1a G433C with MTSET in both conformational states. The reason may arise from the difference in ASIC subtype. Indeed, we are currently working on the ASIC1a, whereas they have used the ASIC2 subtype.

2.5.   Docking of methanethiosulfonate reagents

To visualize the binding of MTS-reagents to C426 or C430 residues, we have performed docking analyses in collaboration with the SIB using AutoDock Vina (259) and SwissDock (260). We added two constraints: the reactive part of the MTS has to point towards the free SH group of the cysteine and a disulfide bond ranging from 2.5 and 3.5 Å. We only included results with a reasonable distance between each reactive part (the SH of the cysteine and the reactive part of the MTS). With these parameters, Justyna Iwaskievicz (SIB) docked each MTS into the extracellular vestibule of both Y426C and G430C mutants. Below are the closest distances obtained between the reactive part of the MTS and the free cysteine. Given that docking distances of Y426C and G430C display similar results, illustrations and discussions presented below are on for the G430C mutant.

	Y426C	G430C
MTSEA-Biotin	4.18 Å	3.93 Å
MTSEA-BiotinCap	4.83 Å	3.74 Å
MTS-PTrEA	3.89 Å	3.44 Å
MTSET	4.30 Å	3.40 Å
MTS-TBAE	3.87 Å	3.56 Å
MTSEA-Fluorescein	4.99 Å	5.30 Å

Table 4 Distances between engineered cysteines and MTS-reagents. Distances are expressed in Å.

The docking of MTSEA-biotin on the crystal structure is depicted in the Figure 43. The whole view of the channel highlights one of the putative entrances for MTS (red arrow) (228). To assess the size of these lateral fenestrations, we used the program ghecom (261), which takes advantage of a pocket detection algorithm covering the proteins with a 3D grid and indicating empty grid points defined as pocket if they satisfy a number of energetic and geometric conditions (261). This program indicated that the size of a lateral fenestration is about 7 to 10 Å. The sliced view below, illustrates that this compound fills the extracellular vestibule close to residue 430. Indeed, the MTSEA-biotin (blue) is located in the middle of the vestibule as a plug that hides the pore.
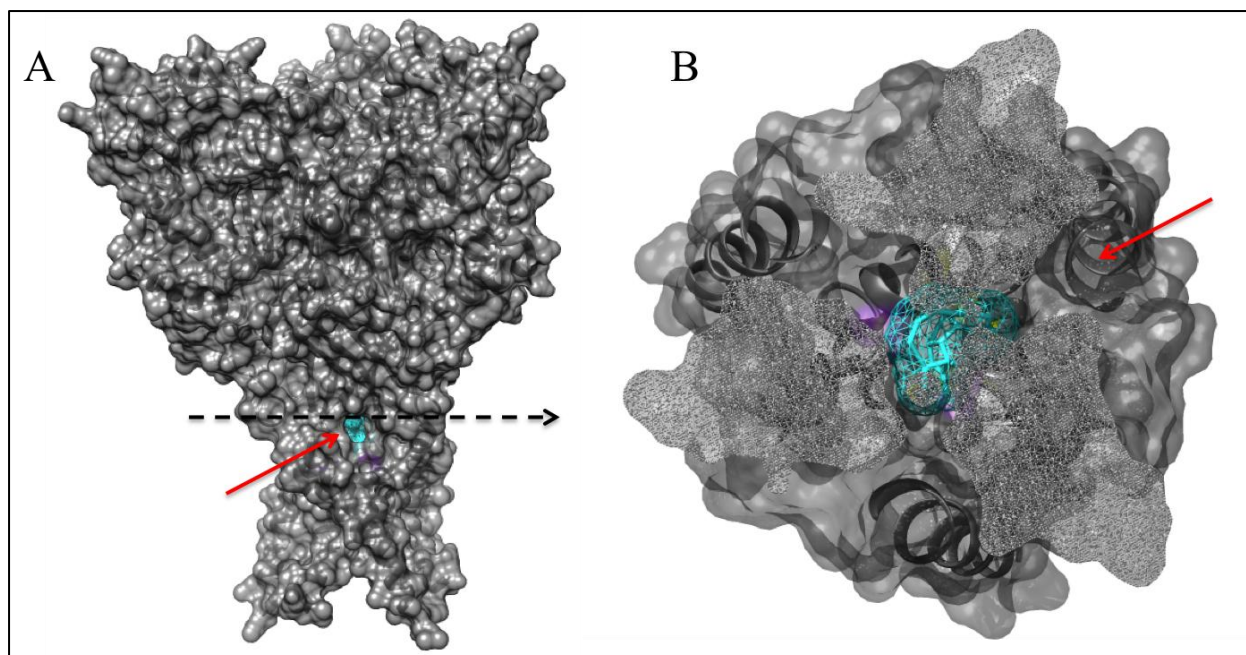
Figure 43 Docking of MTSEA-biotin on the desensitized cASIC1 crystal structure. *A,* Whole view of cASIC1. *B,* Sliced view. The dotted arrow indicates where the channel is sliced. MTSEA-biotin is in blue, G430C in purple and lateral fenestrations are highlighted by the red arrows.

Docking of MTSEA-biotinCap, MTS-PTrEA, MTSET and MTS-TBAE have shown that the extracellular vestibule can accommodate MTS of different shapes and sizes (Figure 44). In addition to the extracellular vestibule, the -biotinCap (in purple) also fills one of the lateral fenestration with its long tail (A). MTS-PTrEA and −TBAE are restricted to the vestibule, in orange (B) and red (D), respectively. The smallest reagent, MTSET, in blue, does not fill the whole vestibule (C). MTSEA-fluorescein is too large to pass through the fenestration and to be accommodated in the vestibule.

We have compared the binding of MTSEA-biotin to Y426C at both alkaline and acidic pH and it appears to be unchanged. This means that even under a desensitized conformation MTSEA-biotin is able to go through the lateral fenestration and reach its binding site.
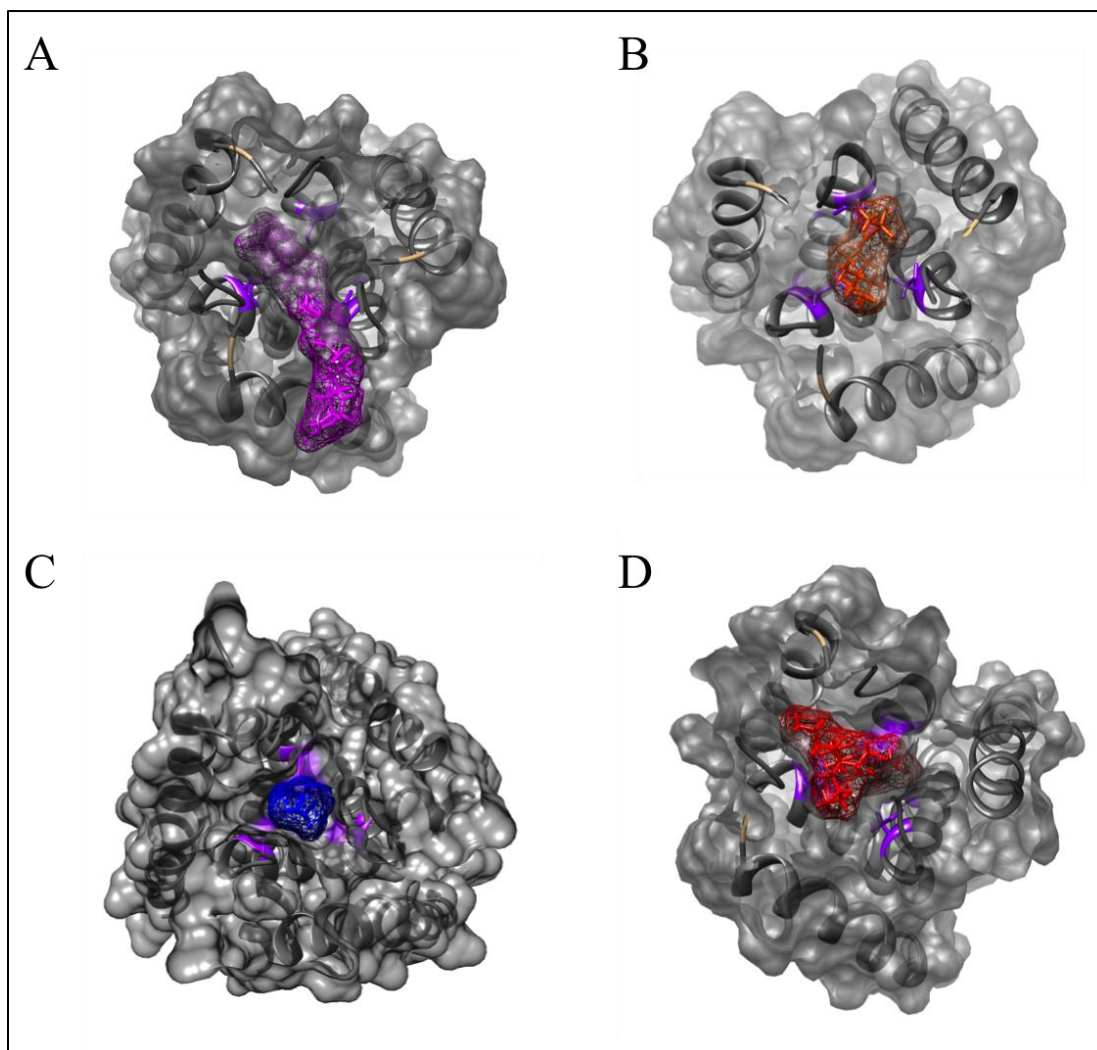
Figure 44 *A-D,* Clipped views of the MTSEA-biotinCap in pink, MTS-PTrEA in orange, MTSET in blue and MTS-TBAE in red, dock on the desensitized cASIC1 crystal structure. G430C is depicted in violet.

In conclusion, these docking experiments illustrate that MTSEA-biotinCap, MTS-PTrEA, MTSET and MTS-TBAE can be accommodated by the ECV. Given that the MTS reagents fill the vestibule, it is difficult to conceive that this binding does not prevent the Na$^+$ flux.

2.6. Association rate constants

As we have clear indications that MTS-reagents do bind the channel, we estimated the association rate constants of these MTS with Y426C and G430C. Specifically, we investigated the accessibility kinetics of MTS to the engineered cysteines of the ECV. Association rate constants range from ~1,000 to ~7,000 $[M^{-1}*s^{-1}]$ independently of the mutant and without any significant difference between compounds, excluding the bulky MTSEA-fluorescein, which displays a lower constant (60 $[M^{-1}*s^{-1}]$). Two main factors can influence this value: The

81

ionization of the sulfhydryl side chain and the steric hindrance (i.e., how difficult it is for the MTS to physically approach and bind the sulfhydryl group). Under our experimental conditions the ionization of Y426C and G430C are not expected to change, so, the parameter modifying the constant is the steric hindrance. It indicates that the bulky MTSEA-fluorescein has more difficulties to bind to Y426C or G430C compared to the smaller MTS-reagents. This suggests that the vestibule can accommodate the MTSEA-fluorescein but that there are some steric hindrances that increase the time required for modifying the cysteine.

Wagner *et al*. studied the GABA binding pocket for the MTSEA-biotin. They showed that a residue located at the mouth of the binding pocket presents a k_2 of ~250,000 [$M^{-1}*s^{-1}$], whereas another one in the deepest part of the pocket has a slower k_2 of ~120 [$M^{-1}*s^{-1}$] (262). The association rate constants that we have observed for the accessibility of MTS-reagents to Y426C and G430C are far from either of these extreme values. However, they are closer to the slower values (~120 [$M^{-1}*s^{-1}$]). This indicates that Y426C and G430C are localized in a somehow confined part of the channel, i.e. the extracellular vestibule.

2.7. Amiloride block of MTS-bound channels

MTS is docking onto Y426C or G430C, does not appear to perturb amiloride binding affinity. However, it is hardly to believe that an amiloride molecule of ~10 x 5 Å is able to weave past the MTS until its binding site located in the middle of the TM2 (G440). As we have been working with the desensitized cASIC1 crystal structure, we cannot rule out that the opening of the extracellular vestibule occurs during the activation of the channel, which would allow for the amiloride binding. To date, the conformation of ASIC1 during its natural open state is not known. Indeed, in the above-mentioned study by Baconguis and Dawson the open-state of ASIC1 is somewhat forced, by the binding of PcTx1, which may not be representative of the open conformation induced by protons. Moreover, PcTx1 binding leads either to a non-selective 10 Å pore at pH 7.25, or to a twisted pore as observed for the first non-functional N- and C-truncated crystal structure (201). Finally, the non-selective channel crystallized at pH 7.25 has almost fully lost its sensitivity for the amiloride. This absence of block further supports the fact that this open-state is not representative of the open ASIC1 conformation.

2.8.   Ion permeation pathway of the crystal structures

Several vestibules and cavities are present along the 3-fold axis of symmetry of the extracellular loop within each of the four ASIC1 crystal structures. At the level of the TM domains, the pathway seems close off. However, the presence of cations in each of the two PcTx1-cASIC1 structures is supported by two observations: firstly, there is an anomalous density feature with a cation trapped in the central vestibule (203) and secondly, there is an ion-binding site at the extracellular end of the TM1, near a lateral fenestration (201). Despite this, however, none of the crystal structures present an electron density feature consistent with the presence of cations in the pore. This goes against observations for other ion channel structures, which clearly show permeant ions and their interaction with pore lining residues. Examples of this include the KcsA K^+, the prokaryotic Cl^-, the Ca^{2+} Orai, or the ligand-gated GLIC channels obtained from soaked crystals in solutions (263-266).

The crystal structure models have been valuable for the interpretation of results obtained in the study of the biophysical properties of ASIC1, such as its activation and the desensitization. As mentioned before, Tolino *et al*., using double mutant analysis, have demonstrated that the tilting of the TM is necessary for ASIC opening (252). Furthermore, through accessibility screening of the TM domains, Li *et al.* have proposed that a narrowing in the external end of the pore is present in the closed state, whereas this narrowing moves further up the pore in the open conformation (256). Moreover, Adams *et al.* have further confirmed that the non-inactivation of deg site bulkier mutant was due to steric hindrance, which blocks the channel in an open conformation (258). None of these studies, however, are able to address the question of ASIC stoichiometry, or the structure-function analysis of the ECV, which requires a biochemical approach and cannot be studied using the crystal structure.

3.   Summary

In our study, we have focused on the structure-function of the extracellular vestibule of ASIC, by investigating the accessibility of the residues Y426C and G430C. We have shown that both residues line the ion permeation pathway (Cd^{2+} experiments) and have identified that larger crosslinkers (BMOE) are able to connect two Y426C (or G430C). This has been confirmed biochemically, by the stabilization of high molecular weight complexes corresponding to tetramers, and functionally, by the inhibition of channel activity. In addition, competitive experiments using MTS-reagents and crosslinkers have supported the binding of MTS to Y426C

and G430C. These MTS-bindings do not prevent the Na$^+$ flux or the amiloride block, which indicates that the ECV is able to accommodate large reagents without blocking the activity of the channel.

Our biochemical approach using crosslinking analysis of hASIC1a supports a homotetrameric organization of the channel. Moreover, our study into the structure-function of the extracellular vestibule suggests that an enlargement in this cavity occurs to allow for amiloride binding despite the presence of bulky MTS, which fills the whole vestibule. The addition of a supplementary subunit might increase the size of the extracellular vestibule, as well as the entire permeation pathway.

Previous studies into the stoichiometry of ENaC/Deg family members have employed either biochemical or electrophysiological techniques, but not a combination of the two, making our study innovative as it makes the link between the structure and function of ASIC1a channels.

- The crosslinking approach we have used focuses on functional ASIC1a expressed at the cell surface. The stabilization of the G433C mutant does not block channel activity and we specifically separate cell surface ASIC from that expressed in the cytosol.
- In the structure-function analysis of the extracellular vestibule, we have tested the accessibility of Y426C and G430C residues for MTS. Competitive interaction between MTS and BMOE allows us to distinguish MTS-labeled from unlabeled channels. Once labeled with MTS, Y426C and G430C are no longer blocked by BMOE. Thus we are certain that the recorded function represents the activity of MTS-modified channels.

We have then tried to interpret our results in function of the crystal structures. It appears that these structures can explain neither the high molecular weight complexes supported by the crosslinking approach, nor the docking of MTSEA-fluorescein in the extracellular vestibule, nor that the amiloride block is not prevented by the binding of the large MTS into the vestibule.

This study adds further evidence that the ion permeation pathway of this crystal channel might be constricted and suggests that:

- subunits have to be closer in order to explain the crosslinking data

- the extracellular vestibule has to be larger to accommodate the MTS-reagents without interfering with the Na^+ flux or amiloride block.

The addition of a supplementary subunit might explain how the tetrameric complex stabilized at the cell surface and our data on the structure-function of the extracellular vestibule.

ENaC

In our published case report, we have functionally characterized the mutation S243P discovered in the *SCNN1A* gene of a PHA1 patient. Our study demonstrated that S243 is involved in Na$^+$ sensing, with both feedback inhibition and Na$^+$ self-inhibition impaired in the αS243P$\beta\gamma$ ENaC channel. This leads to a channel with an exacerbated response to a high Na$^+$ load.

1. Self-inhibition

Several studies have aimed at localizing residues involved in self-inhibition. Vincent Bize demonstrated that both α and γ subunits were required (complementary results of (267) and published in his thesis), with both $\alpha\beta$ and $\beta\gamma$ lacking self-inhibition, but not $\alpha\gamma$ or $\alpha\beta\gamma$. Furthermore, Babini *et al.*, cloned a new ϵENaC subunit from *Xenopus leavis*. $\epsilon\beta\gamma$ channels are functional but display a slower self-inhibition that $\alpha\beta\gamma$. Using a chimeric $\alpha-\epsilon$ construct, they identified that the proximal part of the ECL controlled the speed of self-inhibition (268). Moreover, two specific histidines in the ECL of α and γ subunits (mouse αH282 and γH239 corresponding to human αH255 and γH233) have been implicated, with the mutation of these sites leading to a potentiation of, and a suppression of self-inhibition, respectively (269).

Localization of these residues on the homology model of $\alpha\beta\gamma$ENaC, which is based on the first cASIC1 crystal structure, demonstrates that both histidines are exposed to the environment. Moreover, the residue αS243, which once mutated into proline leads to PHA1, is in the proximity of αH255 (Figure 45). Its replacement by a proline, a residue characterized by an increased conformational rigidity given by the cyclic structure of its side chain, might disrupt the structure of this entire region changing the orientation of the αH255 side chain and impairing the self-inhibition mechanism.
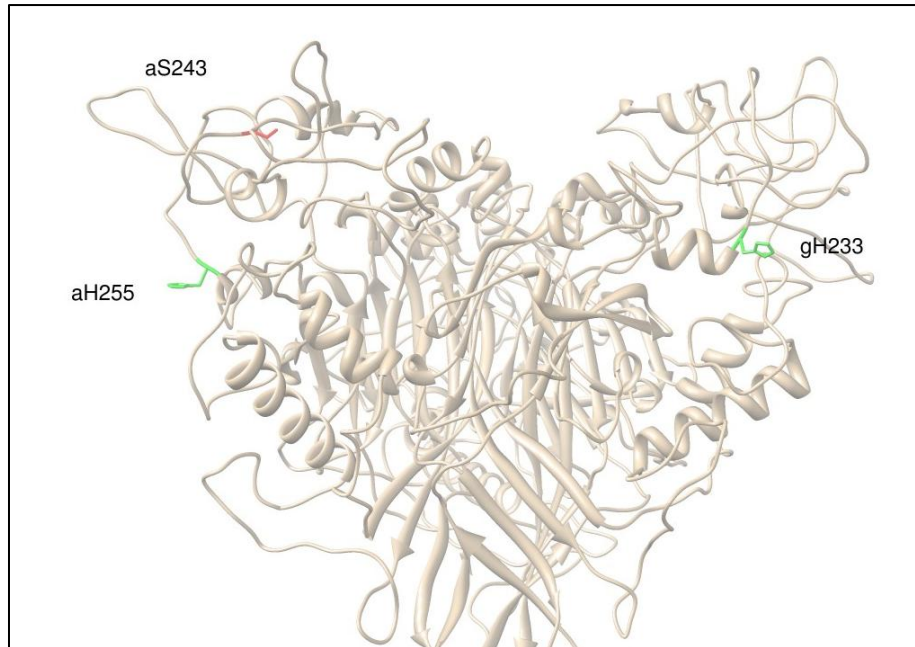
Figure 45 Extracellular loop of αβγENaC. Homology model of αβγENaC based on the first cASIC1 crystal structure. S243 (red) and H255 (green) are both located on the α subunit. H233 (green) is the corresponding αH255 of the γENaC subunit.

2. High Na$^+$ load in the kidneys of a preterm neonate

In the kidney of a baby born at term, the amount of Na$^+$ reaching ENaC is controlled by other transporters located upstream of the channel. Salt-losing diseases such as the Barter or Gitelman syndromes have highlighted the importance of these transporters in Na$^+$ handling; NKCC2 and NCC (67). In addition, Satlin & Palmer have demonstrated that there is no Na$^+$ transport in the CCD of immature rabbit kidneys (250,251). It has also been shown that the transition between foetal and neonatal life correlates with a strong reduction in urinary excreted Na$^+$ (270). Together, these reports could explain the elevated amount of Na$^+$ to which ENaC is exposed to in the kidney of this preterm boy. As the αS243Pβγ channel is hypersensitive to high Na$^+$ load, it responds in an exacerbated way by decreasing its Na$^+$ current and thus Na$^+$ reabsorption.

Perspectives
1. ASIC

It is not be the first time that the use of different methodologies has led to the identification of various stoichiometries for the same channel. For example, the large-conductance mechanosensitive channel MscL, has been identified as having a hexameric, a homopentameric and a homotetrameric organization depending on the methodology used (271-274). The challenge is to find the most reliable technique in order to unveil the correct stoichiometry, of, in our case, the human ASIC1a channel. In my opinion, one of the best techniques to use would be to crystallize ASIC1a in its 2D form. Studies have been performed to compare the accuracy of the 3D versus the 2D crystal structures and as the native protein is embedded in a lipid bilayer, 2D crystals are likely to be more representative (275).

To find an explanation for the discrepancy between our results (homotetramer) and the trimeric stoichiometry of the crystallized chicken ASIC1, it would be interesting to overexpress the human ASIC1a construct into Sf9 cells and then compare the oligomerization pattern of Sf9 with CHO and *Xenopus laevis* cells. Indeed, the difference in the lipid composition between insect and mammalian cells might account for a different oligomerization.

We would like to investigate the physiological roles of ASIC channels. This could be done by screening compounds present in the nervous system and testing if they are able to activate the hASIC1a channel at a physiological pH as with MTS. Potential candidates would be amino acids, serotonin, histamine, acetylcholine, adenosine, or dopamine, to name a few. Alternatively, the knock-down of ASIC-like proteins *in vivo,* in *Drosophila melanogaster* for example, could also determine ASIC functions. Indeed, we have already started this project and using the GAL4/UAS system, we have generated ~30 complete knock-downs (276), among which, 9 gave a lethal phenotype. Limiting the expression of GAL4 to the nervous system leads to a similar phenotype for 6 out of 9 RNAi knock-downs, which share unexpanded wings and a cuticular sclerotization defect. This phenotype is characteristic by a dysfunction occurring at the time of eclosion and involving the neuropeptide Bursicon (277). Now the aim is to look deeper into this pathway in order to determine where these ASIC-like proteins are expressed and what physiological role they may have.

2.   ENaC

Given that self-inhibition is exacerbated in the αS243Pβγ ENaC mutant channel, it would be of interest to test a molecule known to increase the open probability of the channel by specifically inhibiting an exacerbated self-inhibition, such as S3969, shown in the Figure 46 (115). This would further confirm our data and maybe even be a useful treatment in case of new PHA1 linked to αS243Pβγ.
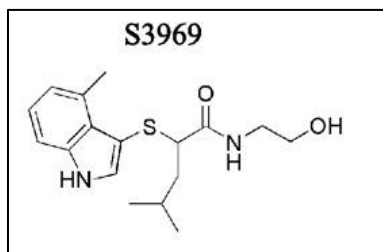
Figure 46 Structure of S3969 (*N*-(2-hydrosyethyl)-4-methyl-2-(4-methyl-1*H*-indol-3-ylthio)pentanamide. Modified from Lu *et al.*, 2008 (115).

Currently, we are working on a novel mutation of the *SCNN1G* gene discovered in a new PHA1 patient. This mutation leads to the replacement of threonine 353 by a proline (T353P) on the γ subunit of ENaC. We have created this mutation and started to investigate its effect on ENaC function, *in vitro,* using *Xenopus laevis* oocytes.

Our preliminary experiments confirm that ENaC loss of function correlates with PHA1 diagnosis. Protein expression analysis via SDS-PAGE shows a cleavage defect of the αβγ complex, which could be responsible for this loss of function. More specifically the post-translational cleavage of the α subunit, normally present when ENaC is expressed at the cell surface is absent (n=2). Moreover, pull down experiments on total lysates, demonstrate that mutated γ is co-purified with α and β subunits but it seems that the efficiency of the pull down is decreased with T353P (n=3). This would support an assembly defect of the αβγT353P channel. These pull down experiments also show an absence of γ cleavage in αβγT353P channels and confirm the previously demonstrated impaired α cleavage.

Bioinformatical analysis excludes the localization of the T353P mutation in a cleavage consensus sequence or near α or γ cleavage sites. This indicates that there is not a direct effect of the mutation on the cleavability of ENaC. Structural analysis of T353P supports our preliminary

results, showing ENaC loss of function, as the substitution of a threonine for a proline is destructive in terms of structural channel stability. This amino acid has a particular conformational rigidity given by the cyclic structure of its side chain. Thus, adding a proline into a α-helix or a β-sheet would disturb the protein's secondary structure. It is difficult to predict what exactly is happening in the patient, the loss of ENaC function could be due to a complete or partial folding defect or the degradation of the mutant channel. However, it is clear that there is a structural problem. Indeed, FoldX studies show that the stability of αβγT353P is lowered by ~2.5 kcal/mol compared to the wild-type channel (278).

Homologous mutations in the α and β subunits do not lead to a similar phenotype. Phenotype conservation would have indicated that γT353P is part of a conserved region important in the promotion of ENaC cleavage. In this case, it suggests that γT353 is not part of a region directly involved in the ENaC cleavage.

As preliminary experiments have been done on total lysates with a rat αENaC His-tagged construct co-expressed with human β and γ subunits, we next have to construct the human α, β and γ His-tagged subunits and then repeat the pull-down experiments on the cell surface expressed pool of channels. The idea is to specifically look at the functional pool of ENaC involved in the transport of Na^+, and to avoid a mixture of immature and mature channels.

Appendix

1.   Primer sequences

Mutant	Forward primer	Reverse primer
C59V	gtgctgctggttgtatgcacggagcgtgt	acacgctccgtgcatacaaccagcagcac
C59V_C61S	gtgctgctggttgtgtccacggagcctgt	acaggctccgtggacacaaccagcagcac
V74C	ccactaccaccattgcaccaagctcgacg	cgtcgagcttggtgcaatggtggtagtgg
Y426C	gagaccattgaacagaagaaagcctgtgagattgcagggctcctg	caggagccctgcaatctcacaggctttcttctgttcaatggtctc
G430C	ggcctatgagattgcatgtctcctgggtgacatcg	cgatgtcacccaggagacatgcaatctcataggcc
G433C	gcagggctcctgtgtgacatcgggg	ccccgatgtcacacaggagccctgc
C466A	ggagctatttgactacgcctacgaggtcattaagcacaagctggcccgacgaggaaaatg	cattttcctcgtcgggccagcttgtgcttaatgacctcgtaggcgtagtcaaatagctcc
C471A	gctatttgactacgcctacgaggtcattaagcacaagctgtgccgacgaggaaaagcccagaaggag	ctccttctgggcttttcctcgtcggcacagcttgtgcttaatgacctcgtaggcgtagtcaaatagc
C497A	ggacgacgtcaaaagacacaacccggccgagagccttcg	cgaaggctctcggccgggttgtgtcttttgacgtcgtcc
C528Stop	cacgttcgaggactttacctgatgagccccgcagg	cctgcggggctcatcaggtaaagtcctcgaacgtg

Supplemental Table 1. Sequences of the primers used for the PCR mutagenesis.

2. **Percent Identity Matrix (Clustal Omega)**

	SCNN1A	SCNN1B	SCNN1G	SCNN1D
SCNN1A	100.00			
SCNN1B	31.41	100.00		
SCNN1G	33.17	35.79	100.00	
SCNN1D	39.12	29.20	29.97	100.00

TM1	SCNN1A	SCNN1B	SCNN1G	SCNN1D
SCNN1A	100.00			
SCNN1B	29.17	100.00		
SCNN1G	25.00	29.17	100.00	
SCNN1D	37.50	33.33	29.17	100.00

TM2	SCNN1A	SCNN1B	SCNN1G	SCNN1D
SCNN1A	100.00			
SCNN1B	48.39	100.00		
SCNN1G	45.16	54.84	100.00	
SCNN1D	54.84	38.71	32.26	100.00

	ASIC1	ASIC2	ASIC3	ASIC4	ASIC5
ASIC1	100.00				
ASIC2	67.38	100.00			
ASIC3	50.70	51.45	100.00		
ASIC4	49.69	46.38	47.35	100.00	
ASIC5	28.85	30.11	30.41	26.71	100.00

TM1	ASIC1	ASIC2	ASIC3	ASIC4	ASIC5
ASIC1	100.00				
ASIC2	58.33	100.00			
ASIC3	41.67	45.83	100.00		
ASIC4	37.50	29.17	50.00	100.00	
ASIC5	29.17	33.33	29.17	20.83	100.00

TM2	ASIC1	ASIC2	ASIC3	ASIC4	ASIC5
ASIC1	100.00				
ASIC2	89.47	100.00			
ASIC3	73.68	78.95	100.00		
ASIC4	78.95	84.21	84.21	100.00	
ASIC5	47.37	52.63	68.42	52.63	100.00

	UN105	UNC8	DEG1	DEL1	MEC4	MEC10
UN105	100.00					
UNC8	33.81	100.00				
DEG1	32.99	35.92	100.00			
DEL1	31.99	32.56	37.36	100.00		
MEC4	35.58	35.65	41.54	40.72	100.00	
MEC10	34.23	32.90	40.53	38.22	20.99	100.00

TM1	UN105	UNC8	DEG1	DEL1	MEC4	MEC10
UN105	100.00					
UNC8	33.33	100.00				
DEG1	25.00	12.50	100.00			
DEL1	16.67	8.33	16.67	100.00		
MEC4	25.00	20.83	16.67	37.50	100.00	
MEC10	30.00	15.00	15.00	35.00	45.00	100.00

TM2	UN105	UNC8	DEG1	DEL1	MEC4	MEC10
UN105	100.00					
UNC8	44.44	100.00				
DEG1	44.44	66.67	100.00			
DEL1	40.74	40.74	48.15	100.00		
MEC4	44.44	55.56	59.26	48.15	100.00	
MEC10	44.44	51.85	59.26	44.44	66.67	100.00

	HyNaC2	HyNaC3	HyNaC4	HyNaC5
HyNaC2	100.00			
HyNaC3	30.02	100.00		
HyNaC4	65.45	30.68	100.00	
HyNaC5	29.21	41.81	27.70	100.00

TM1	HyNaC2	HyNaC3	HyNaC4	HyNaC5
HyNaC2	100.00			
HyNaC3	12.50	100.00		
HyNaC4	16.67	70.83	100.00	
HyNaC5	25.00	20.83	20.83	100.00

TM2	HyNaC2	HyNaC3	HyNaC4	HyNaC5
HyNaC2	100.00			
HyNaC3	48.15	100.00		
HyNaC4	44.44	88.89	100.00	
HyNaC5	62.96	44.44	44.44	100.00

	HtFaNaC	LsFaNaC	HaFaNaC
HtFaNaC	100		
LsFaNaC	69.28	100	
HaFaNaC	65.2	68.74	100

TM1	HtFaNaC	LsFaNaC	HaFaNaC
HtFaNaC	100		
LsFaNaC	100	100	
HaFaNaC	95.83	95.83	100

TM2	HtFaNaC	LsFaNaC	HaFaNaC
HtFaNaC	100		
LsFaNaC	96.3	100	
HaFaNaC	96.3	96.3	100

3. **A crosslinking study of the human Acid-Sensing Ion Channel ASIC1a: evidence for a homotetrameric assembly state at the cell surface**

A crosslinking study of the human Acid-Sensing Ion Channel ASIC1a: evidence for a homotetrameric assembly state at the cell surface.

Delphine Huser, Miguel Xavier van Bemmelen, Ivan Gautschi and Laurent Schild¶.

Department of Pharmacology & Toxicology

Faculty of Biology and Medicine

Lausanne University

Rue du Bugnon 27, CH-1005 Lausanne, Switzerland

¶ Corresponding author:

Laurent Schild

e-mail: Laurent.Schild@unil.ch

phone: +41 21 692 5380

Short title: tetrameric assembly of the human ASIC1a

Key words: Acid-sensing ion channels, ASIC, Epithelial sodium channel, ENaC, structure, subunit assembly, subunit stoichiometry, crosslinking.

Abstract

The chicken acid-sensing ion channel ASIC1 was crystallized as a homotrimer. Previous functional studies on the epithelial sodium channel ENaC, a close member of the same ion channel family, have however provided evidence for a tetrameric channel made of homologous subunits. The oligomeric state of the functional ASIC1 at the cell surface has not been specifically addressed so far.

We have developed a crosslinking approach using the sulfhydryl crosslinker BMOE and engineered cysteines in the extracellular vestibule of the human ASIC1a channel pore to stabilize the functional multimeric complex expressed at the surface of *Xenopus laevis* oocytes or CHO cells. Under reducing conditions, we could identify by western blot four distinct oligomeric states that correspond by mass to multiples of a single ASIC1a subunit. We could show that these oligomeric states identified on SDS-gel are oligomers made of ASIC1a subunits. By optimizing the intersubunit crosslinking between cysteines in the extracellular vestibule, in the first transmembrane helix and in the C-terminus of ASIC1a subunits, we could isolate from the cell surface a major channel complex, which by mass corresponds to four ASIC1a subunits. Similar results were obtained with formaldehyde, a less specific amino-group crosslinking agent. We conclude that the major ASIC1a channel complex expressed at the cell surface has a mass corresponding to a tetramer suggesting that the functional ASIC1 channel has a subunit stoichiometry different from the cASIC1 multimeric structure revealed by crystallography.

Introduction

Acid-sensing ion channels (ASICs) are proton-gated cation channels that belong to the degenerin/epithelial, non-voltage-gated, sodium channel family. Four orthologs of ASICs have been identified in vertebrates. At the subcellular level, ASICs are localized in cell bodies, in dendrites and in post-synaptic dendritic spines, suggesting a role in synaptic transmission. ASIC1 knockout mice have decreased acid-induced inward currents and a reduced long-term potentiation associated either with fear-related behaviors, altered learning and memory processes, or pain sensation (1).

ASIC channels open upon acidification of the extracellular milieu to a pH below 7.0. ASIC channels show a selectivity for Na^+ over K^+, and a slight permeability to Ca^{2+} ions (2). The chicken ASIC1 (cASIC1) was crystalized as a homotrimer (3, 4). Each subunit comprises a large extracellular domain between 2 transmembrane α helices (TM1 and TM2) arranged pseudosymmetrically around a non-conducting pore, a channel conformation that was interpreted as the desensitized state of the channel. The TM2 of each subunit is located close to the three-fold axis, lining the putative ion channel pore, while the TM1 helices lie at the periphery, making most of the contact with the lipid bilayer. The crossing of the TM2 helices identifies an extended physical gate in the transmembrane domain that precludes the flow of ions between the extracellular and the intracellular milieus.

The peptide Psalmotoxin 1 (PcTx1) in the venom of the tarantula *Psalmopoeus cambridgei* inhibits homomeric ASIC1a channels at nanomolar concentrations (5). A crystal structure of ASIC1 bound to psalmotoxin-1 obtained at two different proton concentrations shows a rearrangement both of the inter-subunit interactions at the extracellular domain and of the transmembrane α helices (6). This results in the expansion of the extracellular vestibule and the enlargement of the diameter of the transmembrane channel pore, with little changes in the extracellular domain. These structural features were interpreted as reflecting an open channel conformation, although no permeant ions could be identified in the pore of either of these two ASIC1 structures.

Since the crystallization of ASIC1, the field seems to have settled that ASIC and ENaC channels are trimers made of three homologous subunits. Two recent studies using the atomic force microscopy imaging of solubilized ENaC and ASIC complexes tagged with

antibodies agreed as well with a trimeric subunit assembly of these channels (7, 8). The cASIC1 crystal structures contradict however previous functional and biochemical studies on ENaC that supported a heterotetrameric organization of this channel, made of homologous α, β, and γ subunits (9-12). Additional studies have been performed on ENaC subunit stoichiometry including a fluorescence microscopy study that concluded to an equal number of each subunit in the ENaC channel complex, a model consistent with a previously reported 9 subunit stoichiometry (13, 14).

Taken together, these observations raise intriguing questions about the oligomerization state of ASIC and ENaC channels. A variability in the stoichiometry among members of the ENaC/ASIC/degenerin ion channel family remains conceivable, similarly to what has been reported for ion channels members of the MscL family. Indeed, the early model for the *Escherichia coli* MscL (EcMscL) stoichiometry based on crosslinking and electron microscopy studies was a hexamer (15, 16). The subsequent elucidation of the crystal structure of the *Mycobacterium tuberculosis* (MtMscL) revealed a pentameric oligomerization (17). Finally, the crystal structure of *Staphylococcus aureus* MscL (SaMscL) truncated at the C-terminus was shown to be a tetramer (18).

Thus far, the subunit stoichiometry of a functional ASIC1 as it is expressed at the cell surface has not been specifically addressed. In this report, we have used an intersubunit crosslinking approach to identify the oligomeric state of the human ASIC1a channel at the cell surface. Our results reveal the presence of a functional oligomeric ASIC1a complex at the cell surface made of more than three homologous subunits.

Results

It has been recently reported that intracellular cysteine residues at the C-terminus of ASIC1a participate in the formation of intersubunit disulfide bonds in the presence of hydrogen peroxide (19). In a first set of experiments, we assessed the oligomerization state of wild type ASIC1a and of a mutant lacking the cysteines in the C-terminus (ASIC1a-ΔC_{Ct}), at the cell surface of *Xenopus laevis* oocytes, and after *in situ* crosslinking using the homobifunctional disulfide crosslinker bismaleimidoethane BMOE. BMOE is a short-arm (8 Å) crosslinker for covalent, irreversible conjugation between sulfhydryl groups. Since the formation of intersubunit disulfide bonds in the C-terminus has been reported to affect ASIC1 activity (19), we tested the effect of BMOE (2 mM) applied

intracellularly in oocytes expressing either ASIC1a or ASIC1a-ΔC_{Ct}. As shown in **figure 1A**, the current magnitudes mediated by ASIC1a or the ASIC1a-ΔC_{Ct} mutant were maintained unchanged during the time of the intracellular perfusion with BMOE. The ASIC1a subunit crosslinking was investigated in the same oocytes perfused intracellularly with BMOE, or alternatively, in those injected with the crosslinker, 60 to 180 minutes before current measurements. The Triton-X100-soluble fractions of these oocytes were collected and analyzed by western blot after SDS-PAGE under reducing conditions. The blot in **figure 1B** shows side by side the ASIC1a and ASIC1a-ΔC_{Ct} bands obtained after either perfusion or injection with vehicle or BMOE. In the absence of intracellular BMOE, both forms of ASIC1a migrate as a predominant band at ~70 kDa, size expected for an ASIC1a monomer; a discrete band could be detected around 150 kDa for ASIC1a, which was absent in the case of ASIC1a-ΔC_{Ct}. Upon intracellular application of BMOE, the intensity of the 150 kDa band increased for both constructs. In addition, a specific band could be detected for ASIC1a, at an apparent molecular weight higher than 250 kDa. The estimated mass of the oligomers identified as distinct bands on SDS-PAGE for both constructs, with or without BMOE were (mean±SD, n=7) 72±2, 156±7, and 329±19 kDa for ASIC1a and 73±2 and 164±6 kDa for ASIC1a-ΔC_{Ct}. A band corresponding to the molecular mass expected for a trimeric channel could not be consistently detected. Furthermore, ASIC1a complexes migrating as bands higher than the 330 kDa were not detected under these experimental conditions. The 329 kDa molecular weight band could represent by mass the crosslinking of either four ASIC1a subunits, of two ASIC1a dimers or alternatively, the crosslinking of an ASIC1a trimer with another protein. The differences in the band profile observed between ASIC1a and ASIC1a-ΔC_{Ct} indicate that the C-terminal cysteines participate in the formation of the BMOE-mediated intersubunit bonds that stabilize the different ASIC1a oligomeric forms. These results are consistent with the results obtained by Zha et al. under similar experimental conditions (19).

To further investigate the subunit composition of the ASIC1a multimeric complex, we developed an intersubunit disulfide crosslinking strategy using cysteine residues engineered at positions exposed to the ion permeation pathway at the extracellular entrance of the channel pore and therefore not expected to participate in crosslinking with residues at contiguous channel units (**figure 2**). A recent study using modifications

by thiol-specific reagents of cysteines introduced in the transmembrane helices of *Lamprey* ASIC1 allowed to functionally assess the orientation of the TM1 and TM2 with respect to the channel pore in the open and closed conformations; this functional evidence showed that the external end of TM1 and a well-defined side of the TM2 are exposed to the channel pore (20).

Based on these data, we have introduced cysteines at positions G430 and G433, in the TM2 α helix of ASIC1a that correspond to the side of the helix exposed to the channel pore (**figure 2B**). Two additional cysteine substitutions were performed at position V74 in the prolongation of the external end of the TM1 and at position Y426 in the short loop preceding the TM2, which presumably faces the external vestibule of the ASIC1 pore. Finally, the V74C, Y426C, G433C, and G430C substitutions were generated in the ΔC_{Ct} background of ASIC1a lacking the C-terminal cysteines to avoid a potential crosslinking of the channel subunits with adjacent membrane or cytosolic proteins.

As shown in **Table 1**, all the cysteine mutants were functional: the V74C and G433C mutants show a decreased current, but full activity of V74C could be restored upon extracellular treatment of oocytes with DTT. All these mutants show an increased sensitivity to block by extracellular Cd^{2+}; BMOE drastically and irreversibly decreased the activity of both the Y426C and G430C mutants but not of the V74C and G433C forms. Together, these functional experiments indicate that different thiol ligands or reagents applied from the extracellular side bind to V74C, Y426C, G430C and G433C and that this interaction interferes with the ASIC1a activity. These results are consistent with a location of these residues in the ion permeation pathway.

The oligomeric states of ASIC1a, and of the cysteine mutants in the ΔC_{Ct} background (V74C/ΔC_{Ct}, Y426C/ΔC_{Ct}, G430C/ΔC_{Ct} and G433C/ΔC_{Ct}) were assessed by anti-His-tag western blot analysis under reducing conditions. Crosslinking with BMOE was performed at the cell surface of oocytes and was followed by cell-surface biotinylation and purification on streptavidin beads. The western blot in **figure 3A** shows that, after crosslinking with BMOE, ASIC1a-ΔC_{Ct} runs as a major band corresponding to the mass of a monomer, and as a weaker, ~160 kDa band consistent with an ASIC1a dimer. In contrast, each of the BMOE-treated cysteine mutants, V74C/ΔC_{Ct}, Y426C/ΔC_{Ct}, G430C/ΔC_{Ct} or G433C/ΔC_{Ct}, run as ladders of four distinct bands on SDS-PAGE, with similar migration patterns. As for the experiments in **figure 1B**, we never observed any

additional bands at higher molecular weights (Mw) than those shown in this blot. **Figure 3B** summarizes the migration patterns on SDS-PAGE gels of the ASIC1a-ΔC_{Ct}, V74C/ΔC_{Ct}, Y426C/ΔC_{Ct}, G430C/ΔC_{Ct}, and G433C/ΔC_{Ct} mutants expressed at the cell surface after crosslinking with BMOE. In this graph, each point represents the average molecular weight estimated for each band (bands I to IV), in a series of four independent experiments. This analysis shows the linearity of the distribution of the apparent sizes of the four bands detected for each mutant. Regression analysis of the estimated molecular weights for the four bands of each ASIC1a mutant yielded an average slope of 72±4 kDa, consistent with the mass of a single subunit. The relative intensities of each of the four bands obtained for the ASIC1a-ΔC_{Ct} constructs shown in **figure 3B** are illustrated in **figure 3C**. Except for ASIC1a-ΔC_{Ct}, and for V74C/ΔC_{Ct} that are predominantly in either a monomeric or in a high Mw form, respectively, none of the four bands detected for the other cysteine-substitution mutants is predominant. These experiments identify for each of the mutants and independently of the position of the cysteine substitution, four distinct oligomeric states corresponding by mass to multiples of a single ASIC1a subunit. Since this pattern of four oligomeric states was highly reproducible among the ASIC1a mutants in terms of the apparent mass of each oligomeric state, the next set of experiments were carried out exclusively on the G433C mutant.

If the cysteine residues available for crosslinking were only those engineered in the extracellular vestibule, the homo-bifunctional BMOE would stabilize exclusively dimers of ASIC1a but not trimers or tetramers. The stabilization of oligomers of higher order than dimers requires therefore the participation of additional native cysteines in the intersubunit crosslinking. Candidates are the native cysteine residues C59 and C61 in the TM1 close to G433C in the transmembrane domain (see **figure 2B**). **Figure 4A** displays the oligomerization patterns on SDS-PAGE gels of ASIC1a-ΔC_{Ct}, G433C/ΔC_{Ct}, G433C/C59V/ΔC_{Ct}, and G433C/C59V/C61S/ΔC_{Ct}, after crosslink with BMOE at the cell surface. All these ASIC1a mutants were functional (data not shown). Similarly to what is shown in **figures 1B** and **3A**, cell surface crosslinking with BMOE yields a major 80 kDa band and a faint 170 kDa band for ASIC1a-ΔC_{Ct}, and four distinct bands for the G433C/ΔC_{Ct}. The two high molecular bands of G433C/ΔC_{Ct} (234±8 and 303±17 kDa, n=4) become less accentuated for the mutants carrying either the C59V or the double C59V/C61S substitutions. The bands detected for the G433C/C59V/C61S/ΔC_{Ct} mutant

closely resemble those obtained for ASIC1a-ΔC_{Ct}. The relative intensities of the four bands migrating by mass at 80±10, 160±6, 230±9 and 300±19 kDa (Mw±SD) for the ASIC1a-ΔC_{Ct}, G433C/ΔC_{Ct}, G433C/C59V/ΔC_{Ct}, and G433C/C59V/C61S/ΔC_{Ct} constructs, are represented in **figure 4B** (n=4 experiments). The two highest molecular weight oligomers that represent respectively 24±4% and 10±6% of the total immunostaining in the case of the G433C/ΔC_{Ct} form, are virtually absent in the mutants lacking both the C59 and C61 in the TM1 (0±1% for both oligomers), as is the case for ASIC1a-ΔC_{Ct} (0±1% for both oligomers). Thus, the substitution of both the C59 and C61 cysteines in the TM1 nearly completely reverses the effect of G433C in stabilizing the two high molecular weight ASIC1a channel complexes (234±8 and 303±17 kDa), indicating that these two ASIC1a oligomers result from the crosslink between cysteines in the extracellular vestibule and those in the TM1. The comparison of ASIC1a-ΔC_{Ct} and G433C/C59V/C61S/ΔC_{Ct} shows that crosslinking by BMOE of two G433C residues enhances the stabilization of a complex that by mass corresponds to a dimer. Altogether, our results identify a network of BMOE-mediated cysteine crosslinks that involve G433C in the extracellular vestibule and C59/C61 cysteines in the TM1 that are essential for the stabilization of the high molecular weight ASIC1a channel complexes. Therefore these high molecular weight oligomers of ASIC1a are likely made of homologous ASIC1a subunits and do not represent heteromultimeric complexes with other cell surface proteins.

The identification of four distinct oligomers of ASIC1a on SDS-PAGE gels provides evidence for the existence at the cell surface of a ASIC1a channel complex of a higher oligomeric order than a homotrimer. The other identified ASIC1a oligomers may originate from a unique multimeric ASIC1a complex at the cell surface from which some of the ASIC1a subunits dissociate during SDS-PAGE, due to a limited efficiency of BMOE to crosslink and stabilize all the subunits of the native channel. Alternatively, ASIC1a channels could be present in various oligomeric states at the cell surface, as reported for the MscL channels (21, 22). To differentiate between these two possibilities, we searched for the presence of a predominant ASIC1a oligomeric state at the cell surface by optimizing the efficiency of the crosslinking. Because the C-terminal cysteines participate in intersubunit interactions in the presence of BMOE (see **figure 1B**), we investigated whether these cysteine further stabilize the multimeric ASIC1a channel

complex at the cell surface. We used CHO cells as an alternative expression system because of its wide use as cell system for functional expression of ASIC1a (6, 23, 24); we compared the crosslinking patterns of the ASIC1a and of ASIC1a-G433C mutant, both in the wt and the ΔC_{Ct} background. The functional integrity of these ASIC1a constructs in CHO cells was verified by patch-clamp (data not shown). After incubation of transiently transfected CHO cells in the presence of 2 mM BMOE or vehicle, we analyzed by SDS-PAGE the relative abundance of each of the four stabilized oligomeric states of ASIC1a, ASIC1a-G433C and ASIC1a-G433C/ΔC_{Ct} constructs in cell-surface biotinylated protein fractions. A representative western blot carried out under reducing conditions is displayed in **figure 5A**. In the absence of BMOE, the three constructs are detected mainly as a single band (75±2.4 kDa, n=9), corresponding to that expected for the ASIC1a monomer; under conditions where the monomer is abundant, a fast migrating band of unclear origin and associated with the monomer could be detected, in particular with the ASIC1a-G433C/ΔC_{Ct}, mutant. After BMOE treatment of the intact cells expressing ASIC1a, four well defined bands of similar intensity were observed with estimated molecular weights of 75±2, 160±13, 224±20 and 304±22 kDa (Mw±SD), based on the migration of 2 different standard markers (See **supplementary figure 1**). Introduction of the G433C mutation in the absence of the C-terminal cysteines (ASIC1a-G433C/ΔC_{Ct}) improves the crosslinking efficiency with the bands at 224 and 304 kDa becoming the main oligomeric forms detected. As for the monomer, a fast migrating band was associated with the tetramer at 270±25 kDa. The presence of the native C-terminal cysteines further increases the levels of the 304 kDa band of the ASIC1a-G433C construct, concomitant with a decrease in the intensity of all the other fast migrating bands with molecular weights below 250 kDa. The quantification of the relative intensities of the bands detected by western blotting is shown in **figure 5B**, for each ASIC1a construct on separate panels, with their apparent molecular weight. All the constructs were found as monomers in the absence of BMOE. After BMOE treatment, none of the multimeric forms of the wild type ASIC1a complex expressed at the cell surface represented more than 20% of the total amount of ASIC1a detected in the blot (**figure 5B, left panel**). For the G433C/ΔC_{Ct} (**figure 5B, middle panel**), the two most abundant multimeric forms are the ~224 and ~304 kDa oligomers representing each up to 40% of the total amount of protein. By contrast, the ASIC1a-G433C expressed at the cell surface and crosslinked with BMOE is detected in WB as a major ~304 kDa band

accounting for 59% of the total amount of the channel complex compared to 26 % for the ~224 kDa band (**figure 5B right panel**). For all the constructs, the abundance of the intermediate 270 kDa band was minor compared to that of the ~224 and ~304 kDa bands. Finally, to exclude the potential crosslinking by BMOE of two adjacent ASIC1a channel complexes at the cell membrane, treatment with the crosslinker was also performed on the streptavidin-bound fraction of the ASIC1a channel complex obtained after protein solubilization. Under these conditions, the migration profile of the ASIC1a complex on SDS-PAGE remained qualitatively similar to that obtained when BMOE was directly applied to the cells (see **supplementary figure S2A**).

All the crosslinking experiments performed so far revealed four highly reproducible ASIC1a oligomeric states in oocytes and in CHO cells; they involve crosslinking of specific cysteines at the C-terminus, the extracellular vestibule of the pore and the transmembrane helices of ASIC1 subunits. To finally exclude the possibility that the identified ASIC1a oligomeric states are dependent on the type of crosslinking, we compared the migration band pattern of ASIC1a and the ASIC1a-G433C mutant in cell-surface biotinylated fractions from cells treated with either 2 mM BMOE or formaldehyde (1 or 4%), a less specific, amino group-selective, crosslinking agent. **Figure 6A** shows the ASIC1a oligomeric states detected by western blot for the ASIC1a and ASIC1a-G433C using either type of crosslinker. In the absence of crosslinker the band corresponding by mass to a monomer is predominant, although three faint bands of higher Mw corresponding to dimers, trimers or tetramers could be detected. In the presence of the crosslinkers, the high molecular bands corresponding by mass to trimers and tetramers are the most intense. BMOE and formaldehyde yield qualitatively comparable band patterns; however, in contrast to BMOE where the accumulation of the highest Mw band was predominant only for the ASIC1a-G433C construct, the respective intensities of the 222±16 kDa and 313±22 kDa (Mw±SD, n=3) bands in the ASIC1a and ASIC1a-G433C samples were very similar (**figure 6B**), as expected for a less specific crosslinking agent. In addition, the stabilization of the 313±22 kDa by formaldehyde was dose-dependent **(figure 6A)**, and represented between 70% and 80% of the sum of all oligomeric states identified by western blot **(figure 6B)**. This further supports the presence of a main ASIC1a oligomeric state at the cell surface that corresponds by mass to a homotetrameric channel. In addition, our data favor the hypothesis that the other three lower molecular weight oligomers detected on SDS-PAGE result from the

dissociation of non-covalently linked ASIC1a subunits from the native tetrameric ASIC1a channel complex expressed at the cell surface.

Discussion

Our experiments show that the crosslinking of cysteines located in the extracellular vestibule, in the C-terminal domain, and in the first transmembrane domain of ASIC1a allows a covalent stabilization of ASIC subunit-subunit interactions and the identification of four distinct oligomeric states by SDS-PAGE under reducing conditions. These oligomeric states correspond by mass to multiples of the ASIC1a monomer detected as a 75-80 kDa band. The estimated molecular mass of these four oligomeric states was highly reproducible among different ASIC1a constructs with native or engineered cysteines, using two different crosslinkers BMOE and formaldehyde, and in different cell systems expressing functional ASIC1a channels. Improving the intersubunit crosslinking efficiency by increasing the number of available cysteines for BMOE or by using a less specific crosslinker, formaldehyde, allowed us to identify at the cell surface a predominant ASIC1a oligomer with a molecular weight ~310 kDa, corresponding to that expected for a homotetrameric channel.

Several observations support the notion that the ASIC1a oligomers crosslinked by BMOE and detected by SDS-PAGE/WB under reducing conditions are homomultimers of ASIC1a subunits. First, the apparent Mw of the four different oligomers represent multiples of the mass of a single subunit. Second, we identified the cysteine pairs in the extracellular vestibule (G433C) and in the TM1 (C59V and C61S) that are necessary and sufficient for the stabilization by BMOE of both of the higher molecular weight ASIC1a oligomers with sizes corresponding to trimers and tetramers. Third, since the homobifunctional crosslinker BMOE can bridge S-S distances in the range of 6 to 11 Å (25), it is unlikely that the crosslinking of cysteines engineered in the TM2 transmembrane domain and exposed to the pore (G430C, G433C) stabilizes a multi-channel ASIC1a complex.. Finally, the migration profile was qualitatively similar when the crosslinking was performed directly on the native cells or on solubilized and affinity purified fractions bound to streptavidin beads. It can be expected that this latter procedure minimizes the chances of crosslinking ASIC1a subunits with adjacent surface proteins that could form clusters at the cell membrane. Taken together, these observations support the fact that, under our experimental conditions, cysteine

crosslinking with BMOE occurs exclusively between ASIC1a subunits to stabilize a homomultimeric channel complex present at the cell surface. This specificity in the intersubunit crosslinking of the ASIC1a channel complex can explain the high reproducibility in the estimated mass of the four ASIC1a oligomers identified on SDS-PAGE among different ASIC1a constructs, using different crosslinkers or different cell expression systems.

The crosslink between G433C on the TM2, and native C59 or C61 in the TM1 of the adjacent subunit (figures 3A and 4A) is important for the stabilization of ASIC1a oligomers of higher order than dimers. In addition, the native cysteines at the C-terminus also participate in crosslinking of the ASIC1a. When all these cysteines are available for crosslinking by BMOE, this leads to the stabilization of a predominant ASIC1a oligomer at the cell surface that corresponds by mass to a tetrameric channel. An ASIC1a oligomer of similar mass is detected as well as the predominant ASIC1a complex at the cell surface after crosslinking with 4% formaldehyde. Furthermore, it is remarkable that the increase in the intensity of the signal obtained for the tetrameric form of ASIC1a-G433C correlates with the decrease in the band intensity of the trimer (**figure 5B**). The likely explanation for these observations is that the putative trimeric complex detected by western blot results from an incomplete crosslinking of all the subunits of the ASIC1a tetrameric complex leading to the dissociation of the non-linked subunit during SDS-PAGE. Our data are consistent with a recent report on the effects of hydrogen peroxide on the formation of ASIC1a intersubunit disulfide bonds; hydrogen peroxide stabilizes ASIC1 dimers on SDS-PAGE under non-reducing conditions, but also higher order ASIC1 oligomers of apparent molecular weight similar to those observed in our study (19). These high order ASIC1 oligomers are predominant at the cell surface and were interpreted as inter-trimer complexes (19). Our experiments provide no evidence for a crosslinking between two functional channel complexes at the cell surface.

Our observations are also in accordance with previous functional studies that reported a four subunit stoichiometry of ENaC and FaNaCh (9-12, 26). The epithelial sodium channel, ENaC, and FaNaCh belong to the same ion channel family as ASICs. ENaC is made of 3 homologous subunits, α, β, and γ that share 15-20% identity with ASIC1 and a similar membrane topology (2). Most of the functional studies on ENaC

including channel interaction with different blockers, analysis of specific mutations, expression of subunit concatemeric constructs, and biochemical studies came to the conclusion that ENaC is made of four subunits, 2α, 1β, and 1γ arranged pseudosymmetrically around a single channel pore (9, 10). Similar functional studies have not been performed on ASIC1 before our present report.

The available crystal structures of the C-terminally truncated chicken ASIC1 reveal a trimer (3, 4, 6, 27). These structures are consistent with the predicted membrane topology of ENaC but challenge both the evidence that ENaC is a tetramer, and our present data on the ASIC1a oligomeric state at the cell surface. ASIC1 crystal structures reveal two different conformation states: a closed, non-conducting state that is considered to reflect the desensitized state, and a toxin-bound state with a large open pore. The extracellular domain contains several cavities and vestibules in series along the 3-fold axis of symmetry. Two potential pathways for ions to access the transmembrane pore can be identified: the first one consists of lateral fenestrations at the intersubunit interface, the second along the 3-fold axis of the extracellular domain of the channel. The latter ion pathway remains occluded in all ASIC1 crystal structures available. Nevertheless a crystal structure of a non-functional ASIC1 bound with Psalmotoxin 1 revealed an anomalous density feature consistent with a cation trapped in a central vestibule of the extracellular domain (27). In another ASIC1 crystal structure bound to Psalmotoxin-1 showing an expanded extracellular vestibule and pore, an ion-binding site was identified at the extracellular end of the TM1, close to the entrance of the lateral fenestration of the channel complex (6). However, no electron density features consistent with the presence of cations deep into the pore could be observed in any of the ASIC1 structures interpreted as corresponding to either desensitized or open states. In contrast, the presence of permeant ions and their interactions with pore-lining residues could be resolved from the crystals of KcsA K^+ channels, the prokaryotic Cl^- channel, the Ca^{2+} Orai channel or the ligand-gated GLIC channel (28-31). The absence of permeant ions on the ASIC1 channel pore raises pertinent questions regarding the functional relevance of this non-conducting channel structure. Atomic force microscopy (AFM) imaging on purified ENaC and ASIC1 channel complexes bound to specific antibodies revealed angles between the Fab fragments that are consistent with trimeric channels (7, 8). Since the molecular mass of the ASIC1 or ENaC channel complexes was

not determined biochemically, the relevance of these data remains difficult to assess. Finally, the crystal structure of cASIC1 has been successfully used to provide a structural rationale for different biophysical properties of ASIC1 channel function such as their activation and desensitization (20, 32, 33). However these studies were not designed to specifically address the question of the subunit stoichiometry of ASIC1, and their conclusions cannot be used to refute the tetrameric organization of native ASIC1 channel.

Different subunit stoichiometries have been reported for members of the MscL ion channel family. The early model for the *Escherichia coli* MscL (EcMscL), based on crosslinking and electron microscopy studies was a hexamer (15, 16). The subsequent elucidation of the crystal structure of the *Mycobacterium tuberculosis* (MtMscL) orthologs revealed a pentameric oligomerization (17). Finally, the crystal structure of a form of *Staphylococcus aureus* MscL (SaMscL) truncated at the C-terminus was shown to be a tetramer (18). Furthermore, a single type of MscL can assemble in a mixture of different oligomeric states (22). The structural requirements for the generation of multiple oligomeric forms of MscL channels are unknown. Regarding cASIC1, there is no doubt that the protein, fused to GFP and carrying a truncation of its C-terminus, assembles as a trimer, at least when expressed in insect cells (3, 4, 6, 27). It remains possible that, under these expression conditions, cASIC1 assembles as a mixture of trimeric and tetrameric oligomers, but that only the former are able to generate diffraction-quality crystals. In contrast, we show that when the functional fraction of ASIC1a is chemically stabilized, the oligomeric state of ASIC1a corresponds by size to that of a tetramer.

Knowledge about the structure of ASIC and ENaC channels still remains incomplete. On one hand, the different cASIC1 crystal structures available to date lack sound evidence for their functional relevance. On the other hand, the ASIC1a complex identified at the cell surface as a tetramer requires further structural information to better define subunit organization of the channel complex. Our results will certainly not provide the last words on the subunit stoichiometry of the ENaC/ASIC channels, but hopefully will promote the reevaluation of the cASIC1 crystal structure for its functional relevance.

Methods

Detailed materials and methods are provided in the SI Text.

Cloning, site-directed mutagenesis, *in vitro* RNA transcription, and expression in *Xenopus laevis* oocytes

Healthy stage V and VI *Xenopus laevis* oocytes were pressure-injected with 10 ng of cRNA. ASIC1a wt and mutants constructs were carried out as detailed in the SI Text.

Electrophysiology

Electrophysiological measurements were performed 24–48 h after oocyte injection with cRNA. Macroscopic ASIC1a currents were elicited every 40 s by extracellular pH changes from 7.4 to 6.0 and were measured using either the two-electrode voltage-clamp for whole-cell currents or the cut-open oocyte technique.

Biochemistry

Cell-surface crosslinking and biotinylation of ASIC1a expressed in Xenopus oocytes

Triton 1% (v/v) was used as detergent for the lysis. Crosslinking was done with BMOE at 19°C and biotinylation with NHS-SS-biotin on ice. The lysis buffer was supplemented with 10 mM N-Ethylmaleimide*.*

Transfection, biotinylation, cross-linking, and lysis of CHO-K1 cells. Cells were transfected with Lipofectamine-2000. Cell-surface crosslinking with BMOE or formaldehyde and biotinylation were carried out as for oocytes. Membrane fractions were isolated by centrifugation after lysis of CHO cells in a solution without detergent, and subsequently solubilized.

Pull-Down with nickel-NTA- or Streptavidin-agarose beads,

The Triton X100 soluble fractions from Xenopus oocytes or CHO membranes were used for pull-down assays using either Ni^{2+}NTA- or streptavidin-agarose. The thus isolated fractions were analyzed by western blot using either anti-ASIC1a or anti-His-tag antibody and IRDye-conjugated secondary antibodies. Bands were quantified from images obtained with a LiCor Odyssey scanner using the Odyssey v2.1 software.

Acknowledgements

References

1. Wemmie JA, Taugher RJ, & Kreple CJ (2013) Acid-sensing ion channels in pain and disease. *Nature reviews. Neuroscience* 14(7):461-471.
2. Kellenberger S & Schild L (2002) Epithelial sodium channel/degenerin family of ion channels: a variety of functions for a shared structure. *Physiol Rev* 82(3):735-767.
3. Jasti J, Furukawa H, Gonzales EB, & Gouaux E (2007) Structure of acid-sensing ion channel 1 at 1.9 A resolution and low pH. *Nature* 449(7160):316-323.
4. Gonzales EB, Kawate T, & Gouaux E (2009) Pore architecture and ion sites in acid-sensing ion channels and P2X receptors. *Nature* 460(7255):599-604.
5. Escoubas P, *et al.* (2000) Isolation of a tarantula toxin specific for a class of proton-gated Na+ channels. *J Biol Chem* 275(33):25116-25121.
6. Baconguis I & Gouaux E (2012) Structural plasticity and dynamic selectivity of acid-sensing ion channel-spider toxin complexes. *Nature* 489(7416):400-405.
7. Carnally SM, *et al.* (2008) Direct visualization of the trimeric structure of the ASIC1a channel, using AFM imaging. *Biochem Biophys Res Commun* 372(4):752-755.
8. Stewart AP, Haerteis S, Diakov A, Korbmacher C, & Edwardson JM (2011) Atomic force microscopy reveals the architecture of the epithelial sodium channel (ENaC). *J Biol Chem* 286(37):31944-31952.
9. Firsov D, Gautschi I, Merillat AM, Rossier BC, & Schild L (1998) The heterotetrameric architecture of the epithelial sodium channel (ENaC). *EMBO J* 17(2):344-352.
10. Anantharam A & Palmer LG (2007) Determination of epithelial Na+ channel subunit stoichiometry from single-channel conductances. *J Gen Physiol* 130(1):55-70.
11. Kosari F, *et al.* (1998) Subunit stoichiometry of the epithelial sodium channel. *J Biol Chem* 273(22):13469-13474.
12. Dijkink L, Hartog A, van Os CH, & Bindels RJ (2002) The epithelial sodium channel (ENaC) is intracellularly located as a tetramer. *Pflugers Arch* 444(4):549-555.
13. Eskandari S, *et al.* (1999) Number of subunits comprising the epithelial sodium channel. *J Biol Chem* 274(38):27281-27286.
14. Staruschenko A, Adams E, Booth RE, & Stockand JD (2005) Epithelial Na+ channel subunit stoichiometry. *Biophys J* 88(6):3966-3975.
15. Blount P, *et al.* (1996) Membrane topology and multimeric structure of a mechanosensitive channel protein of Escherichia coli. *EMBO J* 15(18):4798-4805.
16. Blount P, Sukharev SI, Moe PC, Nagle SK, & Kung C (1996) Towards an understanding of the structural and functional properties of MscL, a mechanosensitive channel in bacteria. *Biol Cell* 87(1-2):1-8.
17. Chang G, Spencer RH, Lee AT, Barclay MT, & Rees DC (1998) Structure of the MscL homolog from Mycobacterium tuberculosis: a gated mechanosensitive ion channel. *Science* 282(5397):2220-2226.
18. Liu Z, Gandhi CS, & Rees DC (2009) Structure of a tetrameric MscL in an expanded intermediate state. *Nature* 461(7260):120-124.
19. Zha XM, *et al.* (2009) Oxidant regulated inter-subunit disulfide bond formation between ASIC1a subunits. *Proc Natl Acad Sci U S A* 106(9):3573-3578.

20.   Li T, Yang Y, & Canessa CM (2011) Outlines of the pore in open and closed conformations describe the gating mechanism of ASIC1. *Nature communications* 2:399.

21.   Dorwart MR, Wray R, Brautigam CA, Jiang Y, & Blount P (2010) S. aureus MscL is a pentamer in vivo but of variable stoichiometries in vitro: implications for detergent-solubilized membrane proteins. *PLoS Biol* 8(12):e1000555.

22.   Gandhi CS, Walton TA, & Rees DC (2011) OCAM: a new tool for studying the oligomeric diversity of MscL channels. *Protein Sci* 20(2):313-326.

23.   Jing L*, et al.* (2012) N-glycosylation of acid-sensing ion channel 1a regulates its trafficking and acidosis-induced spine remodeling. *J Neurosci* 32(12):4080-4091.

24.   Schnizler MK*, et al.* (2009) The cytoskeletal protein alpha-actinin regulates acid-sensing ion channel 1a through a C-terminal interaction. *J Biol Chem* 284(5):2697-2705.

25.   Green NS, Reisler E, & Houk KN (2001) Quantitative evaluation of the lengths of homobifunctional protein cross-linking reagents used as molecular rulers. *Protein Sci* 10(7):1293-1304.

26.   Coscoy S, Lingueglia E, Lazdunski M, & Barbry P (1998) The Phe-Met-Arg-Phe-amide-activated sodium channel is a tetramer. *J Biol Chem* 273(14):8317-8322.

27.   Dawson RJ*, et al.* (2012) Structure of the acid-sensing ion channel 1 in complex with the gating modifier Psalmotoxin 1. *Nature communications* 3:936.

28.   Dutzler R, Campbell EB, & MacKinnon R (2003) Gating the selectivity filter in ClC chloride channels. *Science* 300(5616):108-112.

29.   Zhou Y, Morais-Cabral JH, Kaufman A, & MacKinnon R (2001) Chemistry of ion coordination and hydration revealed by a K+ channel-Fab complex at 2.0 A resolution. *Nature* 414(6859):43-48.

30.   Hilf RJ & Dutzler R (2009) Structure of a potentially open state of a proton-activated pentameric ligand-gated ion channel. *Nature* 457(7225):115-118.

31.   Hou X, Pedi L, Diver MM, & Long SB (2012) Crystal structure of the calcium release-activated calcium channel Orai. *Science* 338(6112):1308-1313.

32.   Tolino LA, Okumura S, Kashlan OB, & Carattino MD (2011) Insights into the mechanism of pore opening of acid-sensing ion channel 1a. *J Biol Chem* 286(18):16297-16307.

33.   Roy S*, et al.* (2013) Molecular determinants of desensitization in an ENaC/degenerin channel. *FASEB J*.
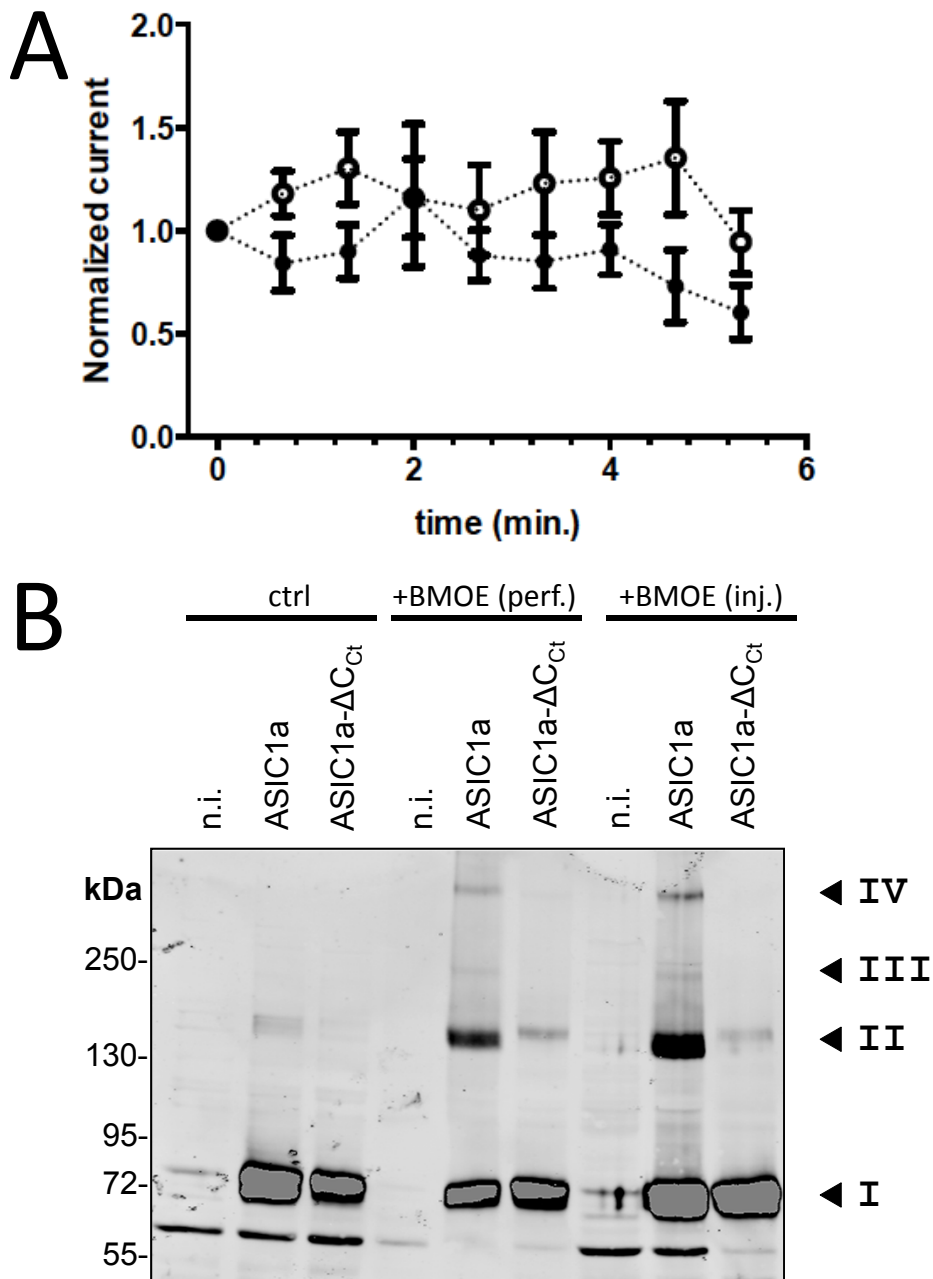
Figure 1

Effects of intracellularly applied BMOE on hASIC1a activity and oligomerization. *A*, Cut-open oocytes expressing either ASIC1a wild type (solid circles, n=18) or ASIC1a-ΔC_{Ct} (open circles, n=17) were intracellularly perfused with 2 mM BMOE; time 0 corresponds to the onset of perfusion with BMOE; currents (m±SD), elicited at pH 6.0 were normalized to the peak current at time zero in the absence of BMOE. *B*, Oligomerization of ASIC1a identified by an anti-ASIC1 western blot from oocytes, not injected (n.i.), or expressing ASIC1a or ASIC1a-ΔC_{Ct} lacking cysteines in the C-terminus, that were either untreated, internally perfused (perf.), or intracellularly injected (inj.) with 2 mM BMOE. Numbers I to IV identify bands that are specific for ASIC1a and represent by Mw multiples of band I.
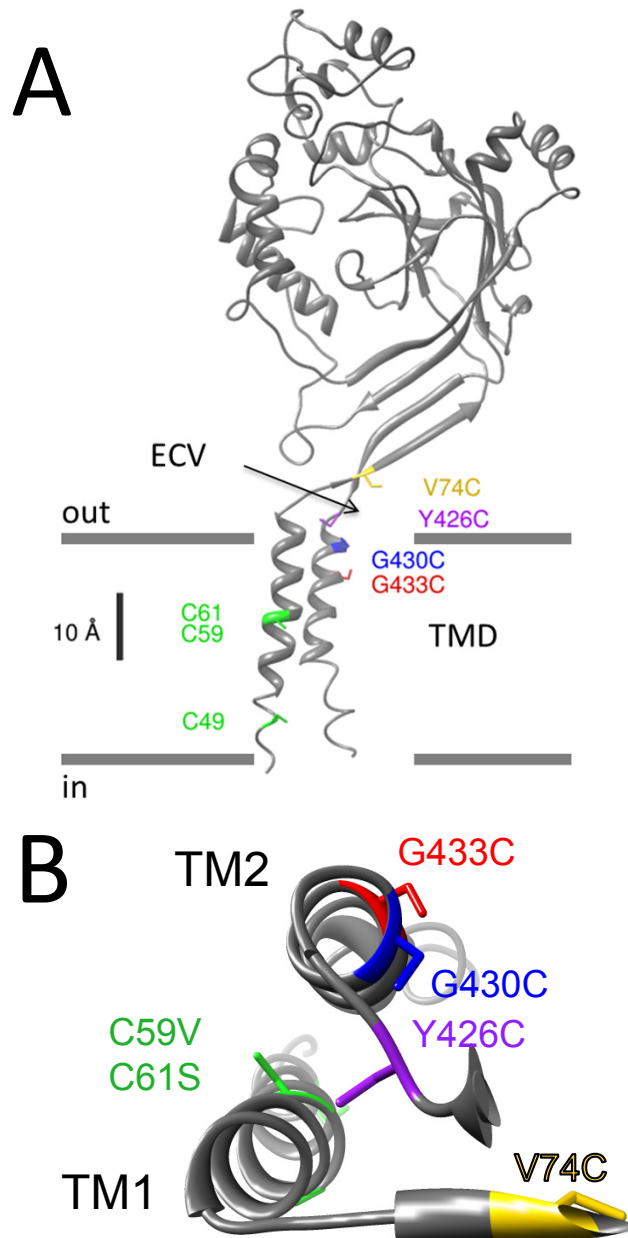
Figure 2

Homology model of a human ASIC1a subunit with cysteine substitutions. *A,* Model structure of a human ASIC1a subunit based on the chicken ASIC1 crystal structure as published in ref (4): the subunit is made on 2 transmembrane α helices (TM1 and TM2); the cysteines C49, C59 and C61 in the transmembrane α helix 1 (TM1) are shown in green. The G430C and G433C in TM2 are exposed to the channel pore (20). The V74C and Y426C are located at the entrance of the channel pore in the extracellular vestibule (ECV). *B,* Top view of the transmembrane α helices TM1 and TM2 of a single ASIC1a subunit, with the pore lining residues G433C and G430C.
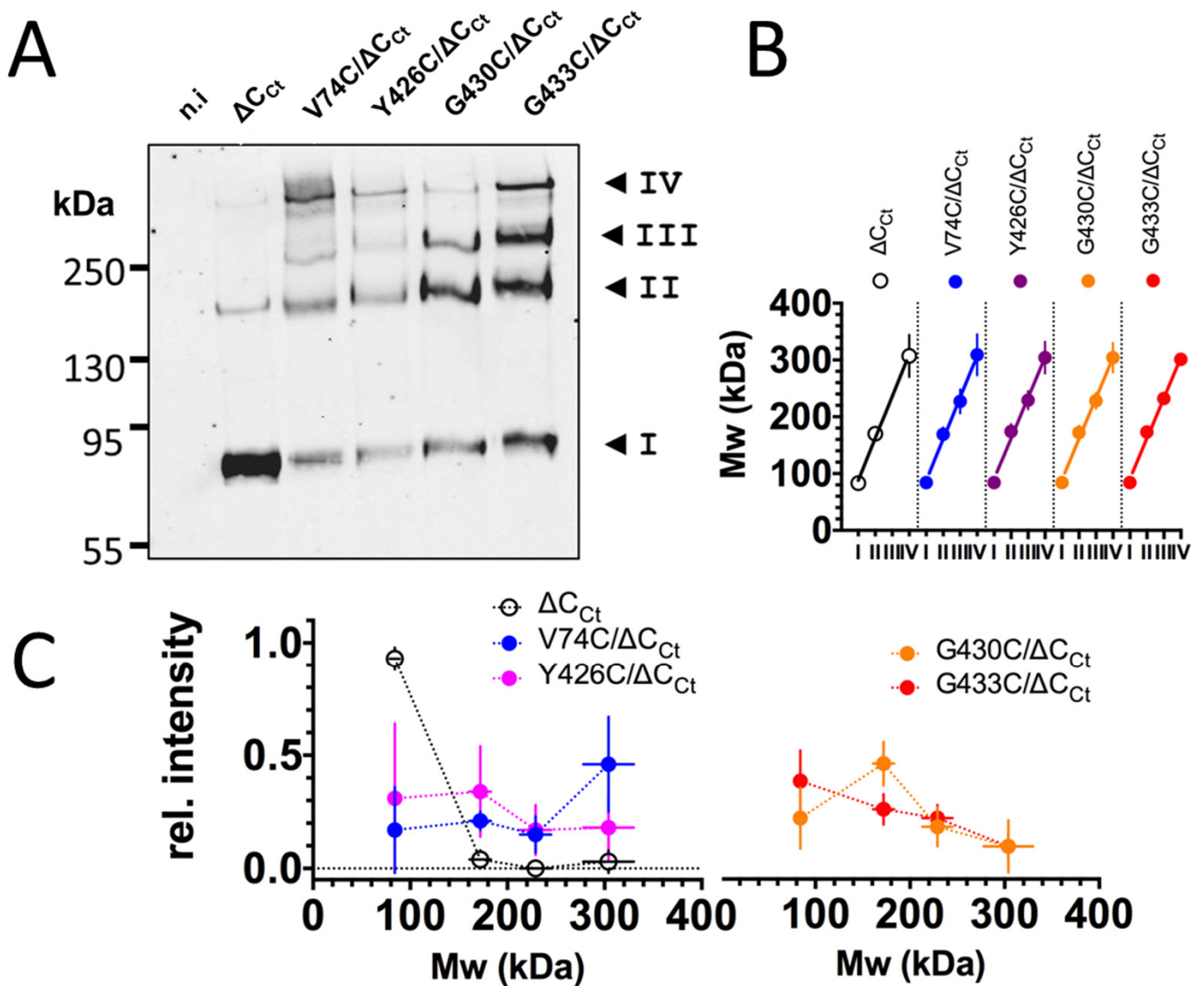
Figure 3

ASIC1 oligomeric states revealed by SDS-PAGE separation after crosslinking of cysteines in the ECV. A, Anti-His-tag western blot of the biotinylated fractions of surface proteins from non-injected oocytes (n.i.), from oocytes expressing either the His$_8$-tagged forms ASIC1a/ΔC_{Ct} (ΔC_{Ct}) lacking cysteines in the C-terminus, or the substitution mutants V74C/ΔC_{Ct}, Y426C/ΔC_{Ct}, G430C/ΔC_{Ct}, and G433C/ΔC_{Ct}. The crosslinking with 2 mM BMOE was performed at the cell surface; the biotinylated surface proteins were affinity-purified on streptavidin beads. Numbers I to IV, as in **figure 1. B,** Apparent Mw values of the ASIC1 oligomers (kDa, mean ±SD) estimated for each of the four main bands (I to IV) resolved by SDS-PAGE (see Methods) for the different constructs, as in A. **C,** Relative intensities (mean, vertical bars ±SD) of the four distinct bands I-IV identified in A: horizontal bars represent SD for the apparent Mw value for each band.
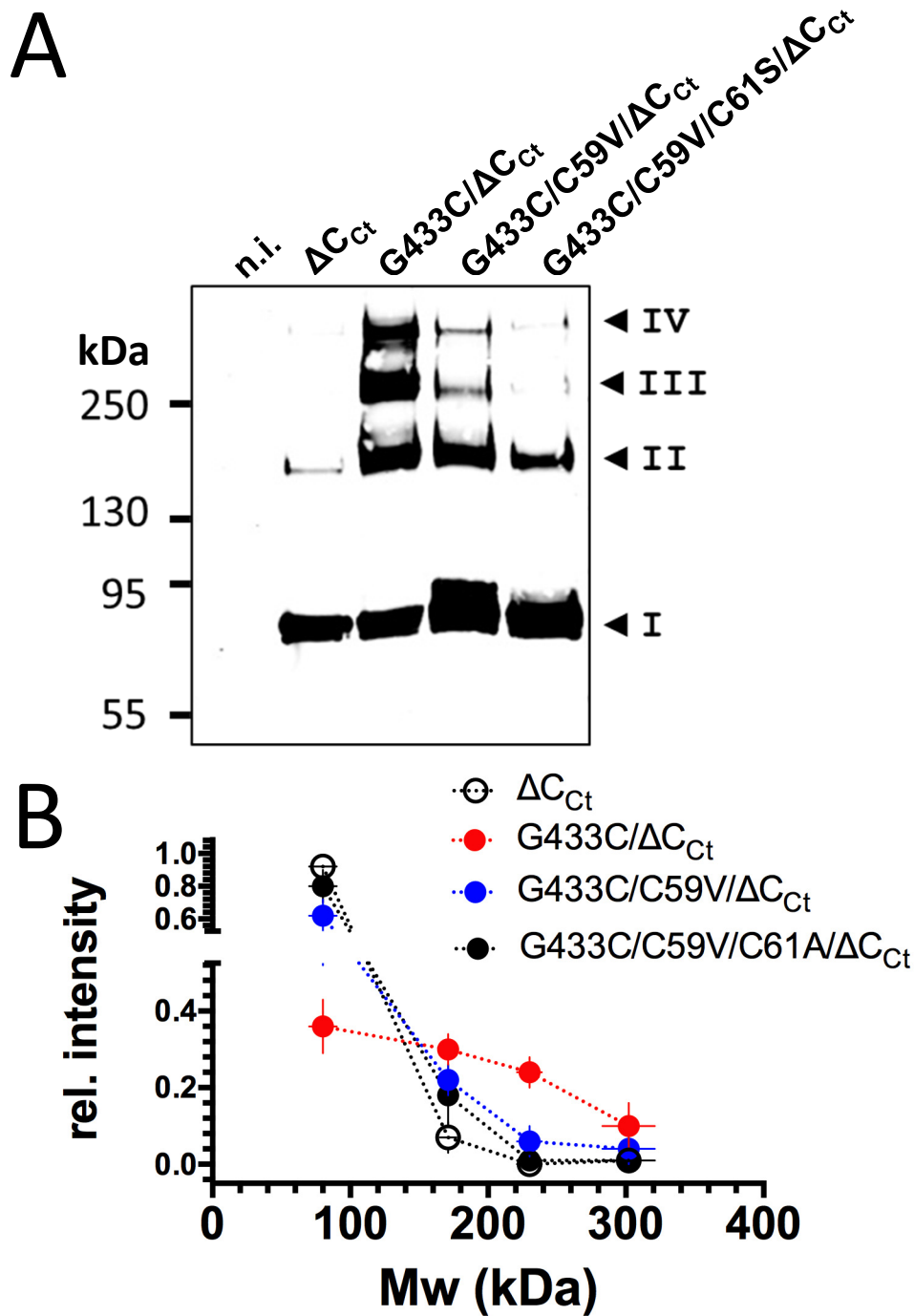
Figure 4

Contribution of the cysteines in the first transmembrane helix (TM1) to the subunit crosslinking by BMOE. *A,* ASIC1a oligomeric states identified by anti-His-tag western blot (using the same experimental procedure as in figure 3A) of the His_8-tagged forms of ASIC1a-ΔC_{Ct} (ΔC_{Ct}), and the cysteine substitution mutant G433C-ΔC_{Ct} associated or not with the C59V or C59V/C61S substitutions (G433C/C59V/ΔC_{Ct} or G433C/C59V/C61S/ΔC_{Ct}). Numbers I to IV have the same meaning as in **figure 1**. *B,* Relative intensities (arbitrary units, mean ±SD, n=4) of the bands identified on SDS-PAGE estimated for ASIC1a-ΔC_{Ct}, G433C/ΔC_{Ct}, G433C/C59V/ΔC_{Ct}, and G433C/C59V/C61S/ΔC_{Ct}. Horizontal bars represent ±SD of apparent molecular weight sizes.

Figure 5

Stabilization of the ASIC1a channel complex at the cell surface of transfected CHO cells. *A,* Anti-His-tag western blot showing ASIC1a oligomeric states obtained from cell surface fractions of proteins expressed by CHO cells and transiently transfected with an empty vector (n.t.), or His$_8$-tagged forms of ASIC1a wt, ASIC1a-G433C/ΔC_{Ct}, or ASIC1a-G433C mutants, and treated with 2 mM BMOE or vehicle. Surface proteins were biotinylated, purified on streptavidin beads and analyzed by western blot.. Numbers I to IV have the same meaning as in figure 3. ***B,*** Relative intensities (mean ±SEM) measured of the different bands detected for the different constructs without (open circles) or with 2mM BMOE (filled circles). Horizontal bars represent apparent Mw values (±SEM) estimated for each band. Significant (** = p<0.01) difference in intensity between bands III and IV for each protein was determined by a paired, two-tailed *t*-test.
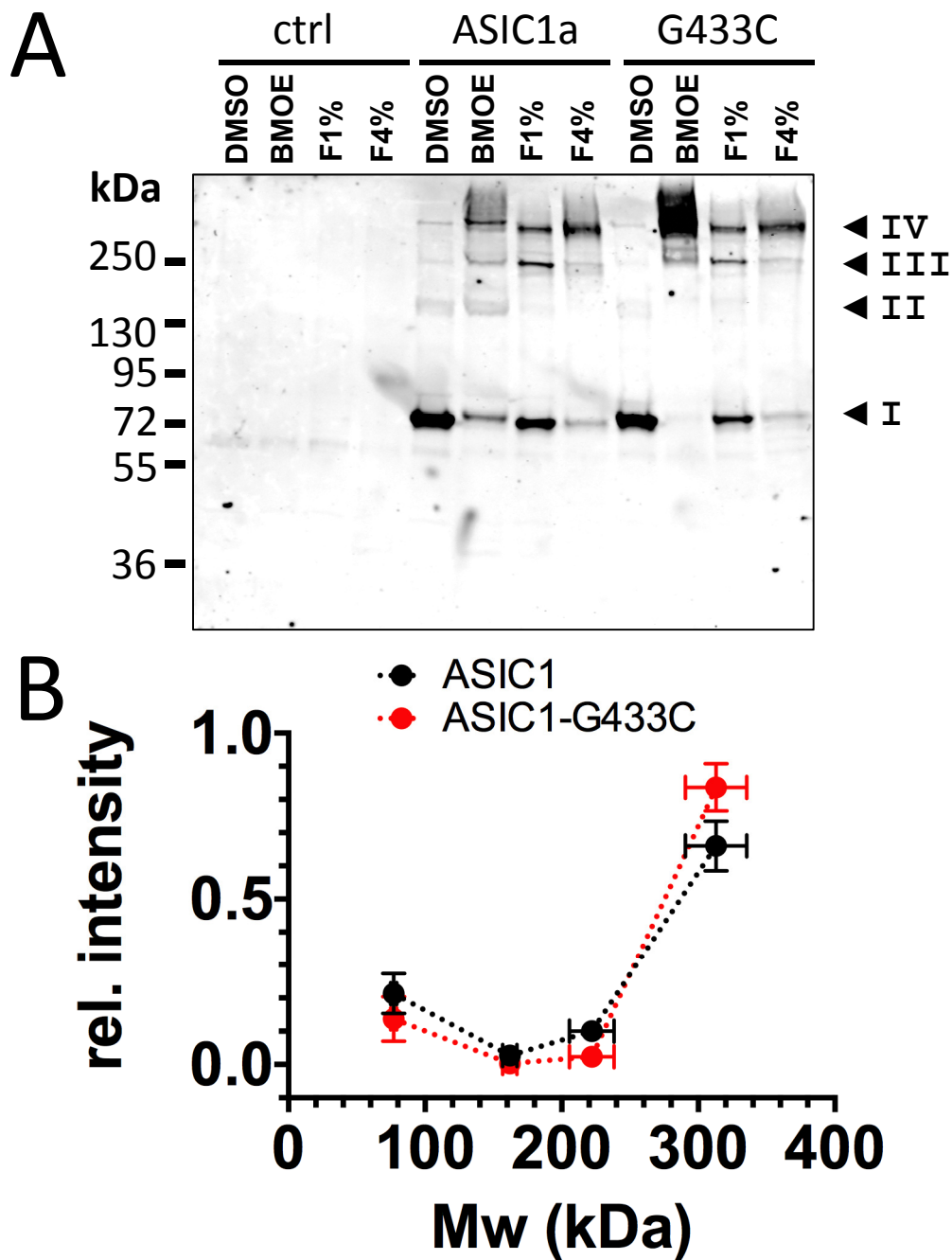
Figure 6.

ASIC1a channel complex at the cell surface of CHO cells after crosslinking with formaldehyde. *A,* Anti-His-tag western blot of the biotinylated fractions of surface proteins in CHO cells transiently transfected either with empty vector (ctrl), or with His$_8$-tagged ASIC1a, or ASIC1a-G433C mutant (G433C). Cells were treated either with vehicle (DMSO), or BMOE (2 mM), or with 1 or 4% formaldehyde (1F, 4F, respectively). Surface proteins were biotinylated, purified on streptavidin beads before western blot analysis. Numbers I to IV have the same meaning as in **figure 1**. *B,* relative intensities of the bands I-IV identified in A from CHO cells expressing ASIC1a or ASIC1a-G433C treated with 4% formaldehyde.

Supplementary Information

Chemicals

Bis(maleimido)ethane (BMOE #22323) was purchased from Pierce Biotechnology (USA). Anti-His-tag monoclonal antibody was from GE Healthcare (#27-4710-01). Polyclonal anti-ASIC1 (#ASC-014) was purchased from Alomone Labs (Israel). Polyclonal goat antibody anti-rabbit IRDye® 800CW (#926-32211), IRDye® 680CW (#926-32221) and goat anti-mouse IRDye® 680CW (#926-68070) were from Li-Cor® Biosciences GmbH (Bad Homburg, Germany). Pre-stained protein molecular weight ladders were from PeqLab Biotechnologie GmbH, Erlangen, Germany (peqGold Protein Marker, #27-2210) or from Thermo Scientific (Spectra Multicolor High Range Protein Ladder, #26625). EZ-link sulfo-NHS-SS-biotin (Pierce, #21331) was used as biotinylation reagent. Immunopure immobilized streptavidin gel was from Thermo Scientific (#20349).

Cloning, site-directed mutagenesis, *in vitro* RNA transcription, and expression in *Xenopus laevis* oocytes

The coding sequence of human ASIC1a was cloned in the pSDEasy vector. An octahistidine coding sequence (H_8) was introduced into the multiple cloning site using XhoI and SalI restriction sites (H_8-ASIC1a).

The ASIC1a construct lacking the cysteine in the C-terminus, H_8-hASIC1a-C466A/C471A/C497A/C528Stop (ASIC1a-ΔC_{Ct}) was used as template for mutagenesis. V74C, Y426C, G430C and G433C cysteine substitutions were introduced by site-directed mutagenesis with the QuickChange kit from Stratagene (see Supplementary Table 1 for primers). C49A, C59V and C61S primers were already described (1). Mutations were verified by sequencing (Synergene Biotech, Zurich, Switzerland).

Complementary RNAs were synthesized *in vitro* with SP6 RNA-polymerase (Promega, Dübendorf, Switzerland) from H_8-ASIC1a cDNA encoding vectors previously linearized with FspI. Healthy stage V and VI *Xenopus laevis* oocytes were pressure-injected with 10 ng of cRNA.

Electrophysiology

Electrophysiological measurements were performed 24–48 h after oocyte injection with ASIC cRNA. Macroscopic ASIC1a currents were elicited every 40 s by rapid changes in extracellular pH from 7.4 to 6.0 and were measured using either the two-electrode voltage-clamp for whole-cell currents or the cut-open oocyte technique when intracellular perfusion was needed, as previously described (1). For the two-electrode voltage clamp experiments, reagents were directly added to the extracellular solutions: Cd^{2+} 10, 100 and 1000 µM, or BMOE 2 mM. In experiments investigating the effects of intracellular BMOE on ASIC1a activity, 100nl of a 10mM BMOE or vehicle (DMSO) solution were injected per oocyte 60 to 180min before electrophysiological measurements. In the cut-open oocyte experiments, he voltage clamp was performed using a Dagan cut-open oocyte voltage clamp apparatus (Dagan Corporation, Minneapolis, MN; model CA-1 high performance oocyte clamp). 24 hours after RNA injection, oocytes were perfused extracellularly and intracellularly. Extracellular solutions contains, in mM: 80 Na-gluconate, 10 HEPES, 10 TEA-Cl, 5 $BaCl_2$, 1 $MgCl_2$ and 0.5 $CaCl_2$, pH 7.5/6.0 adjusted with NMDG. Intracellular side of oocytes was perfused either using a control solution (in mM: 90 K-gluconate, 10 HEPES, 10 KCl, 2 Na-gluconate, 1 $MgCl_2$, 0.2 BAPTA, pH 7.35 adjust with NMDG) or a solution supplemented with 2mM of BMOE. The BMOE perfusion lasts 6 minutes. Oocytes were then intracellularly washed with the control solution.

Expression, cell-surface labeling and crosslinking of His-tagged hASIC1a in CHO cells.

The XhoI-XbaI fragments encoding the His-tagged ASIC constructs were subcloned into pCDNA3.1(+)_zeo (Life Technologies, Zug, Switzerland). CHO-K1 cells were plated on P100 dishes and transfected with 15 µg plasmid DNA per plate using Lipofectamine-2000 (Life-Technologies), according to the manufacturer instructions. After 8-12 h incubation with the transfection mix, fresh medium (DMEM:F12, 3.6% FCS, 1% PenStrep) was added and cells were further incubated for ~24h.

Biochemistry

Pull-Down with nickel-NTA-Agarose beads

Oocytes were lysed with a lysis buffer (LB) containing 1% Triton and, in mM: 100 NaCl, 20 Tris-HCl at pH 7.5, 10 N-Ethylmaleimide (NEM), and a protease inhibitor cocktail containing 1 PMSF and 10 µg/ml each of Leupeptin, Pepstatin and Aprotinin (20 µl LB/oocyte). After 10 min centrifugation at ~15,000g (4°C), the intermediate phase comprising the solubilized protein fraction was recovered and subjected to batch affinity chromatography on nickel-NTA-Agarose beads (Qiagen, Hombrechtikon, Switzerland), incubating 2 h at 4°C in the presence of 20 mM imidazole to reduce non-specific binding.

After 2 min centrifugation at 2,000 rpm, the beads were washed 3 times with LB. 40 µl of sample buffer (25 mM DTT, final concentration) were added to the pellet containing the drained beads and heated at 95°C for 5 min. Bound proteins were then recovered by centrifuging through Evergreen mini-filters (EVE-208).

Cell-surface crosslinking and biotinylation of ASIC1a expressed in Xenopus oocytes.

48h hours after cRNA injection, 30 oocytes were incubated in 1 ml MBS solution supplemented with 2 mM BMOE (5 and 120 min at 19°C). Oocytes were then washed three times and then cell-surface biotinylated as described above. After lysis in SBB supplemented with 10 mM NEM, the biotinylated fraction was affinity-purified as described below.

Control- and BMOE-treated oocytes were labeled by 15 min incubation in ice in 1 ml of biotinylation buffer (in mM: 10 Triethanolamine, 150 NaCl and 2 $CaCl_2$) supplemented with 1 mg/ml biotinylation reagent. After aspiration of the bathing solution, oocytes were incubated for 5 min in 1 ml of quenching buffer (in mM: 192 Glycine, 25 Tris-HCl at pH 7.5, in MBS solution) and subsequently washed 3 times with MBS. Oocytes were finally lysed with a Streptavidin binding buffer (SBB, 20 µl LB/oocyte) containing 1% (v/v) Triton and, in mM: 5 EDTA, 100 NaCl, 40 Tris-HCl (pH 7.5), and protease inhibitor cocktail. The biotinylated fraction was affinity purified from the intermediate phase as described below.

Cell-surface crosslinking and biotinylation of ASIC1a expressed in CHO cells.

Transfected cells were washed with PBS containing 0.1 mM $CaCl_2$ and 1 mM $MgCl_2$ (PBS-CM) and then treated for 5 min at 22°C in the presence of 4 ml PBS-CM containing 2 mM BMOE or vehicle (DMSO, 2% final). Alternatively, cells were incubated with either ¼ diluted (in PBS-CM) or undiluted formaldehyde solution (~4%, SIGMA #HT5014) with $CaCl_2$ and $MgCl_2$ concentrations adjusted to 0.1 and 1 mM, respectively. After washing with chilled PBS-CM, plates were placed on ice in a cold room and cells were incubated for 15 min in the presence of 5 ml PBS-CM supplemented with 0.25 mg/ml of biotinylation reagent. The reaction was quenched by replacing the biotinylation solution with 10 ml of 100 mM Glycine in PBS-CM and further incubation for 20 min in the cold. Lysates were prepared by scraping cells in 3 ml membrane isolation buffer: 50 mM Tris/HCl (pH 7.0 at RT), 150 mM NaCl, 5 mM $MgCl_2$, and protease inhibitor cocktail. Lysates were snap-frozen in liquid nitrogen and stored at -70°C. After thawing, raw lysates were incubated for 30 min on an orbital shaker at 4°C in the presence of 0.1 mg/ml DNaseI (Roche Diagnostics AG, Rotkreuz, Switzerland). The membrane pellet obtained after 30 min centrifugation at 20,000g (4°C) was resuspended in SBB and proteins were solubilized by 45 min incubation on an orbital shaker at 4°C, and centrifuged for 12 min as before.

Affinity purification of biotinylated fractions from oocytes and CHO cells.

The intermediary phase from oocyte lysates and the Triton-soluble fraction from CHO cells were incubated for 1 h at 22°C with 50μl of streptavidin-bead suspension. Beads were washed three times in SBB and bound proteins were then eluted as described for pull-down experiments with nickel beads. Pilot studies using lysates from non-biotinylated oocytes and cells were carried out to assess the absence of non-specific binding of His-tagged hASIC1a to streptavidin (not shown).

In certain experiments, after two washing steps, the streptavidin beads were incubated on an orbital shaker for 20 min at 4°C in the presence of either 1 mM BMOE or vehicle. Reagent was removed by thorough washing before elution with sample buffer.

Western-Blot, Infrared detection.

Proteins were resolved by SDS-PAGE on 5-15% acrylamide gradient minigels for 1 h at 200V along with pre-stained molecular weight markers. Proteins were then electrotransferred onto nitrocellulose (Whatman Protran #10401396) for 2-3h at 100V. After 1 h of blocking at RT in 0.1% (w/v) casein solution, the membrane was incubated overnight with the primary antibody in 1 % milk-TBS-Tween. After three rounds of washing over 20-30 minutes in TBS-Tween, the blot was incubated 1 h in the presence of IRDye-conjugated secondary antibodies diluted 1/12,000 in casein solution. After washing, the blot was scanned with an Odyssey® Infrared Imaging System (LI-COR Biosciences).

Quantitative analysis of intensities and apparent molecular weights of western blot bands.

The intensities of bands were analyzed using the Odyssey 2.1 software. For samples obtained after crosslinking experiments, the intensities of the four bands were added and the relative intensity of each band was calculated. Finally, the average of the ratios measured for each band in individual experiments was calculated and reported for each of the ASIC1a constructs (± SD).

To determine the apparent molecular weight of each band, we analyzed the raw scans with the ImageJ software in order to measure the distances migrated by the molecular weight marker's bands. Then, we plotted those distances against the respective theoretical weight of each band and fitted it to an exponential curve in an Excel sheet (Microsoft). The function of the corresponding curve was used to calculate in each blot the apparent molecular weight value of the ASIC1a-immunostained bands on the basis of their respective migration distances (see supplementary Fig. S1). This protocol was repeated for each gel and lane. Finally, the mean of the thus estimated apparent molecular weights was calculated and reported for each ASIC1a construct (± SD).

References

1.   Pfister Y*, et al.* (2006) A gating mutation in the internal pore of ASIC1a. *J Biol Chem* 281(17):11787-11791.

Supplementary Table 1 Sequences of the primers used for the PCR mutagenesis

Mutant	Forward primer	Reverse primer
V74C	ccactaccaccattgcaccaagctcgacg	cgtcgagcttggtgcaatggtggtagtgg
Y426C	gagaccattgaacagaagaaagcctgtgagattgcagggctcctg	caggagccctgcaatctcacaggctttcttctgttcaatggtctc
G430C	ggcctatgagattgcatgtctcctgggtgacatcg	cgatgtcacccaggagacatgcaatctcataggcc
G433C	gcagggctcctgtgtgacatcgggg	ccccgatgtcacacaggagccctgc
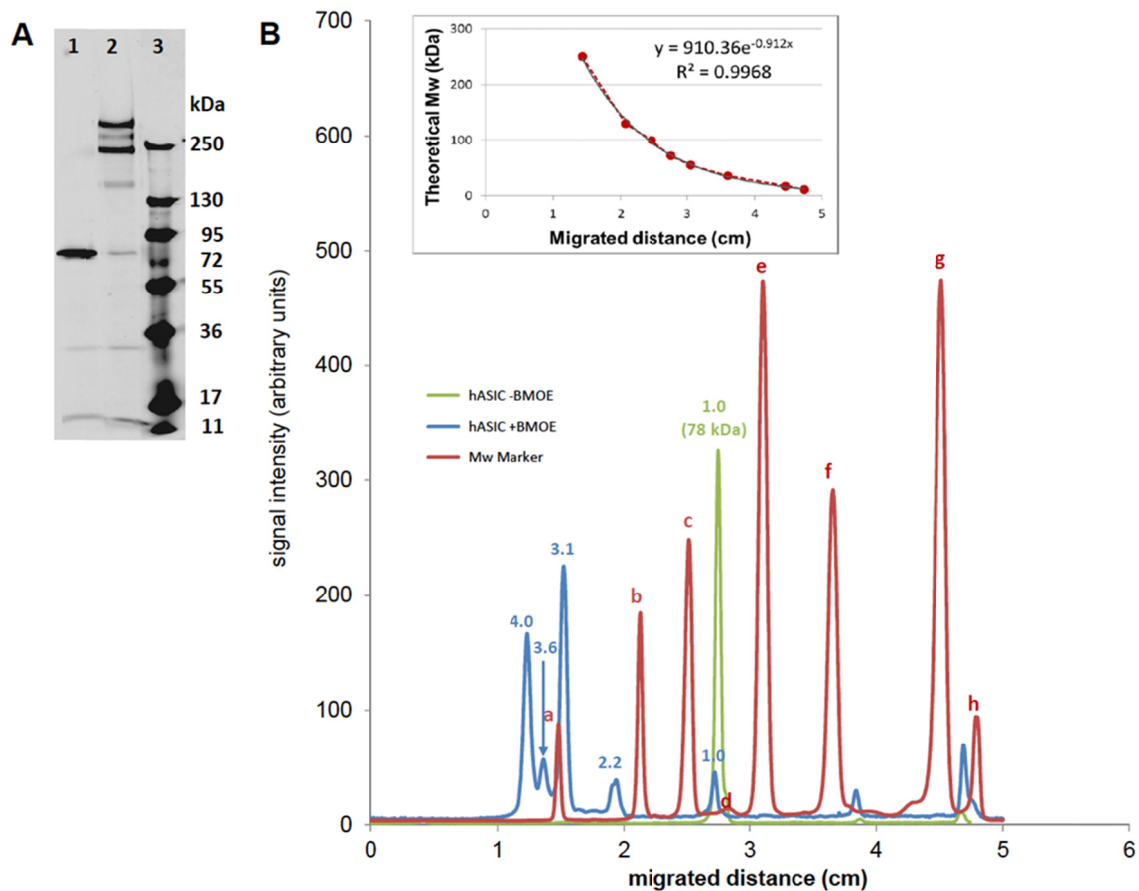
Figure S1

Apparent molecular weight (Mw) determination of ASIC1a bands. Blot (**A**): CHO cells were transiently transfected with G433C-ΔC_{Ct} and incubated for 5 min in the absence (lane 1) or presence (lane 2) of 2 mM BMOE, followed by cell-surface biotinylation. Anti-His-tag western blot of Streptavidin-bound fractions were analyzed with a LI-COR Odyssey scanner. In this example, the original blot has been cropped as to group the relevant lanes. The signal intensity profiles (**B**) for untreated ASIC1a (1, green), BMOE-treated ASIC1a (2, blue), and the molecular weight marker (3, red) are the average of four longitudinal traces drawn along each lane of the blot using the "straight line selection" tool of the ImageJ package. Theoretical Mw values of PeqGold Protein Marker V standards: a, 250; b, 130; c, 95; d, 72; e, 55; f, 36; g, 17; h, 11 kDa. Insert: distances migrated by each Mw standard band measured at the peaks of intensity were plotted against the corresponding theoretical Mw and fitted to an exponential function (insert). This function was used to estimate the apparent Mw values of the ASIC bands from control and BMOE-treated samples. Fold increases in the molecular weights relative to that of the main band in the control sample (78 kDa) are indicated on top of each peak. Experiments carried out using an additional molecular weight marker, Spectra Multicolor High Range Protein Ladder providing two additional high molecular weight standards at 180 and 300 kDa, yielded apparent Mw values for each band that fell within the range of values calculated when using the PeqGold ladder.

A
BMOE (beads) − + −
BMOE (cells) − − +

Band	On-cells crosslinking		On-beads crosslinking	
	Mw±SD	Relative Mw	Mw±SD	Relative Mw
I	75±2	1.0±0.0	77±1.1	1.0±0.0
II	161±13.4	2.2±0.2	167±3.5	2.2±0.0
III	224±19	3.0±0.2	236±6.0	3.0±0.1
III-IV	270±25	3.6±0.3	275±20.6	3.6±0.2
IV	302±26	4.0±0.3	308±11.9	4.0±0.2
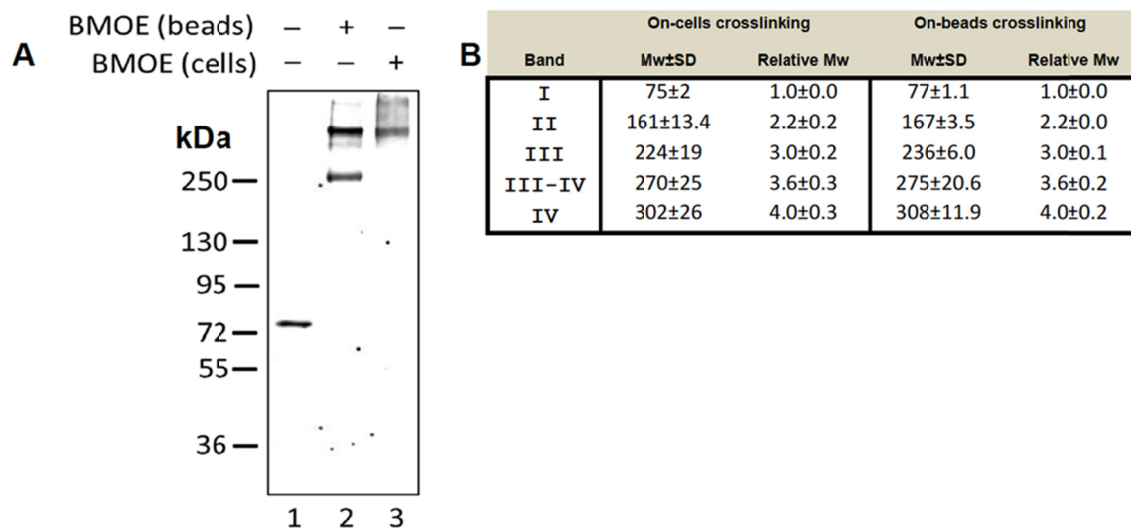
Figure S2

Crosslinking of G433C with BMOE on Streptavidin-agarose beads or at the cell surface. A; Transiently transfected CHO cells were incubated for 5 min at 22°C with either vehicle (DMSO, lanes 1 and 2) or 2 mM BMOE (lane 3). After cell-surface biotinylation, lysates were prepared and subjected to Streptavidin affinity chromatography. After washing, beads were incubated 15 min with either vehicle (lanes 1 and 3) or 1 mM BMOE (lane 2), washed and subsequently eluted by boiling drained beads in sample buffer (see Materials and Methods). After resolution of proteins by SDS-PAGE, control and crosslinked samples were analyzed by anti-His-tag western blotting. **B;** Apparent Mw values of bands I, II, III, III-IV, and IV, estimated as in **Supplementary figure 1**, after crosslinking of ASIC1a subunits by incubation with BMOE of either cells (n=9), or Streptavidin-bound fractions (beads, n=6).

4.   Structure of the methanethiosulfonate reagents and labeling reaction
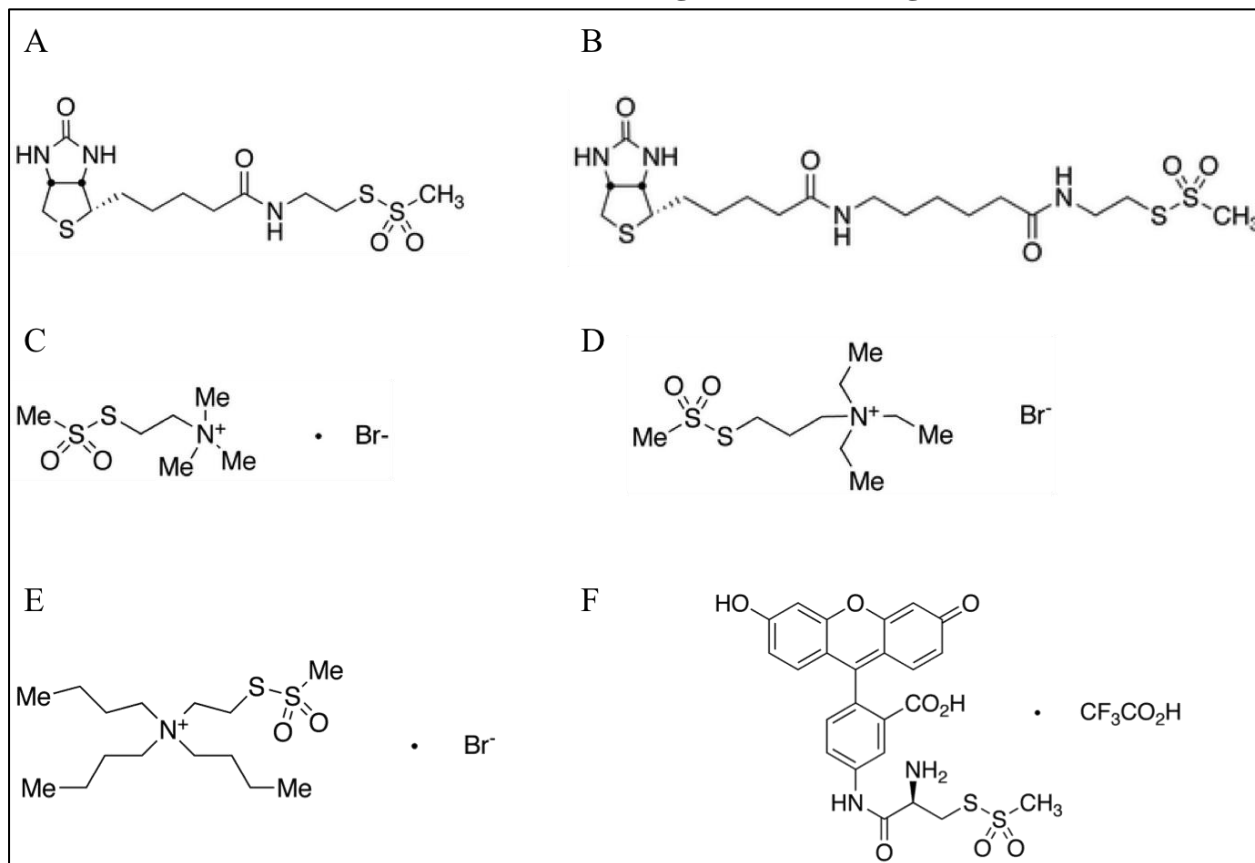
Figure 47 Methanethiosulfonate reagents. *A-F,* MTSEA-biotin, MTSEA-biotinCap, MTSET, MTS-PTrEA, MTS-TBAE, MTSEA-fluorescein, respectively. MTS pictures come from the Toronto Research Chemicals Inc. company website: http://www.trc-canada.com/search_cat.php?Search=MTS&qsearch=Quick+Search.
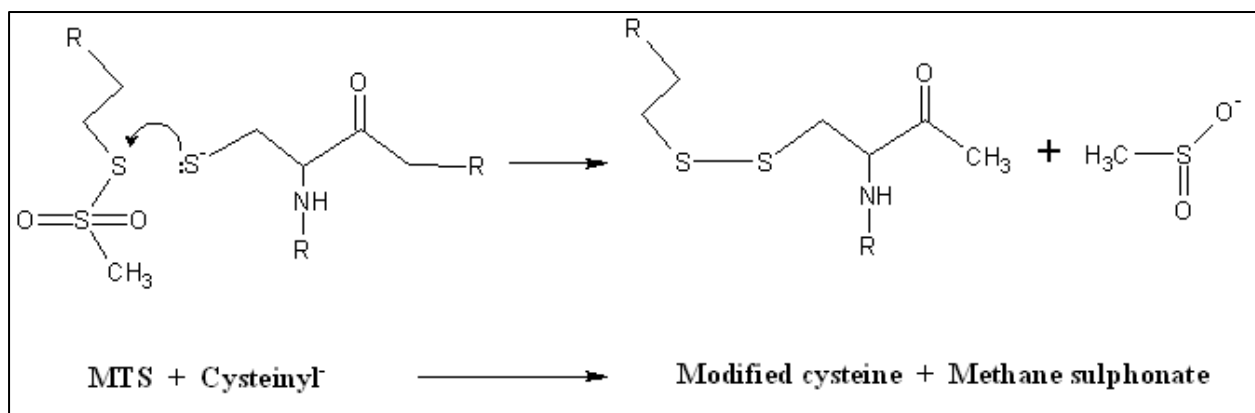
Figure 48 MTS reaction. The cysteinyl group makes a nucleophilic attack on the alkylthio group of the MTS reagent. As result, it forms a disulfide bridge to the thioalkyl moiety and the methanesulfonate part leaves.

Abbreviation	Name	Reference
MTSET	(2-(trimethylammonium)ethyl methanethiosulfonate, Bromide)	T795900
MTSEA-biotin	N-Biotinoylaminoethyl methanethiosulfonate	B394750
MTSEA-BiotinCAP	N-Biotinylcaproylaminoethyl Methanethiosulfonate	B395750
MTS-PTrEA	3-(Triethylammonium)propyl Methanthiosulfonate Bromide	T776300
MTS-TBAE	2-(Tributylammonium)ethyl Methanethiosulfonate Bromide	T773250
MTSEA-Fluorescein	(R)-2-Amino-2-[(5-fluoresceinyl)aminocarbonyl]ethyl Methanethiosulfonate, Trifluoroacetate Salt	A609615

Table 5 Chemical formula and reference numbers of the MTS reagents.

5.   Amiloride dose-response curves
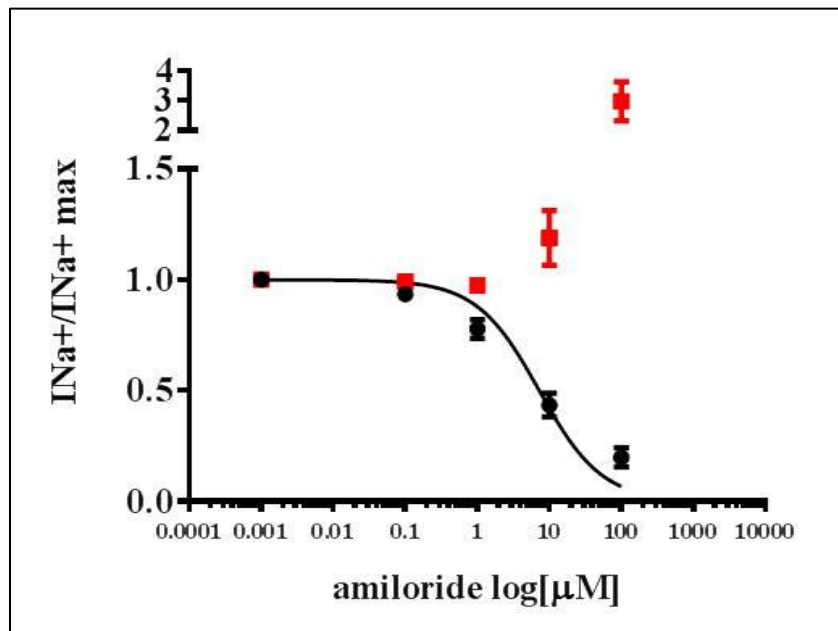
Figure 49 Amiloride dose-response curves. hASIC1a wt is blocked by amiloride with an IC50 of 7.27±1.22 µM (n=8, black curve). The amiloride inhibition of G440A is completely disrupted (in red, n=6).

6.   A homozygous missense mutations in SCNN1A is responsible for a transient neonatal form of pseudohypoaldosteronism type 1

A homozygous missense mutation in *SCNN1A* is responsible for a transient neonatal form of pseudohypoaldosteronism type 1

Mirjam Dirlewanger, Delphine Huser, Maria-Christina Zennaro, Eric Girardin, Laurent Schild and Valerie M. Schwitzgebel

You might find this additional info useful...

Supplemental material for this article can be found at:
http://ajpendo.physiology.org/content/suppl/2011/08/02/ajpendo.00066.2011.DC1.html

This article cites 39 articles, 15 of which can be accessed free at:
http://ajpendo.physiology.org/content/301/3/E467.full.html#ref-list-1

Updated information and services including high resolution figures, can be found at:
http://ajpendo.physiology.org/content/301/3/E467.full.html

Additional material and information about *AJP - Endocrinology and Metabolism* can be found at:
http://www.the-aps.org/publications/ajpendo

This infomation is current as of January 31, 2012.

A homozygous missense mutation in *SCNN1A* is responsible for a transient neonatal form of pseudohypoaldosteronism type 1

Mirjam Dirlewanger,[1]* Delphine Huser,[2]* Maria-Christina Zennaro,[3,4,5] Eric Girardin,[6] Laurent Schild,[2] and Valerie M. Schwitzgebel[1]

[1]*Pediatric Endocrine and Diabetes Unit, Department of the Child and Adolescent, Children's Hospital, Geneva University Hospitals, Geneva;* [2]*Department of Pharmacology and Toxicology, University of Lausanne, Lausanne, Switzerland.* [3]*Institut National de la Sante et de la Recherche Medicale, U970, Paris Cardiovascular Research Center - PARCC;* [4]*Université Paris Descartes;* [5]*Assistance Publique-Hôpitaux de Paris, Hôpital Européen Georges Pompidou, Paris, France; and* [6]*Pediatric Nephrology Unit, Department of the Child and Adolescent, Children's Hospital, Geneva University Hospitals, Geneva, Switzerland*

Dirlewanger M, Huser D, Zennaro MC, Girardin E, Schild L, Schwitzgebel VM. A homozygous missense mutation in *SCNN1A* is responsible for a transient neonatal form of pseudohypoaldosteronism type 1. *Am J Physiol Endocrinol Metab* 301: E467–E473, 2011. First published June 7, 2011; doi:10.1152/ajpendo.00066.2011.—Pseudohypoaldosteronism type 1 (PHA1) is a monogenic disorder of mineralocorticoid resistance characterized by salt wasting, hyperkalemia, high aldosterone levels, and failure to thrive. An autosomal recessive form (AR-PHA1) is caused by mutations in the epithelial sodium channel ENaC with usually severe and persisting multiorgan symptoms. The autosomal dominant form of PHA1 (AD-PHA1) is due to mutations in the mineralocorticoid receptor causing milder and transient symptoms restricted to the kidney. We identified a homozygous missense mutation in the *SCNN1A* gene (c.727T>C/p.Ser243Pro), encoding α-subunit of ENaC (α-ENaC) in a prematurely born boy with a severe salt-losing syndrome. The patient improved rapidly under treatment, and dietary salt supplementation could be stopped after 6 mo. Interestingly, the patient's sibling born at term and harboring the same homozygous Ser243Pro mutation showed no symptom of salt-losing nephropathy. In vitro expression of the αSer243Pro ENaC mutant revealed a slight but significant decrease in ENaC activity that is exacerbated in the presence of high Na^+ load. Our study provides the first evidence that ENaC activity is critical for the maintenance of salt balance in the immature kidney of preterm babies. Together with previous studies, it shows that, when the kidney is fully mature, the severity of the symptoms of AR-PHA1 is related to the degree of the ENaC loss of function. Finally, this study identifies a novel functional domain in the extracellular loop of ENaC.

hyponatremia; hyperkalemia; mineralocorticoid resistance; aldosterone; salt wasting

PSEUDOHYPOALDOSTERONISM TYPE 1 (PHA1) is a rare disease characterized by a resistance to mineralocorticoids that presents in the neonatal period or early infancy with a salt-wasting nephropathy, dehydration, hyperkalemia, and failure to thrive. Two major clinical forms of PHA1 have been described (17). The autosomal dominant renal form of PHA1 (AD-PHA1) involves loss-of-function mutations of the mineralocorticoid receptor (MR), encoded by the *NR3C2* gene located on chromosome 4q31.1 (38, 39). More than 40 mutations have been

described in both sporadic and familial cases (7, 16, 26, 36). This form of mineralocorticoid resistance is restricted to the kidney and shows moderate clinical features, with renal symptoms typically improving with age. The autosomal recessive form of PHA1 (AR-PHA1) is caused by loss-of-function mutations in the genes encoding the epithelial Na channel (ENaC) α-, β-, and γ-subunits. Symptoms are usually multisystemic, including a severe salt-losing nephropathy causing dehydration with hyperkalemia and recurrent episodes of pulmonary infection, congestion, coughing, and wheezing (21, 32); a cutaneous phenotype with eczematous rash of the skin has been reported (23, 34). The symptoms are usually persistent and more severe than in AD-PHA1. Recently, clinical improvement with age has been reported in patients with AR-PHA1 (2, 18, 28).

In the kidney, the MR is expressed exclusively in the aldosterone-sensitive distal nephron (ASDN), which includes the connecting tubule and the collecting duct (12). The ASDN is the site involved in the fine regulation of Na^+ absorption and K^+ secretion to balance the daily intake of these electrolytes. After binding aldosterone the MR undergoes a conformational change, and the ligand-receptor complex is translocated to the nucleus, allowing transcription of aldosterone-induced genes, including ENaC and various signaling factors (4–6, 15, 16, 27, 37–39).

ENaC colocalizes with the MR and is expressed in the ASDN of the kidney but also in other tight epithelia such as the colon, the respiratory tract, and salivary glands. In the kidney, ENaC is essential for the maintenance of the extracellular fluid and blood pressure and also plays a crucial role in K^+ homeostasis. In the distal lung airways, ENaC regulates fluid absorption at the air-liquid interface, thereby determining the rate of mucociliary transport (11).

ENaC is a heteromeric protein composed of homologous subunits and provides an electrogenic sodium transport pathway from the lumen into the cell (20). The α-subunit is required for ENaC function, whereas the β- and γ-ENaC are important for maximal channel activity. The reabsorbed Na^+ is then transported out of the cell into the interstitium by the Na^+/K^+ ATPase pump located on the basolateral membrane. In the ASDN, ENaC is the rate-limiting step in Na^+ reabsorption. The electrogenic ENaC-mediated Na^+ absorption in the ASDN provides the necessary driving force for K^+ secretion in this part of the nephron.

In the present study, we describe a novel Ser243 to Pro mutation in the α-ENaC subunit that is associated with a

---

transient AR-PHA1 diagnosed in a preterm patient with a severe salt-losing nephropathy. Our observations shed a new light on the role of ENaC in the maturing kidney and on the genotype-phenotype relations found in AR-PHA1.

METHODS

Subjects. We studied a family presenting with an autosomal recessive form of PHA1 and sequenced the MR and ENaC genes. The parents were Sri Lankan first-degree cousins in good general health. The older child presented with clinical and laboratory characteristics of PHA1 at 16 days of age and was the index case. Informed consent was obtained from all of the family members.

Biochemical assays. Aldosterone concentrations were measured in the serum by direct radioimmunoassay with a Diagnostic Products kit (ISO 15189). The plasma renin activity (PRA) ($ng \cdot ml^{-1} \cdot h^{-1}$) was measured by direct radioimmunoassay after an incubation period at 37°C (INC Biomedical). Sweat tests and concentrations of Cl^-, Na^+, and K^+ were measured according to the cystic fibrosis foundation consensus report: normal values of $Cl^- \leq 39$ mmol/l and $Na^+ \leq 60$ mmol/l (14).

Genomic DNA isolation and sequencing. Genomic DNA was extracted from peripheral blood leukocytes by salt extraction, as described previously (26). All coding exons and the intron-exon flanking regions of the *NR3C2* gene, coding for the MR, as well as the *SCNN1A, SCNN1B,* and *SCNN1G* genes were amplified with 13 pairs of primers (see Supplemental Table S1; Supplemental Material for this article is available online at the *AJP-Endocrinology and Metabolism* web site). Direct sequencing of PCR products was then performed by the ABI Prism Big Dye Terminator version 3.1 Cycle Sequencing Kit (Applied Biosystems, Foster City, CA) on an ABI Prism 3700 DNA Analyzer. The identified mutation was confirmed on a second PCR product and on a second DNA sample.

Site-directed mutagenesis, RNA in vitro transcription, and expression in Xenopus laevis oocytes. The human α-, β-, and γ-ENaC subunits were cloned in the pBSK vector and linearized by *Not*I, and capped cRNA was in vitro synthesized by SP6 polymerase. α-ENaC Ser[243] to proline mutant (α-S243P) and Ser[243] to cysteine (α-S243C) were obtained by site-directed mutagenesis using Stratagene's Quick-Change protocol. Healthy stage V and VI *Xenopus laevis* oocytes were pressure-injected with 10 ng of human ENaC cRNA (with equal amounts of α-, β-, and γ-subunits). Oocytes were kept at 19°C in either a low Na^+ incubation solution containing (in mM) 10 NaCl, 0.82 $MgSO_4$, 0.41 $CaCl_2$, 0.33 $Ca(NO_3)_2$, 80 *N*-methyl-D-glucamine (NMDG), 2 KCl, and 5 HEPES or a high Na^+ incubation solution containing (in mM) 85 NaCl, 1 KCl, 2.4 $NaHCO_3$, 0.82 $MgSO_4$, 0.41 $CaCl_2$, 0.33 $Ca(NO_3)_2$, 10 HEPES, and 4.08 NaOH.

Electrophysiology. Electrophysiological measurements were made 16–24 h after injection. The oocytes expressing ENaC were studied using the standard two-electrode voltage clamp technique, using a Dagan TEV voltage clamp amplifier (Dagan, Minneapolis, MN), the Digidata 1322 digitizer, and the PClamp 9 data acquisition and analysis package (Axon Instruments, Molecular Devices, Sunnyvale,

CA). The two electrodes contained a 1 M KCl solution. All electrophysiological experiments were performed at room temperature (22°C). The holding potential was -100 mV. The composition of the perfusion solution was (in mM) 120 NaCl, 2.5 KCl, 1.8 $CaCl_2$-^2H_2O, and 10 HEPES-H^+ for the Na^+ solution; NaCl was replaced by 120 mM NMDG-HEPES or KCl for the perfusion solutions devoid of Na^+. To determine amiloride-sensitive currents, we added amiloride (Sigma) in a separated fraction of each test solution at a final concentration of 10 μM. Inward Na^+ current was generated by switching solution without Na^+ (NMDG or KCl) to perfusion solution containing 120 mM of Na^+. In the experiment with proteases, the oocytes were exposed to 5 μg/ml trypsin (Sigma-Aldrich Chemie) in the 120 mM NaCl perfusion solution.

Biotinylation. For surface biotinylation 16–30 h after cRNA injection, oocytes were incubated in 1 ml of biotinylation buffer containing 1 mg/ml NHS-SS-Biotin (Sigma-Aldrich Chemie) or MTSEA-biotin (*N*-biotinylaminoethyl methanethiosulfonate; Toronto Research Chemicals) for 15 min at 4°C. Oocytes were washed twice and then incubated 5 min at 4°C with 2 ml of the high Na^+ incubation solution. Thirty oocytes per condition was lysed with 20 μl lysis buffer/oocyte. Oocytes were vortexed and centrifuged for 10 min at 12,000 rpm (4°C). The intermediate phase was withdrawn, and a sample of each lysate was kept as a control of "total lysate fraction." Lysates were then incubated overnight with 40 μl of streptavidin beads (Immunopure Immobilized Streptavidin Gel; Perbio) at 4°C.

Statistical analyses. Student's *t*-test was used for statistical analysis. Data are expressed as means ± SE.

RESULTS

Clinical course. The index case issuing from consanguineous parents was born prematurely at 32 wk of gestation by vaginal delivery following premature rupture of the membranes. The patient's birth weight was 1,645 g (between the 10th and 50th percentile, growth curve adjusted for ethnicity and age) (24). The newborn developed hypotonia and feeding problems, and no respiratory distress was noted. On day 16 of life, severe hyponatremia associated with hyperkalemia and mild metabolic acidosis (pH 7.30) was discovered. Plasma renin activity was elevated, as was the plasma aldosterone level (Table 1). Fractional sodium excretion (FENa) was increased, and the urinary Na^+/K^+ ratio was 7.6 (normal value <2), confirming salt wasting (Table 1) (18, 25). These results were consistent with the diagnosis of PHA1. Treatment with cation exchange resin (0.5 $g \cdot kg^{-1} \cdot day^{-1}$) and NaCl (6 $mmol \cdot kg^{-1} \cdot day^{-1}$) supplementation was introduced. At 7 wk after birth, evolution of the FENa and serum Na^+ values normalized under treatment, reaching values comparable with the patient's sibling born at term (Fig. 1). Salt supplementation could be stopped at 6 mo of life without subsequent salt-losing episodes.

Table 1. *Clinical characteristics of the family members with PHA1*

ID	Age	Genotype	Aldosterone, ng/dl	PRA, $ng \cdot ml^{-1} \cdot h^{-1}$	Na^+, mmol/l	K^+, mmol/l	FENa, %
Index patient	2 wk	−/−	2088	>500	106	7.9	5.52
Index patient	6 mo	−/−	148	2.33	139	4.5	0.11
Brother	2 wk	−/−	1058	220	136	5.9	0.12
Brother	4 mo	−/−			140	4.7	
Mother	36 yr	±	5.0	1.00	139	4.1	NA
Father	40 yr	±	14.0	1.93	140	4.2	NA

PHA1, pseudohypoaldosteronism type 1; PRA, plasma renin activity; FENa, fractional sodium excretion. −/−homozygous; ±heterozygous for Ser[243]Pro (S243P) mutation. Normal values for aldosterone 19–141 (premature infant), 5–90 (full-term infant), and 4–30 ng/dl (adult). Normal values for PRA 11–167 (premature infant), 2.35–37 (full-term infant), and 0.82–3.68 $ng \cdot ml^{-1} \cdot h^{-1}$ (adult). Na^+ 131–145 mmol/l (newborn). K^+ 3.6–5.9 mmol/l (newborn). FENa <2%.
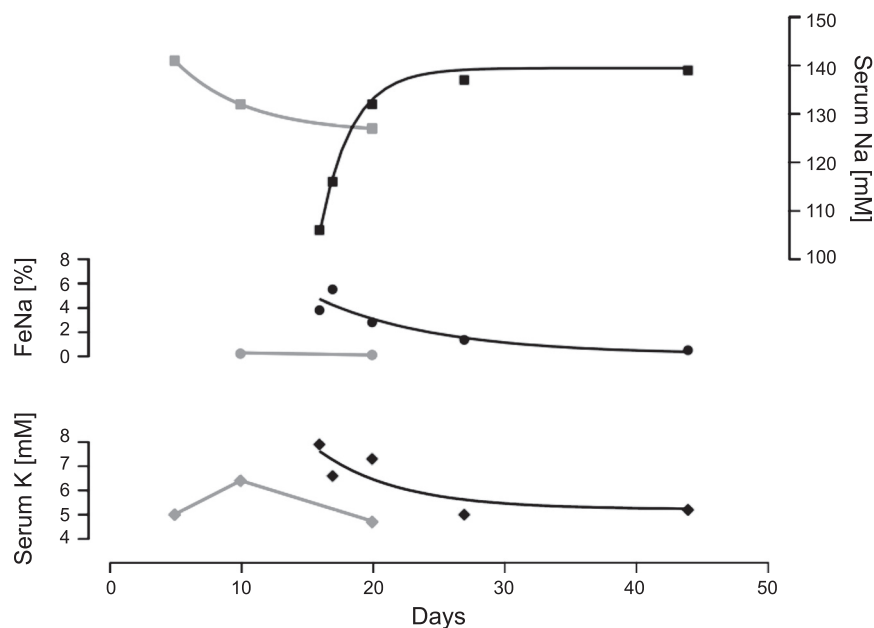
Fig. 1. Serum Na^+ and K^+ as well as fractional excretion for sodium (FENa) in the 2 family members harboring the homozygous S243P α-epithelial Na channel mutation. Postnatal normalization of FENa in the index case born prematurely (black dots). Hyponatremia (black squares) improves as K^+ and FENa decrease in the index case (black diamonds and dots). Normonatremia, kalemia, and normal FENa in the brother born at term (gray squares, diamonds, and dots, respectively).

The second child of the same parents was born at term also by vaginal delivery and did not develop any electrolyte abnormality, and urinary Na^+/K^+ ratio, as well as the FENa, was normal (0.36; Table 1). However, the aldosterone level and PRA at 2 wk of age was above the normal range for age (Table 1). Sweat tests were performed in both brothers. The chloride concentration was normal for both children [38 and 16 mmol/l, respectively, ($n \leq 39$ mmol/l)], excluding the diagnosis of cystic fibrosis. Sweat sodium concentrations were normal [53 and 27 mmol/l ($n = 9$–72 mmol/l)]. Both parents showed normal values of aldosterone and PRA without any electrolyte disturbances (Table 1).

Genetic analysis. Given the exclusive renal symptoms of index case, we initially hypothesized an AD-PHA1 and performed direct sequencing of the *NR3C2* coding exons and the intronic exon-flanking regions for confirmation. No mutation was found in the NR3C2 amplified from the index case. Subsequent analysis of the genes coding for the subunits of the epithelial sodium channel ENaC revealed a homozygous c.727T>C mutation in exon 4 of the *SCNN1A* gene, substituting a proline (Pro) for serine (Ser) at position 243 (Ser243Pro) in the α-ENaC subunit. No other mutations were detected in the *SCNN1B* and *SCNN1G* genes coding for the β- and γ-ENaC subunits, respectively. Both the index case and the patient's younger asymptomatic brother were homozygous carriers of the same Ser243Pro mutation (α-S243P), whereas the mother and the father were heterozygous. The Ser243 residue lies in the large extracellular domain of ENaC within the second cysteine-rich domain and is highly conserved among the α-, β-, and γ-ENaC subunits of different species from amphibian to mammalian (Supplemental Fig. S1).

Functional analysis of the mutant α-ENaC. The ENaC α-S243P mutant was expressed in *Xenopus* oocytes for functional analysis. Representative tracings of the Na^+ current mediated by ENaC wild type (WT) and ENaC α-S243P mutant are shown in Fig. 2, *A* and *B*. The rapid substitution of an external solution devoid of Na^+ ions to a solution containing 120 mM Na^+ generated a robust inward current characterized by a large peak current followed by a current relaxation to a steady-state current after 10 s. The steady-state current was inhibited by the addition of 10 μM amiloride to the bathing solution. The α-S243P mutant exhibits an amiloride-sensitive, inward Na^+ current that is qualitatively similar to WT, but quantitatively the current magnitude is lower. This decrease in the steady-state current magnitude is summarized in Fig. 2, *C* and *D*. ENaC current was measured in oocytes expressing either ENaC WT or the α-S243P mutant after overnight incubation of the oocytes in a high or low Na^+-containing medium. Since ENaC is constitutively open when expressed at the cell surface, extracellular Na^+ equilibrates with the intracellular Na^+ and thus determines both the extra- and intracellular Na^+ loads (1). Under both conditions, the S243P mutant exhibits a lower amiloride-sensitive current (Fig. 2C). The overnight incubation in a high Na^+ medium (85 mM NaCl) of oocytes expressing ENaC WT or the S243P mutant results in a significant decrease in ENaC current compared with oocytes preincubated overnight in a low Na^+ medium (10 mM NaCl). This phenomenon has been described extensively and is called feedback inhibition of the channel in response to an increase in intracellular Na^+ load (1). The feedback inhibition of ENaC serves to prevent excessive accumulation of intracellular Na^+ ions that could be toxic for the cell. Compared with WT ENaC, the reduction in the amiloride-sensitive Na^+ current expressed by the α-S243P mutant was more pronounced (80%) after overnight incubation in the high Na^+-containing medium than in the low Na^+ medium (30% decrease) (Fig. 2, *C* and *D*). These experiments show that the α-S243P mutation is associated with a partial but significant loss of function. In addition, this loss of function is exacerbated under conditions favoring a high intracellular Na^+ load as if the α-S243P mutation makes the channel hypersensitive to feedback inhibition in the presence of a high Na^+ load.

The ENaC current relaxation from the maximal peak current to its steady state is a fast adaptive process dependent on the permeating Na^+ ions, termed ENaC self-inhibition (8). We asked whether this physiological inhibitory response to extra-

Fig. 2. Epithelial Na channel (ENaC)-mediated Na$^+$ currents in oocytes expressing ENaC wild type (WT) and ENaC α-S243P mutant. *A* and *B*: representative recordings of amiloride-sensitive Na$^+$ current in oocytes expressing ENaC WT αβγ-WT and ENaC α-S243Pβγ mutant. *C*: absolute amiloride-sensitive steady-state Na$^+$ currents measured in oocytes incubated for 24 h (see METHODS) in a low Na$^+$-containing solution (closed bars; *n* = 12 experiments) and in a high Na$^+$ solution (open bars; *n* = 8 experiments). Oocytes expressed either αβγ-WT or α-S243Pβγ mutant. *D*: relative changes in the ENaC-mediated amiloride-sensitive current in oocytes expressing the α-S243Pβγ mutant relative to those expressing ENaC αβγ-WT after incubation in a low Na$^+$-containing solution (closed bars) and in a high Na$^+$ solution (open bars). **$P < 0.01$; ***$P < 0.001$.
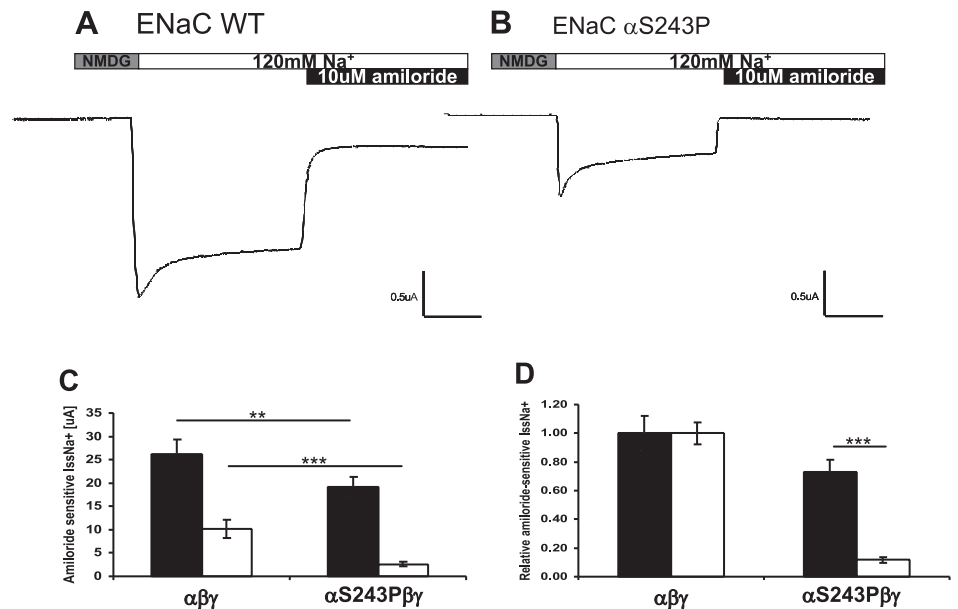
cellular Na$^+$ ions was modified in the α-S243P mutant. Self-inhibition was defined as the ratio of the maximal peak current over the steady-state current measured at 20 s (Iss/Ipeak); the higher the ratio, the lower the ENaC self-inhibition. The data in Fig. 3 show that for ENaC WT and α-S243P mutant, the self-inhibition is independent of the incubation conditions in high or low Na$^+$ medium. The ratio Iss/Ipeak for the α-S243P mutant was significantly decreased for the S243P mutant compared with ENaC WT, indicating a slightly stronger apparent self-inhibition for the channel mutant. The kinetic parameters of the self-inhibition of the S243P mutant, obtained from the exponential fit of the Na$^+$ current decrease, were similar for both the ENaC WT and mutant channel (data not shown). Thus the apparent stronger feedback inhibition determined by the Iss/Ipeak ratio is likely due to a lower steady-state current for the α-S243P mutant, as shown in Fig. 2.

We have verified that the reduction of ENaC-mediated current for the α-S243P mutant was not due to a lower
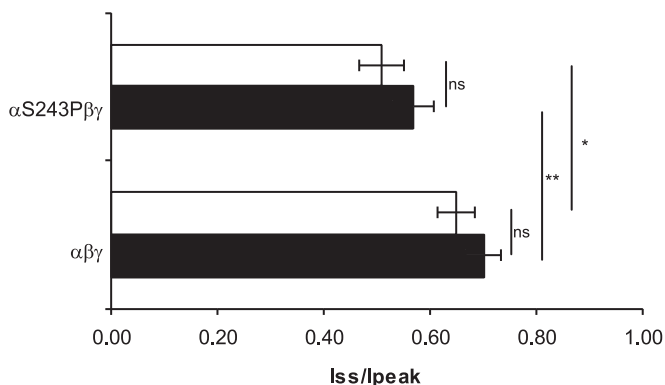
Fig. 3. ENaC self-inhibition of the WT channel and the α-S243P mutant. Channel self-inhibition was defined as the ratio of the steady-state current (Iss) measured after 20 s over the peak current (Ipeak) (see Fig. 2, *A* and *B*). Closed and open bars, low and high Na$^+$ incubation conditions, respectively. Iss/Ipeak ratio for the α-S243Pβγ and the WT was 0.57 ± 0.04 and 0.70 ± 0.03, respectively (Student's *t*-test; $P < 0.05$, *n* = 12), and 0.51 ± 0.04 vs. 0.65 ± 0.04 (Student's *t*-test; $P < 0.01$, *n* = 8).

expression of ENaC at the cell surface. Mutant and WT channels at the cell surface were labeled with biotin and affinity purified on streptavidin beads. Western blots in Fig. 4 using an anti-α-ENaC antibody show the intracellular (unbound fraction to streptavidin beads) and surface expression (bound fraction to streptavidin beads) of the ENaC mutant compared with the WT. Both intracellular and surface expression of the ENaC WT or α-S243P mutant were comparable, and therefore, changes in the expression of the α-S243P mutant at the protein level cannot account for the observed decrease in amiloride-sensitive current. In addition, we also tested the possibility that the α-S243P mutation may change channel affinity for amiloride. Both ENaC WT and S243P mutant have comparable affinities for amiloride with an IC$_{50}$ of 0.29 (± 0.08; *n* = 12) and 0.15 μM (± 0.04; *n* = 12), respectively.

The parents of the index case are heterozygous for the α-S243P mutation and do not show any phenotype related to alterations in the Na$^+$ balance or to changes in the plasma level of aldosterone. We have reproduced the heterozygous genotype in the *Xenopus* oocytes by coinjecting equal amounts of cRNA encoding for the ENaC WT and the α-S243P mutant (1.5 ng of each cRNA), with β- and γ-subunits. Compared with the ENaC WT, the α-S243P shows a significant reduction in the channel activity (60%), and the coexpression of the ENaC WT and mutant generated an amiloride-sensitive current that in magnitude was intermediate to that of the WT and the mutant (Fig. 5). Such reduction in ENaC activity observed upon expression of the α-S243P mutant alone or with the ENaC WT is consistent with a gene dosage effect. Considering the absence of phenotype of the heterozygous parents, our data suggest that the kidney can tolerate a 40% reduction in ENaC activity without any consequence for the maintenance of Na$^+$ homeostasis.

What is the mechanism underlying the partial loss of ENaC function due to the α-S243P mutation? Several mechanisms regulate ENaC at the cell surface. One mechanism associated with the activation of ENaC at the cell surface involves a proteolytic cleavage of the α- and the γ-subunit of the ENaC

A

Unbound fraction

B
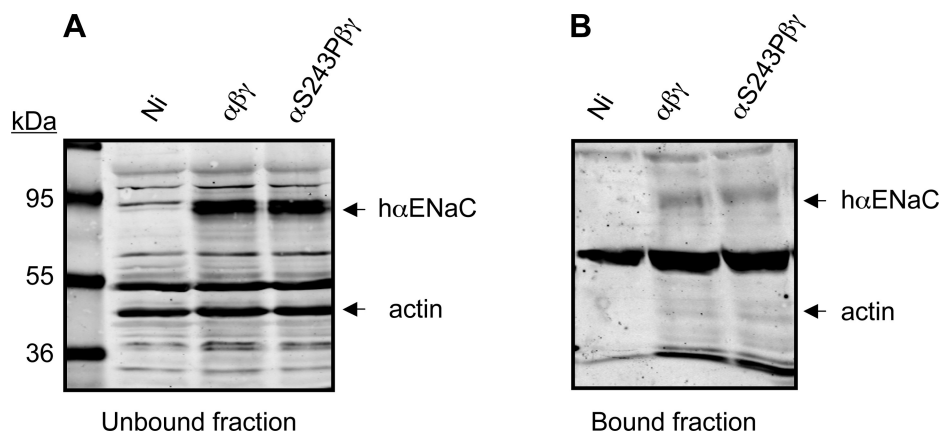
Bound fraction

Fig. 4. Surface expression of ENaC WT and α-S243P mutant. *A*: Western blot using anti-α-ENaC (hαENaC) and anti-actin antibodies of the unbound fraction to streptavidin beads (non-biotinylated fraction) of total proteins from oocytes expressing ENaC WT or the α-S243P mutant. *B*: similar Western blot of the biotinylated fraction of total proteins bound to streptavidin beads representing the surface expression of α-ENaC WT and mutant. Ni, negative control.

complex by serine proteases at specific sites in the extracellular domain (29); this channel activation can be reproduced using low concentrations of external trypsin in *Xenopus* oocytes (9). Although α-S243 is not part of a consensus target sequence for serine proteases, we verified that the loss of function of the α-S243P mutant channel was not due to a resistance to cleavage and channel activation by serine proteases. Experiments in Fig. 6 confirm the partial loss of function of the α-S243P mutant after overnight incubation in a low or high Na^+ medium. In the presence of trypsin, both the WT and the mutant show an approximately twofold increase in channel activity; the reduced activity of the α-S243P still remained significant compared with the WT, even in the presence of trypsin. These experiments indicate that the α-S243P mutant retains its sensitivity to activation by extracellular trypsin, but the loss of function of the channel mutant cannot be overcome by trypsin; thus the mechanism underlying the channel loss of activity is a more general mechanism that is independent of the channel activation by proteolytic cleavage.

The substitution of the α-Ser^{243} by a proline is expected to markedly change the architecture of the protein at this specific site, since Pro is often found in bends of folded proteins. We could observe that a more conserved substitution of the Ser^{243} by cysteine was without effect on ENaC activity. Actually, after overnight incubation in a high Na^+ medium, α-S243Cβγ, did not display a steady-state current that was significantly

different from the WT (15.7 μA ± 3.14; $n = 24$, $P = 0.08$). Thus it is likely that the S243P mutation in the α-ENaC introduces important steric changes in an extracellular domain that is important for ENaC activity and its modulation.

DISCUSSION

In this study, we have identified in a patient with a transient form of AR-PHA1 a novel homozygous mutation in the *SCNN1A* gene, leading to a Ser^{243} to Pro substitution of the α-ENaC subunit. This patient was born prematurely at week 32 and presented renal symptoms only, characterized by a severe salt-wasting nephropathy with extremely high levels of aldosterone. Within 2 wk of treatment with salt supplementation and cation exchange resin, clinical symptoms rapidly improved, and serum and urinary Na^+ values normalized. Blood analyses performed at 6 mo of age still revealed an elevated aldosterone level but without electrolyte disturbances. The patient's younger brother born at term with the same homozygous α-S243P mutation did not show any renal salt-wasting phenotype, only an elevated plasma aldosterone.

In premature infants the urinary loss of sodium exceeds the daily intake, leading to a negative Na^+ balance in most infants less than 28 wk of gestational age (GA) (3, 10). A positive balance is achieved only after 32 wk of GA, which is due to continuing kidney maturation responsible for a decrease in renal fractional excretion of sodium. The cellular mechanisms for the limited capacity of the kidney to retain Na^+ before term have not been completely elucidated.

Microperfusion of cortical collecting ducts isolated from 1-wk-old rabbits with immature kidneys showed no significant Na^+ transport, and no conducting ENaC channels could be observed by patch-clamp technique (30, 31). To the extent that the immature kidney of newborn rabbits is a representative model of the premature human kidney, the paucity of active ENaC channels may certainly contribute to the reduced capacity of the immature kidney to reabsorb Na^+ ions. In addition, a relative insensitivity of the immature kidney to aldosterone has been demonstrated in the newborn rat and rabbit, suggesting that the plasma mineralocorticoids play a limited role in regulating renal distal Na^+ absorption in the early postnatal life (35).

The transition from the fetal to the neonatal life is characterized by a dramatic decrease in the urinary Na^+ excretion. Clearance studies using diuretics have suggested that nephron segments downstream of the proximal tubule are responsible
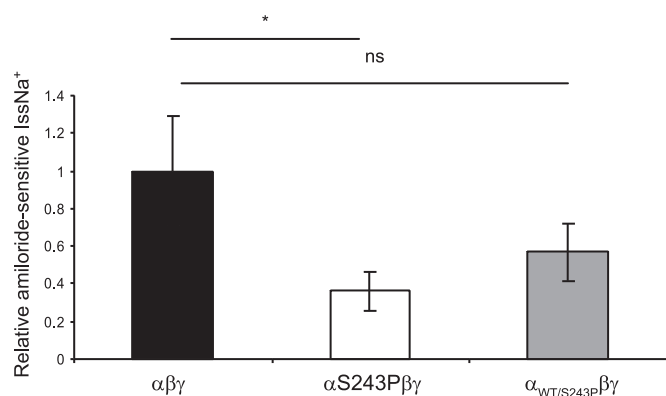
Fig. 5. Reconstitution of the heterozygous genotype for the α-S243P mutation. Equal amounts of cRNA (1.5 ng) for the ENaC WT and for the α-S243P mutant were injected. Oocytes were incubated overnight in a high Na^+-containing medium (85 mM NaC1); $n = 10$ oocytes/condition obtained from 2 frogs. *$P < 0.05$. ns, Not significant.

Fig. 6. ENaC channel activation by trypsin. The addition of trypsin (5 μg/ml) in the external medium (open bars) significantly increased the current of the mutant α-S243Pβγ and the WT 2.6- and 1.9-fold, respectively, after incubation in a low Na^+ medium and 3- and 2.2-fold, respectively, after incubation in a high Na^+ medium. The number of oocytes ranged from 17 to 26. ***$P < 0.001$; **$P < 0.01$.
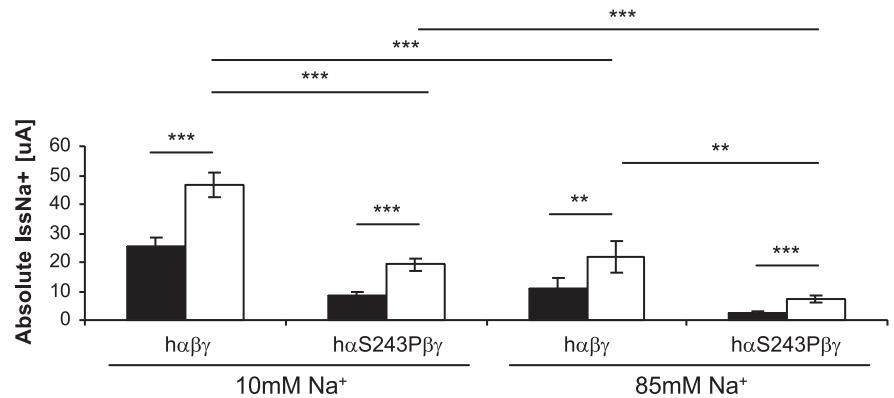
for the sharp increase in Na^+ absorption during the early postnatal life (33). Patch-clamp studies on rabbit neonates have shown that the product of the number of ENaC channel times the channel open probability increases 30-fold between the 1st and the 2nd wk after birth (31).

The index case shows a urinary Na^+ excretion, as measured by the UNa^+/K^+ ratio, more than three times higher than expected for a preterm infant of 32 wk of GA (3). The identification of the α-S243P ENaC loss of function mutation in this patient is the most likely explanation for the patient's abnormally high UNa^+/K^+ and the high plasma aldosterone level. The evidence α-S243P mutation results in a channel loss of function confirms the diagnosis of AR-PHA1. Our observation represents the first direct evidence that ENaC plays a crucial role for achieving a Na^+ balance starting a 32 wk of GA, since a slight decrease in ENaC activity due to the α-S243P mutation has dramatic consequences on distal Na^+ absorption and can precipitate a severe salt-wasting nephropathy in a premature baby.

The rapid clinical improvement of our patient during the first weeks of life is likely due to kidney maturation associated with an increase in the expression of ENaC channels as well as other Na^+ transporters in or upstream of the distal nephron. This is supported by the fact that the patient's younger brother, carrying the same genotype but born at term, never developed the renal symptoms but had a slightly elevated plasma aldosterone level. This further indicates that limited loss of function of the α-S243P ENaC mutation is not sufficient to precipitate an AR-PHA1 when the kidney maturation is nearly completed at term. However, we cannot exclude potential epigenetic changes contributing to the different phenotypes, as sometimes observed in monozygotic twins.

The parents of the index case, heterozygous for the mutations, do not show any sign of a Na^+-losing nephropathy despite an estimated 40% reduction in ENaC activity. Similarly, the partial loss of ENaC function due to the mutation α-S243P has no effects on airway fluid clearance or on the electrolyte composition of the sweat. These observations point out the importance of compensatory mechanisms in the kidneys, lungs, and other organs expressing ENaC to overcome a limited reduction of its activity.

Clinical improvements of AR-PHA1 have already been reported, but in most cases patients exhibit salt-losing episodes if they are not supplemented with dietary salt (13, 18, 28). Clinical improvement is usually associated with missense mutations or mutations in the β- or γ-subunits, resulting in only

partial but not complete loss of ENaC function. The slight reduction in ENaC activity of the α-S243P mutant fully supports the notion that the clinical evolution of the AR-PHA1 is related to the degree of ENaC loss of function caused by the genetic mutations. A partial loss of function of ENaC in the ASDN is likely to be compensated by an increased Na^+ absorption in the upstream nephron segments. The late distal nephron also responds to elevated plasma levels of aldosterone by increasing the expression of the thiazide-sensitive NaCl cotransporter (NCC) (22). Recently, an increased level of NCC protein in the urine of a patient with AR-PHA1 was reported and supports the hypothesis of a compensatory Na^+ absorption in the distal nephron (2, 19). This upregulation of the activity of the NCC likely represents a compensatory mechanism to reabsorb Na^+ and to maintain Na^+ balance in the mature kidney but not in an immature kidney at the GA of 32 wk.

In the premature kidney, an elevated delivery of Na^+ is expected in the distal part of the nephron where ENaC is expressed and can result from upstream immature functional Na^+ transporters; we tried to experimentally reproduce this situation with oocytes expressing ENaC by overnight incubation in a high Na^+ medium, leading to intracellular Na^+ load. Interestingly, it was under such a high Na^+ load that we observed the most important loss of ENaC function. We still do not understand the molecular mechanism underlying this effect, but it may also contribute to the salt-losing episode after birth and the rapid clinical improvement of our preterm patient. Indeed, as the Na^+ transporters mature in the nephron segments upstream of the ASDN, the distal Na^+ delivery decreases, and under these conditions we can expect from our data that the degree of ENaC loss of function is reduced.

Finally, the S243P mutation identifies a novel functional domain in the extracellular loop of the channel that may link ENaC activity to changes in chronic extracellular Na^+ load. The S243 residue is located in the extracellular loop of ENaC. Further studies are needed to investigate the precise mechanisms involved in the ENaC sensing of external Na^+ ions.

In conclusion, our study provides the first genetic evidence that ENaC activity is critical for the maintenance of salt balance in the immature kidney of preterm babies. Furthermore, it shows that the severity of the symptoms of AR-PHA1 is related to the degree of the ENaC loss of function. Finally, this study identifies a novel functional domain in the extracellular loop of ENaC that is important for channel regulation.

REFERENCES

1. **Abriel H, Horisberger JD.** Feedback inhibition of rat amiloride-sensitive epithelial sodium channels expressed in Xenopus laevis oocytes. *J Physiol* 516: 31–43, 1999.
2. **Adachi M, Asakura Y, Muroya K, Tajima T, Fujieda K, Kuribayashi E, Uchida S.** Increased Na reabsorption via the Na-Cl cotransporter in autosomal recessive pseudohypoaldosteronism. *Clin Exp Nephrol* 14: 228–232, 2010.
3. **Al-Dahhan J, Haycock GB, Nichol B, Chantler C, Stimmler L.** Sodium homeostasis in term and preterm neonates. III. Effect of salt supplementation. *Arch Dis Child* 59: 945–950, 1984.
4. **Alvarez de la Rosa D, Canessa CM, Fyfe GK, Zhang P.** Structure and regulation of amiloride-sensitive sodium channels. *Annu Rev Physiol* 62: 573–594, 2000.
5. **Barbry P, Hofman P.** Molecular biology of Na$^+$ absorption. *Am J Physiol Gastrointest Liver Physiol* 273: G571–G585, 1997.
6. **Bastl CP, Hayslett JP.** The cellular action of aldosterone in target epithelia. *Kidney Int* 42: 250–264, 1992.
7. **Belot A, Ranchin B, Fichtner C, Pujo L, Rossier BC, Liutkus A, Morlat C, Nicolino M, Zennaro MC, Cochat P.** Pseudohypoaldosteronisms, report on a 10-patient series. *Nephrol Dial Transplant* 23: 1636–1641, 2008.
8. **Bize V, Horisberger JD.** Sodium self-inhibition of human epithelial sodium channel: selectivity and affinity of the extracellular sodium sensing site. *Am J Physiol Renal Physiol* 293: F1137–F1146, 2007.
9. **Chraibi A, Vallet V, Firsov D, Hess SK, Horisberger JD.** Protease modulation of the activity of the epithelial sodium channel expressed in Xenopus oocytes. *J Gen Physiol* 111: 127–138, 1998.
10. **Delgado MM, Rohatgi R, Khan S, Holzman IR, Satlin LM.** Sodium and potassium clearances by the maturing kidney: clinical-molecular correlates. *Pediatr Nephrol* 18: 759–767, 2003.
11. **Donaldson SH, Boucher RC.** Sodium channels and cystic fibrosis. *Chest* 132: 1631–1636, 2007.
12. **Doucet A, Katz AI.** Mineralcorticoid receptors along the nephron: [^{3}H]aldosterone binding in rabbit tubules. *Am J Physiol Renal Fluid Electrolyte Physiol* 241: F605–F611, 1981.
13. **Edelheit O, Hanukoglu I, Gizewska M, Kandemir N, Tenenbaum-Rakover Y, Yurdakok M, Zajaczek S, Hanukoglu A.** Novel mutations in epithelial sodium channel (ENaC) subunit genes and phenotypic expression of multisystem pseudohypoaldosteronism. *Clin Endocrinol (Oxf)* 62: 547–553, 2005.
14. **Farrell PM, Rosenstein BJ, White TB, Accurso FJ, Castellani C, Cutting GR, Durie PR, Legrys VA, Massie J, Parad RB, Rock MJ, Campbell PW 3rd; Cystic Fibrosis Foundation.** Guidelines for diagnosis of cystic fibrosis in newborns through older adults: Cystic Fibrosis Foundation consensus report. *J Pediatr* 153: S4–S14, 2008.
15. **Garty H.** Regulation of the epithelial Na+ channel by aldosterone: open questions and emerging answers. *Kidney Int* 57: 1270–1276, 2000.
16. **Geller DS, Rodriguez-Soriano J, Vallo Boado A, Schifter S, Bayer M, Chang SS, Lifton RP.** Mutations in the mineralocorticoid receptor gene cause autosomal dominant pseudohypoaldosteronism type I. *Nat Genet* 19: 279–281, 1998.
17. **Hanukoglu A.** Type I pseudohypoaldosteronism includes two clinically and genetically distinct entities with either renal or multiple target organ defects. *J Clin Endocrinol Metab* 73: 936–944, 1991.
18. **Hanukoglu A, Edelheit O, Shriki Y, Gizewska M, Dascal N, Hanukoglu I.** Renin-aldosterone response, urinary Na/K ratio and growth in pseudohypoaldosteronism patients with mutations in epithelial sodium channel (ENaC) subunit genes. *J Steroid Biochem Mol Biol* 111: 268–274, 2008.
19. **Hanukoglu A, Hanukoglu I.** Clinical improvement in patients with autosomal recessive pseudohypoaldosteronism and the necessity for salt supplementation. *Clin Exp Nephrol* 14: 518–519, 2010.
20. **Kellenberger S, Schild L.** Epithelial sodium channel/degenerin family of ion channels: a variety of functions for a shared structure. *Physiol Rev* 82: 735–767, 2002.
21. **Kerem E, Bistritzer T, Hanukoglu A, Hofmann T, Zhou Z, Bennett W, MacLaughlin E, Barker P, Nash M, Quittell L, Boucher R, Knowles MR.** Pulmonary epithelial sodium-channel dysfunction and excess airway liquid in pseudohypoaldosteronism. *N Engl J Med* 341: 156–162, 1999.
22. **Kim GH, Masilamani S, Turner R, Mitchell C, Wade JB, Knepper MA.** The thiazide-sensitive Na-Cl cotransporter is an aldosterone-induced protein. *Proc Natl Acad Sci USA* 95: 14552–14557, 1998.
23. **Martin JM, Calduch L, Monteagudo C, Alonso V, Garcia L, Jorda E.** Clinico-pathological analysis of the cutaneous lesions of a patient with type I pseudohypoaldosteronism. *J Eur Acad Dermatol Venereol* 19: 377–379, 2005.
24. **Nanayakkara KK, Samarakoon AB, Perera BH, De Silva AW, Nanayakkara CD.** Size of Sri Lankan newborns at birth. *J Obstet Gynaecol* 31: 311–314, 2011.
25. **Polito C, La Manna A, Maiello R, Nappi B, Siciliano MC, Di Domenico MR, Di Toro R.** Urinary sodium and potassium excretion in idiopathic hypercalciuria of children. *Nephron* 91: 7–12, 2002.
26. **Pujo L, Fagart J, Gary F, Papadimitriou DT, Claes A, Jeunemaitre X, Zennaro MC.** Mineralocorticoid receptor mutations are the principal cause of renal type 1 pseudohypoaldosteronism. *Hum Mutat* 28: 33–40, 2007.
27. **Riepe FG.** Clinical and molecular features of type 1 pseudohypoaldosteronism. *Horm Res* 72: 1–9, 2009.
28. **Riepe FG, van Bemmelen MX, Cachat F, Plendl H, Gautschi I, Krone N, Holterhus PM, Theintz G, Schild L.** Revealing a subclinical salt-losing phenotype in heterozygous carriers of the novel S562P mutation in the alpha subunit of the epithelial sodium channel. *Clin Endocrinol (Oxf)* 70: 252–258, 2009.
29. **Rossier BC, Stutts MJ.** Activation of the epithelial sodium channel (ENaC) by serine proteases. *Annu Rev Physiol* 71: 361–379, 2009.
30. **Satlin LM, Palmer LG.** Apical K$^+$ conductance in maturing rabbit principal cell. *Am J Physiol Renal Physiol* 272: F397–F404, 1997.
31. **Satlin LM, Palmer LG.** Apical Na$^+$ conductance in maturing rabbit principal cell. *Am J Physiol Renal Fluid Electrolyte Physiol* 270: F391–F397, 1996.
32. **Schaedel C, Marthinsen L, Kristoffersson AC, Kornfalt R, Nilsson KO, Orlenius B, Holmberg L.** Lung symptoms in pseudohypoaldosteronism type 1 are associated with deficiency of the alpha-subunit of the epithelial sodium channel. *J Pediatr* 135: 739–745, 1999.
33. **Schoeneman MJ, Spitzer A.** The effect of intravascular volume expansion of proximal tubular reabsorption during development. *Proc Soc Exp Biol Med* 165: 319–322, 1980.
34. **Speiser PW, Stoner E, New MI.** Pseudohypoaldosteronism: a review and report of two new cases. *Adv Exp Med Biol* 196: 173–195, 1986.
35. **Stephenson G, Hammet M, Hadaway G, Funder JW.** Ontogeny of renal mineralocorticoid receptors and urinary electrolyte responses in the rat. *Am J Physiol Renal Fluid Electrolyte Physiol* 247: F665–F671, 1984.
36. **Uchida N, Shiohara M, Miyagawa S, Yokota I, Mori T.** A novel nonsense mutation of the mineralocorticoid receptor gene in the renal form of pseudohypoaldosteronism type 1. *J Pediatr Endocrinol Metab* 22: 91–95, 2009.
37. **Verrey F, Pearce D, Pfeiffer R, Spindler B, Mastroberardino L, Summa V, Zecevic M.** Pleiotropic action of aldosterone in epithelia mediated by transcription and post-transcription mechanisms. *Kidney Int* 57: 1277–1282, 2000.
38. **Zennaro MC.** Mineralocorticoid resistance. *Steroids* 61: 189–192, 1996.
39. **Zennaro MC, Lombès M.** Mineralocorticoid resistance. *Trends Endocrinol Metab* 15: 264–270, 2004.

1. Hille, B. (2001) *Ion channels of excitable membranes*, 3rd ed., Sinauer, Sunderland, Mass.
2. Golubovic, A., Kuhn, A., Williamson, M., Kalbacher, H., Holstein, T. W., Grimmelikhuijzen, C. J., and Grunder, S. (2007) *J Biol Chem* **282**, 35098-35103
3. Lingueglia, E., Champigny, G., Lazdunski, M., and Barbry, P. (1995) *Nature* **378**, 730-733
4. Chalfie, M., and Wolinsky, E. (1990) *Nature* **345**, 410-416
5. Driscoll, M., and Chalfie, M. (1991) *Nature* **349**, 588-593
6. Liu, J., Schrank, B., and Waterston, R. H. (1996) *Science* **273**, 361-364
7. Katsura, I., Kondo, K., Amano, T., Ishihara, T., and Kawakami, M. (1994) *Genetics* **136**, 145-154
8. Zelle, K. M., Lu, B., Pyfrom, S. C., and Ben-Shahar, Y. (2013) *G3 (Bethesda)* **3**, 441-450
9. Adams, C. M., Anderson, M. G., Motto, D. G., Price, M. P., Johnson, W. A., and Welsh, M. J. (1998) *The Journal of cell biology* **140**, 143-152
10. Darboux, I., Lingueglia, E., Champigny, G., Coscoy, S., Barbry, P., and Lazdunski, M. (1998) *J Biol Chem* **273**, 9424-9429
11. Liu, L., Johnson, W. A., and Welsh, M. J. (2003) *Proc Natl Acad Sci U S A* **100**, 2128-2133
12. Liu, L., Leonard, A. S., Motto, D. G., Feller, M. A., Price, M. P., Johnson, W. A., and Welsh, M. J. (2003) *Neuron* **39**, 133-146
13. Liu, T., Starostina, E., Vijayan, V., and Pikielny, C. W. (2012) *J Neurosci* **32**, 11879-11889
14. Thistle, R., Cameron, P., Ghorayshi, A., Dennison, L., and Scott, K. (2012) *Cell* **149**, 1140-1151
15. Younger, M. A., Muller, M., Tong, A., Pym, E. C., and Davis, G. W. (2013) *Neuron*
16. Zhong, L., Hwang, R. Y., and Tracey, W. D. (2010) *Current biology : CB* **20**, 429-434
17. Studer, R. A., Person, E., Robinson-Rechavi, M., and Rossier, B. C. (2011) *Physiological genomics* **43**, 844-854
18. Ussing, H. H. (1960) *J Gen Physiol* **43**, 135-147
19. Palmer, L. G., and Frindt, G. (1986) *Proc Natl Acad Sci U S A* **83**, 2767-2770
20. Canessa, C. M., Horisberger, J. D., and Rossier, B. C. (1993) *Nature* **361**, 467-470
21. Canessa, C. M., Schild, L., Buell, G., Thorens, B., Gautschi, I., Horisberger, J. D., and Rossier, B. C. (1994) *Nature* **367**, 463-467
22. Lingueglia, E., Voilley, N., Waldmann, R., Lazdunski, M., and Barbry, P. (1993) *FEBS letters* **318**, 95-99
23. Ota, T., Suzuki, Y., Nishikawa, T., Otsuki, T., Sugiyama, T., Irie, R., Wakamatsu, A., Hayashi, K., Sato, H., Nagai, K., Kimura, K., Makita, H., Sekine, M., Obayashi, M., Nishi, T., Shibahara, T., Tanaka, T., Ishii, S., Yamamoto, J., Saito, K., Kawai, Y., Isono, Y., Nakamura, Y., Nagahari, K., Murakami, K., Yasuda, T., Iwayanagi, T., Wagatsuma, M., Shiratori, A., Sudo, H., Hosoiri, T., Kaku, Y., Kodaira, H., Kondo, H., Sugawara, M., Takahashi, M., Kanda, K., Yokoi, T., Furuya, T., Kikkawa, E., Omura, Y., Abe, K., Kamihara, K., Katsuta, N., Sato, K., Tanikawa, M., Yamazaki, M., Ninomiya, K., Ishibashi, T., Yamashita, H., Murakawa, K., Fujimori, K., Tanai, H., Kimata, M., Watanabe, M., Hiraoka, S., Chiba, Y., Ishida, S., Ono, Y., Takiguchi, S., Watanabe, S., Yosida, M., Hotuta, T., Kusano, J., Kanehori, K., Takahashi-Fujii, A., Hara, H., Tanase, T. O., Nomura, Y., Togiya, S., Komai, F., Hara, R., Takeuchi, K., Arita, M., Imose, N., Musashino, K., Yuuki, H., Oshima, A., Sasaki, N., Aotsuka, S., Yoshikawa, Y.,

Matsunawa, H., Ichihara, T., Shiohata, N., Sano, S., Moriya, S., Momiyama, H., Satoh, N., Takami, S., Terashima, Y., Suzuki, O., Nakagawa, S., Senoh, A., Mizoguchi, H., Goto, Y., Shimizu, F., Wakebe, H., Hishigaki, H., Watanabe, T., Sugiyama, A., Takemoto, M., Kawakami, B., Watanabe, K., Kumagai, A., Itakura, S., Fukuzumi, Y., Fujimori, Y., Komiyama, M., Tashiro, H., Tanigami, A., Fujiwara, T., Ono, T., Yamada, K., Fujii, Y., Ozaki, K., Hirao, M., Ohmori, Y., Kawabata, A., Hikiji, T., Kobatake, N., Inagaki, H., Ikema, Y., Okamoto, S., Okitani, R., Kawakami, T., Noguchi, S., Itoh, T., Shigeta, K., Senba, T., Matsumura, K., Nakajima, Y., Mizuno, T., Morinaga, M., Sasaki, M., Togashi, T., Oyama, M., Hata, H., Komatsu, T., Mizushima-Sugano, J., Satoh, T., Shirai, Y., Takahashi, Y., Nakagawa, K., Okumura, K., Nagase, T., Nomura, N., Kikuchi, H., Masuho, Y., Yamashita, R., Nakai, K., Yada, T., Ohara, O., Isogai, T., and Sugano, S. (2004) *Nature genetics* **36**, 40-45

24.   Waldmann, R., Champigny, G., Bassilana, F., Voilley, N., and Lazdunski, M. (1995) *J Biol Chem* **270**, 27411-27414

25.   Firsov, D., Schild, L., Gautschi, I., Merillat, A. M., Schneeberger, E., and Rossier, B. C. (1996) *Proc Natl Acad Sci U S A* **93**, 15370-15375

26.   Giraldez, T., Afonso-Oramas, D., Cruz-Muros, I., Garcia-Marin, V., Pagel, P., Gonzalez-Hernandez, T., and Alvarez de la Rosa, D. (2007) *Journal of neurochemistry* **102**, 1304-1315

27.   Garty, H., and Palmer, L. G. (1997) *Physiol Rev* **77**, 359-396

28.   McNicholas, C. M., and Canessa, C. M. (1997) *J Gen Physiol* **109**, 681-692

29.   Duc, C., Farman, N., Canessa, C. M., Bonvalet, J. P., and Rossier, B. C. (1994) *The Journal of cell biology* **127**, 1907-1921

30.   Kretz, O., Barbry, P., Bock, R., and Lindemann, B. (1999) *The journal of histochemistry and cytochemistry : official journal of the Histochemistry Society* **47**, 51-64

31.   Lin, W., Finger, T. E., Rossier, B. C., and Kinnamon, S. C. (1999) *The Journal of comparative neurology* **405**, 406-420

32.   Lienhard, D., Lauterburg, M., Escher, G., Frey, F. J., and Frey, B. M. (2012) *PLoS One* **7**, e37898

33.   Brouard, M., Casado, M., Djelidi, S., Barrandon, Y., and Farman, N. (1999) *Journal of cell science* **112** (**Pt 19**), 3343-3352

34.   Mauro, T., Guitard, M., Behne, M., Oda, Y., Crumrine, D., Komuves, L., Rassner, U., Elias, P. M., and Hummler, E. (2002) *The Journal of investigative dermatology* **118**, 589-594

35.   Hernandez-Gonzalez, E. O., Sosnik, J., Edwards, J., Acevedo, J. J., Mendoza-Lujambio, I., Lopez-Gonzalez, I., Demarco, I., Wertheimer, E., Darszon, A., and Visconti, P. E. (2006) *J Biol Chem* **281**, 5623-5633

36.   Ji, H. L., Zhao, R. Z., Chen, Z. X., Shetty, S., Idell, S., and Matalon, S. (2012) *American journal of physiology. Lung cellular and molecular physiology* **303**, L1013-1026

37.   Nie, H. G., Chen, L., Han, D. Y., Li, J., Song, W. F., Wei, S. P., Fang, X. H., Gu, X., Matalon, S., and Ji, H. L. (2009) *J Physiol* **587**, 2663-2676

38.   Firsov, D., Robert-Nicoud, M., Gruender, S., Schild, L., and Rossier, B. C. (1999) *J Biol Chem* **274**, 2743-2749

39.   Loffing, J., and Schild, L. (2005) *Journal of the American Society of Nephrology : JASN* **16**, 3175-3181

40.   Grunder, S., Firsov, D., Chang, S. S., Jaeger, N. F., Gautschi, I., Schild, L., Lifton, R. P., and Rossier, B. C. (1997) *EMBO J* **16**, 899-907

41.   Kellenberger, S., Gautschi, I., and Schild, L. (2002) *J Physiol* **543**, 413-424
42.   Sakai, H., Lingueglia, E., Champigny, G., Mattei, M. G., and Lazdunski, M. (1999) *J Physiol* **519 Pt 2**, 323-333
43.   Schaefer, L., Sakai, H., Mattei, M., Lazdunski, M., and Lingueglia, E. (2000) *FEBS letters* **471**, 205-210
44.   Snyder, P. M., Bucher, D. B., and Olson, D. R. (2000) *J Gen Physiol* **116**, 781-790
45.   Waldmann, R., and Lazdunski, M. (1998) *Current opinion in neurobiology* **8**, 418-424
46.   Schild L, S. E., Gautschi I, Firsov D. (1997) *J Gen Physiology* **109**, 15-26
47.   Adams, C. M., Snyder, P. M., and Welsh, M. J. (1999) *J Biol Chem* **274**, 15500-15504
48.   Alijevic, O., and Kellenberger, S. (2012) *J Biol Chem* **287**, 36059-36070
49.   Kellenberger, S., Gautschi, I., and Schild, L. (2003) *Mol Pharmacol* **64**, 848-856
50.   Benos, D. J., Simon, S. A., Mandel, L. J., and Cala, P. M. (1976) *J Gen Physiol* **68**, 43-63
51.   Palmer, L. G., and Andersen, O. S. (1989) *Biophys J* **55**, 779-787
52.   Palmer, L. G. (1985) *J Membr Biol* **87**, 191-199
53.   Kellenberger, S., Auberson, M., Gautschi, I., Schneeberger, E., and Schild, L. (2001) *J Gen Physiol* **118**, 679-692
54.   Kellenberger, S., Gautschi, I., and Schild, L. (1999) *Proc Natl Acad Sci U S A* **96**, 4170-4175
55.   Kellenberger, S., Hoffmann-Pochon, N., Gautschi, I., Schneeberger, E., and Schild, L. (1999) *J Gen Physiol* **114**, 13-30
56.   Sheng, S., Li, J., McNulty, K. A., Avery, D., and Kleyman, T. R. (2000) *J Biol Chem* **275**, 8572-8581
57.   Hansson, J. H., Nelson-Williams, C., Suzuki, H., Schild, L., Shimkets, R., Lu, Y., Canessa, C., Iwasaki, T., Rossier, B., and Lifton, R. P. (1995) *Nature genetics* **11**, 76-82
58.   Boucher, R. C. (2007) *Journal of internal medicine* **261**, 5-16
59.   Thelin, W. R., and Boucher, R. C. (2007) *Current opinion in pharmacology* **7**, 290-295
60.   Boucher, R. C. (2007) *Annual review of medicine* **58**, 157-170
61.   Malagon-Rogers, M. (1999) *Pediatr Nephrol* **13**, 484-486
62.   Keszler, M., and Sivasubramanian, K. N. (1983) *Am J Dis Child* **137**, 738-740
63.   Mall, M., Grubb, B. R., Harkema, J. R., O'Neal, W. K., and Boucher, R. C. (2004) *Nature medicine* **10**, 487-493
64.   Palmer, L. G., and Andersen, O. S. (2008) *J Gen Physiol* **132**, 607-612
65.   Edwards, C. R., Stewart, P. M., Burt, D., Brett, L., McIntyre, M. A., Sutanto, W. S., de Kloet, E. R., and Monder, C. (1988) *Lancet* **2**, 986-989
66.   Funder, J. W., Pearce, P. T., Smith, R., and Smith, A. I. (1988) *Science* **242**, 583-585
67.   Rossier, B. C., Staub, O., and Hummler, E. (2013) *FEBS letters* **587**, 1929-1941
68.   Nikolaeva, S., Pradervand, S., Centeno, G., Zavadova, V., Tokonami, N., Maillard, M., Bonny, O., and Firsov, D. (2012) *Journal of the American Society of Nephrology : JASN* **23**, 1019-1026
69.   Rakova, N., Juttner, K., Dahlmann, A., Schroder, A., Linz, P., Kopp, C., Rauh, M., Goller, U., Beck, L., Agureev, A., Vassilieva, G., Lenkova, L., Johannes, B., Wabel, P., Moissl, U., Vienken, J., Gerzer, R., Eckardt, K. U., Muller, D. N., Kirsch, K., Morukov, B., Luft, F. C., and Titze, J. (2013) *Cell metabolism* **17**, 125-131
70.   Wang, Q., Horisberger, J. D., Maillard, M., Brunner, H. R., Rossier, B. C., and Burnier, M. (2000) *Clinical and experimental pharmacology & physiology* **27**, 60-66
71.   Boron, W. F., and Boulpaep, E. L. (2005) *Medical physiology : a cellular and molecular approach*, Updated ed., Elsevier Saunders, Philadelphia, Pa.

72. Loffing, J., Zecevic, M., Feraille, E., Kaissling, B., Asher, C., Rossier, B. C., Firestone, G. L., Pearce, D., and Verrey, F. (2001) *American journal of physiology. Renal physiology* **280**, F675-682

73. Masilamani, S., Kim, G. H., Mitchell, C., Wade, J. B., and Knepper, M. A. (1999) *J Clin Invest* **104**, R19-23

74. Dahlmann, A., Pradervand, S., Hummler, E., Rossier, B. C., Frindt, G., and Palmer, L. G. (2003) *American journal of physiology. Renal physiology* **285**, F310-318

75. Alvarez de la Rosa, D., Li, H., and Canessa, C. M. (2002) *J Gen Physiol* **119**, 427-442

76. Bens, M., Chassin, C., and Vandewalle, A. (2006) *Pflugers Arch* **453**, 133-146

77. Morris, R. G., and Schafer, J. A. (2002) *J Gen Physiol* **120**, 71-85

78. Chraibi, A., Vallet, V., Firsov, D., Hess, S. K., and Horisberger, J. D. (1998) *J Gen Physiol* **111**, 127-138

79. Harris, M., Firsov, D., Vuagniaux, G., Stutts, M. J., and Rossier, B. C. (2007) *J Biol Chem* **282**, 58-64

80. Vallet, V., Chraibi, A., Gaeggeler, H. P., Horisberger, J. D., and Rossier, B. C. (1997) *Nature* **389**, 607-610

81. Vuagniaux, G., Vallet, V., Jaeger, N. F., Hummler, E., and Rossier, B. C. (2002) *J Gen Physiol* **120**, 191-201

82. Vuagniaux, G., Vallet, V., Jaeger, N. F., Pfister, C., Bens, M., Farman, N., Courtois-Coutry, N., Vandewalle, A., Rossier, B. C., and Hummler, E. (2000) *Journal of the American Society of Nephrology : JASN* **11**, 828-834

83. Hughey, R. P., Mueller, G. M., Bruns, J. B., Kinlough, C. L., Poland, P. A., Harkleroad, K. L., Carattino, M. D., and Kleyman, T. R. (2003) *J Biol Chem* **278**, 37073-37082

84. Kleyman, T. R., Carattino, M. D., and Hughey, R. P. (2009) *J Biol Chem* **284**, 20447-20451

85. Rossier, B. C., and Stutts, M. J. (2009) *Annu Rev Physiol* **71**, 361-379

86. Wakida, N., Kitamura, K., Tuyen, D. G., Maekawa, A., Miyoshi, T., Adachi, M., Shiraishi, N., Ko, T., Ha, V., Nonoguchi, H., and Tomita, K. (2006) *Kidney international* **70**, 1432-1438

87. Kellenberger, S., Gautschi, I., Rossier, B. C., and Schild, L. (1998) *J Clin Invest* **101**, 2741-2750

88. Staub, O., Abriel, H., Plant, P., Ishikawa, T., Kanelis, V., Saleki, R., Horisberger, J. D., Schild, L., and Rotin, D. (2000) *Kidney international* **57**, 809-815

89. Staub, O., Dho, S., Henry, P., Correa, J., Ishikawa, T., McGlade, J., and Rotin, D. (1996) *EMBO J* **15**, 2371-2380

90. Fakitsas, P., Adam, G., Daidie, D., van Bemmelen, M. X., Fouladkou, F., Patrignani, A., Wagner, U., Warth, R., Camargo, S. M., Staub, O., and Verrey, F. (2007) *Journal of the American Society of Nephrology : JASN* **18**, 1084-1092

91. Abriel, H., and Horisberger, J. D. (1999) *J Physiol* **516 (Pt 1)**, 31-43

92. Fuchs, W., Larsen, E. H., and Lindemann, B. (1977) *J Physiol* **267**, 137-166

93. Garty, H., and Benos, D. J. (1988) *Physiol Rev* **68**, 309-373

94. Palmer, L. G., Sackin, H., and Frindt, G. (1998) *J Physiol* **509 (Pt 1)**, 151-162

95. Chraibi, A., and Horisberger, J. D. (2002) *J Gen Physiol* **120**, 133-145

96. Guyton, A. C. (1991) *Science* **252**, 1813-1816

97. Crowley, S. D., Gurley, S. B., Oliverio, M. I., Pazmino, A. K., Griffiths, R., Flannery, P. J., Spurney, R. F., Kim, H. S., Smithies, O., Le, T. H., and Coffman, T. M. (2005) *J Clin Invest* **115**, 1092-1099

98. Freis, E. D., Wanko, A., Wilson, I. M., and Parrish, A. E. (1958) *Journal of the American Medical Association* **166**, 137-140

99. Bonny, O., and Hummler, E. (2000) *Kidney international* **57**, 1313-1318

100. Hummler, E., Barker, P., Gatzy, J., Beermann, F., Verdumo, C., Schmidt, A., Boucher, R., and Rossier, B. C. (1996) *Nature genetics* **12**, 325-328

101. Barker, P. M., Nguyen, M. S., Gatzy, J. T., Grubb, B., Norman, H., Hummler, E., Rossier, B., Boucher, R. C., and Koller, B. (1998) *J Clin Invest* **102**, 1634-1640

102. McDonald, F. J., Yang, B., Hrstka, R. F., Drummond, H. A., Tarr, D. E., McCray, P. B., Jr., Stokes, J. B., Welsh, M. J., and Williamson, R. A. (1999) *Proc Natl Acad Sci U S A* **96**, 1727-1731

103. Belot, A., Ranchin, B., Fichtner, C., Pujo, L., Rossier, B. C., Liutkus, A., Morlat, C., Nicolino, M., Zennaro, M. C., and Cochat, P. (2008) *Nephrology, dialysis, transplantation : official publication of the European Dialysis and Transplant Association - European Renal Association* **23**, 1636-1641

104. Chang, S. S., Grunder, S., Hanukoglu, A., Rosler, A., Mathew, P. M., Hanukoglu, I., Schild, L., Lu, Y., Shimkets, R. A., Nelson-Williams, C., Rossier, B. C., and Lifton, R. P. (1996) *Nature genetics* **12**, 248-253

105. Geller, D. S., Rodriguez-Soriano, J., Vallo Boado, A., Schifter, S., Bayer, M., Chang, S. S., and Lifton, R. P. (1998) *Nature genetics* **19**, 279-281

106. Botero-Velez, M., Curtis, J. J., and Warnock, D. G. (1994) *The New England journal of medicine* **330**, 178-181

107. Shimkets, R. A., Warnock, D. G., Bositis, C. M., Nelson-Williams, C., Hansson, J. H., Schambelan, M., Gill, J. R., Jr., Ulick, S., Milora, R. V., Findling, J. W., and et al. (1994) *Cell* **79**, 407-414

108. Salako, L. A., and Smith, A. J. (1970) *Br J Pharmacol* **38**, 702-718

109. Bull, M. B., and Laragh, J. H. (1968) *Circulation* **37**, 45-53

110. Bentley, P. J. (1968) *J Physiol* **195**, 317-330

111. Baer, J. E., Jones, C. B., Spitzer, S. A., and Russo, H. F. (1967) *J Pharmacol Exp Ther* **157**, 472-485

112. Kerem, E., Bistritzer, T., Hanukoglu, A., Hofmann, T., Zhou, Z., Bennett, W., MacLaughlin, E., Barker, P., Nash, M., Quittell, L., Boucher, R., and Knowles, M. R. (1999) *The New England journal of medicine* **341**, 156-162

113. Mora-Lopez, F., Bernal-Quiros, M., Lechuga-Sancho, A. M., Lechuga-Campoy, J. L., Hernandez-Trujillo, N., and Nieto, A. (2012) *European journal of pediatrics* **171**, 997-1000

114. Randrianarison, N., Clerici, C., Ferreira, C., Fontayne, A., Pradervand, S., Fowler-Jaeger, N., Hummler, E., Rossier, B. C., and Planes, C. (2008) *American journal of physiology. Lung cellular and molecular physiology* **294**, L409-416

115. Lu, M., Echeverri, F., Kalabat, D., Laita, B., Dahan, D. S., Smith, R. D., Xu, H., Staszewski, L., Yamamoto, J., Ling, J., Hwang, N., Kimmich, R., Li, P., Patron, E., Keung, W., Patron, A., and Moyer, B. D. (2008) *J Biol Chem* **283**, 11981-11994

116. Randrianarison, N., Escoubet, B., Ferreira, C., Fontayne, A., Fowler-Jaeger, N., Clerici, C., Hummler, E., Rossier, B. C., and Planes, C. (2007) *J Physiol* **582**, 777-788

117. Price, M. P., Snyder, P. M., and Welsh, M. J. (1996) *J Biol Chem* **271**, 7879-7882

118. Waldmann, R., Champigny, G., Bassilana, F., Heurteaux, C., and Lazdunski, M. (1997) *Nature* **386**, 173-177

119. Akopian, A. N., Chen, C. C., Ding, Y., Cesare, P., and Wood, J. N. (2000) *Neuroreport* **11**, 2217-2222
120. Grunder, S., Geissler, H. S., Bassler, E. L., and Ruppersberg, J. P. (2000) *Neuroreport* **11**, 1607-1611
121. Waldmann, R., Bassilana, F., de Weille, J., Champigny, G., Heurteaux, C., and Lazdunski, M. (1997) *J Biol Chem* **272**, 20975-20978
122. Wiemuth, D., Assmann, M., and Grunder, S. (2013) *Channels (Austin)* **8**
123. Coric, T., Zheng, D., Gerstein, M., and Canessa, C. M. (2005) *J Physiol* **568**, 725-735
124. Hesselager, M., Timmermann, D. B., and Ahring, P. K. (2004) *J Biol Chem* **279**, 11006-11015
125. Kellenberger S, S. L. (2002) *Physiol Rev.* **82**, 735-767
126. Yermolaieva, O., Leonard, A. S., Schnizler, M. K., Abboud, F. M., and Welsh, M. J. (2004) *Proc Natl Acad Sci U S A* **101**, 6752-6757
127. Pfister, Y., Gautschi, I., Takeda, A. N., van Bemmelen, M., Kellenberger, S., and Schild, L. (2006) *J Biol Chem* **281**, 11787-11791
128. Coscoy, S., de Weille, J. R., Lingueglia, E., and Lazdunski, M. (1999) *J Biol Chem* **274**, 10129-10132
129. Askwith, C. C., Cheng, C., Ikuma, M., Benson, C., Price, M. P., and Welsh, M. J. (2000) *Neuron* **26**, 133-141
130. Bässler EL, N.-A. T., Geisler HS, Ruppersberg JP, Gründer S. (2001) *J Biol Chem* **276**, 33782-33793
131. Sutherland, S. P., Benson, C. J., Adelman, J. P., and McCleskey, E. W. (2001) *Proc Natl Acad Sci U S A* **98**, 711-716
132. Zhang, P., and Canessa, C. M. (2002) *J Gen Physiol* **120**, 553-566
133. Sherwood, T. W., and Askwith, C. C. (2009) *J Neurosci* **29**, 14371-14380
134. Chen, C. C., England, S., Akopian, A. N., and Wood, J. N. (1998) *Proc Natl Acad Sci U S A* **95**, 10240-10245
135. Champigny, G., Voilley, N., Waldmann, R., and Lazdunski, M. (1998) *J Biol Chem* **273**, 15418-15422
136. de Weille, J. R., Bassilana, F., Lazdunski, M., and Waldmann, R. (1998) *FEBS letters* **433**, 257-260
137. Benson, C. J., Xie, J., Wemmie, J. A., Price, M. P., Henss, J. M., Welsh, M. J., and Snyder, P. M. (2002) *Proc Natl Acad Sci U S A* **99**, 2338-2343
138. de Weille, J., and Bassilana, F. (2001) *Brain research* **900**, 277-281
139. Wemmie, J. A., Taugher, R. J., and Kreple, C. J. (2013) *Nature reviews. Neuroscience* **14**, 461-471
140. Poirot, O., Vukicevic, M., Boesch, A., and Kellenberger, S. (2004) *J Biol Chem* **279**, 38448-38457
141. Alvarez de la Rosa, D., Krueger, S. R., Kolar, A., Shao, D., Fitzsimonds, R. M., and Canessa, C. M. (2003) *J Physiol* **546**, 77-87
142. Wemmie, J. A., Askwith, C. C., Lamani, E., Cassell, M. D., Freeman, J. H., Jr., and Welsh, M. J. (2003) *J Neurosci* **23**, 5496-5502
143. Krishtal, O. A., Osipchuk, Y. V., Shelest, T. N., and Smirnoff, S. V. (1987) *Brain research* **436**, 352-356
144. Miesenbock, G., De Angelis, D. A., and Rothman, J. E. (1998) *Nature* **394**, 192-195

145. Wemmie, J. A., Chen, J., Askwith, C. C., Hruska-Hageman, A. M., Price, M. P., Nolan, B. C., Yoder, P. G., Lamani, E., Hoshi, T., Freeman, J. H., Jr., and Welsh, M. J. (2002) *Neuron* **34**, 463-477

146. Zha, X. M., Wemmie, J. A., Green, S. H., and Welsh, M. J. (2006) *Proc Natl Acad Sci U S A* **103**, 16556-16561

147. Wu, P. Y., Huang, Y. Y., Chen, C. C., Hsu, T. T., Lin, Y. C., Weng, J. Y., Chien, T. C., Cheng, I. H., and Lien, C. C. (2013) *J Neurosci* **33**, 1828-1832

148. Ahn, Y. J., Kim, H., Lim, H., Lee, M., Kang, Y., Moon, S., Kim, H. S., and Kim, H. H. (2012) *BMB reports* **45**, 489-495

149. Chu, X. P., and Xiong, Z. G. (2013) *Adv Exp Med Biol* **961**, 419-431

150. Immke, D. C., and McCleskey, E. W. (2001) *Nature neuroscience* **4**, 869-870

151. Choi, D. W. (1988) *Neuron* **1**, 623-634

152. Xiong, Z. G., Zhu, X. M., Chu, X. P., Minami, M., Hey, J., Wei, W. L., MacDonald, J. F., Wemmie, J. A., Price, M. P., Welsh, M. J., and Simon, R. P. (2004) *Cell* **118**, 687-698

153. Wahlgren, N. G., and Ahmed, N. (2004) *Cerebrovasc Dis* **17 Suppl 1**, 153-166

154. Gao, J., Duan, B., Wang, D. G., Deng, X. H., Zhang, G. Y., Xu, L., and Xu, T. L. (2005) *Neuron* **48**, 635-646

155. Pignataro, G., Simon, R. P., and Xiong, Z. G. (2007) *Brain* **130**, 151-158

156. Xiong, Z. G., Pignataro, G., Li, M., Chang, S. Y., and Simon, R. P. (2008) *Current opinion in pharmacology* **8**, 25-32

157. Mitchell, W. G., and Grubbs, R. C. (1956) *Science* **123**, 223-224

158. Somjen, G. G. (1984) *Brain research* **311**, 186-188

159. Velisek, L., Dreier, J. P., Stanton, P. K., Heinemann, U., and Moshe, S. L. (1994) *Exp Brain Res* **101**, 44-52

160. Ziemann, A. E., Schnizler, M. K., Albert, G. W., Severson, M. A., Howard, M. A., 3rd, Welsh, M. J., and Wemmie, J. A. (2008) *Nature neuroscience* **11**, 816-822

161. Friese, M. A., Craner, M. J., Etzensperger, R., Vergo, S., Wemmie, J. A., Welsh, M. J., Vincent, A., and Fugger, L. (2007) *Nature medicine* **13**, 1483-1489

162. Price, M. P., Lewin, G. R., McIlwrath, S. L., Cheng, C., Xie, J., Heppenstall, P. A., Stucky, C. L., Mannsfeldt, A. G., Brennan, T. J., Drummond, H. A., Qiao, J., Benson, C. J., Tarr, D. E., Hrstka, R. F., Yang, B., Williamson, R. A., and Welsh, M. J. (2000) *Nature* **407**, 1007-1011

163. Lu, Y., Ma, X., Sabharwal, R., Snitsarev, V., Morgan, D., Rahmouni, K., Drummond, H. A., Whiteis, C. A., Costa, V., Price, M., Benson, C., Welsh, M. J., Chapleau, M. W., and Abboud, F. M. (2009) *Neuron* **64**, 885-897

164. Price, M. P., McIlwrath, S. L., Xie, J., Cheng, C., Qiao, J., Tarr, D. E., Sluka, K. A., Brennan, T. J., Lewin, G. R., and Welsh, M. J. (2001) *Neuron* **32**, 1071-1083

165. Fromy, B., Lingueglia, E., Sigaudo-Roussel, D., Saumet, J. L., and Lazdunski, M. (2012) *Nature medicine* **18**, 1205-1207

166. Bianchi, L. (2007) *Molecular neurobiology* **36**, 254-271

167. Zha, X. M. (2013) *Molecular brain* **6**, 1

168. Smith, M. L., von Hanwehr, R., and Siesjo, B. K. (1986) *Journal of cerebral blood flow and metabolism : official journal of the International Society of Cerebral Blood Flow and Metabolism* **6**, 574-583

169. Basbaum, A. I., Bautista, D. M., Scherrer, G., and Julius, D. (2009) *Cell* **139**, 267-284

170. Yen, Y. T., Tu, P. H., Chen, C. J., Lin, Y. W., Hsieh, S. T., and Chen, C. C. (2009) *Molecular pain* **5**, 1

171. Diochot, S., Baron, A., Salinas, M., Douguet, D., Scarzello, S., Dabert-Gay, A. S., Debayle, D., Friend, V., Alloui, A., Lazdunski, M., and Lingueglia, E. (2012) *Nature* **490**, 552-555

172. Bohlen, C. J., Chesler, A. T., Sharif-Naeini, R., Medzihradszky, K. F., Zhou, S., King, D., Sanchez, E. E., Burlingame, A. L., Basbaum, A. I., and Julius, D. (2011) *Nature* **479**, 410-414

173. Mazzuca, M., Heurteaux, C., Alloui, A., Diochot, S., Baron, A., Voilley, N., Blondeau, N., Escoubas, P., Gelot, A., Cupo, A., Zimmer, A., Zimmer, A. M., Eschalier, A., and Lazdunski, M. (2007) *Nature neuroscience* **10**, 943-945

174. Duan, B., Wu, L. J., Yu, Y. Q., Ding, Y., Jing, L., Xu, L., Chen, J., and Xu, T. L. (2007) *J Neurosci* **27**, 11139-11148

175. Baron, A., Waldmann, R., and Lazdunski, M. (2002) *J Physiol* **539**, 485-494

176. Roza, C., Puel, J. L., Kress, M., Baron, A., Diochot, S., Lazdunski, M., and Waldmann, R. (2004) *J Physiol* **558**, 659-669

177. Hruska-Hageman, A. M., Wemmie, J. A., Price, M. P., and Welsh, M. J. (2002) *Biochem J* **361**, 443-450

178. Zha, X. M., Costa, V., Harding, A. M., Reznikov, L., Benson, C. J., and Welsh, M. J. (2009) *J Neurosci* **29**, 8438-8446

179. Arias, R. L., Sung, M. L., Vasylyev, D., Zhang, M. Y., Albinson, K., Kubek, K., Kagan, N., Beyer, C., Lin, Q., Dwyer, J. M., Zaleska, M. M., Bowlby, M. R., Dunlop, J., and Monaghan, M. (2008) *Neurobiology of disease* **31**, 334-341

180. Wong, H. K., Bauer, P. O., Kurosawa, M., Goswami, A., Washizu, C., Machida, Y., Tosaki, A., Yamada, M., Knopfel, T., Nakamura, T., and Nukina, N. (2008) *Human molecular genetics* **17**, 3223-3235

181. Babini, E., Paukert, M., Geisler, H. S., and Grunder, S. (2002) *J Biol Chem* **277**, 41597-41603

182. Sherwood, T. W., Lee, K. G., Gormley, M. G., and Askwith, C. C. (2011) *J Neurosci* **31**, 9723-9734

183. Hauser, K. F., Foldes, J. K., and Turbek, C. S. (1999) *Experimental neurology* **160**, 361-375

184. Yang, H. Y., Fratta, W., Majane, E. A., and Costa, E. (1985) *Proc Natl Acad Sci U S A* **82**, 7757-7761

185. Li, W. G., Yu, Y., Zhang, Z. D., Cao, H., and Xu, T. L. (2010) *Molecular pain* **6**, 88

186. Duan, B., Wang, Y. Z., Yang, T., Chu, X. P., Yu, Y., Huang, Y., Cao, H., Hansen, J., Simon, R. P., Zhu, M. X., Xiong, Z. G., and Xu, T. L. (2011) *J Neurosci* **31**, 2101-2112

187. Staruschenko, A., Dorofeeva, N. A., Bolshakov, K. V., and Stockand, J. D. (2007) *Developmental neurobiology* **67**, 97-107

188. Immke, D. C., and McCleskey, E. W. (2003) *Neuron* **37**, 75-84

189. Paukert, M., Babini, E., Pusch, M., and Grunder, S. (2004) *J Gen Physiol* **124**, 383-394

190. Wang, X., Li, W. G., Yu, Y., Xiao, X., Cheng, J., Zeng, W. Z., Peng, Z., Xi Zhu, M., and Xu, T. L. (2013) *J Neurosci* **33**, 4265-4279

191. Birdsong, W. T., Fierro, L., Williams, F. G., Spelta, V., Naves, L. A., Knowles, M., Marsh-Haffner, J., Adelman, J. P., Almers, W., Elde, R. P., and McCleskey, E. W. (2010) *Neuron* **68**, 739-749

192. Wang, J. Q., Chu, X. P., Guo, M. L., Jin, D. Z., Xue, B., Berry, T. J., Fibuch, E. E., and Mao, L. M. (2012) *Frontiers in physiology* **3**, 164

193. Allen, N. J., and Attwell, D. (2002) *J Physiol* **543**, 521-529

194. Voilley, N., de Weille, J., Mamet, J., and Lazdunski, M. (2001) *J Neurosci* **21**, 8026-8033
195. Ugawa, S., Ishida, Y., Ueda, T., Inoue, K., Nagao, M., and Shimada, S. (2007) *Biochem Biophys Res Commun* **363**, 203-208
196. Dube, G. R., Lehto, S. G., Breese, N. M., Baker, S. J., Wang, X., Matulenko, M. A., Honore, P., Stewart, A. O., Moreland, R. B., and Brioni, J. D. (2005) *Pain* **117**, 88-96
197. Yu, Y., Chen, Z., Li, W. G., Cao, H., Feng, E. G., Yu, F., Liu, H., Jiang, H., and Xu, T. L. (2010) *Neuron* **68**, 61-72
198. Muto, S., Imai, M., and Asano, Y. (1993) *Br J Pharmacol* **109**, 673-678
199. Hoagland, E. N., Sherwood, T. W., Lee, K. G., Walker, C. J., and Askwith, C. C. (2010) *J Biol Chem* **285**, 41852-41862
200. Qadri, Y. J., Berdiev, B. K., Song, Y., Lippton, H. L., Fuller, C. M., and Benos, D. J. (2009) *J Biol Chem* **284**, 17625-17633
201. Baconguis, I., and Gouaux, E. (2012) *Nature* **489**, 400-405
202. Chen, X., Kalbacher, H., and Grunder, S. (2006) *J Gen Physiol* **127**, 267-276
203. Dawson, R. J., Benz, J., Stohler, P., Tetaz, T., Joseph, C., Huber, S., Schmid, G., Hugin, D., Pflimlin, P., Trube, G., Rudolph, M. G., Hennig, M., and Ruf, A. (2012) *Nature communications* **3**, 936
204. Anangi, R., Chen, C. C., Lin, Y. W., Cheng, Y. R., Cheng, C. H., Chen, Y. C., Chu, Y. P., and Chuang, W. J. (2010) *Toxicon : official journal of the International Society on Toxinology* **56**, 1388-1397
205. Chagot, B., Escoubas, P., Diochot, S., Bernard, C., Lazdunski, M., and Darbon, H. (2005) *Protein Sci* **14**, 2003-2010
206. Diochot, S., Baron, A., Rash, L. D., Deval, E., Escoubas, P., Scarzello, S., Salinas, M., and Lazdunski, M. (2004) *EMBO J* **23**, 1516-1525
207. Blanchard, M. G., Rash, L. D., and Kellenberger, S. (2012) *Br J Pharmacol* **165**, 2167-2177
208. Peigneur, S., Beress, L., Moller, C., Mari, F., Forssmann, W. G., and Tytgat, J. (2012) *FASEB J* **26**, 5141-5151
209. Matricon, J., Gelot, A., Etienne, M., Lazdunski, M., Muller, E., and Ardid, D. (2011) *Eur J Pain* **15**, 335-343
210. Karczewski, J., Spencer, R. H., Garsky, V. M., Liang, A., Leitl, M. D., Cato, M. J., Cook, S. P., Kane, S., and Urban, M. O. (2010) *Br J Pharmacol* **161**, 950-960
211. Ikeuchi, M., Kolker, S. J., Burnes, L. A., Walder, R. Y., and Sluka, K. A. (2008) *Pain* **137**, 662-669
212. Izumi, M., Ikeuchi, M., Ji, Q., and Tani, T. (2012) *Journal of biomedical science* **19**, 77
213. Behan, A. T., Breen, B., Hogg, M., Woods, I., Coughlan, K., Mitchem, M., and Prehn, J. H. (2013) *Cell death and differentiation*
214. Coryell, M. W., Wunsch, A. M., Haenfler, J. M., Allen, J. E., Schnizler, M., Ziemann, A. E., Cook, M. N., Dunning, J. P., Price, M. P., Rainier, J. D., Liu, Z., Light, A. R., Langbehn, D. R., and Wemmie, J. A. (2009) *J Neurosci* **29**, 5381-5388
215. Coryell, M. W., Ziemann, A. E., Westmoreland, P. J., Haenfler, J. M., Kurjakovic, Z., Zha, X. M., Price, M., Schnizler, M. K., and Wemmie, J. A. (2007) *Biological psychiatry* **62**, 1140-1148
216. Dwyer, J. M., Rizzo, S. J., Neal, S. J., Lin, Q., Jow, F., Arias, R. L., Rosenzweig-Lipson, S., Dunlop, J., and Beyer, C. E. (2009) *Psychopharmacology* **203**, 41-52
217. Snyder, P. M., McDonald, F. J., Stokes, J. B., and Welsh, M. J. (1994) *J Biol Chem* **269**, 24379-24383

218. Canessa, C. M., Merillat, A. M., and Rossier, B. C. (1994) *Am J Physiol* **267**, C1682-1690
219. Snyder, P. M., Cheng, C., Prince, L. S., Rogers, J. C., and Welsh, M. J. (1998) *J Biol Chem* **273**, 681-684
220. Dijkink L, H. A., van Os CH, Bindels RJ. (2002) *Pflugers Arch.* **444**, 549-555
221. Coscoy, S., Lingueglia, E., Lazdunski, M., and Barbry, P. (1998) *J Biol Chem* **273**, 8317-8322
222. Firsov D, G. I., Merillat AM, Rossier BC, Schild L. (1998) *EMBO J.* **17**, 344-353
223. Kosari, F., Sheng, S., Li, J., Mak, D. O., Foskett, J. K., and Kleyman, T. R. (1998) *J Biol Chem* **273**, 13469-13474
224. Eskandari, S., Snyder, P. M., Kreman, M., Zampighi, G. A., Welsh, M. J., and Wright, E. M. (1999) *J Biol Chem* **274**, 27281-27286
225. Stryer, L., and Haugland, R. P. (1967) *Proc Natl Acad Sci U S A* **58**, 719-726
226. Staruschenko, A., Medina, J. L., Patel, P., Shapiro, M. S., Booth, R. E., and Stockand, J. D. (2004) *J Biol Chem* **279**, 27729-27734
227. Anantharam A, P. L. (2007) *J Gen Physiology* **130**, 55-70
228. Jasti J, F. H., Gonzales EB, Gouaux E. (2007) *Nature* **449**, 316-323
229. Collier, D. M., and Snyder, P. M. (2011) *J Biol Chem* **286**, 6027-6032
230. Stewart, A. P., Haerteis, S., Diakov, A., Korbmacher, C., and Edwardson, J. M. (2011) *J Biol Chem* **286**, 31944-31952
231. Gao, Y., Liu, S. S., Qiu, S., Cheng, W., Zheng, J., and Luo, J. H. (2007) *Biochem Biophys Res Commun* **359**, 143-150
232. Carnally, S. M., Dev, H. S., Stewart, A. P., Barrera, N. P., Van Bemmelen, M. X., Schild, L., Henderson, R. M., and Edwardson, J. M. (2008) *Biochem Biophys Res Commun* **372**, 752-755
233. Zha, X. M., Wang, R., Collier, D. M., Snyder, P. M., Wemmie, J. A., and Welsh, M. J. (2009) *Proc Natl Acad Sci U S A* **106**, 3573-3578
234. Gonzales EB, K. T., Gouaux E. (2009) *Nature* **460**, 599-604
235. Snyder, P. M., Olson, D. R., and Bucher, D. B. (1999) *J Biol Chem* **274**, 28484-28490
236. Schild, L., Schneeberger, E., Gautschi, I., and Firsov, D. (1997) *J Gen Physiol* **109**, 15-26
237. Takeda, A. N., Gautschi, I., van Bemmelen, M. X., and Schild, L. (2007) *J Biol Chem* **282**, 31928-31936
238. Gimpl, G., Klein, U., Reilander, H., and Fahrenholz, F. (1995) *Biochemistry* **34**, 13794-13801
239. Marheineke, K., Grunewald, S., Christie, W., and Reilander, H. (1998) *FEBS letters* **441**, 49-52
240. Samways, D. S., Harkins, A. B., and Egan, T. M. (2009) *Cell Calcium* **45**, 319-325
241. Salinas, M., Rash, L. D., Baron, A., Lambeau, G., Escoubas, P., and Lazdunski, M. (2006) *J Physiol* **570**, 339-354
242. Baron, A., Diochot, S., Salinas, M., Deval, E., Noel, J., and Lingueglia, E. (2013) *Toxicon : official journal of the International Society on Toxinology* **75**, 187-204
243. Smart, O. S., Goodfellow, J. M., and Wallace, B. A. (1993) *Biophys J* **65**, 2455-2460
244. Li, T., Yang, Y., and Canessa, C. M. (2010) *J Biol Chem* **285**, 31285-31291
245. Springauf, A., Bresenitz, P., and Grunder, S. (2011) *J Biol Chem* **286**, 24374-24384
246. Gandhi, C. S., Walton, T. A., and Rees, D. C. (2011) *Protein Sci* **20**, 313-326
247. Swamy, M., Siegers, G. M., Minguet, S., Wollscheid, B., and Schamel, W. W. (2006) *Sci STKE* **2006**, pl4
248. Hajdu, J., Wyss, S. R., and Aebi, H. (1977) *Eur J Biochem* **80**, 199-207

249. Metz, B., Kersten, G. F., Hoogerhout, P., Brugghe, H. F., Timmermans, H. A., de Jong, A., Meiring, H., ten Hove, J., Hennink, W. E., Crommelin, D. J., and Jiskoot, W. (2004) *J Biol Chem* **279**, 6235-6243
250. Satlin, L. M., and Palmer, L. G. (1996) *Am J Physiol* **270**, F391-397
251. Satlin, L. M., and Palmer, L. G. (1997) *Am J Physiol* **272**, F397-404
252. Tolino, L. A., Okumura, S., Kashlan, O. B., and Carattino, M. D. (2011) *J Biol Chem*
253. Warne, T., Chirnside, J., and Schertler, G. F. (2003) *Biochim Biophys Acta* **1610**, 133-140
254. Schagger, H., and von Jagow, G. (1991) *Anal Biochem* **199**, 223-231
255. Green, N. S., Reisler, E., and Houk, K. N. (2001) *Protein Sci* **10**, 1293-1304
256. Li, T., Yang, Y., and Canessa, C. M. (2011) *Nature communications* **2**, 399
257. Passero, C. J., Okumura, S., and Carattino, M. D. (2009) *J Biol Chem* **284**, 36473-36481
258. Adams, C. M., Snyder, P. M., Price, M. P., and Welsh, M. J. (1998) *J Biol Chem* **273**, 30204-30207
259. Trott, O., and Olson, A. J. (2010) *Journal of computational chemistry* **31**, 455-461
260. Grosdidier, A., Zoete, V., and Michielin, O. (2011) *Nucleic Acids Res* **39**, W270-277
261. Kawabata, T. (2010) *Proteins* **78**, 1195-1211
262. Wagner, D. A., and Czajkowski, C. (2001) *J Neurosci* **21**, 67-74
263. Dutzler, R., Campbell, E. B., and MacKinnon, R. (2003) *Science* **300**, 108-112
264. Hilf, R. J., and Dutzler, R. (2009) *Nature* **457**, 115-118
265. Hou, X., Pedi, L., Diver, M. M., and Long, S. B. (2012) *Science* **338**, 1308-1313
266. Zhou, Y., Morais-Cabral, J. H., Kaufman, A., and MacKinnon, R. (2001) *Nature* **414**, 43-48
267. Bize, V., and Horisberger, J. D. (2007) *American journal of physiology. Renal physiology* **293**, F1137-1146
268. Babini, E., Geisler, H. S., Siba, M., and Grunder, S. (2003) *J Biol Chem* **278**, 28418-28426
269. Sheng, S., Perry, C. J., and Kleyman, T. R. (2004) *J Biol Chem* **279**, 31687-31696
270. Schoeneman, M. J., and Spitzer, A. (1980) *Proc Soc Exp Biol Med* **165**, 319-322
271. Blount, P., Sukharev, S. I., Moe, P. C., Nagle, S. K., and Kung, C. (1996) *Biol Cell* **87**, 1-8
272. Blount, P., Sukharev, S. I., Moe, P. C., Schroeder, M. J., Guy, H. R., and Kung, C. (1996) *EMBO J* **15**, 4798-4805
273. Chang, G., Spencer, R. H., Lee, A. T., Barclay, M. T., and Rees, D. C. (1998) *Science* **282**, 2220-2226
274. Liu, Z., Gandhi, C. S., and Rees, D. C. (2009) *Nature* **461**, 120-124
275. De Zorzi, R., Nicholson, W. V., Guigner, J. M., Erne-Brand, F., and Venien-Bryan, C. (2013) *Biophys J* **105**, 398-408
276. Duffy, J. B. (2002) *Genesis* **34**, 1-15
277. Peabody, N. C., Diao, F., Luan, H., Wang, H., Dewey, E. M., Honegger, H. W., and White, B. H. (2008) *J Neurosci* **28**, 14379-14391
278. Schymkowitz, J., Borg, J., Stricher, F., Nys, R., Rousseau, F., and Serrano, L. (2005) *Nucleic Acids Res* **33**, W382-388